LEABHARLANN CHOLÁISTE NA TRÍONÓIDE, BAILE ÁTHA CLIATH | TRINITY COLLEGE LIBRARY DUBLIN
Ollscoil Átha Cliath | The University of Dublin

Terms and Conditions of Use of Digitised Theses from Trinity College Library Dublin

Copyright statement

All material supplied by Trinity College Library is protected by copyright (under the Copyright and Related Rights Act, 2000 as amended) and other relevant Intellectual Property Rights. By accessing and using a Digitised Thesis from Trinity College Library you acknowledge that all Intellectual Property Rights in any Works supplied are the sole and exclusive property of the copyright and/or other IPR holder. Specific copyright holders may not be explicitly identified. Use of materials from other sources within a thesis should not be construed as a claim over them.

A non-exclusive, non-transferable licence is hereby granted to those using or reproducing, in whole or in part, the material for valid purposes, providing the copyright owners are acknowledged using the normal conventions. Where specific permission to use material is required, this is identified and such permission must be sought from the copyright holder or agency cited.

Liability statement

By using a Digitised Thesis, I accept that Trinity College Dublin bears no legal responsibility for the accuracy, legality or comprehensiveness of materials contained within the thesis, and that Trinity College Dublin accepts no liability for indirect, consequential, or incidental, damages or losses arising from use of the thesis for whatever reason. Information located in a thesis may be subject to specific use constraints, details of which may not be explicitly described. It is the responsibility of potential and actual users to be aware of such constraints and to abide by them. By making use of material from a digitised thesis, you accept these copyright and disclaimer provisions. Where it is brought to the attention of Trinity College Library that there may be a breach of copyright or other restraint, it is the policy to withdraw or take down access to a thesis while the issue is being resolved.

Access Agreement

By using a Digitised Thesis from Trinity College Library you are bound by the following Terms & Conditions. Please read them carefully.

I have read and I understand the following statement: All material supplied via a Digitised Thesis from Trinity College Library is protected by copyright and other intellectual property rights, and duplication or sale of all or part of any of a thesis is not permitted, except that material may be duplicated by you for your research use or for educational purposes in electronic or print form providing the copyright owners are acknowledged using the normal conventions. You must obtain permission for any other use. Electronic or print copies may not be offered, whether for sale or otherwise to anyone. This copy has been supplied on the understanding that it is copyright material and that no quotation from the thesis may be published without proper acknowledgement.

Simulation of Microcrack Growth and Repair in Living Bone

Pietro Tisbo

Department of Mechanical and Manufacturing Engineering

Trinity College Dublin

A thesis submitted to the University of Dublin, Trinity College, part fulfilment of the requirements of application for the degree of

Doctor of Philosophy

Outputs of the simulator 112
Simulation of crack growth in fatigue tests 113
Simulation of broken processes 127
Biological reactions 133
Wolff's law simulation 135
Simulation of crack growth and repair 136
Results of the simulator for military training 138
New cracks 146
Probability of failure 149
Simulation of special scenarios 151
Mechanostat signal model 155
Chapter 6: Discussion 157
Conclusions 165
Appendix: List of Matlab™ scripts and functions 168
Bibliography 172

TRINITY COLLEGE
2 4 MAY 2013
LIBRARY DUBLIN

Thesis 9856

Table of Contents

Declaration 5
Acknowledgments 6
Abstract 7
Nomenclature 8
Introduction 9
Analysis of the problem 9
Bone micro structural anatomy 10
Damage in cortical bone 12
Damage in trabecular bone 14
Repair 15
This project's goal 16
Chapter 1: Literature review 19
Bone crack theory 19
Bone microstructure 29
Stress on bone 30
Crack formation 33
Damage detection in bone 36
Osteocyte Processes 48
Bone repair 49
Bone remodelling 51
Factors influencing bone properties 60
Stress fractures during military training 61
Simulation 63
Summary 64
Chapter 2: Methods 67
Chapter 3: Theoretical model 73
Bone cracking under fatigue stress 73
Damage Detection 77
Mechanostat model 84
Bone repair theory 84
Variation in bone density 88
Simulation of the risk of fracture in lower limbs for military personnel 89
Chapter 4: The simulator model 94
Chapter 5: Results 112

Acknowledgments

It has been an honour and a pleasure to work in the last few years in Trinity College Dublin as a postgraduate student. I will take a few words here to thank all the people who made it possible for me to have such an extraordinary experience.

First of all I would like to thank my supervisor, Prof. David Taylor, for all the help, encouragement and support he has given me since I first came to Ireland for the interview until now. It is rare to meet a person so in love with his work and so eager to transmit his knowledge to his students.

My thanks go also to the other members of the Bone for Life group, especially to the other PhD (former) students whose work contributed to shape the simulation: Gerardo Presbitero, Lauren Mulcahy and Clodagh Dooley. They have been wonderful companions in this research and it is because of their help that this work has been completed.

For the financial support I would like to thank Science Foundation Ireland for funding this project and therefore allowing the completion of this work.

Finally, I need to thank my family, especially my mother, for the help and the support that they have given to me, even from afar.

Declaration

I declare that the present work has not previously been submitted as an exercise for a degree at this or any other University.

The thesis consists entirely of my own work except where references indicate otherwise.

The library of the University of Dublin, Trinity College, may lend or copy this thesis upon request.

Nomenclature

The following table shows the most common abbreviations I have used in this work.

BMU	Bone Multicellular Unit
RankL	Receptor activator of NFκ B Ligand
Rank	Receptor activator of NFκ B
OPG	Osteoprotegrin
OC	Osteoclast
OB	Osteoblast
2a	Crack Length
a	½ Crack Length
2d	Distance between osteons
d	½ Distance Between osteons
K	Stress intensity
ΔK	Stress intensity range
ΔK_{th}	Stress intensity range threshold
$\Delta\sigma$	Stress range
σ	Stress
Δa	Crack growth because of fatigue
BP	Broken processes
IV	Initial value
δs	Displacement
MLO-Y4	Osteocyte-like cells.

Abstract

As they are the structural components of the body, bones are subjected to the accumulation of damage because of cyclical stress (fatigue). The fatigue damage in bone takes the form of microscopic cracks (microcracks) that span the bone structure and with time can become a danger for the bone. Bones are able to repair damage by detecting the microcracks and using specialized cells that remove the old bone and replace it with new, undamaged bone. The goal of this work was to create a system able to simulate the mechanics of microcrack growth and repair in living bone knowing the properties of bone and the stress it is going to sustain.

The system has been built with the Simulink™ suite of the program Matlab™. It was composed of three sub models: the first to simulate crack growth under stress, the second to simulate how the damage done by the crack is translated into a biological signal and the third to mimic the cellular reactions that come into action to repair the damage.

The system has been applied to simulate different situations, from reproducing the behaviour of cracks in fatigue experiments to predicting the risk of fracture in army trainees. The results have shown that the system is able to simulate the mechanics of bone microcrack accumulation, detection and repair in accordance to the literature on the topic and the experimental data used as references. The system was also able to simulate special conditions, like the presence of diseases or the use of drugs that alter the biochemical reactions that regulate repair.

Keywords: Bone, Fatigue, Microcracks, Simulation, Repair, Damage

and tend to bring the whole bone to failure (2). It is a known fact that the body is able to identify the cracks and act accordingly, but how the body detects this damage is less clear at the moment and still a topic of debate (3). Because of this I will have to make a choice about which theory of damage signalling I will follow. For this model the choice will be on the "scissors model" developed in our research group and I will show, in detail, this signal model in this work, but I will also show a simulation of the "mechanostat" theory, which theorizes the bone cells acting as transducers, feeling the increase of stress at the tip of the crack. After the body receives the signal that damage has occurred, it starts a series of chemical processes that turn precursor cells into the cells that will repair the damage. Those processes are known in principle but there are still many unclear factors, like what inhibits and improves reactions. I will have to make assumptions about this part and simplify the reactions to have a number of coefficients small enough to have a smooth simulation but still big enough to be realistic and versatile. The last part of this study will focus on the long term effects of repair. Many studies have shown how repaired bone is stronger that the original bone for healthy subjects (4), while in presence of diseases like osteoporosis or osteopetrosis the repair seems to reduce the overall strength of the bones (5). The system will use a simple mechanism to simulate this effect altering the properties of bone, based on the chemical processes that start the repair. The system applies the variations to cracks and bone structure to the initial values, allowing for a closed loop. At every cycle of the simulation the parameters are updated for the next, creating a dynamical depiction of the behaviour of bone.

Bone micro structural anatomy

Bone material is composed of both cellular mass and an extracellular matrix. The cellular component is composed of osteocytes, osteoclasts, osteoblasts and their precursors that are enclosed in the matrix. The matrix, composed of mineralized bone and collagen fibres, is the part that determines the mechanical properties of bone and has a very heterogeneous structure as can be seen from Figure 1.

Introduction

In all vertebrate animals the skeletal structure provides support for movement and protection for the most delicate organs in the body. Bones are hard, sturdy organs that grant an impressive number of features to vertebrates, allowing them to sustain their size, run, fly and swim. But even as they are resilient, bones accumulate damage during everyday activity and exceptional traumatic events. If the damage is not extreme, bones can still recover their functionality given rest and time. The damage accumulated is constantly repaired by the bone cells themselves, with a mechanism that allows them to find it and operate on it. The fatigue damage accumulated in normal activities shows itself in the form of microcracks, with sizes of the order of a tenth of a millimetre, those microcracks are detected by the body that generates cell units that remove the old bone together with the cracks and replace it with new bone, free from damage (1).

These constant processes of damage accumulation, detection and repair are the focus of this study. My goal is to understand these processes, give them a quantitative description and finally generate a coherent simulation, able to predict the behaviour of bone in given cases of stress and damage. To do so I will analyze the processes step by step and I will form theories about their behaviour. Those theories will be the base of my simulation, whose results will be confronted with the experimental data available from literature and with the results of experiments from the project group. Combining the different steps of simulation I will have a complex simulator that covers almost all the aspects of the cycle of bone damage and repair, from the birth of damage to its repair.

Analysis of the problem

The topic of bone damage and repair cycles needs to be analyzed by a multitude of different scales as bone is a complex object on three different scales, from the macro-scale (shape of the bone, size) to the nano-scale (the cellular processes that form the repair, the composition of bone) and that affect its response to damage. The most common cause of damage and failure in bone is accumulated fatigue damage. This damage can be seen in the form of microcracks spanning the bone material, cracks that tend to grow fast when very small and then slow down their growth when they reach a certain size (around a tenth of millimetre). Only a few cracks in specific instances manage to grow beyond that size, but those who do usually after that start growing out of control

structure of the bone, similar to ties and struts in engineering, with the added bonus of being able to rearrange their directions to those of the lines of stress (10).

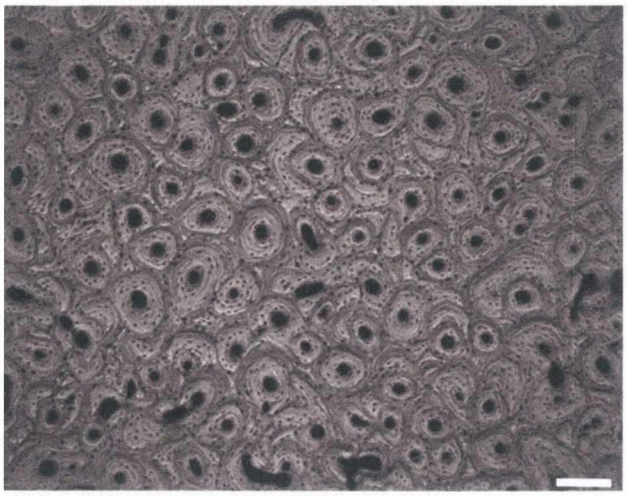

Figure 2. Cortical bone cross-section, showing the osteons and their Haversian channels. Image from Shahar *et al* (11)

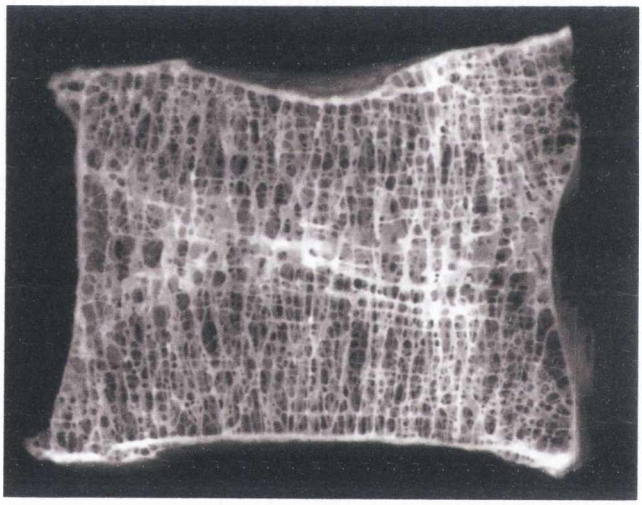

Figure 3. Section of a human vertebra. The image shows the reticular shape of trabecular bone. From Mosekilde *et al* (12)

Damage in cortical bone

Observing more in detail cortical bone it's possible to start meeting microcracks between osteons (Figure 4). Those are the physical results of the stresses applied to the bone. They are roughly elliptical in shape, ranging between 100 μm and 400 μm in length and approximately with their axes parallel to the bone's longitudinal direction (13). The osteons act as barriers for the growth of those cracks, which are able to grow very fast until they meet an osteon (14). Sometimes osteons fail to stop cracks, in those cases the

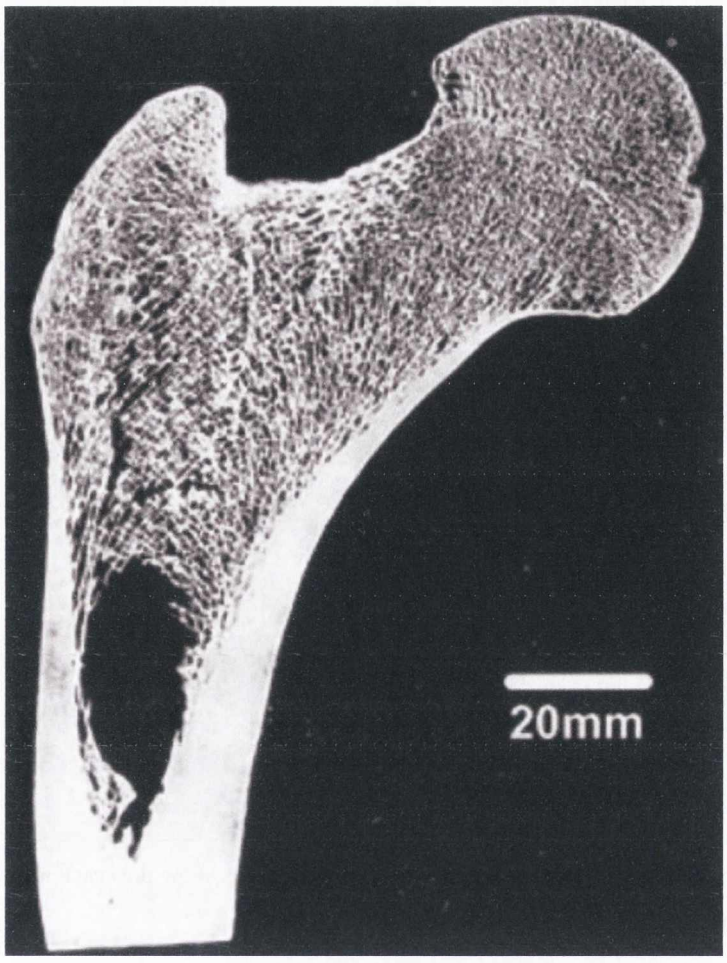

Figure 1. Section of bone, showing cortical and trabecular bone structures. The trabecular bone is the spongy central section and the cortical bone is the compact section which can be seen in the outer and lower parts of the bone. Extracted from Gray (6).

The compact and porous structures are characteristics respectively of cortical and trabecular bone (7). The first (Figure 2) is the main component of the cortex, the outer shell of bones and provides the stiffness and resilience of bone. The cortex composes around 80% of the skeleton's weight. Its primary constituents are the osteons, cylindrically shaped units that are around 0.2 mm in diameter and several millimetres long. The osteons are themselves composed of lamellae; concentric, thin slices of material that surround the Haversian canal, where the nerves and blood vessels of the bone are placed (8). The osteons have an important part to play in determining the resistance of bone to microcrack growth (9). The trabecular or spongy bone (Figure 3) is the component of the inner part of flat bones, like vertebrae and the pelvis, and of the head of long bones. It is arranged, as the name suggests, in a porous structure similar to a sponge, with plates (trabeculae) and rods of bone that surround the bone marrow. Their role is to support the

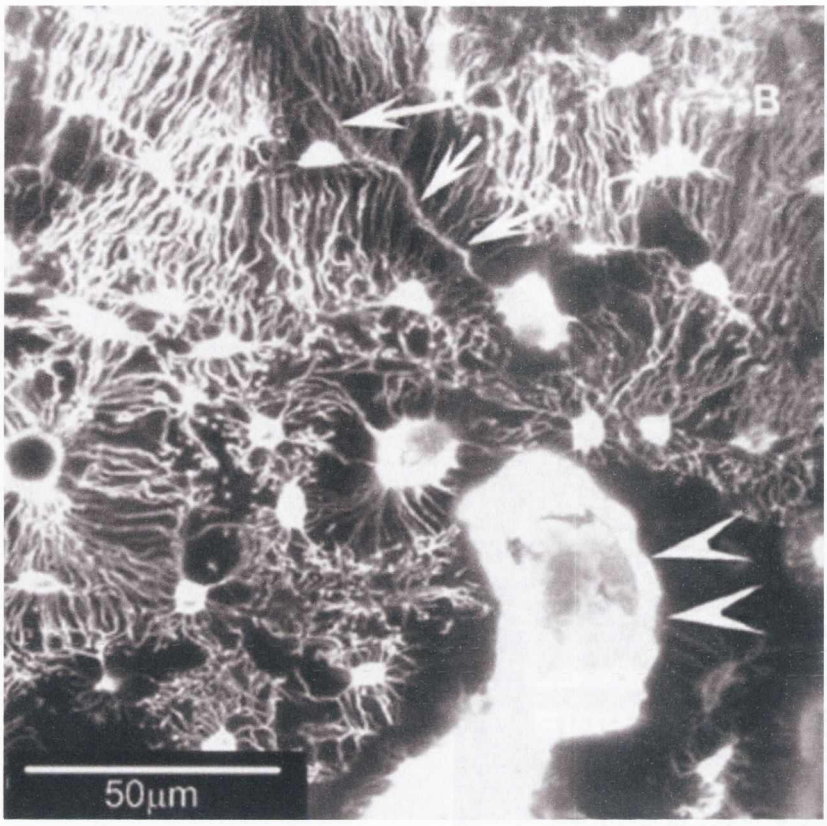

Figure 5. Microscopic image showing a crack and the BMU travelling towards it. The arrows show the crack and the triangles show the BMU approaching it to repair it. From Colopy *et al* (17)

Damage in trabecular bone

In trabecular bone the mechanics of damage are a bit different, as can be expected from a spongy structure. Trabeculae are thin slices of mineralized bone ranging between 10 μm and 100 μm in size(18). Cracks are not impeded in growth by anything, but they don't have the immediate destructive effect that can be observed in a more compact structure, instead a failed trabecula reduces the overall integrity of the material. Partially failed trabeculae can be repaired by BMUs (Basic Multicellular Unit, see next paragraph for details) but when they are completely broken they heal like bones, with the formation of a small callus (Figure 6). When this phenomenon does not occur the quality of the material is compromised, as it happens in elderly or osteoporotic patients (15).

crack will grow more energetic and usually will cause the failure of the whole bone, as is typical of the fracture mechanics of brittle materials (2).

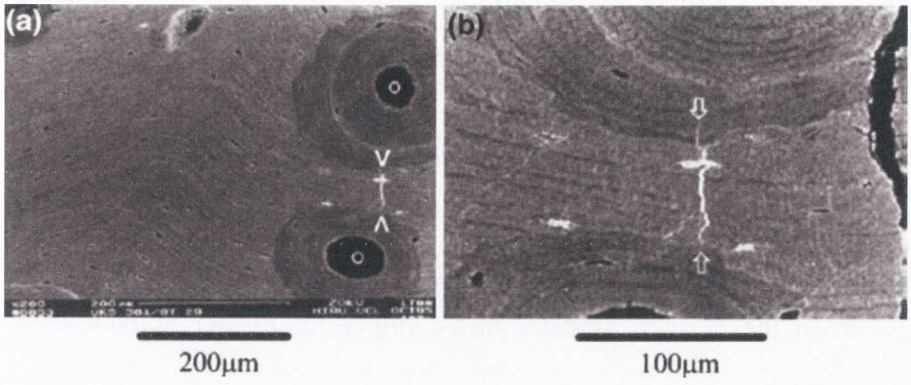

Figure 4. Damage on cortical bone: the cracks are marked by arrows that show also where they stop. The image shows how cracks are impended in their growth from the presence of osteons. The images are at two different scales to show both the osteons (a) and the details of the crack (b). From Boyde (15)

When I observe bone at this scale I can notice how it appears even less homogeneous than before. Osteocytes are linked to each other by a network of processes, shaped like tree branches that allow communication between cells (Figure 5). Cracks can cross a consistent number of processes and the strain they are experiencing can break them, this breaking could be a way for the body to detect the damage caused by the cracks (16).

activator of NFκ B Ligand (RANKL) and its receptors, receptor activator of NFκ B (RANK) and osteoprotegrin (OPG), along with other factors, such as ephrins and interleukins(23). It has been established that the RANKL-RANK-OPG signalling pathway is a main actor in the activation of bone remodelling by BMUs. RANKL causes the activation and differentiation of osteoclasts from their inactive precursors, and so it stimulates bone remodelling. Osteoclast activation occurs as RANKL binds to the RANK receptor on the cell surface of both precursors and mature osteoclasts. OPG, a member of the TNF superfamily, functions by binding to and sequestering RANKL, impeding the resorption. It binds to it on the surface of osteoblasts, impeding further activation of osteoclasts (24).

The action of a BMU restores the bone to an undamaged state, but the new bone is not usually equal in quality to the old bone. An increase of bone mass has been noticed in healthy subjects that engage in physical activities (25) and people that are forced to long periods of inactivity have shown significant reduction in bone mass(26). Furthermore diseases like osteoporosis have been shown to affect the remodelling process by unbalancing it towards a reduction of the density of bone (27).

This project's goal

The goal of this project is to craft a simulation model that predicts the behaviour of fatigue microcracks in compact bone and the reaction of the body to this damage. I want to create a model that can give a prediction of how the length of a bone microcrack is affected by fatigue stress accumulation and by the repair action of the body. To obtain this goal I will individually address the processes that affect the cracks as follows:

- Simulating the growth of the microcracks in a bone under fatigue stress at every cycle of fatigue, knowing the stress applied to the bone, the number of cracks and their sizes at the beginning of the simulation and the physical properties of the bone surrounding them.
- Calculating the damage inflicted by the microcracks, simulating the signal released by the cells around a crack, knowing the size of the crack and the stress applied to the bone
- Simulating the biological processes that are activated by the signal of damage and activate the repair, by reproducing the chain of cell reactions that stimulate the formation of a BMU and the effects of the BMU on the crack length.

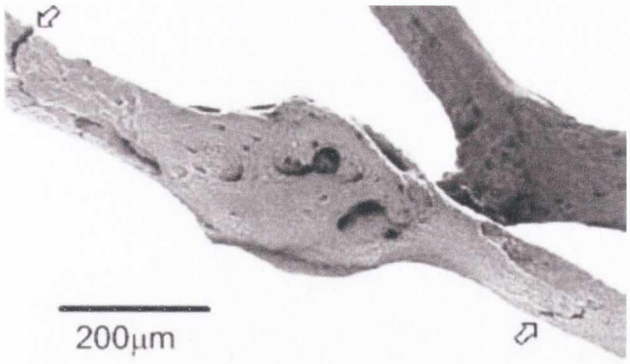

Figure 6. Repair in trabecular bone, the arrows show the surface microcracks. It is also visible the callus formed by the repair. Image from Boyde (15)

Repair

The presence of damage alerts the body to repair it. There are specialized cells that work to repair the damage in the bone. Osteoclasts remove the damaged bone material while osteoblasts replace it with new bone(19). They are usually present in bone tissue as inactive cells, waiting for the body to release substances that trigger their activation(20). When they became active the cells arrange themselves in a BMU (basic multicellular unit) that travels toward the crack to repair it. A typical BMU (Figure 7) is composed like a cone of osteoclasts followed by a cone of osteoblasts, the former eat the damage while the latter create new bone, the BMU moves like a single unit, travelling towards the damage once it has been formed (21).

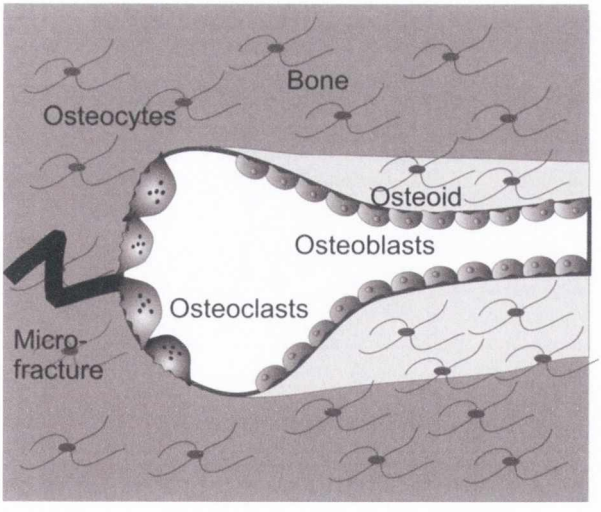

Figure 7. Schematic of a BMU (not to scale). The image shows the basilar mechanics of BMU repair, with osteoclasts removing the old bone and osteoblast depositing new bone in its place. From Ryser *et al* (22)

The substances that are thought to promote activation of the cells composing a BMU are, among others, members of the tumour necrosis factor family especially the receptor

- Additionally, I will simulate the reaction to the birth of new cracks in the system and the effects that repair can have on the overall strength of bone to analyze the system in special long term scenarios.
- At the end of this work I will use the simulator to reproduce the living bone behaviour of military conscripts during the first weeks of training, observing the similarities between the results of the simulation and the data available from the studies on this champion of real life data.

The result will be to have a system that can realistically simulate the behaviours observed in experimental data and that can be used to simulate different scenarios. I want to achieve a simulation which is able to replicate multiple cracks at the same time, allowing for a set of inputs and output that can reduce the scatter usually found in experiments. I expect the simulation of crack damage to give results that approximate those that can be found in physical experiments. As the exact details of how the body reacts to damage are not completely clear, the simulation of biological processes is based on a simplified model of the chain of reactions which brings the BMU to act, because of this it would be excessive to expect it to give a great level of quantitative accuracy in its results, I expect it to give good qualitative finding, like showing a targeted repair and the increase of repair activity with increased load. The simulation of the effects that the repair process has on the strength of bone is based on the variables in the biological processes simulation, so I expect it to give only qualitative results in the special scenarios where I will apply it. I am looking for a system which is versatile enough to be able to simulate different conditions, from variable load condition to the presence of diseases.

levels, but it is in this size that the nature of bone as a composite material can be analyzed in detail.

This analysis is composed of three parts that focus on 3 different scales, the micro scale for the crack growth by fatigue, a slightly smaller scale to detect the broken processes that define the behaviour of repair following the "scissors model" and finally the scale of molecular processes to simulate the RankL-OPG pathway that promotes the formation of the BMU.

After deciding the scale of the analysis to perform the next step is to get information on how the crack grows and how its behaviour can be predicted. Regarding crack growth a formula is provided in Taylor *et al* 1995 (28) that has been used in many different works and which was used as a component of the system in this project (Equation 1).

$$da/dN = C(\Delta K - \Delta Kth)^n + C'(\Delta K)^{n'}((d-a)/d)^m$$

Equation 1. Crack growth rate from Taylor et al (28)

Here da/dN is the rate of crack growth per cycle and ΔK is the stress intensity range which is related to the cyclic stress range, $\Delta\sigma$ and the crack length, 2a, through the standard fracture mechanics equation (Equation 2):

$$\Delta K = F\,\Delta\sigma\,(\pi a)^{1/2}$$

Equation 2. Stress intensity range from the classic fracture mechanic theory, as reported by Taylor *et al* (28)

F is a constant which depends on the geometry of the crack. Cracks are roughly elliptical in shape: the authors assumed a constant aspect ratio c/a=4.5. C, C', m, n and n' are constants, d is the distance between osteons and ΔK_{th} is the stress intensity range threshold required for the crack to grow following the standard fracture behaviour. Units for C and C' are such that da/dN is given in mm/cycle with ΔK in $MPa(m)^{1/2}$. The first term in Equation 1 describes the growth of the crack when it is relatively long; the second term describes short-crack growth, which decreases as the crack approaches a barrier a distance d from the initiation point. Each term is regarded as zero if it becomes negative. In cortical bone cracks are usually seen to stop at the cement lines surrounding secondary osteons, so d can represent the spacing between osteons.

Equation 1 is shown and used to analyze the microcrack growth and its relation with the ability of body to repair In Taylor 1997 (2). Since the equation is composed of 2 parts,

Chapter 1: Literature review

The problem of how bones accumulate damage and repair has interested scientists, biologists, physicians and engineers since the first studies have detected how fatigue damage accrues in it and how bone, as a living material, can repair itself to ensure its long life, retaining a light structure. So the literature on this topic is large and its works are written by people coming from many different backgrounds, with their various points of view. Since the problem is multidisciplinary to create a simulation of bone behaviour it is necessary to understand the problem from different points of view, so the sources needed for this project are actually varying from engineering to biological to medical. The following review roughly mirrors the steps undergone in the development of the system, and will show the papers that suggested the choices to configure it.

Bone crack theory

The first step in analyzing a problem is to picture the scale I am going to work with. In Taylor 2007 (18) it is stated that the subject is a hierarchical one which must be viewed on different levels: the scales of interest are three, called the macro, micro, and nano scale, though it is admitted that these divisions are somewhat arbitrary and can overlap each other. Moreover, despite some unique characteristics, bone is a composite material, on which investigation can be performed in the same way it is used to investigate other similar materials. The three scales are then defined as follows.

The macro scale is the scale that humans can easily detect without optical instruments, i.e. the bone size and shape, As the mechanical properties of the bone follow a gradient of change from one location to another along the structure, it is hard to say where the material ends and the structure begins so the analysis is conducted on a whole bone, depicted by size, shape and density.

The micro scale is where hints of a microstructure become more visible. In Taylor 2007 (18) evidence suggests that the main mechanics that control the fracture are found at the 0.1–1 mm scale. This scale is also the scale where it is easier to detect repair as the BMU is a cluster of cells 200 μm in diameter.

The nano scale is under 1 μm of size down to molecular dimensions. The processes of damage and repair on this scale are less understood than those ones on the larger size

one of the most important hypotheses of my model.

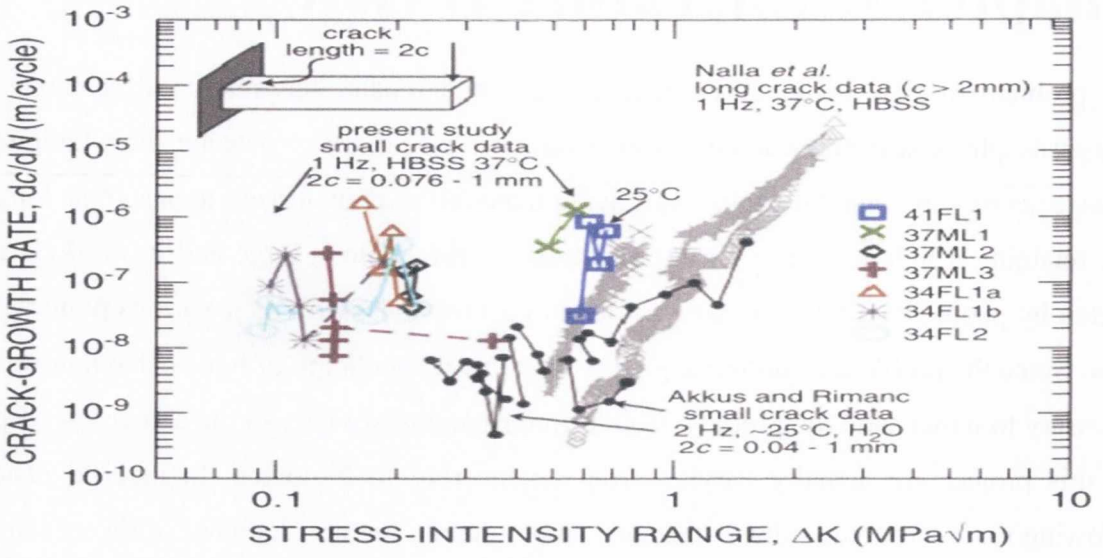

Figure 8. Experimental results for Stress Intensity Range vs. Crack Growth Rate. The figure shows the relation between crack growth rate and stress intensity range for different cracks in different bones. From (33)

An analysis done on crack growth and shape variation is done by means of experimental analysis in Lee *et al* 2000 (13) where the experiments show the size and the shape of cracks from various bones. This paper shows that microcracks are normally present in bone and are elliptical in shape, approximately 400 μm long and 100 μm wide. This paper doesn't focus too much on the growth but instead focuses on the shape and the position of cracks; it is from this shape that the analysis on the stress in cracks is made.

An analysis focused on crack density, directly correlated to the finding in Lee *et al* (13) is presented by O'Brien *et al* 2003 (34), along with the technique of bone staining with a sequence of chelating agents used to show the number of cracks at different number of cycles. In this paper the bones are analyzed with a microscope and the behaviour of crack density with cycles of fatigue is pictured. The analysis shows also the growth of cracks in a two dimensional image obtained by the microscope analysis. Figure 9 shows how a crack can develop with fatigue. The microcrack propagates from one of its ends in only one direction both transversally and longitudinally, keeping the ratio of crack length to width almost constant. This important finding allowed a great deal of successive analysis, including mine, to consider the cracks by defining only their length, reducing the problem to a single dimension. Another finding is that crack density tends to increase mainly at the beginning of the experiments and when nearing fracture as shown in Figure 10.

one regarding the small crack behaviour and another focusing on bigger cracks, to comply with the actual behaviour of microcracks in bone, the study finds that since the small crack behaviour shows a growth involving a decrease of rate with increasing length, precise control of crack length could be possible even for a nonintelligent system, such as bone.

This behaviour was then confirmed analytically by David Taylor the following year, in Taylor 1998 (29) where the parameters for growth are analyzed using theories from fracture mechanics (in particular the change of strain energy of the bone) and data from an experiment done in 1989 from Shaffler (30) that measured the variation in elastic modulus of the bone because of microcracks. From the variation of elastic modulus the parameters (crack length, crack growth rate and stress intensity) are detected and the theory described in the formula confirmed.

Other works from the David Taylor (31) (32) continue the studies on this formula and provide variations to it. The main variation is the insertion of stochastic variables to cover the effects of scatter on the experimental data. This choice proves to be effective, as, while this model was hard to set up initially, having a large number of degrees of freedom, it proved to be capable of predicting a wide variety of experimental data, including: crack density, length and other damage variables; stress/life data, and the effect of specimen size. It was also possible to simulate the increased density of cracks that occurs in older people.

In Kruzic *et al* 2006 (33) there are some experiments done on human cortical bone that confirm the results of the latest version of Equation 1, when compared to them. Actually the paper provides very few data, as the cracks are just 7 and they are from 6 different samples coming from 3 bodies (Figure 8), but the data about cracks of this size are actually very rare, so they are a welcome addition. The results show how small cracks grow at lower stress intensities than larger cracks and confirm the existence of a "stable" length of cracks where physiological stresses are unable to cause crack growth, which is

The behaviour of crack growth, and especially the discontinuous point where crack growth rate changes from dropping to rising is also analyzed in O'Brien *et al* 2006 (35) where the results of 5 years of experiments on bone microdamage are described, including those presented in O'Brien *et al* 2003 (34). These experiments are performed by applying fatigue load to the bones of animals that have been previously stained with dies. The results of these experiments find that the cracks that bring bones to failure always present some degree of rupturing of the osteons (Figure 11), which can be seen as a criterion to determine when crack growth changes its behaviour from dropping to rising.

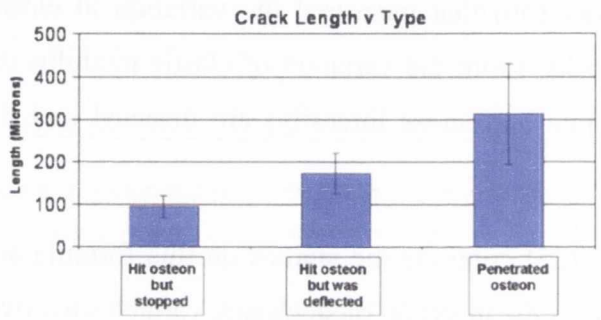

Figure 11. Mean crack length at the time of encountering an osteon for cracks of three categories: cracks which stopped at the osteon, cracks deflected by the osteon and cracks which penetrated the osteon. The values show how almost all the larger cracks present some degree of rupturing of the osteons. From O'Brien *et al* (35)

a will be later analyzed in more detail.

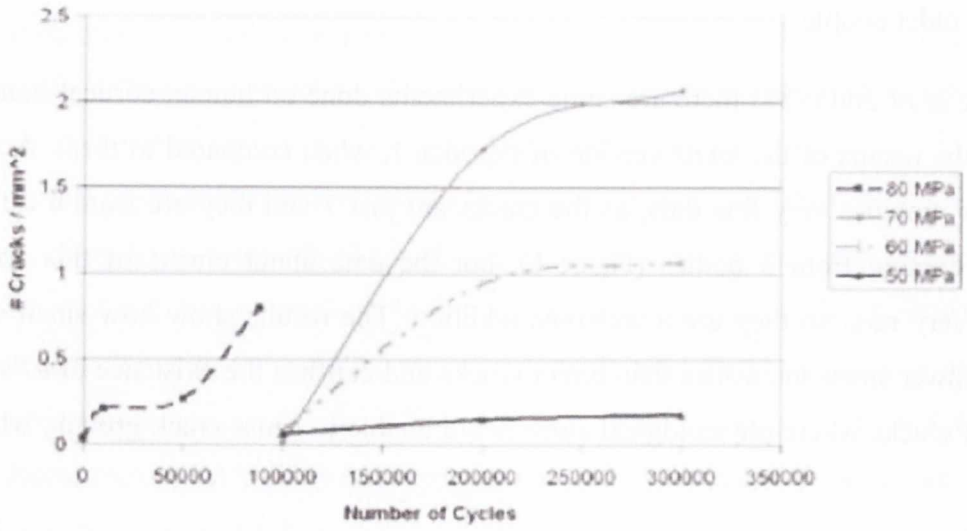

Figure 12. Mean numerical crack density versus number of cycles for four stress ranges, from O'Brien *et al* 2005 (36). The graph shows how the density increases mainly in the first cycles of stress application and when the bone is approaching failure, remaining otherwise stable during the experiments. It also shows how with increasing stress there is an increase in crack density.

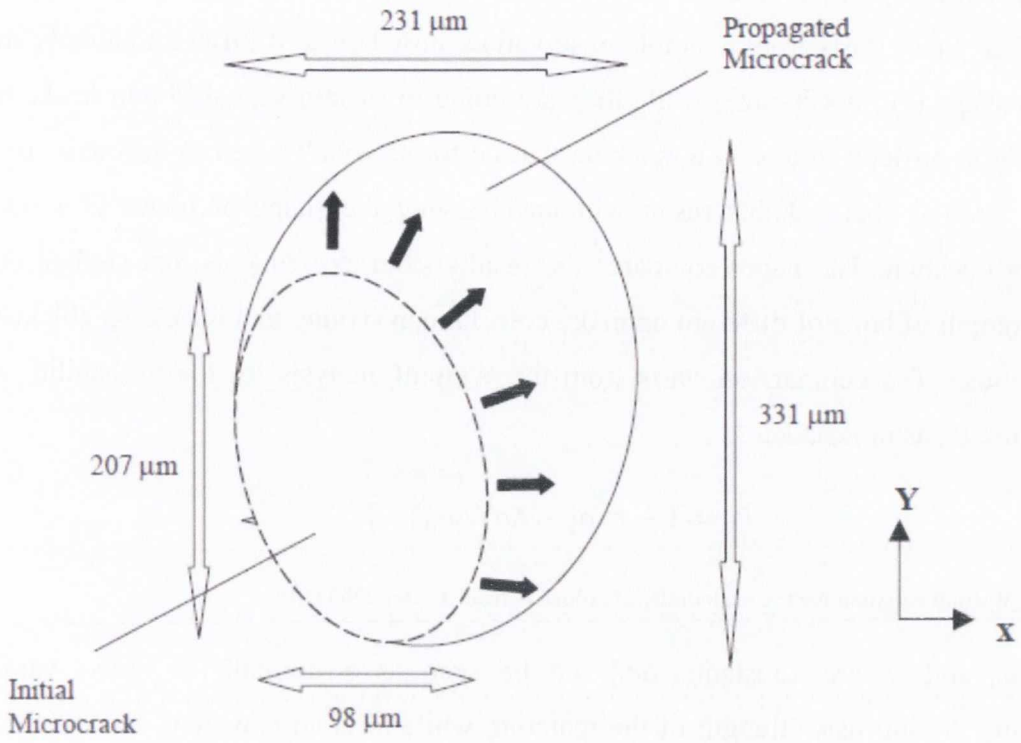

Figure 9. Schematic of a crack from O'Brien *et al* (34). This schematic measures the aspect of a crack and its propagation with stress, showing how the ratio between crack length and width remains roughly constant, between 4 and 4.5.

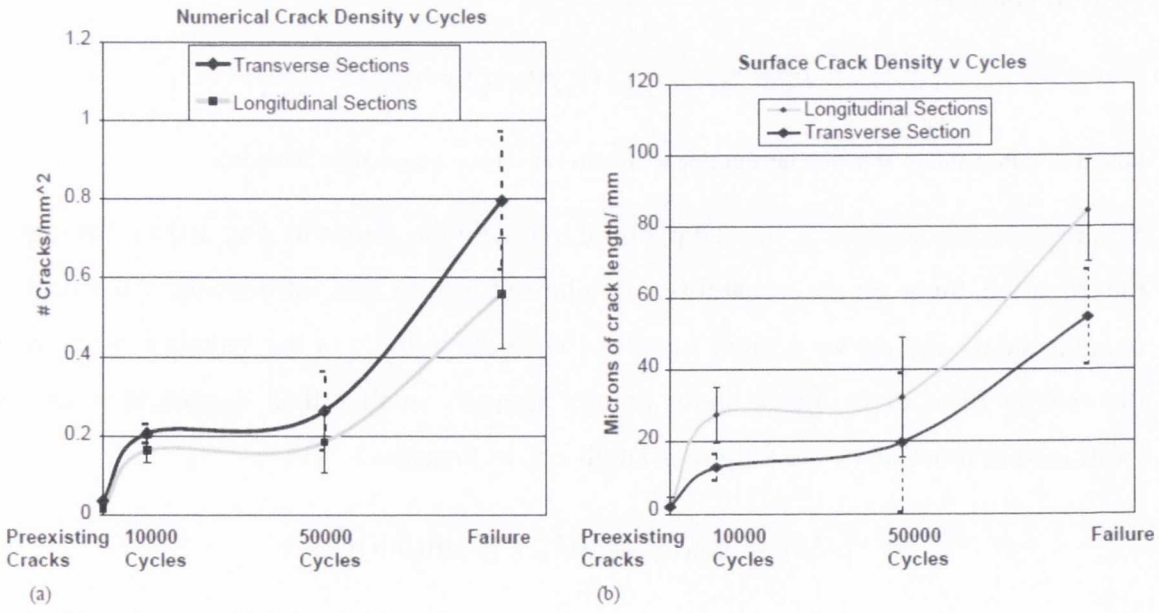

Figure 10. Crack density against fatigue cycles from O'Brien *et al* (34). The graphs show how cracks tend to increase their number mainly at the beginning of the experiments (when the stress is applied) and when the bone is approaching failure.

The paper written by Taylor in 2000 (38) offers an analysis of the effect of size on fatigue in bone. The paper starts from a simple observation: how bones of different animals are similar in shape (but not in size) while they are going to sustain very different loads. In engineering is difficult to design a machine that performs equally well at different sizes and how biology obtained this result without changing the shape of bones is a very interesting question. The paper compares the results from experiments that studied the fatigue strength of bone of different animals: cow, human (young and old), dog, chicken, rat and mouse. The comparison starts from the Weibull analysis for the probability of crack failure P_f, as in Equation 3

$$P_f = 1 - \exp[-(\Delta\sigma/\Delta\sigma_0^*)^m]$$

Equation 3. Weibull equation for the probability of failure P_f from Taylor 2000 (38)

Where $\Delta\sigma_0^*$ and m are constants; $\Delta\sigma_0^*$ can be seen as a normalizing stress value, representing the intrinsic strength of the material, while m is an exponent. Equation 3 is then modified to include what can be called the "weakest link" concept: as fatigue failure happens because of a single defect, the larger the specimen, the higher the probability that the failure occurs. The probability of failure for a sample of a different volume Vs would be as in Equation 4:

$$P_f = 1 - \exp[-(V_s/V_{so})(\Delta\sigma/\Delta\sigma_0^*)^m]$$

Equation 4. Probability of failure introducing a variation of volume from Taylor 2000 (38)

Where V_{so} is the volume of the sample used to obtain the constants $\Delta\sigma_0^*$ and m. Arranging the equation for a given probability of failure (e.g. 0.5) and introducing a constant to explain the results for very small samples (when the volume of the sample is very small the results from experiments show fatigue strength smaller than expected) it can be expressed in function of the fatigue strength $\Delta\sigma_0$ in Equation 5

$$\Delta\sigma_0 = \Delta\sigma_0^*[-(V_{so}/(V_s + V^*)\ln(0.5)]^{1/m}$$

Equation 5. Fatigue strength expressed as a stress where the probability of failure is 0.5 from Taylor 2000 (38)

Where V* is a constant that allows better results in case of very small samples and has a value similar to the volume of a single osteon. Comparing the results for different animals the paper shows how the fatigue strength of bone decreases with its size. This means that the increased fatigue risk intrinsic in bigger bones is compensated by an increased quality

In Shelton *et al* 2003 (37) the authors have measured fatigue crack propagation rates in cortical bone. The goal of the paper was to observe the crack propagation in bone during fatigue tests. The 20 specimens of the shape shown in Figure 13 were extracted from 5 pairs of equine cannon bones (the third metacarpal). The specimens were tested by means of servo hydraulic machine systems and the opening of the cracks was measured by applying an extensometer to the front face of each sample with elastic bands. Crack length was measured observing the change in compliance of the specimen as the crack growth (as the two values are related to each other through a fifth order polynomial), when the tests were over the crack length was measured optically on the fractured specimens, showing a value of crack length ± 5% different from the pre-calculated value. The fatigue tests themselves were performed under ΔK control, varying the value of ΔK gradually during the tests. The paper shows the results for 7 specimens as the remaining were lost during setup or experiments, the results show a value of ΔK_{th} of 2.0 MPa $\cdot$ $m^{1/2}$ for low values of ΔK and plots of da/dN against ΔK for dorsal specimens (lateral specimens' cracks always deviated from the desired path and ran longitudinally, making the analysis impossible). The method used for the experiments and the parameters observed in them can be easily applied to the system and the value of ΔK_{th} obtained in this paper gives realistic results in the simulation when applied to bovine bone.

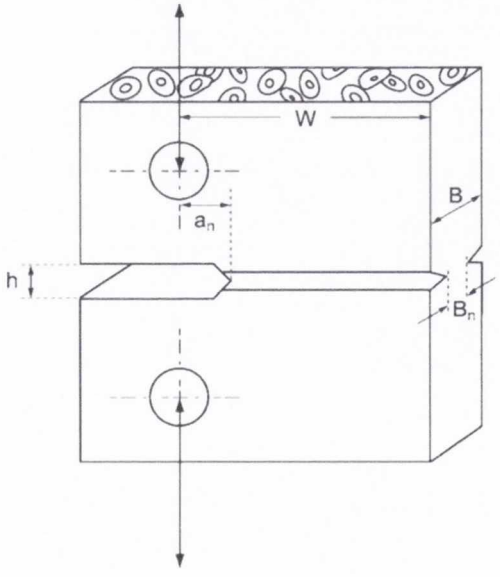

Figure 13. Geometry of the specimen used in Shelton *et al* for transverse crack growth measurements.(Initial values of W = 20.32 mm, B = 5.0 mm, B_n = 3.0 mm and a/W = 0.5). These samples are used to show the resistance to crack of equine bone.

Dataset	AD Gaussian	AD Weibull	Number of cracks	R^2 linear plot
1	15.05	13.44	672	0.92
2	0.74	0.71	25	0.97
3	1.28	0.98	96	0.94
4	0.72	0.69	34	0.95
5	0.55	0.43	60	0.97
6	3.22	1.8	120	0.95
7	4.88	3.45	48	0.78
8	14.91	8.97	190	0.84
9	3.01	1.75	84	0.93
10	4.53	1.92	95	0.91

Figure 14. Table showing the AD scores for all the datasets from Presbitero *et al* (39). The scores for the Weibull distribution fittings are lower than those for the Gaussian fit, proving that Weibull distributions are more fit to describe crack size distributions.

of bone itself; this quality can be obtained by the histological differences, in the bones of larger animals there is the growth of secondary osteons that act as barriers for crack growth, while in smaller animals like rats and mice secondary osteons are not present. Also the orientation of lamellae can improve the strength of bone and its resistance to fatigue damage. Another result that is found by the paper is that the fatigue failure stress is compatible with *in vivo* loads, showing that the repair process is necessary to ensure bone wellbeing.

Many parameters used in the simulation come from the analyses done in Presbitero *et al* 2012 (39), in this paper the authors suggested that the lengths of microcracks in bone could be described by standard statistical forms like Weibull or Gaussian distribution and that the constants describing a distribution would vary with the conditions of bone, effectively representing its state regarding fatigue damage. To prove this hypothesis the authors applied statistical analyses to ten data sources from different studies on bone loaded both *in vivo* and in vitro and to two simulations. The simulations' data were obtained by calculating the distance between the osteonal barriers in images taken from transverse sections of osteonal bone in the first simulation and from computer generated images composed of circles representing the osteons randomly placed for the second simulation. The statistical analysis was done by plotting the data in terms of cumulative probability as a function of crack length, where cumulative probability represents the probability (between 0 and 1) that the length is smaller or equal the given length, so that they form curves. The curves are then compared to Gaussian and Weibull distributions though the Anderson-Darling approach to assess the goodness of either fit. The results show how in all cases the Weibull distribution is more similar to the real distribution than the Gaussian (see Figure 14). Using Weibull distributions to define the entire set of microcracks in bone after fatigue tests allows the use of just 2 parameters to describe the whole situation of the bone; this method of representing cracks is very compatible with the simulation, as it allows putting the results in a format that can be easily compared to experimental data.

osteon fibres can have and accordingly name the osteons as transverse, longitudinal or alternate (Figure 16). They describe the properties of the finite element model used to simulate the osteons, showing two versions of it, one with the Haversian canal (applied as non compressible) and one where the Haversian canal is missing. The osteon model then is subjected to a 10% deformation in 4 cases, as a full or empty osteon with and without the Haversian canal and the corresponding variation of stiffness of the lamellae is shown. The goal of the study is not a quantitative analysis but it is explicitly said as a way to determine the relative viability of the various possible geometrical arrangements. The study offers many new possible explanations on the structure of lamellae in transverse osteons, from their small number (because having more would be redundant from a structural view) to their increasing sturdiness near the axis, as they are subjected to a greater load.

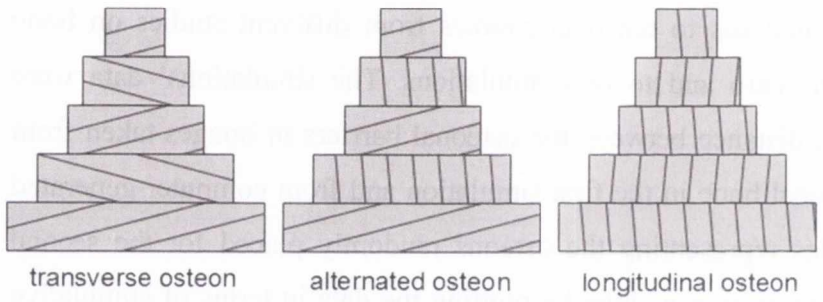

Figure 16. Scheme of the fibre orientation of the lamellae in each type of osteon. This image (from Martin *et al* (41) and used in DeMicheli *et al* (40)) provides the difference in the fibre orientation of transverse, alternated and longitudinal osteons.

Stress on bone

I have also found useful to study a few papers that concentrate their analysis on the macroscopic scale of bone, to detect how the model needed to be loaded. In some papers, like Taylor & Kuiper (42), the analysis of stress fractures has offered a good insight on how the bones are loaded and how this loading reflects itself on the structure of the bone. In this paper the authors use the volume of loaded bone and its loading to predict the probability of failure during "*in vivo*" loading of human legs, analyzing the stress that loads the bone during various activities. This stress is analyzed by a finite element method that shows the volume subject to the maximum load (Figure 17).

Bone microstructure

The role of osteons as barriers to the growth of cracks offers the occasion of studying papers that focus on the microstructures in the bone as a key factor for its physical properties. In Shahar *et al* 2011 (11) a study on the spatial arrangement of osteons is performed. This offers a useful help for the evaluation of the distance between them, which is an important input of the system. The analysis is done on microscopic images of ovine and canine compact bone. After obtaining the results of the microscopic observation and the measurement of the arrangement of the osteons in quantitative form, the paper creates a simple model of the osteonal arrangement that follows the rule that every Haversian Canal restricts the possible area where new canals can be formed (a cherry-pit model), to confirm the theory that there is an order in the arrangement of osteons. As optimizing factor they use SDD (Shorter Distance Distribution), the distribution of the distances of the osteocytes from the canals, as the osteocytes that are too far from the canals have reduced nutritional supplies (see Figure 15). The results provide an order for the distribution of the osteons which is coherent with the observation of real life distributions of osteons, proving that osteonal growth is dependent from the spatial arrangement of previous osteons, instead that being completely random.

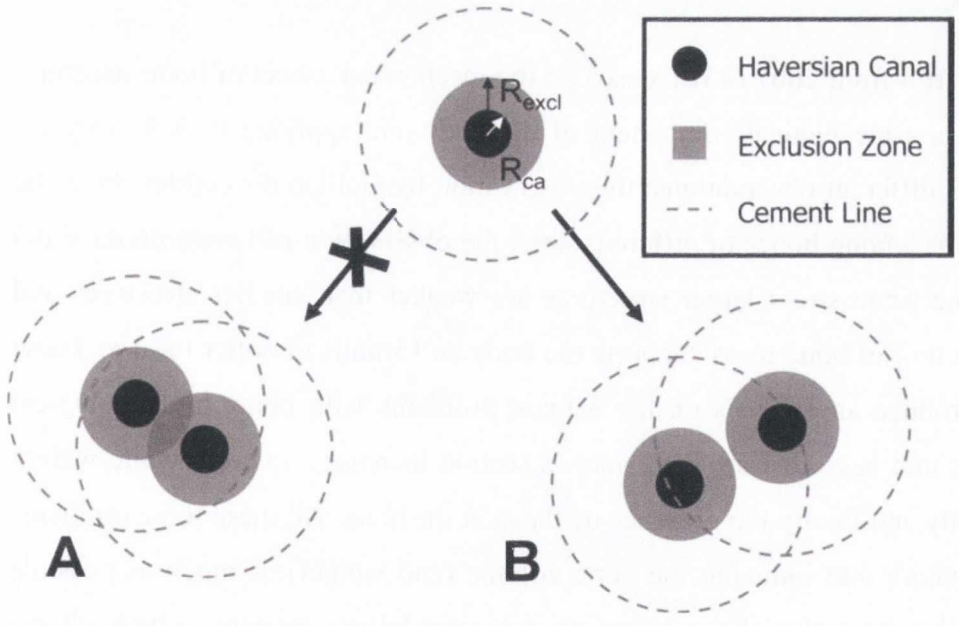

Figure 15. How the exclusion zone rule works. The addition in A is unsuccessful as the new osteon overlaps the exclusion zone of the first one; in B the addition is successful. From Shahar *et al* (11)

A paper from DeMicheli *et al* (40) provides an analysis concentrates on the osteons and on their own anisotropic behaviour. The authors define the various arrangements that

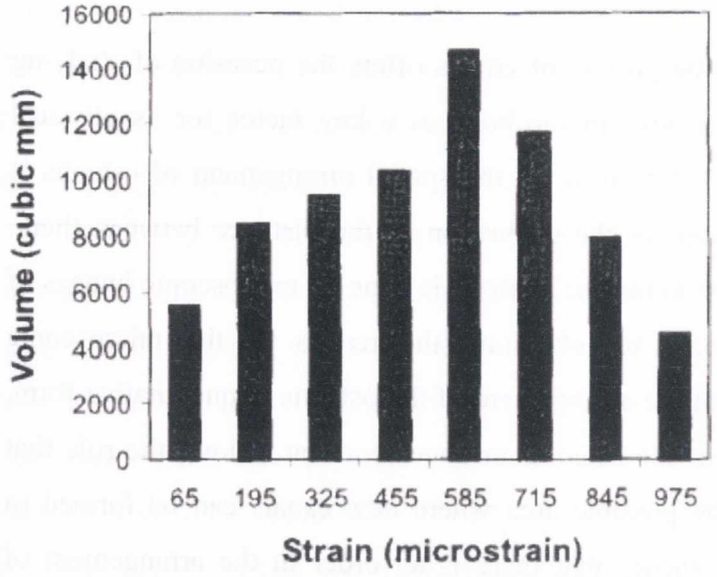

Figure 18. Histogram of Strain per Volume in the FE model shown in Figure 17, from Taylor & Kuiper(42). This graph shows how different sections of the bone are subject to different stress, allowing recognition of the volume of bone subject to the higher load.

Figure 18 has allowed me to estimate the part of volume of the bone subject to the maximum stress, so that I can apply this knowledge to the data about crack density to obtain how many cracks need to be analyzed by the system to predict the behaviour of a bone under stress.

A paper from Martin from 2007 (43) focuses on the mechanical aspect of bone structure, observing bone as a mechanical component of the body and applying to it 3 analyses, stemming from 3 different observations: the observation by Galileo de' Galilei about the difference in shape among bones of different sizes; the observation of Leonardo da Vinci on how under the same stress larger structures are weaker than smaller structures and finally how each unit of bone mass supports the body as 15 units of softer tissues. These observations introduce an analysis on the 3 main problems with bone: high biological cost, proportions that have to vary with size, as section increases squarely while weight increases cubically and finally the presence of flaws in the bone. All these three problems have "pushed" nature into reducing the bone volume (and weight) as much as possible without sacrificing strength. The solution is the remodelling process, which allows extended lifetime to bones, so that smaller bones can be used instead of larger ones. Remodelling reduces the average size of the cracks allowing for a longer life of bone.

Another study performed by Genk *et al* (26) has used a portable device to detect total foot force in-shoe and to plot the variations of stress on the foot during activities like

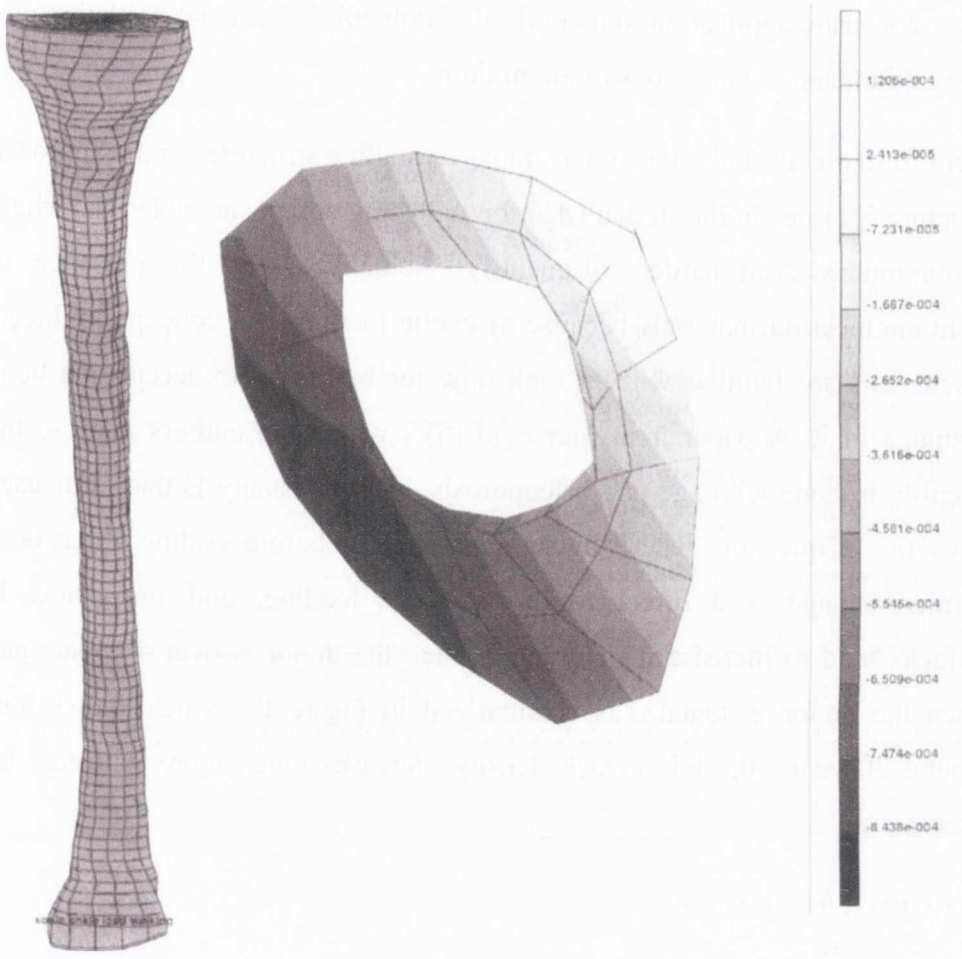

Figure 17. FE Model from Taylor & Kuiper (42). The differently shaded parts represent the volume of bone subject to the different strains. This allows to observe the distribution of load along the bone when subject to a load.

A histogram (Figure 18) shows in a more readable format the results from this analysis

paper suggests a stochastic application to quantify the probabilities of crack initiation and propagation in titanium and in two alloys of aluminium.

Bone is different from metals and it has not a simple crystalline structure, so the approach to its microstructure is more similar to that used for analyzing composite materials, where microcrack initiation is even harder to quantify. Actually, while the presence of microdamage in engineering materials because of cyclic loading is a concept engineers and material scientists are familiar with, it took time for biologists to accept that bone could have damage in it. A paper from Burr *et al* (5) , where the authors analyze the increase in fragility in bone with age and osteoporosis, offers an analysis that is focused in answering a series of questions where, by staining the bone before loading, it has been proven that microdamage is a direct result of cyclic loading, and finds how in experiments cracks tend to increase their number when the donor is over 40 years and especially when the donor is female, as summarized in Figure 19, which shows how starting at around 30 years, the microcrack density increases much more with age for women than for men.

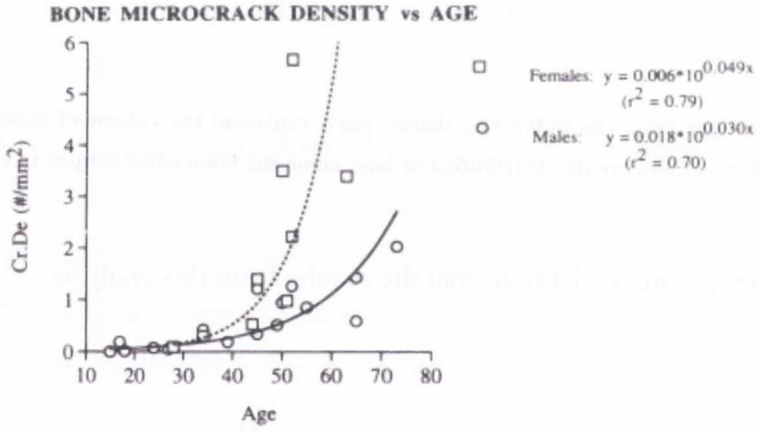

Figure 19. Microcrack Density with age for men and women from Burr *et al* (5). The two lines start to diverge after 25 years of age, marking the difference in microcrack density between men and women, which becomes more extreme with increasing age.

A paper approaching the structural problem in crack initiation and propagation is Sahar *et al* (47). In this paper the problem is analyzed in its entirety, stating the social cost of fractures and the importance of microdamage in their occurrence. The paper approaches the microdamage at different scales, separately shown in its parts by the method used. The first part is about optical microscopy and laser confocal microscopy, the first methods used to identify the existence of microdamage and the difference between

standing and running working towards the goal to predict the loss in bone mass experienced by astronauts after long periods in reduced gravity. It applies a modal analysis to obtain the values of frequency and stress amplitude (based on body weight) for running standing and walking. These results regarding the individual loads are included in an enhanced daily load stimulus (EDLS) model used to prescript an exercise regime for preventing the bone loss of astronauts going to the moon or to Mars.

The topic of walking stress on human bone has been analyzed also in a recent paper from Pang *et al* (44), where the forces acting on the tibia have been measured by video based motion captures and applied to a specially modified finite element model. In this model the local density of bone has been used as a variable of the elements, so that the variation in bone density can be observed in the tibia model during the gait.

The majority of papers and studies on crack growth are real-life experiments, used to prove and analyze the behaviour of cracks. Even if experiments are not directly converted into components of a simulating system, knowing the way they were performed and the results they brought allows to better engineer the system and to prepare it for adapting its results to theirs, allowing a better comparison of results.

Crack formation

The birth of cracks because of fatigue stress is an important topic for structural engineering and countless studies have investigated it since the beginning of the previous century, when it was demonstrated how microcracks are the cause of fatigue damage. The study of fatigue in hard biomaterials is relatively younger, as fatigue in bone was first reported in studies around 50 years ago [Evans 1957 (45)] and so the mechanics of crack formation in bone are investigated with an eye to the results already obtained in engineering materials. Fatigue is firstly a stochastic process, showing a good deal of scatter even in controlled experiments. In a paper from 1980 (46) Ghonem makes an attempt to offer a mathematical prediction of microcrack initiation and growth in metals. The paper illustrates crack birth as an effect of the different microstresses that load the crystallographic clusters of grains of material at the nano and meso scale, where the nano scale is the scale of the grains and the meso scale is when the surfaces of the clusters are evident. This difference generates micro-yields of the single grains and clusters, which have different loads on them at every instant of the fatigue load. From this theory the

presence of uncarbonated apatite in the region of cracks. Various experiments with loads combined with spectrum analyses in near real time show how the load changes the chemical arrangement of the bone, showing that the matrix of bone is affected by load and offering a way to directly observe crack initiation and growth in bone.

The density of cracks is a value often found in literature, but I need a volumetric density, while in literature it is easier to find a surface density. In Taylor and Lee (32) I have found an equation (Equation 6) that measures crack volumetric density knowing the stress on the bone.

$$\rho_V = A\sigma_{max}^{b}$$

Equation 6. Crack Volumetric Density based on Stress, from Taylor and Lee (32)

Where ρ_V is the volumetric density and A and b are constants. In the same paper the constants are calculated as $A = 3.40*10^{-4}$ and b= 1.69. Combining the results of Equation 6 with the data on the stressed volume I can calculate the number of cracks that are subjected to the greater stress and compile the system's input accordingly.

Damage detection in bone

How the bone detects damage is not exactly known at the moment. Different theories are developed but actually there is almost no evidence that can effectively "rule out" a theory in favour of another, just a number of clues that point to the different solutions. Two theories are principally followed: one that states that the body detects the damage sustained reacting with the substances released by the cell processes that span the microcracks, which are ruptured by the displacement of the surface of cracks; and the mechanostat theory, which sustains that the body has a mechanism, similar to a transducer, able to detect the stress applied, and therefore the variation of stress around cracks. Our research group has conducted researches in the first theory, so I will use mainly the "scissors model" for simulating damage detection, but an alternative version including the mechanostat theory will be shown, this way the differences between the two possible approaches can be discussed.

The ability of the BMU to "sense" the damage is been proved in literature. A paper from Burr (48) explored the possibility of BMU "steering" (the change of direction of a BMU to reach damaged bone). To perform this analysis the author proposes a simple theoretical model of crack repair, calculating the amount of crack length removed by repair as a

microcracks and diffuse damage. The paragraphs composing this part describe the results obtained in understanding the mechanics of damage accumulation and the experiments used to obtain those results. The second part is about the use of electron microscopy. As the SEM has a depth of field which is almost 500 greater than an optical microscope, the analysis at this level shows a very different image of the bone. The bone appears riddled with voids, as blood vessels, resorption spaces and canaliculi that affect the crack growth in ways that are complex to understand and impossible to observe at greater scales. The second to last part shows the results of an analysis by transmission electron microscopy, which allows observing the so called "ultrastructure" of bone, as in Figure 20.

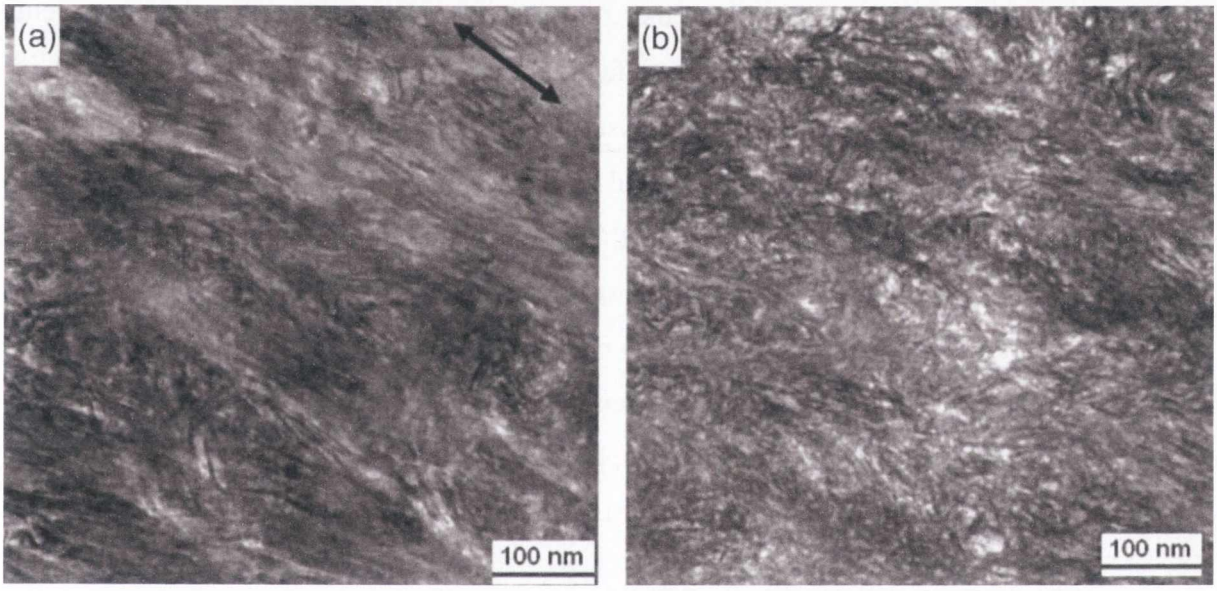

Figure 20. Ultrastucture of mouse bone before (a) and after (b) fatigue, showing how the tissue is damaged at a nano-scale. From Sahar *et al* (47)

Observing the bone at this level of magnification offers the chance of examining the morphological and crystalline arrangement of mineral apatites and crystal–collagen interactions. The damage at this scale takes the form of destroyed collagen fibrils, ripped from their regular shape. Observing at even greater magnification the fatigue-affected crystals of apatite look opaque, less crystalline and the authors suggest that the crystals have shifted to an amorphous state. Similar analyses on osteoporotic bones show how the collagen fibrils are characterized by an irregular and random arrangement and a reduction of diameters, which together could give an explanation of the reduced strength of bone caused by the disease, but the paper lists as contradictory the different results obtained in this topic. The last part of the paper shows the effects of spectroscopic analyses on bone that observe the variation of chemical structure in the damaged bone. The results show a

Where Cr.Le is the mean crack length, iCr.Le is the mean initial crack length, On.Ar is the mean osteonal area (equivalent to the area of the BMU) and finally Rs.Ar is the number of resorption spaces per mm^2. Equation 7 suggests that a graph of mean crack length against resorption density (Cr.Le vs. Rs.Ar) should be linear; its intercept should represent iCr.Le, the mean crack length without remodelling and the slope should represent On.Ar, the mean osteonal area. Comparing Equation 7 with the graph from experimental data in Figure 21 the hypothesis of linearity was confirmed, but the value of the slope/On.Ar is much greater than expected, with a value of 1.66×10^6 μm^2, equivalent to a BMU that has the diameter of 1.4mm, much larger than the 200 μm found experimentally. The author suggested that this extremely large value does not represent the physical area of the BMU but an "effective area", a region centred on the BMU's position where its osteoclasts can detect, steer toward and repair the microcracks. The discussion chapter of the paper discussed the mechanisms that could cause steering, reasoning that the BMU could be activated by stress load, moving along the direction of maximum stress until the signal from apoptotic osteocytes surrounding a crack is found in the "effective area", so that the BMU "steers" toward the crack to repair it. This paper addressed the issue of how "smart" is the remodelling process and how much of the repair process is a routine of the organism, as opposed to an emergency procedure tailored to solve a problem (in this case, microdamage).

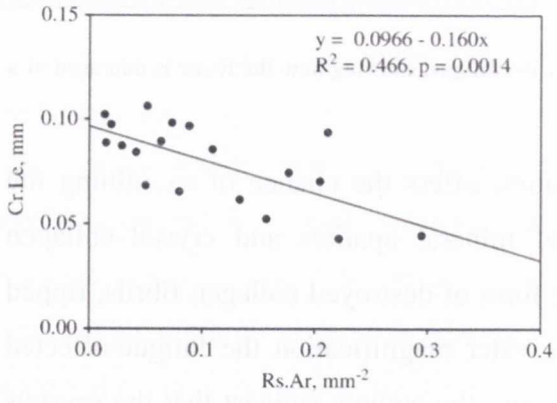

Figure 21. Resorption spaces vs. average crack length. The picture from Burr (48) shows a linear correlation between damage and repair, suggesting that the repair is not a stochastic process but a targeted one and that BMUs are able to "steer" to reach the cracks when they are not on their "trajectory".

This paper gave an answer to this question by pointing to a crucial detail of remodelling: if it were stochastic it would need a much larger number of BMU that those found *in vivo*. The details on how bone detects damage and what can be the trigger to repair can still be

function of the size of the BMU and its speed. The analysis was performed supposing that the BMU is "untargeted" and so it crosses the microcrack at a random location. The result of the analysis is in Equation 7

$$Cr.Le = iCr.Le - (On.Ar \times iCr.Le)\ Rs.Ar$$

Equation 7. Relation between Crack Length and Resorption Area

For estimating crack-face displacement there is a well-known solution for a 2D crack, originally formulated by Irwin (52) (Equation 8).

$$\delta T = \frac{2\sigma}{E}(1 - \nu^2)\sqrt{a^2 - x^2}.$$

Equation 8. Crack Face displacement for a 2d crack, from Irwin (52)

Here σ is the applied tensile stress, E is Young's modulus, υ is Poisson's ratio, 'a' is the half-length of the crack and x is distance along the shorter axis of the crack, measured from the crack centre. Maximum displacement occurs in the middle of the crack (x = 0). From the work of Taylor *et al* (51) I have Equation 9 that describe the displacement along the shorter axis of the crack:

$$\delta T(x) = \left(f\left(\frac{b}{a}\right)^{0.1} \frac{\sigma}{E}(1 - \nu^2)\sqrt{(a^2 - x^2)} \right) \times \cos(\beta)\cos(\beta),$$

$$\delta s(x) = \left(f\left(\frac{b}{a}\right)^{0.1} \frac{\sigma}{E}(1 - \nu^2)\sqrt{(a^2 - x^2)} \right) \times \sin(\beta)\cos(\beta).$$

Equation 9. Displacement along the shorter axis of a crack from Taylor *et al* (51).

In Equation 9 δT(x) is the tensile displacement in the x direction and δs is the shear displacement along the same direction. The constant f has the following values: in isotropic material f = 1.53; in orthotropic material f = 2.0 for tensile displacement and 3.25 for shear. In Taylor *et al* 2006 (16) the authors propose a computer simulation able to study the dynamics of the crack/repair/adaptation cycle, conduct experiments to observe what happens to cells and cellular processes in the vicinity of cracks and finally develop a theoretical model that predicts the strength of the signal knowing crack length and applied stress, showing in the end that the characteristics of the cellular transducer were similar to those in the original specification. In Hazenberg *et al* 2006 (50) the simulation is done in a FEM environment and the experiments are done on 31 samples of bovine bones submitted to a UV microscopy to show the ruptured processes. The FEM models of samples are then compared to the actual samples to confirm the validity of the

unclear, but it is certain that remodelling is not a stochastic routine of the body, but for the main part a reaction to a damage that can be a risk for the performance of the bone.

The theory of signal based on rupturing processes starts from the analysis of the shape of a crack, first deduced from experiments depicted in Taylor *et al* 1998 (49) and then completed in Lee *et al* 2000(13). The elliptical shape of the crack and its ratio length: width of 4:1 provides information on the geometry and allows the use of known formulas to calculate shear and tensile displacement of the crack faces.

There are two ways in which cells may be fractured. Firstly, cells immediately ahead of the crack tip may experience a strain which is sufficiently high to break them; secondly, the relative displacements of the crack faces may be sufficient to fracture cellular processes: the long, thin extensions of the cell which link one cell to another, via gap junctions. Some of these processes will pass across the crack faces. The fracture strengths of osteocytes was showed by Hazenberg *et al* (50) to not be of importance, since even under a 'worst case' scenario with a long crack (2a=300 mm) and a high applied stress (80MPa) the calculated tensile strain on the osteocytes was much less than their failure strain. Thus, in both compressive and tensile loading, the proposed mode of failure is cutting of the cell process by the shearing motion between crack faces.

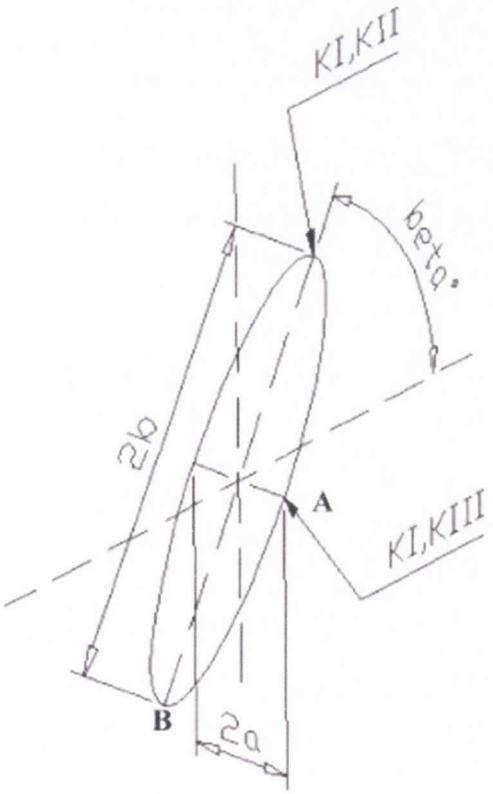

Figure 22. The geometry of a crack embedded in cortical bone from Taylor *et al* (51). The crack appears oval, with the longer axis 2b and the shorter 2a in a 4.5 ratio.

with the methods required to control the presence of substances like RankL and OPG in it. Other than those levels also the values of cell viability and apoptosis are provided by the experiment. The damage to the cells was applied using acupuncture needles of four different diameters: 160, 300, 400 and 800 μm. In all the experiments it can be seen how damage increases the level of RankL and reduces the level of OPG; the levels of low or zero damage keep a stable level of RankL, while with the rise of damage the response of RankL almost doubles, but this response slows when the damage goes over a threshold (400 μm), becoming similar to that observed for lower damages when damages reach values as high as 800 μm. This suggests that 400 μm is the ideal level of damage for a cellular response. The behaviour of OPG usually mirrors in reverse those of RankL, suggesting that when RankL is higher OPG binds to it becoming harder to detect. Viability of cells shows that the presence of damage reduces viability when it is around 300 and 400 um, instead than in control, at 160 and 800 um. There is no significant variation of toxicity until 800 um, while apoptosis shows variation only at 400 um. In the end all the experiments show that damage alters the release of RankL and OPG by cells, hinting that injury size is important for the body to arrange a response. The results from these experiments confirm that with increasing damage the release of RankL is higher, proving a reaction to damage as shown in Figure 23.

simulation. Hazenber *et al* (9) depict the role of osteocytes in bone repair and how their production of RankL alters the balance of osteoclasts and osteoblasts triggering the action of BMU and targeting them to the crack repair. The paper shows various results regarding the effects of bone microstructure, bone adaptation and osteocyte actions and concludes that initiation, propagation and arrest of microcracks are affected by microstructural features and the nano-composition of bone. The paper then provides evidence by literature to suggest that microcracks are repaired by a targeted remodelling process. Because it is still unknown how this process is regulated at a cellular level, the paper lists the 2 mechanisms for bone damage signalling: one mechanism focused on ruptured cell processes that cause up-regulation of RANKL and the second mechanism where microdamage accumulation causes apoptosis in the osteocytes, which triggers osteoclastic activity. This second mechanism was expanded by discussing the results from Noble et al (53) that have found how resorption cavities tend to appear where the bone has microcracks. The use of MLO-Y4 cell cultures to replicate osteocytes have shown how microdamage does not cause significant variations on the number of dead cells compared with the control, but cells near the damage have an increased release of substances that promote osteoclast and osteoblast activation. In the final summary is suggested that the rupture of osteocyte processes could be the mechanism that unifies both the mechanisms depicted above.

After that it concludes that a common pathway might be present where osteocyte apoptosis can be caused by ruptured processes, leading to an up-regulation of RANKL which stimulates osteoclastic activity with the formation of BMUs. In McNamara and Prendergast (3) the authors try to answer if the strain stimuli or the microdamage is the trigger for the repair. To do so they model bone behaviour using both strain and damage as triggers for the repair, with the needed algorithms. The model is then iterated with different stimuli to see which stimulus triggers the reaction expected from bone. The results suggest that the bone repair is caused from both damage and strain, but not at the same time, when damage is below a certain value a strain-based sensor is more realistically the way the body detects damage, while with higher damage values it needs to shift completely to a damage-based sensor to show a realistic behaviour.

Another paper supporting the theory that broken osteocyte processes are sensors for damage is Mulcahy *et al* (54), which uses a cell culture experiment to investigate the effects of damage on bone cells. In the paper the experiment is depicted in detail together

in prostaglandin from the osteons in the cell culture. In a following paper Burger and Klen-Nulend (56) present studies about the correlation between stress and remodelling of bone observing the bone structure at a nano scale. The studies observe the integrity of the the integrity of the lacuno-canalicular network, both the cellular part and the porosity. The experiments show how the porosity conducted the signal to the cellular part by bringing to it the factors produced in the osteocytes, by the same way the cells use to remove waste. The paper also assumes that fatigue microdamage will interfere with the integrity of the osteocytic and lacuno-canalicular network by severing osteocyte processes in the first and breaking canaliculi in the second. Increased permeability between canalicular channel and mineralized matrix will decrease the fluid drag forces in the channel. Fatigue damage may create a situation similar to disuse at the level of the osteocyte cell body, disrupting the communication between osteocytes and bone surface. Accumulation of fatigue damage generates bone remodelling, which starts with osteoclast recruitment. Active recruitment of osteoclasts by osteocyte signalling could be difficult to reconcile with this disrupted communication. Disrupted communication could act as a reverse trigger, interrupting an active suppression of osteoclasts by osteocytes, thereby allowing resorption. Also situations of microgravity and their effect to the bone are analyzed with this theory, as cells are probably unaffected by the different gravity, but they could be affected by the different load, even if it concludes that data in effective microgravity are scarce and extremely expensive to obtain. The studies which followed were described in, among others, Kneil-Nulend *et al* 2005 (57) where the authors found a linear proportion between Nitric Oxide (considered a possible candidate for intercellular communication within the 3D network of bone cells) release and rate of fluid shear stress. Also in Vatsa *et al* (58) a combination of confocal laser scanning microscopy and nano-computed tomography was used to determine the 3D morphology and alignment of long axes of osteocytes and osteocyte lacunae to analyze the role of mechanosensing in the bone formation. The results of these applications that can be observed in the Figure 24 and Figure 25 show how the osteocytes in fibula tend to have an elongated shape, while in calvariae the shape is rounder. In vitro studies on the MLO-Y4 cells show how a round shape is more sensitive than a flat one to mechanical stress, noticing that calvarial bones are subject to smaller stresses than longer bone, a rounder shape could allow them to be more sensitive, giving thus the same response in different bone. The authors propose that if osteocytes are sensors of stress for the bone, then the morphological differences between osteocytes in different bones are connected to the differences in stress between

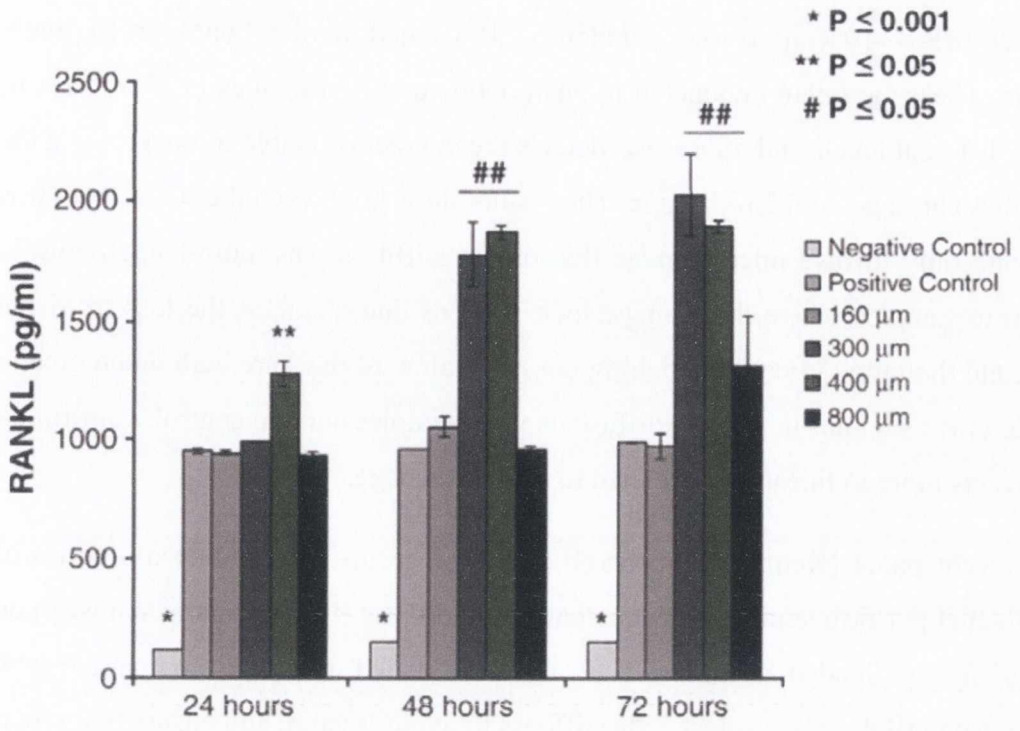

Figure 23. Values of RankL in YMLO-4 cell culture after damage. From Mulcahy *et al* (54). The levels of low or zero damage keep a stable level of RankL, while with the rise of damage the response of RankL almost doubles, but this response slows when the damage goes over a threshold (400 µm), becoming similar to that observed for lower damages when damages reach values as high as 800 µm. This suggests that 400 µm is the ideal level of damage for a cellular response.

Figure 23 shows how the presence of RankL in damaged cells is bigger than in the undamaged control sample. This is coherent with the theory that states how the repair triggering substances are released when cells are damaged. It shows how cells react to damage with an increased release of RankL while the negative (undamaged) control sample keeps a low level of RankL during the experiment. It can be noted how the 800 µm sample has a different behaviour than expected, as probably the damage has caused fatal damage to some of the cells.

The mechanostat hypothesis is based on the assumption that the fluid in the canalicular extracellular matrix pressing on the osteocytes causes them to release some signal molecule that triggers the repair. Actually the osteocytes work as sensors for strain which is directly transmitted to them by the fluid. In a paper from Klein-Nulend (55) the theory is described as a transducer-like mechanism to trigger release of signal by an analysis done upon in vitro cells. The paper shows the machine used for the application of stress to the cells and the details of the experiments conducted. The experiments show an increase

Herman *et al* (60) pose the question if bone reacts more to diffuse microdamage (microcracks below 10 μm in size, randomly distributed in the bone) or to linear microcracks. The experiment conducted to answer this question applies *in vivo* stress to rat ulnae at different levels and afterwards detects the number of viable osteocytes and the loss of stiffness because of microdamage. The results show how when the stress level was able to create only diffuse microdamage the loss in stiffness was almost negligible in comparison to samples where the damage took form of linear cracks; the loss of viable osteocytes and the intracortical remodelling observed after 14 days are both much greater in the linear crack samples that in the diffuse damage samples and the control, confirming that bone reacts more to linear damage than to diffuse damage.

In a very recent paper [Kennedy *et al* (61)] the same group has conducted a series of experiments that perform gene expression analyses and IHCs (Immunohistochemistry) on a sample of *in vivo* loaded rat ulnae. The rats were loaded at a level compatible with strong exercise until their bones lost 25% stiffness to avoid fracture and ensure that repair manifests itself. The ulnae mRNA levels were then measured to examine key factors like RankL, OPG VEGF, and M-CSF; then to determine the source and location of apoptotic and pro-osteoclastogenic signals ICH is performed. The results at 3 and 7 days from loading showed a RankL increase and an OPG decrease, while VEGF increased significantly only at 7 days from loading and M-CSF did not increase at all. The IHC analysis (Figure 26) showed how RankL was scarcely found near the damage, but its concentration increased with increased distance until reaching a maximum at 200 μm from the damage afterwards it decreased with increased distance from the damage. OPG was greatly present near the damage, decreasing with increased distance; same pattern was observed with VEGF. The results show how the reaction to damage can be observed in the osteocytes surrounding the damage and how the different actors have different

the same bones.

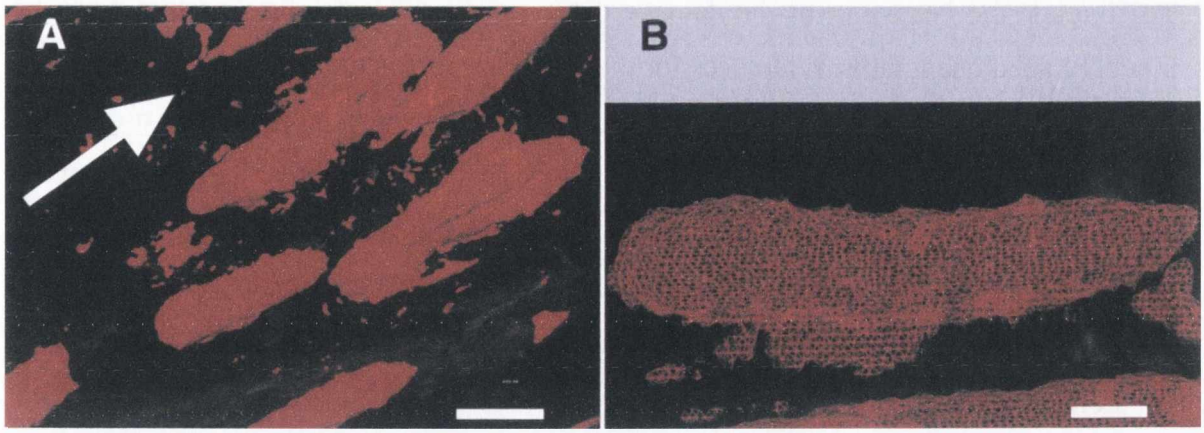

Figure 24. 3D reconstruction of single osteocytes in adult mouse fibula by using confocal laser scanning microscopy scans from Vatsa *et al* (58). The fibula tends to have an elongated shape.

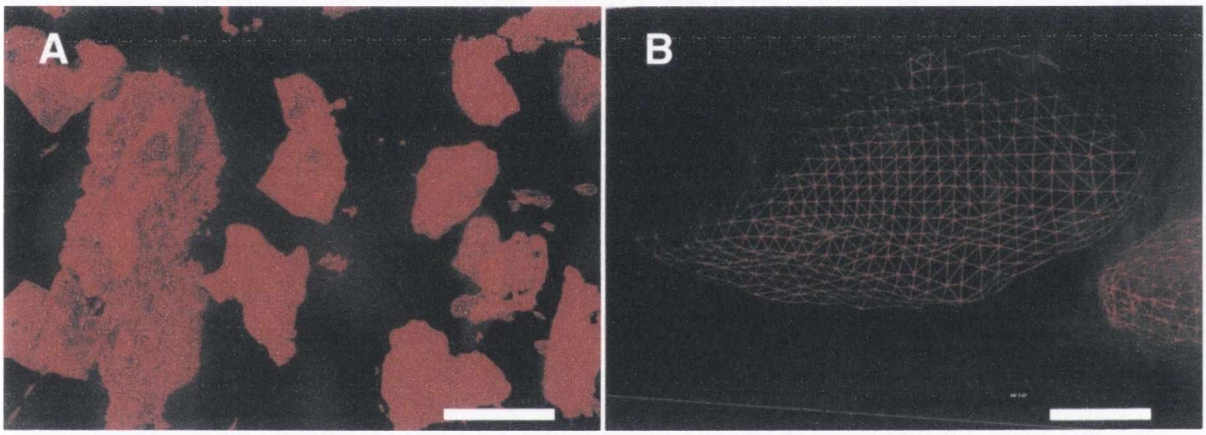

Figure 25. 3D reconstruction of single osteocytes in adult mouse calvaria by using confocal laser scanning microscopy scans from Vatsa *et al* (58). Instead of the elongated shapes of the fibula this calvaria appears rounder.

In (59) Lemaire *et al* model various possible means for the body to detect stress and create a multiphysical model that incorporates more effects than classical models for stress detection. The model incorporates piezoelectricity, ionic electro-diffusive transport, micro porosity and fluid flow effects to offer an evaluation of these mechanics and their macro and microscopic effects on the mechanics of bone cell stress detection. The use of this model and its application show that even if the classical fluid shear models are sufficient to simulate the macroscopic effects of stress detection, a multiphysical model has the possibility to explain even microscopic effects at cellular level, like piezoelectricity and microporosity, which affect the formation of bone.

Osteocyte Processes

To simulate the behaviour of the damage detection mechanism following the "scissors model" I need quantitative references for the histological structure of osteocyte processes in bone. In Mullender *et al* (62) I can find a good reference for the density of osteocytes in various animals. The paper shows the results of analyses performed on bones from 30 animals of 5 different species: cow, pig, monkey, rat and rabbit. The femoral heads of those animals were extracted, sectioned and stained to obtain samples whose morphometric parameters were measured using a microscope and a digital camera. The osteocyte density was measured using the microscope and a digitizing system, with special attention to avoid double counts of osteocytes (the osteocytes can be identified twice in two successive sections). The density of osteocytes was then measured according to Equation 10

$$N.Ot.Nc/BV = \frac{(100\% - double\ counts)}{100\%} \times \frac{N.Ot.Nc/B.Ar}{t}$$

Equation 10. Number of osteocyte nuclei per bone volume unit. From Mullender *et al* (62)

With $N.Ot.Nc$ as number of osteocyte nuclei, BV as bone volume B.Ar as the bone section area (mm^2) and t as the section thickness (mm). The results show how the density of osteocytes is inversely proportional to the size of the animal, ranging from 30000 mm^{-3} for cows to 90000 mm^{-3} for rats.

The data from Mullender *et al* (62) can give interesting insight on the spatial arrangement of osteocyte processes when combined with the results obtained by Sugawara *et al* (63). This paper shows the results of experiments to define the three-dimensional geometry of osteocytes by observing stained calvarias from embryonic chicks using confocal microscopy and reconstructing the 3D image of the osteocytes with the help of specific software. The 3D images (one sample is in Figure 27) were used to obtain a quantitative description of the dendritic processes topology using a program initially developed to analyze neurite morphology and adapted to osteocytes. Finally the surface area and volume of osteocytes were measured with another program. The results give the number of processes per osteocytes, the length of the processes and their spatial arrangement.

timing in their activation.

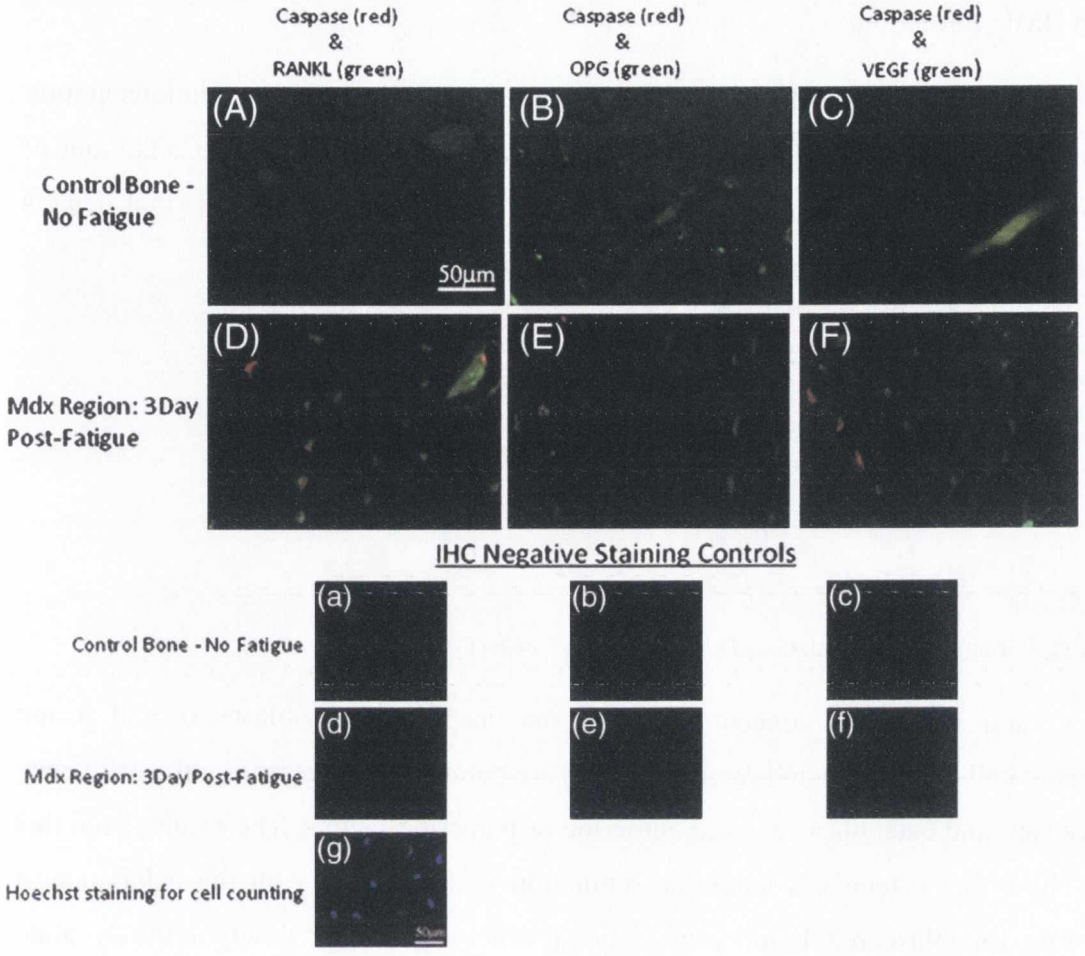

Figure 26. Fluorescence photomicrographs of IHC double-staining from the microdamage from Kennedy *et al* (61)

As both the mechanostat and "scissors" models have substantial evidence supporting them there is no reason to exclude one. Since strain and displacement in a given shape and material have a direct correspondence it is very difficult that one of them will be ruled out soon. In this project I will mainly follow the ruptured processes theory for triggering the damage signal, but I will also show how to model the mechanostat hypothesis. For a simulation actually the difference between the two theories is very small, as all I need to make a trigger is a transfer function that changes the status of cracks into a signal for the body, so even if the status is converted in strain or displacement, it actually changes only the transfer function(s) used in that part of the simulator, but the differences in how the body detects the damage can cause a distortion in some of the results.

developed in the creation of a pathway simulating the different concentrations of the actors in BMU formation.

Other papers focus more on the mechanics of bone remodelling and the relations among its actors. Komarova *et al* (65) define a mathematical model to simulate the behaviour of bone remodelling, which is composed by a system of differential equations that depicts the dynamics of cell population (Equation 11 and Equation 12).

$$\frac{dx_1}{dt} = \alpha_1 x_1^{g_{11}} x_2^{g_{21}} - \beta_1 x_1$$

Equation 11. Variation in the population of osteoclasts in the model by Komarova *et al* (65)

$$\frac{dx_2}{dt} = \alpha_2 x_1^{g_{12}} x_2^{g_{22}} - \beta_2 x_2$$

Equation 12. Variation in the population of osteoblasts in the model by Komarova *et al* (65)

Where x_1 and x_2 are the concentration of osteoclasts and osteoblasts, α_i and β_i are activities of cell production and removal and g_{ii} are parameters representing the efficiency of osteoclast- and osteoblast- derived autocrine or paracrine factors. The results from this system show that osteoclasts autocrine regulation is compatible with the behaviour of cells, while osteoblasts regulation seems much less active, reacting slowly in the dynamic simulation.

A following paper from Komarova *et al* (22) provides an improved simulation. Focusing on trabecular remodelling it offers a model able to recreate the behaviour of cells regarding the spatial coordinates of RankL and OPG fields. This way Equation 11 is changed into Equation 13

$$\partial_t x_1 = \alpha_1 x_1^{g_{11}} - \beta_1 x_1 - \zeta \nabla \cdot (y_1 \nabla \phi_R) + k_1 \frac{\phi_R}{\lambda + \phi_R} \theta(y_1) x_1$$

Equation 13. Variation of the population of osteoclasts from Komarova *et al* (22)

And, regrouping the new elements, into Equation 14

$$\partial_t x_1 = \alpha_1 x_1^{g_{11}} - \beta_1 x_1 - C1 + C2$$

Equation 14. Compact form of the variation of the population of osteoclasts from Komarova *et al* (22)

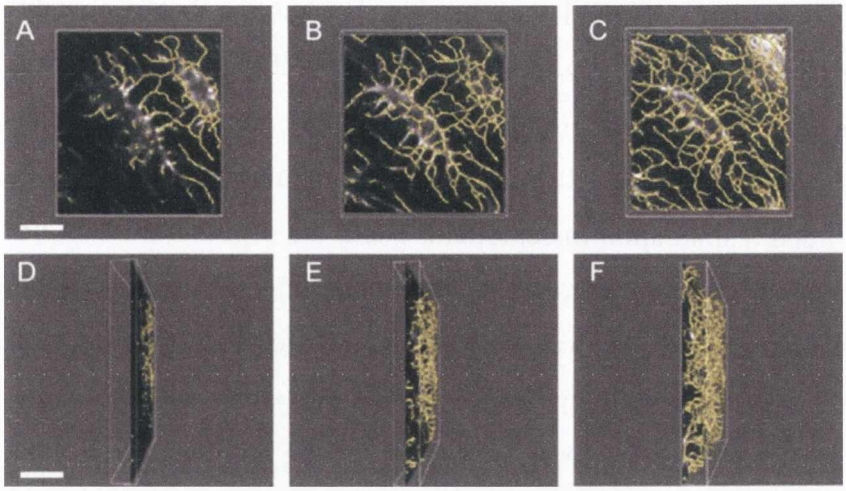

Figure 27. Image of a dendritic tree from (63). Fluorescence-positive sites (white region) showing the histotomography of osteocytes obtained by microscopy. The yellow line shows the topology of the dendritic tree of osteocytes made by the computer program. (A–C) View from the vascular side, (D–F) sagittal views of A to C. Bar = 10 μm

Bone repair

The mechanics of bone repair at a cellular level are the most complex part of the simulation, at least conceptually. Since the repair is done by cells arranged in a BMU the balance of osteoclasts and osteoblasts is important for the results of repair. Since the problem is on a cellular scale most works on the topic are from a biological point of view, and actually biological studies tend to apply poorly in a simulation model, because of the large number of parameters involved and the unclear correlation between them. This is the reason the literature on the topic is big and complex, but all papers have a couple of points in common: that both osteoclasts and osteoblasts interact with each other, so the number of osteoclasts is affected by the number of osteoblasts and vice versa.

An interesting analysis on a cell differentiation, not connected directly to the bone, but very versatile, can be found by Ardelean *et al* (64). In this paper the researchers suggested a *cell-differentiation system* for predicting the differentiation with time of DNA into stem cells and then into different tissue cells. Actually it uses a word generation algorithm to simulate the variation of cells of one type into another, and then adds cardinality to the sets composed of the same words to track both their numbers and their age, which can trigger different transformations. It is a complex system, too complex for including it in the bone repair system at this level of research because of its different scale, but it prompted the idea of including the differentiation of cells in the system, idea that was

dangerous level of stress can be more harmful than leaving the damage that is already present. To answer this question the paper provides a simulation of fatigue load for two different regimes (a "moderate" regime of 10000 cycles in 2000 increments and an "intense" regime of 20000 cycles a day per 100 increments, the amount of total cycles is the same for both regimes) and a simulation of remodelling and the 4 possible cases are observed trying the two load regimes both with and without modelling. The results of the four cases (Figure 28) show that while for the low load regime the presence or absence of modelling does not cause any substantial difference, when the stress is higher the presence of remodelling causes an increased risk of failure for the simulated trabecula because of the removed material, finding how remodelling can be a danger if not accompanied by a period of rest.

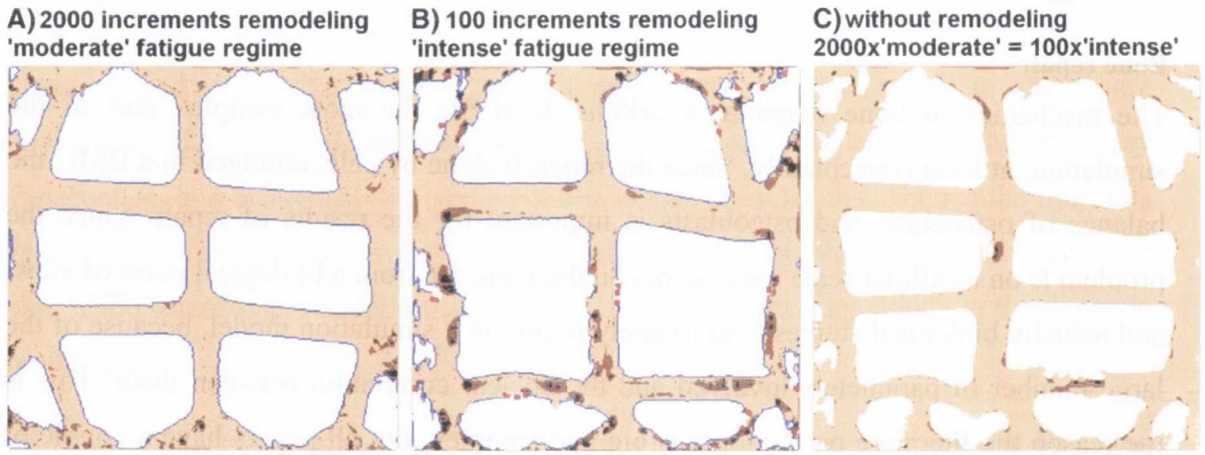

Figure 28. The results of moderate and intense fatigue, with and without remodeling, for an equivalent number of loading cycles. From van Oers *et al* (67)

In 1995 (68) Martin used a mathematical model to simulate the effects of the experiments made by Burr and his co-workers (19). The paper starts its analysis from the equation of fatigue as written in Equation 15

$$N_f = k\,\sigma^{-q}$$

Equation 15. Equation of fatigue used by Martin in 1995 (68).

Equation 15 poses the number of cycles to failure as a function of stress and 2 constants q and k. The idea is to meld the accumulation of damage by fatigue with a repair model of osteonal remodelling. On the basis of the equation of fatigue the accumulation of damage is done as a function of loading rate and stress as in Equation 16

Where y_i represents the population of active cells, C1 describes the motion of active osteoclasts in the field of RankL and ζindicates the effectiveness of the migration. C2 represents the stimulating action of RankL on osteoclasts via RankL-Rank binding (k_1 is the reaction rate coefficient).This generates a system able to simulate both mono-dimensional and bi-dimensional models.

The book "Skeletal Tissue Mechanics" from Martin, Sharkley and Burr (1) is an overview on mechanical and biological properties of bone. The section about bone remodelling offers a description of the action of the BMU in the repair of bone and provides in its results the time of activation, the travel time and finally the mineralization time that mark the remodelling process. According to this book typically a BMU requires 3 days to be activated, it moves at a speed of 40 μm/day and requires a further 10 days before mineralisation of tissue begins. The estimated time for a BMU to be activated by and tunnel through a new crack is thus about 18.5 days.

Bone remodelling

One of the most interesting features of bone is the ability of grow stronger after repairing damage. This property, first coded in Wolff's law, has been observed, for instance, in tennis players that, using one arm much more than the other, are found with an increased bone mass on the "active" arm. The processes that bring this change in the body are not understood in detail at the moment, but the studies that focus on this are extremely varied and interesting. Of notice is Nowlan *et al* (66), where the effects of Wolff's Law are theorized and observed from an anthropological point of view, observing how the changes in subsistence strategy of humans have brought modern men and women to have lighter bones than our ancestors, which were used to sustain greater stresses than us. The authors generate an algorithm that defines the possibility for genes to be transmitted by analyzing the growth of bone and its improvement in ash content during life and then simulating the "choice" of parents for new generations, basing it on an assessment of fitness for the subsistence strategy. The results show, as expected, a reduction in size and strength during the generations and are in line with the variation between archaeological finds for earlier Homo species and modern femora, providing that the reduction in size and strength can be correlated to the different daily loads.

In van Oers *et al* (67) I have a different approach, presenting the remodelling as a paradox, questioning if the removal of material from a bone when it is subjected to a

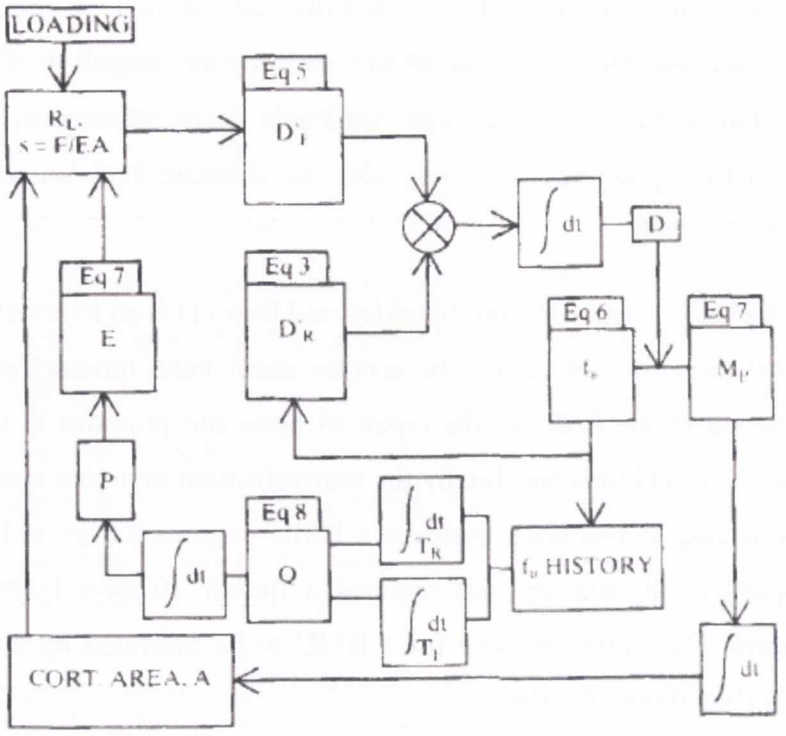

Figure 29. Flow Chart for the model from Martin 1995 (68)

The mathematical system is simple, as the paper is from 1995, and its range of effectiveness is limited, because of its intrinsic instability, but it is one of the earlier attempts to simulate bone mechanics.

In a paper from Bruenzi *et al* (69) the simulation of bone remodelling incorporates the shape of a BMU in its calculations. The author offers a mathematical model where the cells are triggering their activation based not only on time and concentration but on the position they have along the bone. The position is shown as 1-dimensional, to simplify the calculations. The results show a group of cells that moves by generating bone mass without changing its shape. Some properties of BMU get linked to the kinetic properties of the cells in the system, such as differentiation and elimination rates, that can be seen as effects of the cell counts in a particular time point. This approach can explain how the BMU travels along the bone without changing its shape and that the heterogeneity of a BMU, which is vital to the effectiveness of the repair, can be caused by the spatial

$$D'_F = k_D \Phi_D$$

Equation 16. Damage accumulation from Martin 1995 (68)

Where D'_F is damage formation rate and Φ_D is a coefficient composed of stress and loading rate representing the damage potential. On the other hand the damage reduction rate D'_R is defined as in Equation 17

$$D'_R = Df_a \pi r_c^2 F_s$$

Equation 17. Damage reduction rate from Martin 1995 (68)

Where D is the damage, r_c is the radius of the BMU, F_s is the coefficient that covers all the mechanics that could apply and aren't defined and f_a is the activation frequency, the number of BMUs that reach the damage in an unit of time (1 day). The simulation starts with a "normal" level of stress so that the amount of bone removed and added is the same one, leaving the damage at an equilibrium level D_0, it is then supposed that the fatigue challenge is in the form of an extra damage potential Φ_{DF} that is added to the damage potential at the equilibrium Φ_{D0} keeping the bone damage at the equilibrium level D_0. The experiments from Burr allow to obtain an estimate of the value of the damage potential at the equilibrium Φ_{D0} and the amount of porosity is obtained by the history of f_a, supposed in a sigmoidal dose-response relationship with current damage D. From porosity the author obtains a value for Young's modulus E, which is considered constant during the simulation. The effect of strengthening of bone after damage is simulated as an increased area of bone cross-section, reducing the stress linearly; it is modelled depending on the amount of damage either as a linear proportional apposition of lamellar bone with load or a woven bone fixed apposition independent from load. The model was written in basic code and its schematic can be seen in Figure 29.

osteoblast precursors, as shown in Table 1. The 4 model structures are validated by control theory procedures (perturbation and frequency response) showing the different osteoblast differentiation rates and bone volume variation to obtain the model structure that regulates the model into behaving the more realistically and the results show that the Model Structure 2 allows for the simulated BMU to be the most responsive and efficient, when compared to the other 3 model structures analyzed. After finding the correct model structure another analysis performed by perturbation of the parameters of the model (first only one at the time, then progressively increasing the number of parameters under perturbation) to find their more realistic combination. From the results the authors found that it can be postulated that TGF-β could have an action in increasing the apoptosis rate of osteoblasts and that this effect, when included in the model, can improve its adherence to the idealized response curve representing the realistic behaviour.

Table 1: Model structures showing the different expressions of RankL and OPG in active and precursors osteoblasts from Pivonka *et al* (20). 0=no expression, 1=full expression

Model Structure	Osteoblast precursor — OB_p		Active osteoblast — OB_a	
	RankL	OPG	RankL	OPG
MS1	0	1	1	0
MS2	1	0	0	1
MS3	1	1	0	0
MS4	0	0	1	1

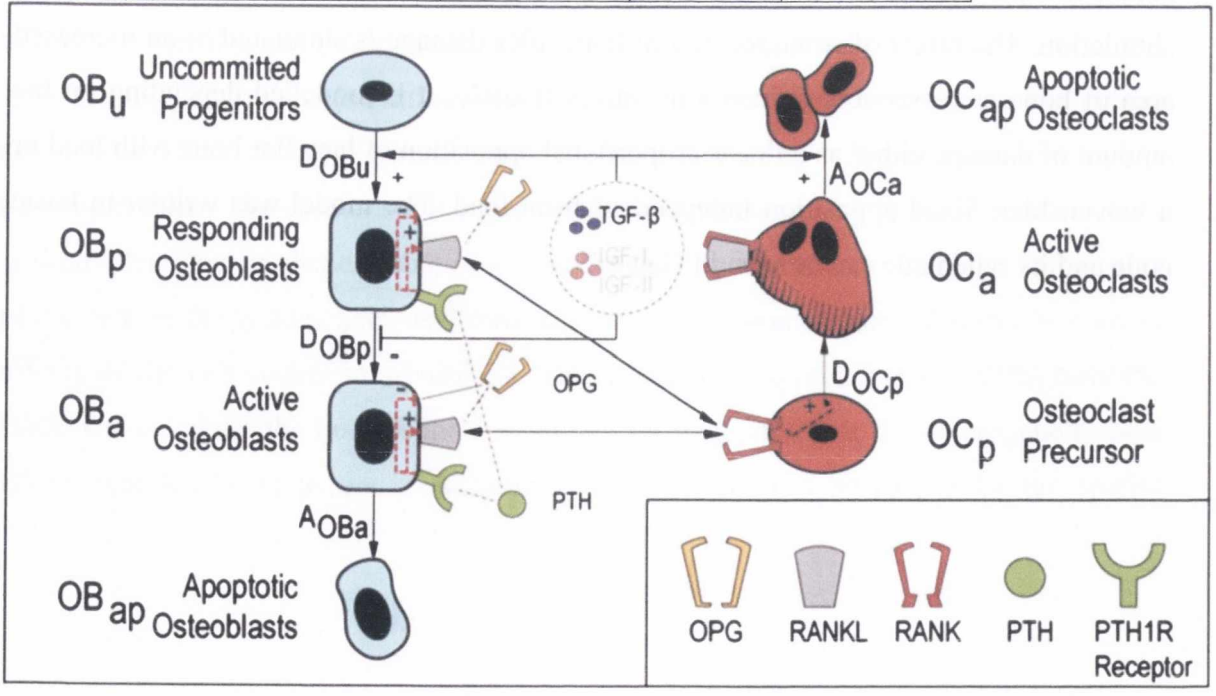

distribution of its effects (Figure 30).

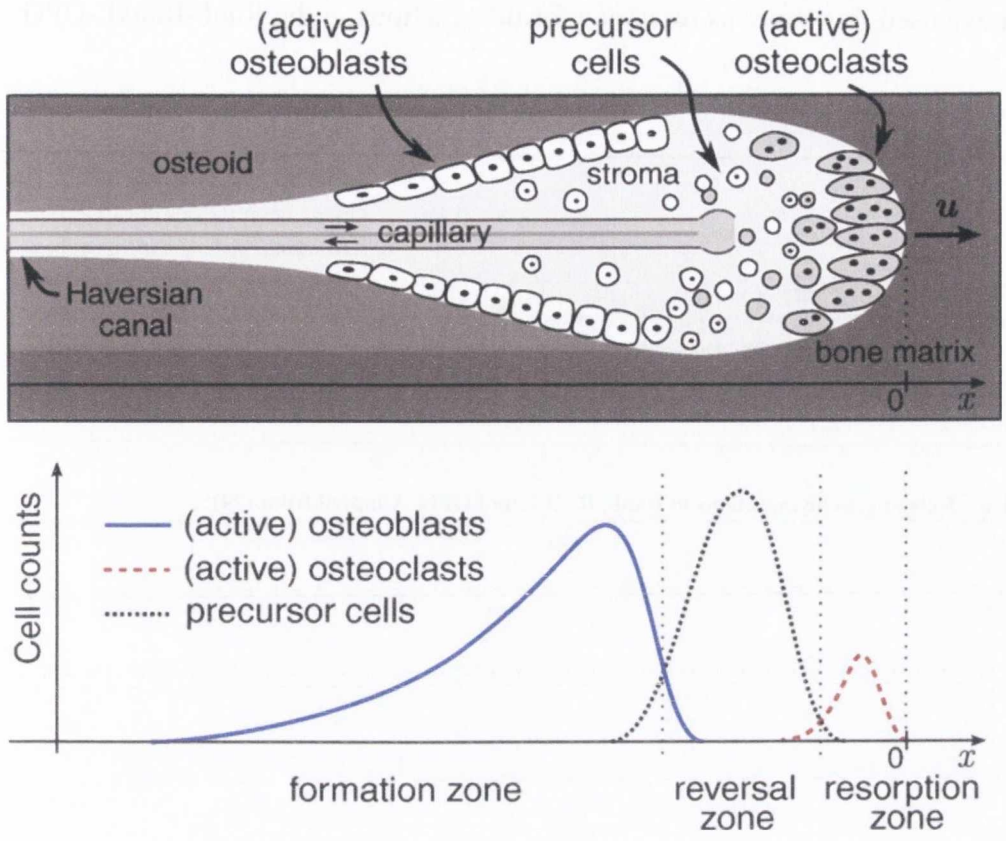

Figure 30. Above: a schematic figure of the internal organisation of a cortical BMU. Below: a schematic plot of the number of cells present at each position along the BMU. From (69)

One of the papers that had the biggest influence on the simulation of biological processes in the model was written by Pivonka *et al* (20) and has addressed the study to the systems biology theory that has allowed simulating the reactions involved in the creation of the BMU. Starting from the link between RankL, Rank and OPG, the paper shows a system of equations that gives as a final result the variation of volume caused by the BMU. The equations have evaluated also the effect of TGF-β, which I haven't included as a variable in the simulator. Then the paper creates a model on a relatively large section of bone affected by a number of BMUs, to simplify the results and cover for local variability. The model is brought to a stable state and then perturbed to observe its reactions to the perturbation. 4 kinds of osteoclasts (precursors, receptors, active and apoptotic) and 3 of osteoblasts (apoptotic, active and precursors) are simulated as actors in the Rank-RankL-OPG pathway with the added effect of TGF-β and vitamin D (Figure 31). The reactions are modelled by the equation of Hill (that is shown as π to abbreviate it in the paper) and then the balance of cells is defined by state equations. The model is analyzed in 4 different structures, with different expressions of RankL and OPG in the osteoclast and

characterized by rapidly remodelling bone, which causes bone mass loss, fractures and even death. I have used this paper as reference for the reactions in the Rank-RankL-OPG pathway.

Gene	Mutation	Disease
RANK	18 bp duplication	Familial expansile osteolysis
	27 bp duplication	Early onset Paget's disease
	15 bp duplication	Expansile skeletal hyperphosphatasia
RANKL	Deletion of amino acids 145-177	Autosomal recessive osteopetrosis
	A single nucleotide change (596T-A) in exon 8 of both alleles	Autosomal recessive osteopetrosis
	Deletion of two nucleotides (828_829delCG)	Autosomal recessive osteopetrosis
OPG	Deletion making OPG inactive	Juvenile Paget's disease
	20 bp deletion resulting in premature termination of OPG translation	Juvenile Paget's disease

Figure 32. Negative effects of genetic mutations in Rank, RankL and OPG. Adapted from (24)

Figure 31. Schematic illustration of bone–cell population model: (a) osteoblastic cell line and (b) osteoclastic cell lines taken into account together with RANK–RANKL–OPG pathway (DOB, DOC…differentiation rates of osteoblasts and osteoclasts; EOB, EOC…elimination/apoptosis rates of osteoblasts and osteoclasts; RANKL binds to RANK and promotes differentiation of OCp; OPG binds to RANKL and so inhibits OCp differentiation). From Pivonka *et al* (20)

To simulate the interactions that bring the BMU to activate I have studied a book from Uri Alon about systems biology (70). This book introduced the Hill equation (Equation 18), the equation that simulates the activation or repression of a gene both in its classical version and in a simplified version. The Hill equation is as follows

$$f(X) = \beta * \frac{X^n}{X^n + K_A^n}$$

Equation 18. Hill Equation

The equation regulates the concentration of the activated actor f as function of X, the concentration of the unbound activating actor. The constants β, K_A and n are respectively the growth coefficient regulating the maximum level of the activated actor, the half concentration coefficient representing the concentration of X necessary to have an activated actor of $\beta/2$ and the Hill coefficient, a shape factor for the equation. The book showed the interactions of three-actor systems and found in the possible interactions a network motif, a specific combination of reactions that appears in the great majority of biological systems. This motif was the feed forward loop (FFL). Of 13 possible combination of FFL only two are statistically found in biology, one coherent and another incoherent. A FFL combination is called coherent when the final sign is positive, meaning that the final reaction is activating, while an incoherent FFL has a repressive final reaction. The final part of this chapter explained the effects of the FFL, showing how when the activation of the last actor requires both the other two actors (AND condition) the FFL acts as a delay on the activation of the last actor, while the OR condition (requiring either the first or the second actor to be active to activate the last) acts as a delay on the deactivation of the last actor.

A paper describing the reactions between the actors of bone repair is (24). This paper describes in detail the structure, function and effects of RankL, Rank and OPG on bone cells. It also describes the different diseases that are caused by genetic variations of these three actors, like osteopetrosis, a disease which completely inhibits the activation of osteoclasts, or Paget's disease, a disease usually manifesting in young age and

The most prominent effect of bisphosphonates is the reduction of active BMUs, but this paper's results showed how not only the BMU's were reduced in number but also their effectiveness in resorption was smaller than in control for doses of bisphosphonate equal or higher than the treatment dose for osteoporosis. It should be noted that the results for doses higher than the treatment doses did not differ much from the results for treatment doses. This study shows how the bisphosphonates also have the effect to reduce the activity of osteoclasts in the BMU without reducing the activity of osteoblasts, reducing the imbalance between bone created and removed in osteoporotic patients and slowing bone loss.

Factors influencing bone properties

The mechanical properties of bone are not homogeneous, as the bone itself is not a material whose structure is fixed. Many factors can affect the bone material, its microstructure and alter its remodelling process, changing in the long run its properties. Because of the vital function that bones have in everyday life and the high social cost of fracture (72), knowing what makes bone stronger or weaker is of the utmost importance, even if the implementation of those effects in the simulation is not trivial. Majumdar *et al* (73) have shown how after a wrist fracture, the costs of another fracture are so high that pursuing a therapy to reduce the probability of further accidents is always convenient from an economical and social point of view, even applying the strictest criteria for costs. Aging is the most common cause of bone strength degradation (27) as it affects both the macroscopic properties and the microscopic structures that offer protection against crack growth. Various studies both on humans (74) and on animals (75) point how the reduction in hormones caused by menopause corresponds to a reduction of bone quality and an increase of both crack length and density and that therapies targeted to offset this reduction can be effective in improving the quality of remodelling (76) . Other studies have proved how physical activity improves the overall quality of bones (77) (25) while disuse reduces it (78) and that the application of vibration can offset the loss of bone mass in case of forced immobility (79). A paper from Notomi *et al* (80) describes the details and results of an experiment to measure how heavy training can make bones stronger. The experiment involved 30 rats of 4 weeks of age that were divided in three groups: the sedentary, running and jumping group. The sedentary group was left to rest, the running group was trained by having the rats run a treadmill at given speeds for growing amounts of speed and time during the days of training until 24 m/min for 60 minutes and finally

Allen *et al* (71) analyzed the effects of bisphosphonates, one of the more widespread class of drugs used in the treatment of osteoporosis, by observing the changes in dogs after treatment. 84 adult female beagles were treated for 1 year with doses of alendronate and risendronate. After the treatment the dogs' bones were analyzed with the microscope to observe variation in their BMUs' resorption parameters (Figure 33).

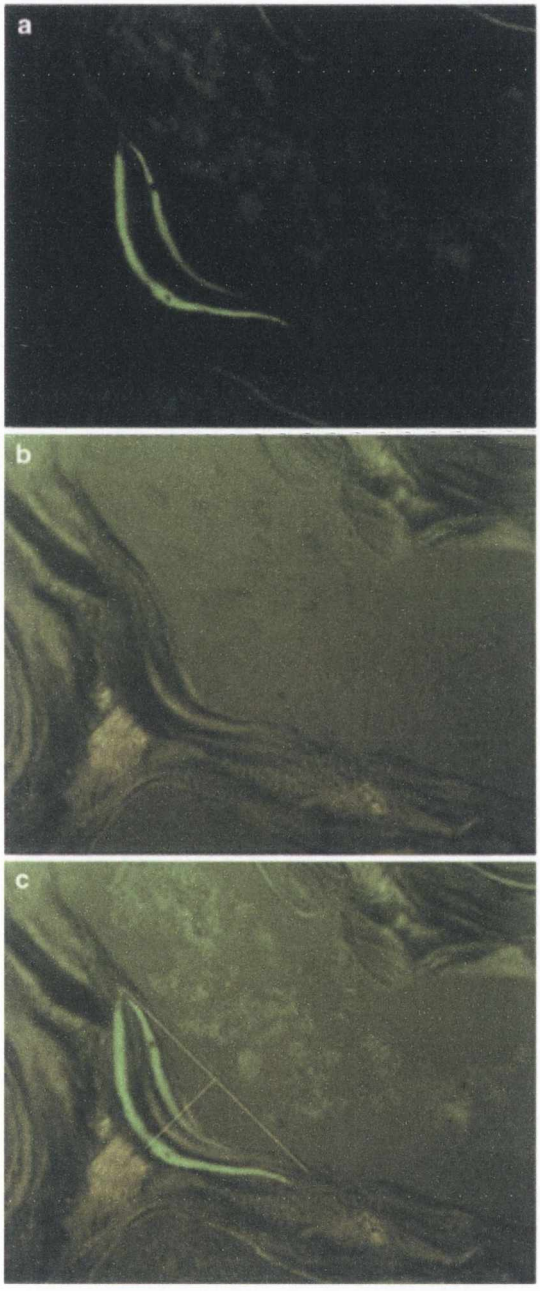

Figure 33. Photomicrographs of a typical basic multicellular unit (BMU) from Allen *et al* (71). (a) BMU viewed with epifluorescence to identify calcein labelling (indicates active bone remodelling). (b) BMU viewed with polarized light to identify the cement line (indicates the limit to erosion of the remodelling unit). (c) Overlay of the two images used for BMU morphology measurement with lines showing how the surface of the BMU resorption cavity was estimated for assessment of resorption cavity width and depth.

of fractures and injuries. The paper (82) offers the results of a study performed on 1224 midshipmen of the U.S. Navy in 2000, observing the incidence of stress fractures (3% for men, 8% for women) in relation to the characteristics of the trainees: demographics, previous sport activity, physical strength, bone mineral density, total body mineral content and bone mineral density and body weight. For the women screenings were also performed for eating disorders, menstrual status, tibia length, anxiety and structural bone geometry. The authors concluded that a possible concurrent cause of stress fractures in trainees could be the excessive loss of weight during training, as the balance of energy (calories obtained by food – calories spent in exercises) is negative.

Very different results appear from the paper (83). In this paper the results of a 1983 study on 295 male recruits in the Israeli Army were shown. The study was conducted by keeping tabs of those 295 recruits for all the 14 weeks of basic training, allowing them to contact the medical staff in case pain or other symptoms of stress fractures appeared. During the study 171 recruits presented with symptoms suggesting stress fractures and 91 had been found affected by stress fractures after examination by scintigraphy and radiography. The paper suggests that this elevated ratio of stress fractures compared to US studies could be because of the scrupulous follow up of the participants in the study, while in the US statistics the stress fractures were recorded only when the soldiers were found to have stress fractures at morning sick call. Another hypothesis was that the study was conducted by making the soldiers and their commanders acutely aware of the risk of stress fractures. This could have influenced the soldiers to seek medical attention after feeling pain; while unaware subjects would have not sought medical attention for what they would have thought was a temporary or rheumatic pain (on the other hand it could be that the increased awareness could have influenced the samples, possibly causing psychosomatic effects). In fact a more recent paper (almost 25 years after (83)) has found how the incidence of stress fractures in the Israeli army has been reduced in the past 25 years(84). This later study shows how the enforcing of a minimum sleep requirement (6 hours), the use of more comfortable shoes and a screening for risk factors, together with the reduction of the cumulative marching and running have reduced the incidence of stress fractures by 62%. It shows the effort done by the Israeli army and proves its effectiveness by evaluating the effectiveness of reduced marching and minimum sleep on 276 soldiers. This results show how fatigue damage is a threat of the health of bones of

the jumping group's rats were trained using a special equipment: the rats wore leather jackets that connected them to a hinged bar with a weight on it and forced them to stand on their back limbs; they were forced to jump by electrically stimulating their tails. The weight on the bar was increased during the training from 0.5 to 0.9 kg. After the training the rats were sacrificed and their bones (the 3rd 4th and 5th vertebrae and both femurs) harvested for testing. The bones were tested for mineralization, were mechanically tested to observe their mechanical properties and finally examined in the SEM to report the structural parameters of their cortical and trabecular tissues. The results showed how the jumping group (and to a lesser extent the running group) exhibited an improvement of the mechanical properties between 20% and 33%. The experiments proved that anaerobic training can increase the strength of bone and its mechanical properties. This paper has been used as a reference for confirming the results of the simulator about the variation of strength of the bone as result of remodelling. Even if human and murine physiologies are different, for example rats have a much faster metabolism than humans and so the process is faster for them than it would appear in the simulation, the results from this experiment confirm the order of magnitude of the variation of strength I can expect after an extensive period of training.

Stress fractures during military training

A good source of data on fatigue damage accumulation *in vivo* comes from statistics regarding stress fractures in military recruits, as military recruits are people whose bone are under a load of stress much higher during the training than it was during their so called "civilian life". The army has standard training; because of this the condition of loading is homogeneous among the samples, helping in the setup of the study. The studies on the incidence of stress fractures on military recruits are also important for their prevention, fractures require hospitalization of the recruit and the time to recover is long and expensive for the army. A good reference for this kind of data is in the book Physical Fitness and Physical Training for Military Performance (81). This book is a medical manual in use by the U.S. Army and covers many of the topics that regard military healthcare. The section I have used covers the fitness and training topics, starting with a digression on muscle and bone mechanics and moving into the topics required to understand the problems that can arise during the training. One of the final sections of this chapter describes the increased risk of stress fractures in military recruits and provides an extensive amount of numerical data from different army sections, showing the incidence

accordingly. It examines the effect of changing the initial stress range, running the same simulation 10 times at each stress level to obtain some simple statistics. The simulation makes many assumptions about bone geometry and loading implied, and therefore is not expected to give precise predictions. Nevertheless, the results have several very realistic features, like how bones can adapt to unusual (but not extreme) loads: the simulation shows adaptation at around 40 MPa but stress fractures appear at 60 MPa.

Summary

The literature on bone properties is extremely vast and new findings are published constantly. In developing a simulation of bone microcrack behaviour is necessary to determine a set of theories to follow to model the behaviour of the different mechanics and to choose a set of experimental data to confront the results of the simulator and validate them. To simulate the crack growth with stress I have adopted the model developed by Taylor and Prendergast in 1995(28) and successively developed in further publications(2)(29)(31). This model applies the laws of fracture mechanics to the fatigue behaviour of bone, developing a specific variation of these laws which includes the effects of the microstructure of bones on microcrack growth. The simulation of repair required a model for the formation of a BMU that I have developed independently, but inspiring it to the model from Pivonka *et al*(20) and applying the techniques shown in the book from Alon(70). The way the body detect the damage is not yet clear, but the "scissors" model developed by Hazenberg *et al* (50) (9) and the mechanostat theories developed by Klein-Nulend *et al* (55) (57) are both valid explanations of how bone cells "feel" the damage, and they have been both used in this simulation to show their differences and similarities. To validate the results of the simulator regarding dead bone I have used the results of experiments from O'Brien(34), from Burr(21) and from Presbitero(39), while the results for living bone have been compared to results from Martin(48). The increase in bone strength with training has been compared to the results from Notomi *et al* (80) regarding rat bone strengthening with increased load. To complete the simulator of biological processes and obtain the parameters it requires, I have used the results of the experiments from Mulcahy *et al*(54), whose results from MLOY-4 cells report the values of RankL and OPG after damaging the osteocytes. The results of BMU analysis and simulations of their behaviour has been previously shown, for example by Pivonka *et al* (20), as studies where the repair is independent from the mechanical state of the bone (number and size of microcracks), while has been proved that cracks can be

military recruits, but also that this threat can be addressed and prevented by adopting specific procedures and ensuring rest to the trainees.

Simulation

Since the goal of the work is to provide a simulation of bone behaviour, papers involving a simulation are the main part of the analyzed literature. Actually, almost all the papers that have been mentioned so far have some degree of simulation as part of them, as it is necessary if the behaviour of a system has to be predicted. Common methods to simulate the behaviour of bone cells are finite element analysis (85) and less commonly neural network interfaces (86)(87). More advanced studies try to model entire limbs by approaching the problem with a multibody method (88)(89) (90) (sample image in Figure 34) .The papers containing the simulations that inspired the blocks of the model have been noted before and will be referenced in their appropriate sections in the current research, but there are a couple of papers that depict simulations not directly included in the model, but that nonetheless inspired the main shape of the project and its layout.

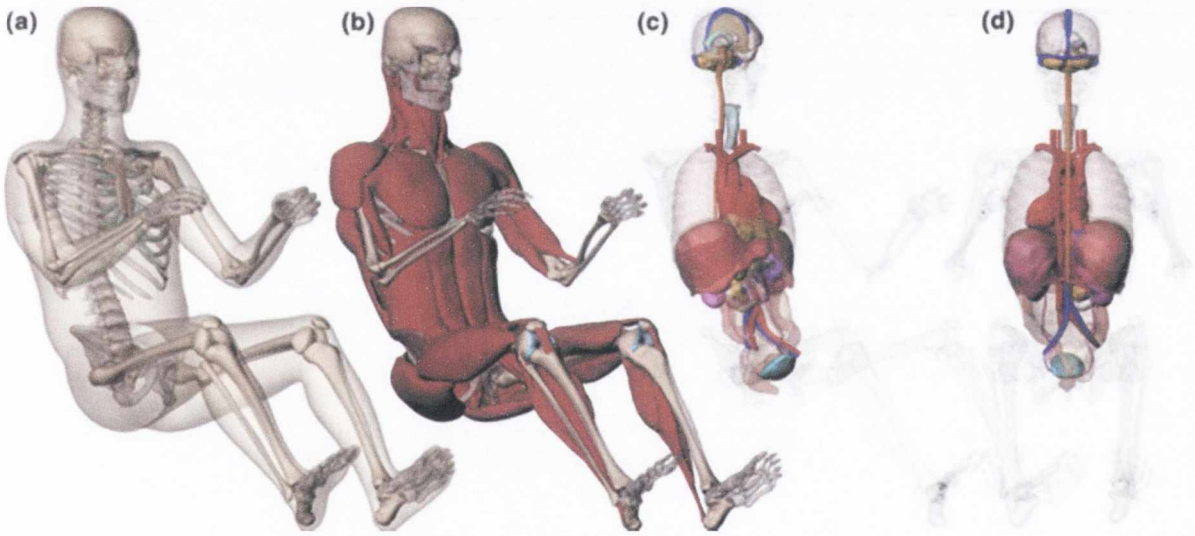

Figure 34. Summary of M50 CAD model. (a) Exterior skin and skeletal structure. (b) Muscle and ligamentous structures within the knee. (c) Organ components of the M50 model with detailed image of brain structures. (d) Posterior view of organ structures. From Gayiz *et al* (90)

A paper with a large scale view of the whole problem is Taylor & Lee 2003 (91). This paper analyzes the problem on a large scale and (re)introduces the importance of using stochastic variables to preview scatter in the crack behaviour. It also provides a simple but effective simulation of the behaviour of living bone. The author sets a simulation where a bone is represented by a tube under cyclic load in compression. The model is then focused on a slice of this bone 450 μm long, by choosing the number of cracks

detected by the bone and healed, no study until now has been able to see the interaction between the damage and the repair, for example to see if the repair prioritizes cracks because of their age or because of their size. This system has been created with the intent of covering these "blank spots" of the mechanics of bone microdamage, by showing them with a system able to simulate multiple cracks.

As a final note, the results of the simulation of the number of processes spanning a crack have caused the writing of a paper which has been published in the journal Biomechanics and Modelling in Mechanobiology in 2012 (92). The methods used in the paper are the same used in this simulation, so they will be shown in detail in the following chapters, along with the results obtained.

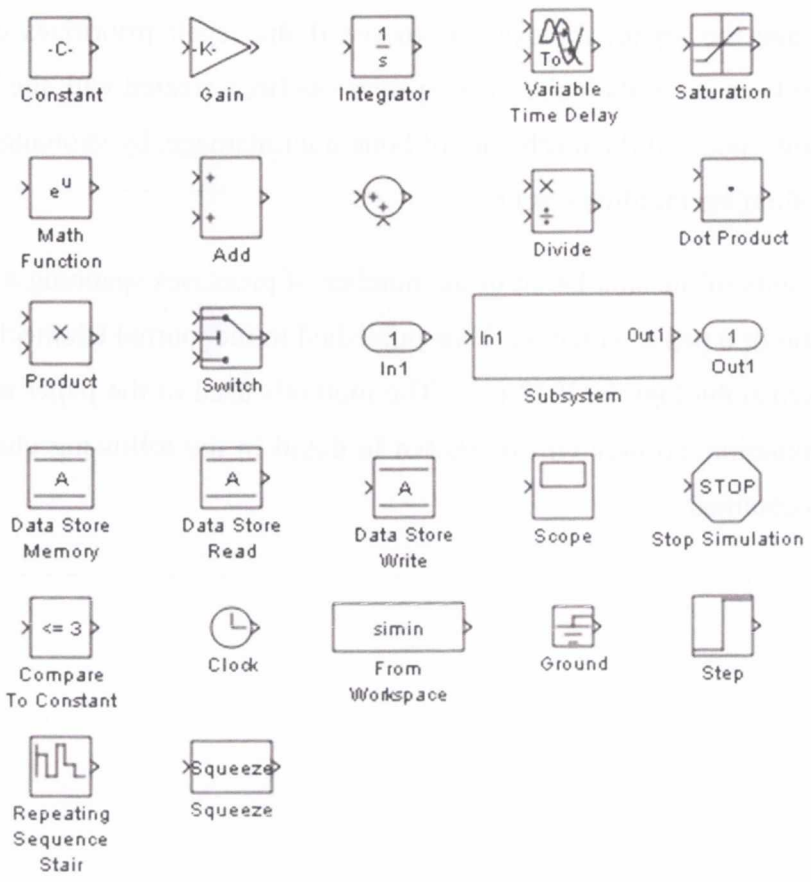

Figure 35. Simulink blocks used in the simulation.

The blocks are described below, starting from the top left and moving left.

Constant: the block most often used in the simulator. It is a source block that outputs a constant signal through the simulation time.

Gain: this triangle shaped block multiplies the input signal by a constant. It is a very common block in control theory applications. It is mainly used in the system to change the units of the signal when needed.

Integrator: this block integrates the signal over the simulation time. The use of this block allows for the solving of differential equations.

Variable Time Delay: this block delays the top input by a number of time units given by the bottom input. It allows for predicting behaviours that happen during the simulation, like the birth of new cracks, or time delayed effects, like the time required for a BMU to reach the crack.

Chapter 2: Methods

For modelling the system I chose to use the Simulink™ suite from the Matlab™ program. This choice was initially made to make use of the modularity of a Simulink™ model, which can have its parts switched and improved without changing the whole model. This has allowed updating of the system properties during the duration of the research process as the results from the group were being submitted and it allows deactivating of the parts that are not needed in a given analysis, like the repair when analyzing dead bone. Finally the nature of a control theory program works very well for simulating a closed loop system such as the bone damage and healing system.

Simulink is a suite of Matlab that is usually used for simulating complex systems for control theory applications; it is a graphical interface that allows the hierarchical building of systems and subsystems connected to each other. The typical Simulink model appears as a white sheet where geometrical shapes are connected to each other by arrows like a flow chart. The arrows represent the flux of signals in the model while the shapes, or "blocks", are the main components of the system, being the source of the signals and representing the operations applied to them. The blocks are chosen from an extensive library made available by the program and represent various kinds of functions, from linear applications like integrations and delays to algorithmic functions like sum and gain (multiplication by a scalar) to model wide utilities like inputs and outputs (called "sources" and "sinks"). Blocks can also interface with Matlab to exchange variables and to use its functions to convert the signals in the model. Simulink can be used to generate analyses on models that reproduce time dependent phenomena like the motion of a pendulum; the program simulates the behaviour of the system in a dynamical environment and offers the states of all the variables of the system during the simulation time.

In Figure 35, there is a list of all the blocks used in the simulator

Data Store Memory: this block memorizes model wide data to be used in different subsystems that are not connected to each other. It needs to be placed in the model to use the following two blocks.

Data Store Read: this block reads the data written in the Data Store Memory so that it can be used as source of a signal.

Data Store Write: this block writes its input signal in the Data Store Memory so that it can be used in other parts of the system.

Scope: this block is the most common sink of data. It outputs its input signal by plotting it in a screen and can be used to write the data in the Matlab workspace for further analyses.

Stop Simulation: this block stops immediately the simulation if the signal input has the logical value TRUE. It is used in the system to stop the simulation when the value of crack length grows to unrealistic values.

Compare to Constant: this block compares the numerical value of its input signal to a constant and releases a logical signal of TRUE or FALSE accordingly.

Clock: the clock block outputs a signal equal to the time of simulation.

From Workspace: this source block takes variables from the Matlab workspace and uses them as inputs for the system. It can give both constant and time dependent values, using different formats.

Ground: this block outputs a constant value of zero. It is also used to avoid leaving unconnected ports.

Step: this source block outputs a constant output of zero until a given time, after that time it gives a constant value different from zero.

Repeating Sequence Stair: this source block outputs a sequence of discrete values and repeats it until the end of the simulation. It is used in the system to reproduce variable load conditions.

Squeeze: this block "squeezes" the input signal's dimensions, removing singleton dimensions. A singleton dimension is a dimension whose size is zero. For example a

Saturation: the saturation block limits the input signal to a range of values. If the value of the input signal is beyond the upper or lower limit it gets changed to the nearest allowed limit. It is used in the simulator to avoid physically impossible situations like negative lengths of cracks.

Math Function: this block covers a series of different mathematical functions, which are applied to the input signal. Among the possible functions that this block can replicate are square root, power and trigonometric functions like sine and tangent. When the function is changed the symbol in the block changes to show which function is applied.

Add or Sum: these blocks have different names and shapes but have the same function, adding together the values of the input signals. The reason for the different shapes is that this block is often used for adding the control signal to the source signal in a looped control system, so it is easier to use when the two inputs aren't parallel to each other.

Divide: this block divides the top input by the bottom input. It can be changed to product

Dot Product: this block multiplies two or more arrays by the rules of scalar product.

Product: this block multiplies two or more signals following the rules of vector product. It can be changed to divide.

Switch: this block passes through the top signal if the middle (or control) signal meets the conditions; else it lets the bottom signal pass through. The conditions are defined by modifying the blocks parameters, among the possible conditions are the relation of the control signal with zero or a constant.

Input: this block represents the input in a subsystem; its name appears in the subsystem block when in the main system.

Subsystem: this block is used to arrange the blocks in hierarchically organized subsystems. Near its input and output arrows are listed the names of its inputs, to make easier connections.

Output: this block is the output in a subsystem; its name appears in the subsystem block when it is displayed in the main system.

a + is the splitting of data. The last shape (Crack Length) represents the output it has this shape when the output is dynamic (for an equation or a simulation) and the shape of a document when the output is static (like for a script).

Finally I have made use of the Matlab suit Simbiology to simulate the biological reactions that happen at the cellular level in reaction to damage. Simbiology is a graphic interface that allows one to simulate the behaviour of a biological system knowing the species in it and the laws that connect them. The program also allows scanning of the parameters of the laws that regulate the species offering the variation of behaviour of the system relatively to variation in the parameters.

The system is composed of 3 parts; each part simulates one step of the bone life process and is directly correlated to the experiments done by one of our group's researchers during this project. The next two chapters describe the theoretical model which was developed and how it was implemented in the Simulink environment.

2x1x4 vector would be changed in a 2x4 vector. It is used in the simulator to convert the data in an easier to read format.

To explain some of the logical steps that have been done to compile the simulator I have made use of the programming capabilities of Matlab in the form of scripts that perform the calculations requested, while the scripts themselves can be found in the appendix, their workings will be shown in the form of logical flow charts like the one in Figure 36.

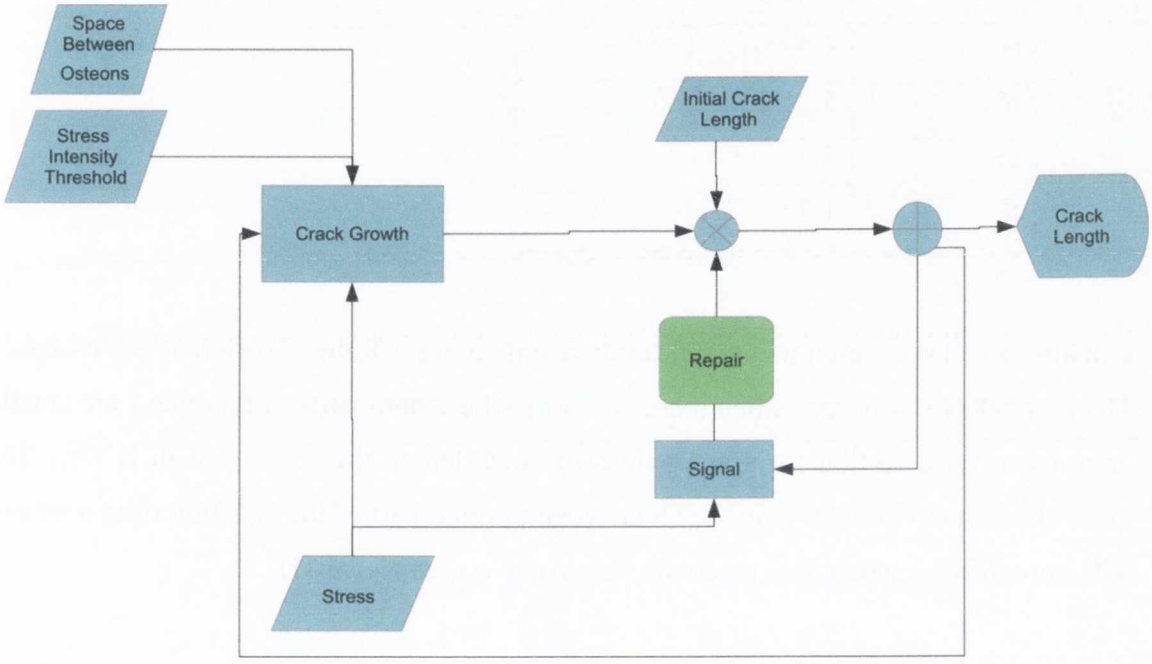

Figure 36. The flowchart showing the flux of information in the model. The trapeziums represent the inputs, in this case the initial value of crack length, the stress, the stress intensity threshold and the space between osteons. The square blocks represent the operations that the system performs on its data, like translating crack length into crack growth and broken processes or broken processes in repair. The square representing the operation to translate signal in repair has rounded corners and a different colour to show that the equations' parameters are purely predicted quantities, not directly correlated to experimental data (but verified against them). The circle with an X inside represent sum of data, in fact the crack length is formed by the sum of crack initial value, crack growth with stress and repair (negative). The circle with the + symbol represents the splitting of data, in fact the value of crack length is used in every cycle as the input for the calculation of crack growth and signal while being affected by the values of repair and crack growth. The output of the system is the value of crack length at every cycle.

Where the trapezium represents the input while the squares represent the operations, the Repair operation is in a rounded rectangle of a different colour to show how the parameters of the equations used in that operation have been deducted mathematically, while all the others operations are regulated from analytical representations of the phenomena involved. The circle with an X represents the sum of data and the circle with

Values the constants of this equation have been deduced and estimated by experiments on dead bone in (29). I have used the values in Table 2 for the simulation

Table 2: Parameters for equation 1. Units for C and C' are such that da/dN is given in mm/cycle with ΔK in MPa(m)$^{1/2}$. Data from Taylor *et al* (29)

Parameter	Value
C	3.46×10^{-7}
C'	1.51×10^{-4}
n	4.5
n'	5
m	3
F	1.22

Equation 1 can be plotted in a graph for different values offering 2 different behaviours. The first behaviour occurs when there is a zone where both parts of Equation 1 are smaller or equal to zero, so that for given values of crack length the crack growth is zero. This means that cracks smaller than the value when the first part of the equation rises over zero will stop growing when they reach the value of a=d (see Figure 37).

Chapter 3: Theoretical model

The simulation focuses its scope on the status of cracks in bone. The goal is to create a closed loop simulation that follows the three main processes alternating themselves in bone: damage accumulation, damage detection and repair.

The processes can be roughly divided in three parts

Bone cracking under fatigue stress

Bone detecting damage

Bone repairing the damage

The main variable in the system will be the length of the cracks. The cracks can grow because of stress or get repaired by the repair process. The crack length "a" can be predicted by Equation 19, which I used to explain the model used for this simulation.

$$a = a_0 + \Delta a(t,a) - \Delta r(t,a)$$

Equation 19. Components of Crack Length with time.

Where a_0 is half the crack size at the beginning of the analysis, Δa is the crack growth with time, a function of a and t and finally Δr is the repair effect, a function of time and a. Providing that a_0 can be obtained by experimental data I need to define Δa and r.

Bone cracking under fatigue stress

As far as the fatigue analysis goes, the bone behaviour can be depicted as similar to that of an orthotropic brittle material, in many previous works this kind of analysis has been conducted and there is a large number of equations to describe this behaviour in these materials.

Taylor *et al* (28) proposed the Equation 1 for compact bone

$$da/dN = C(\Delta K - \Delta K_{th})^n + C'(\Delta K)^{n'}((d-a)/d)^m$$

Equation 1: Crack Growth Rate per cycle. From Taylor & Prendergast 1995(28)

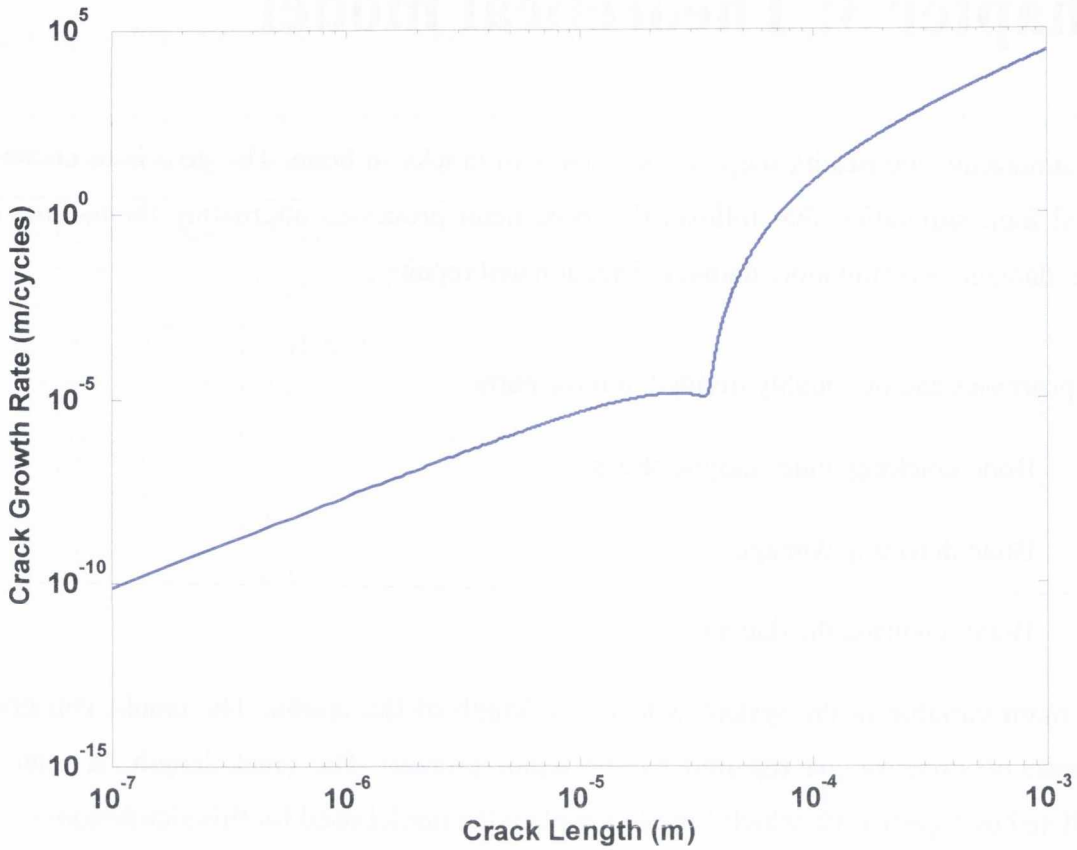

Figure 38. Crack Growth Rate against Crack Length for "unstable" cracks

For the purpose of simulating bone under stress, the first behaviour is what I expect from experiments when the stress is low, with the results moving to the second behaviour as the stress rises and the probability of failure increases. Knowing which kind of behaviour I can expect from a crack allows me to foresee the results of the simulation before even running it. Analyzing Equation 1 and rearranging it I can see what combination of values defines the different behaviours. To have a strictly positive value I need to find the combination of values that makes it so that the value of the function is never zero.
Rearranging Equation 1 I can obtain Equation 20

$$d > (\Delta Kth)^2 / \pi(\Delta\sigma F)^2$$

Equation 20. Balance of parameters for an unstable crack.

Equation 20 shows the characteristics of an inherently unstable crack, namely a crack that has no equilibrium point in its growth. As can be seen in this relation d, F and ΔK_{th} are all properties of the bone depending on its geometry, the geometry of the crack and the resistance of the material to crack propagation while $\Delta\sigma$ is the stress applied, that means

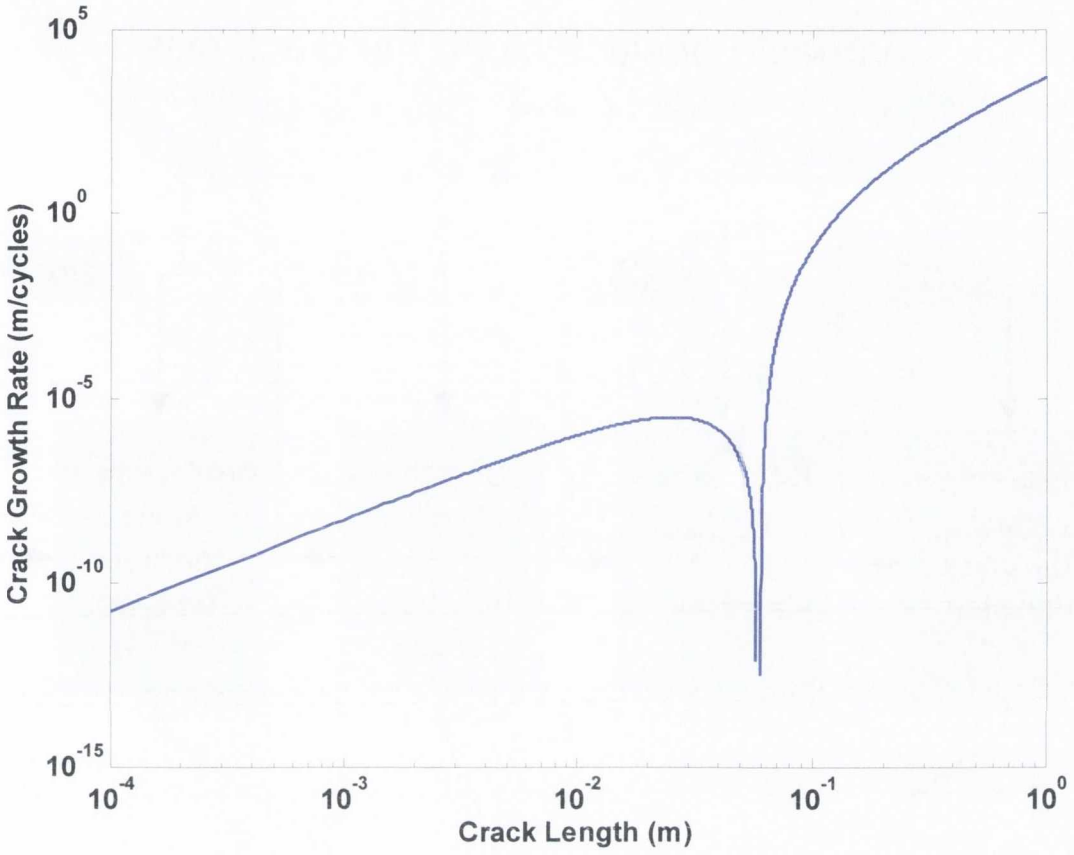

Figure 37. Crack growth rate against crack length for "stable" crack size.

The second behaviour occurs when the conditions for the first are not met, namely when there is no point in the function's domain where the value of the function is zero, as shown in Figure 38. This behaviour means that every crack, no matter how small, will grow to failure with time.

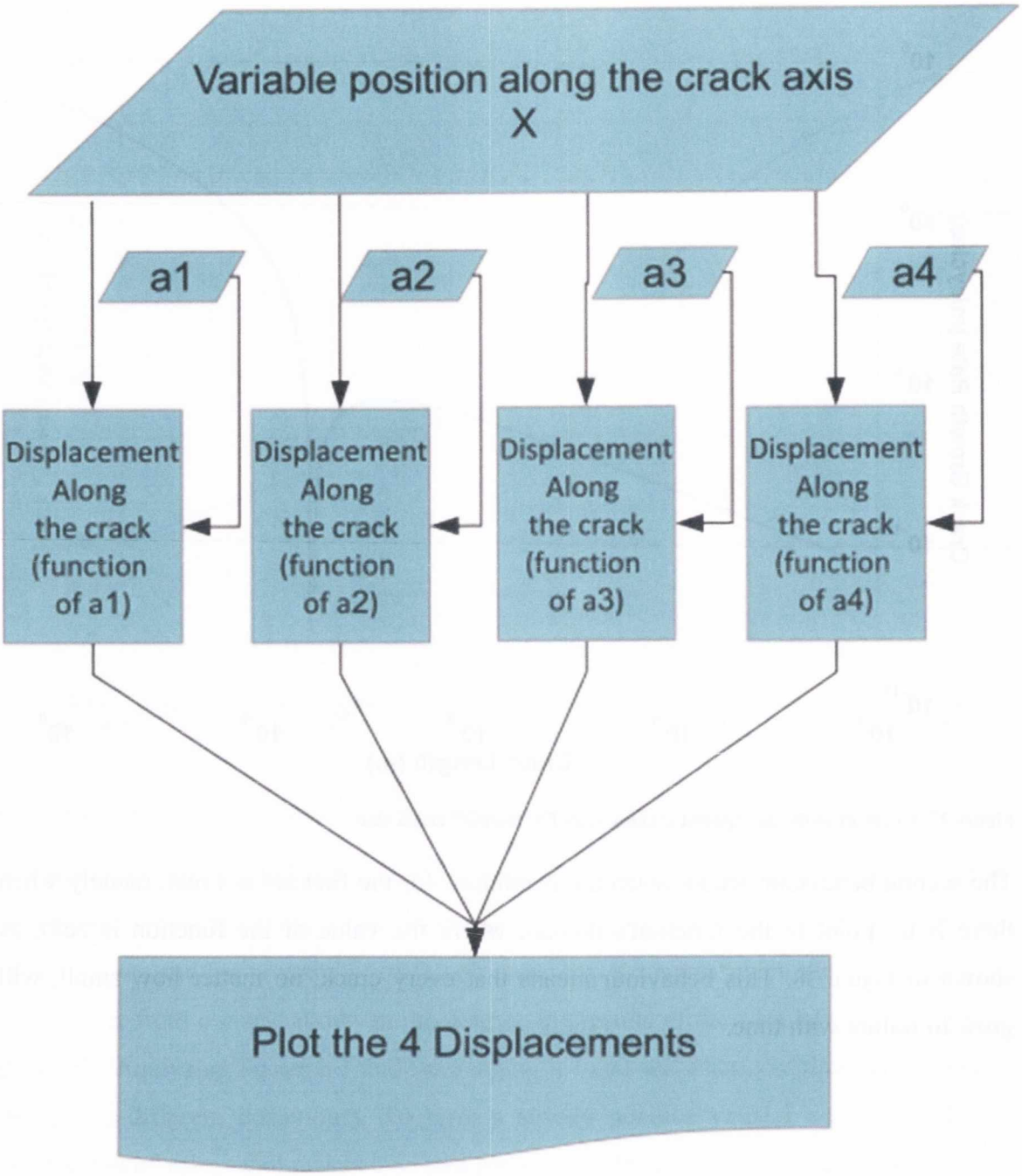

Figure 39. Flowchart explaining the steps of the script calculating the displacement Δs for 4 cracks of different length. The 4 arrays X1, X4 representing the points on the axes of the cracks are inputs together with their lengths *a* to the equation to obtain Δs. The 4 resulting arrays representing Δs for every value of X are then plotted together in the same graph.

The second step was to analyze what happens while keeping the length of the crack constant and varying the stress. Figure 40 shows the flow of information for another Matlab program which performs its analysis on a 100 μm crack under 4 different stresses.

that cracks that are stable for low values of stress do not enjoy the same stability at higher levels of stress. Moreover as d and ΔK_{th} are variable along the bone and mainly obtainable by experiments there is no definite way apart from a statistical analysis to predict exactly which values I can expect for every given crack.

Damage Detection

To simulate an effect of repair it is necessary that the system has a way to detect the damage. In control theory this usually means that a sensor is in place to detect the levels of the signal which needs repairing. In biology there are certain mechanisms that act as "sensors" for the body to detect damage and trigger a repair effect, to be more specific bone damage has to be "sensed" by cells to be able to release the substances that promote repair.

There is still uncertainly about how fatigue damage in the form of microcracks gets detected by bone cells.

The "scissors model"

The presence of cracks in bone material can cause fractures in osteocytes or in the processes that connect them to each other, the broken cells will release many chemical agents into their surroundings, any one of which could act as a signal.

In that Hazenberg *et al* (50) the failure displacement has been defined as $2\delta s > 0.2um$, but further studies (still unpublished at the time of this writing) have shown that the way processes break is more an effect of localized fatigue than a pure cutting effect. Because of this, in this first analysis I will suppose that the stress has been applied for a sufficient number of cycles so that the fatigue effect is the same as the supposed cutting effect, while remaining much less than the number of cycles that can cause fatigue failure in the surrounding bone.

Modifying the equations shown by Hazenberg *et al* (50) I was able to create small programs and functions with Matlab to show the behaviour of processes in different situations. A flow chart representing the behaviour of one of these programs (the text of the programs can be found in the appendix) is in Figure 39. The program calculates displacement along the shorter axis of 4 cracks of different size (a1..a4) and plots it in relation to the position along the axis (x1..x4).

length of the crack. Performing a simulation of ovine bone, to know how many processes cross the crack I have followed the experimental data found in Mullender *et al* (62), which trend suggests a plausible ovine osteocyte density of 40000mm^{-3} and the number of processes per osteocyte has been set as 100 following Sugawara *et al* (63). Assuming that the processes are randomly oriented in space I can model that one sixth of them are crossing the plane of the crack. Knowing the osteocyte density and the number of osteocytes I can measure the number of processes that are crossing any given area in the bone and that, for example, in ovine bone the processes along a crack are spaced by 4.4 μm so the number of processes crossing the axis of a 400 μm crack is 91 (400/4.4)
I have automated this procedure in another Matlab™ program (cfr. appendix) that can be seen in a simple form in Figure 41:

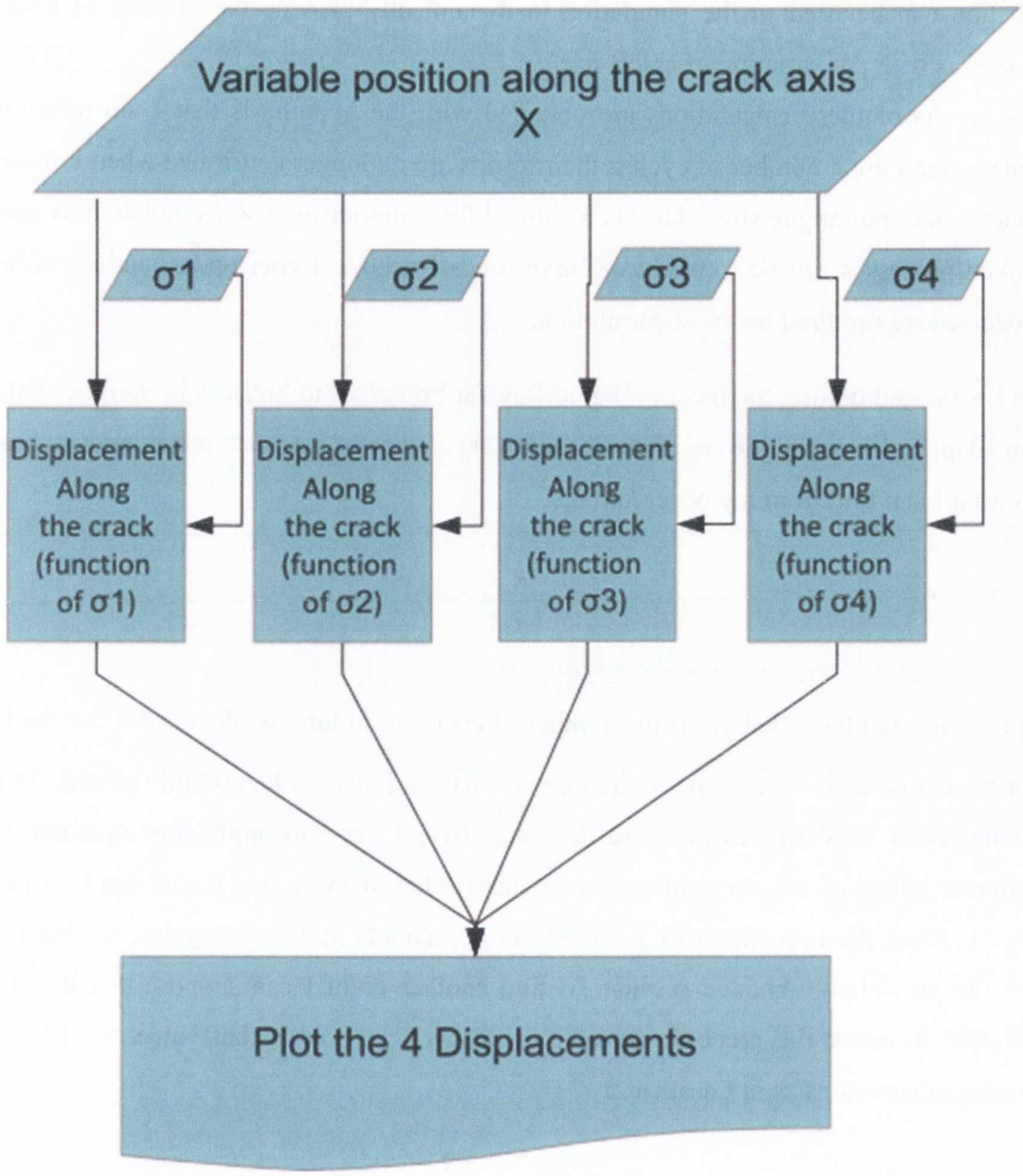

Figure 40. Flowchart showing the flux of data in the script to simulate the displacement in a 100 μm cracks under 4 different degrees of stress. The array X representing the points in the crack is the input of 4 equations made with the 4 different levels of stress. The outputs Δs1, ..,Δs4 are plotted on the same graph.

These models can give a good picture of the differences in percentage of broken processes for cracks at the various lengths, but for including an amount of damage in the simulation I need the exact number of broken processes, so I have created a function which does this job directly.

NUMBER OF BROKEN PROCESSES

Having the fraction of length where the processes will be broken allows the number of broken processes to be guessed knowing the total number of processes that forms on the

function can be used in the simulation to dynamically provide the number of broken processes with the variation of crack size.

The results of these calculations are obtained with the hypothesis that I am observing bones after a great number of cycles; their results are no longer confirmed when I observe bones when the fatigue stress has been applied for a shorter time. To simulate how many broken processes can be found at different times I need a deeper understanding of how processes are ruptured by the shear motion.

As I have said before, the most probable way for processes to break is by fatigue. Thus I can adapt a classic fatigue equation (Equation 21) and try to calculate its parameters based on what I can find from my observations.

$$N_f = \frac{K_F}{(\Delta s)^n}$$

Equation 21. Fatigue life expectation, adapted from (52)

In Equation 21 I have that N_f is the number of cycles to failure, while n and K are the two constants that define the shape of the fatigue curve (a line on a logarithmic graph). As the parameters I need to calculate are the latter two, I need to apply this equation at 2 different points of the curve to obtain its shape. One of these two points can be when I have reached the hypothesis I have used before, namely at 100000 cycles, so that I can use the previously obtained results. To find another point I can suppose that the shear required to break the processes in one single cycle is double that value. So I have a system of equations as in Equation 22

$$(0.2)^n = \frac{K_F}{100000}$$

$$(0.4)^n = K_F$$

Equation 22. Parameters for osteocyte processes fatigue life.

And that gives the values for n= 16.7 and $K_F = (0.4)^{16.7}$

To apply the results of this equation I have created another Matlab™ script that uses this formula to simulate when the processes in a crack are going to rupture, applying the previous results about the shear on every process and obtaining how many cycles can a process stand before being broken. A flowchart of the script is in Figure 42, while the text is in the appendix

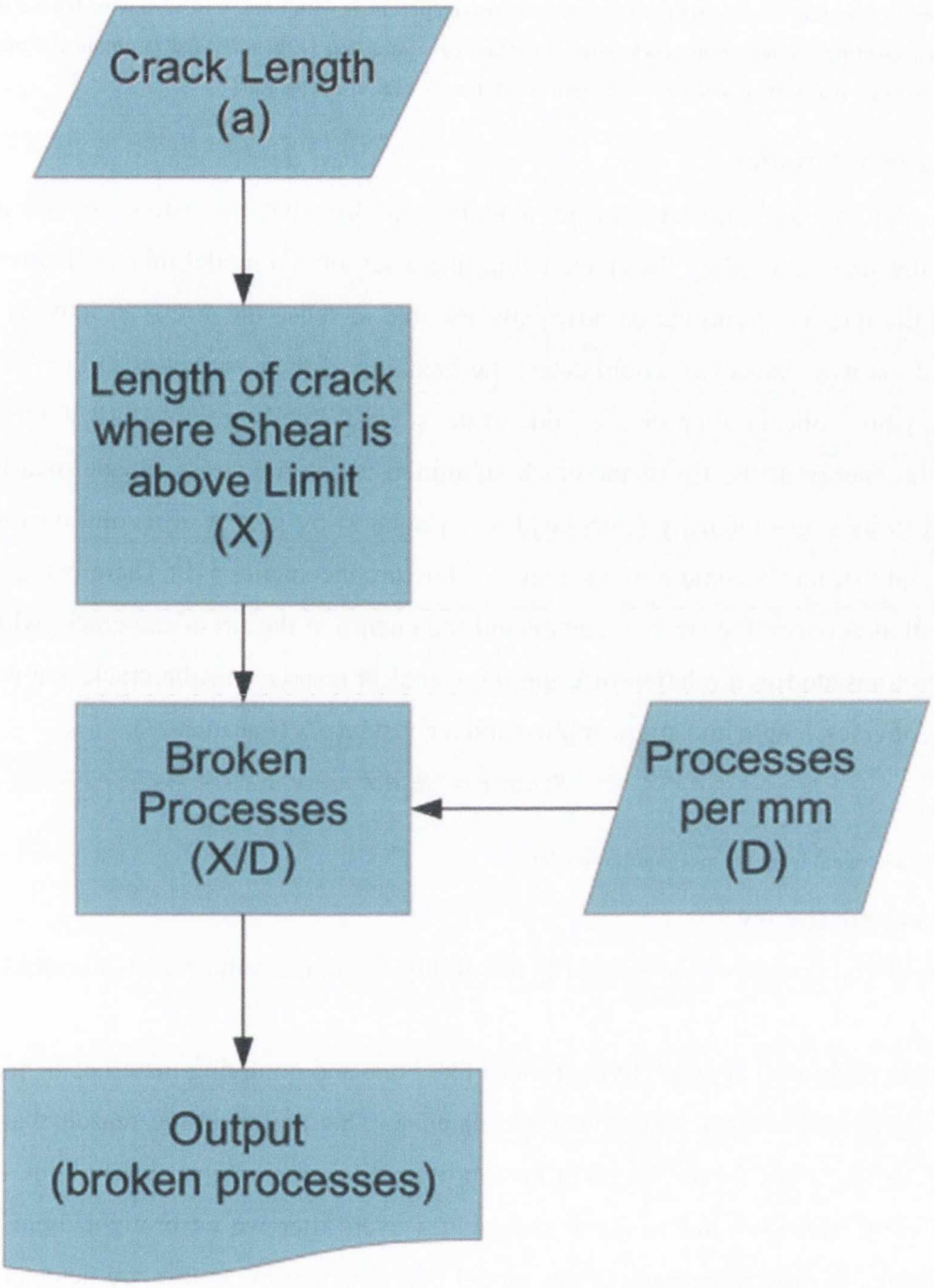

Figure 41. Flowchart of the script to calculate the number of broken processes Bp in a crack of length a. The array a containing the various possible crack lengths is changed in X that represents the portion of crack with a shear greater than the limit. The value of X gets divided by d, representing the density of processes to obtain Br, which gets plotted.

And from the program in Figure 41 I have created a Matlab function which provides the number of broken processes for a given crack knowing its length. (See appendix).This

crack lengths to obtain X, the part of the crack with broken processes with time. X is subtracted from a to obtain I1..I4, representing the length of crack without broken processes that is then divided to obtain the number of intact processes, that is then plotted in the same graph for all 4 the crack lengths.

Mechanostat model

The model for mechanostat damage signalling implies that the osteocytes are able to detect the stress caused by the crack acting like a sensor. To model this mechanics I will ignore the internal workings on how cells are able to sense the stress, exactly as I have ignored the way osteocytes could detect the breaking of their processes in the "scissors" model, while concentrating on the value of the stress the cells are able to feel. On a local scale the energy at the tip of the crack submitted to fatigue stress can be measured as related to its stress intensity (calculated in Equation 2) by means of a solution found by Irwin and that has become a fundamental in fracture mechanics (45) There is a quadratic correlation between the stress intensity and the energy at the tip of the crack, which can be then translated in a relation offering the signal in response to the crack, knowing the values of crack length and stress applied and a constant K_g (Equation 23).

$$Signal = K_g a \sigma^2$$

Equation 23. Signal from the mechanostat model.

Bone repair theory

The third component of the system is the ability to simulate the repair of cracks by the body.

The main difference between living tissues like bone and nonliving materials is the ability of living tissues to grow and regenerate damage. This ability is the reason that allows living tissues to last for the length of human life while remaining relatively light, to adapt to different lifestyles and to repair themselves even after we've brought them beyond their limits, in most situations. In this model I assume that the cracks are detected by the body and that the trigger of this detection is a molecule called RankL (Receptor Activator for Nuclear Factor κ B Ligand). I have made so that in the simulator this molecule is released when the processes spanning a crack are broken by the stress applied on the crack itself that under the stress undergoes a strain, when this strain is big enough the processes spanning from cell to cell that are in the area of the crack are ruptured and their destruction releases RankL, which triggers the creation of a BMU (Bone multicellular units).

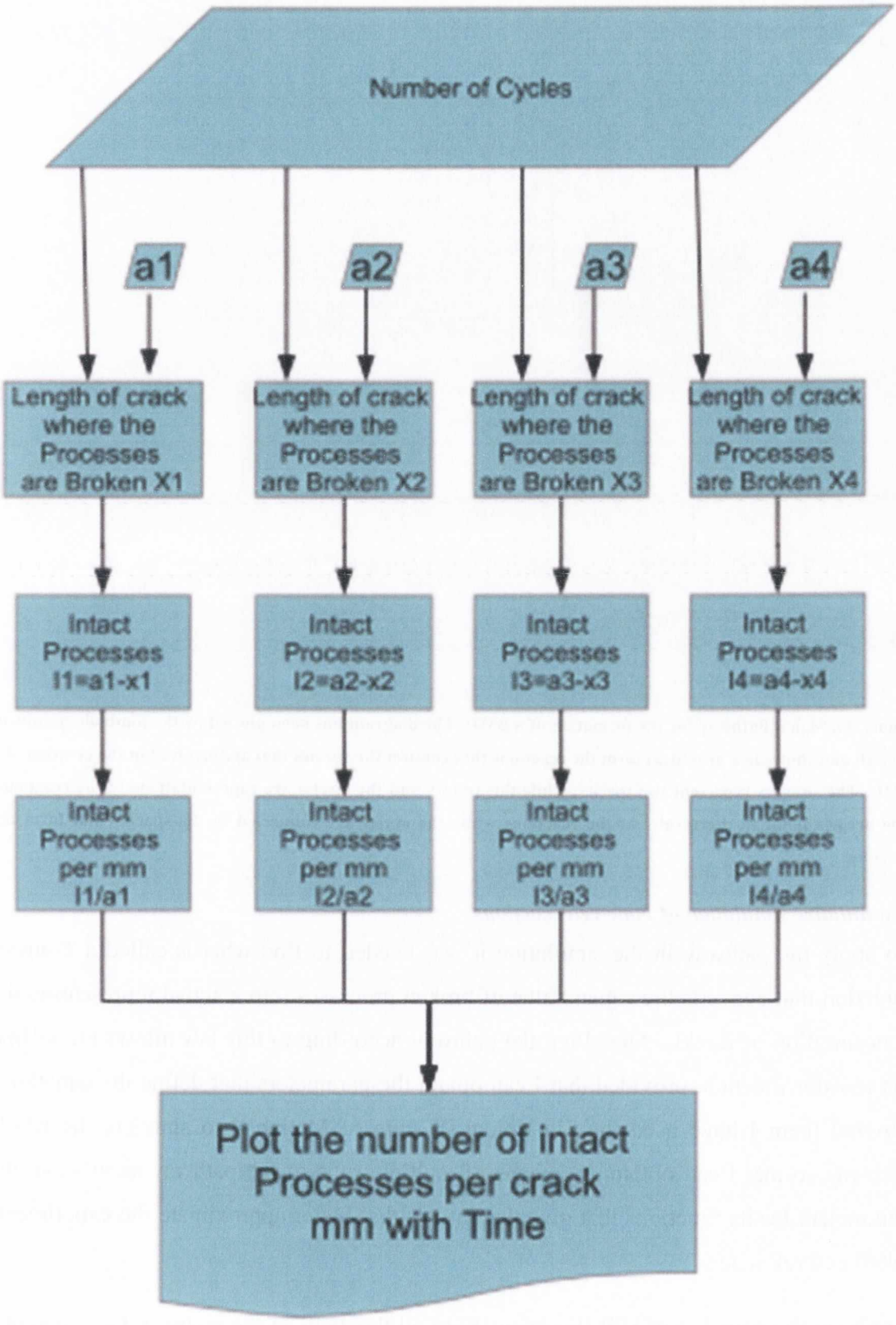

Figure 42. Flowchart explaining the script that predicts the number of intact processes on 4 cracks of size a1..a4 with the flowing of time. The array representing time is evaluated in the first row of blocks together with the

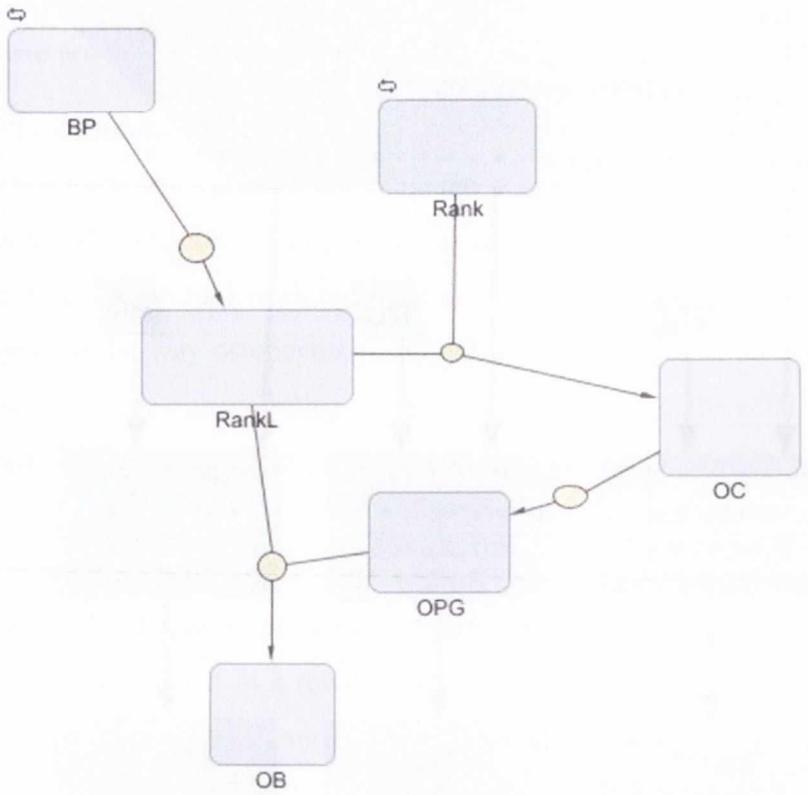

Figure 44. Signal Pathway for the formation of a BMU. The diagram has been plotted by the Simbiology suite of Matlab and shows in a graphical form the reactions that connect the species that are involved in the creation of a BMU. The squares represent the species, while the arrows and the circles are representations of the reactions. The arrows point to the results of the reactions while the cycles are connected to the species that form the reaction.

Quantitative simulation of bone cell reactions

To apply the pathway in the simulation it was needed to find what is called a Transfer Function that converts the signal value of broken processes into a signal representing the concentration of RankL. Modelling the pathway according to this law allows me to find the transfer function, provided that I can obtain the parameters that define the equations. To find them I have used the Simbiology™ suite of Matlab™ to simulate the whole pathway so that I can obtain, by means of multiple runs of the pathway simulation, the parameters for its functions that give the outputs that better approximate the experiments taken as a reference.

Applying the equation of Hill (Equation 18) to all the steps in the pathway I can obtain a system that represents the whole process. This system is composed of 5 equations in 5 variables and 15 parameters. Varying those parameters I have infinite possible outputs of

A BMU is organized into a "cutting cone" of osteoclasts reabsorbing bone followed by a cluster of osteoblasts reforming the bone to fill the defects left by osteoclasts (Figure 43). In the adult human the osteoblasts do not recover all the defects and some are left; this is one of the reasons for which the human bone mass decreases with years.

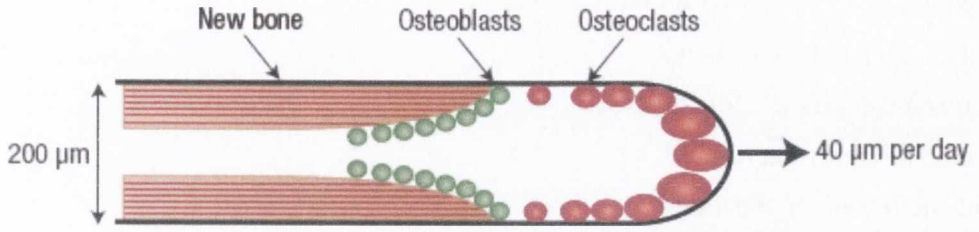

Figure 43. Schematic of a BMU from Taylor *et al* (93). The osteoclasts remove old bone while the osteoblasts place new bone. The schematics shows also the size of a BMU and its speed while travelling the bone.

To create a BMU RankL has to start a series of biological reactions with other actors like Rank and OPG (osteoprotegerin). As of today there are theories and experiments proving that also other factors, especially members of the TNF family of receptors, affect BMU formation but for the simulation I will use a simple model of the pathway that shows only 3 actors: RankL, Rank and OPG. The pathway I have chosen for this simulation is as follows: RankL binds with Rank on the surface of the cell to activate Osteoclasts, Osteoclasts release OPG that binds with RankL (so acting as a repressor on the first reaction) to activate Osteoblasts. My repair simulation starts with transforming the number of broken processes along the crack to a concentration of RankL, models the chain of reactions that create a BMU as a cluster of Osteoclasts and Osteoblasts and finally, when the BMU is completed, applies the effect of repair on the size of the crack, closing the loop of the simulation, as shown in Figure 44.

Table 3: Variables for the biological pathway

Variable	Description	Value
N1	Hill coefficient for equation 1	1
K1	Activation coefficient for equation 1	30
B1	Maximal Expression level for eq. 1	0.6
N2	Hill coefficient for equation 2	2
K2	Activation coefficient for equation 2	5
B2	Maximal Expression level for eq. 2	5.5
N3	Hill coefficient for equation 3	1
K3	Activation coefficient for equation 3	8
B3	Maximal Expression level for eq. 3	1.6
N4	Hill coefficient for equation 4	1
K4	Activation coefficient for equation 4	3
B4	Maximal Expression level for eq. 4	2.75
N5	Hill coefficient for equation 5	1
K5	Activation coefficient for equation 5	3
B5	Maximal Expression level for eq. 5	2.75

Once the equations simulating the pathway have been obtained, I can use them in the simulation to obtain when the BMU is formed in relation to the presence of broken processes, making this formation a trigger for the repair effect.

Variation in bone density

The balance between removed bone and new bone is not perfect, and this is a fact clearly established by the scientific community (67). Usually, for healthy young humans and animals, the process of repair generates a better quality of bone, mainly because the new bone has been cleaned from the damage that was inflicted to the old bone, but also because of the efficiency of the balance between bone mass removed and added that results in a higher density of bone. When this balance get disrupted by factors like aging and diseases, the density of bone decreases after repair and the local benefit of restoring the bone to an undamaged state is offset by the decreasing quality of the bone. The strengthening or weakening of the bone structure because of the repair can be simulated using the signals obtained by the simulation of the RankL-Rank-OPG pathway that provide the number of osteoclasts and osteoblasts that I can find in the BMU. The

this system, but among whose infinite solutions I need to calculate the combination of parameters that gives the most realistic results. To solve this problem I have used Simbiology, which as the name suggest is a utility for the simulation of biological processes and the evaluation of their parameters, by using the results obtained by Lauren Mulcahy (54) as references for the precision of the results. Even with the computational assistance offered by modern PCs, so many parameters required some extra planning to be calculated. To avoid excessive load on the computer I first applied the parameter scan on the first few steps of the signal pathway, narrowing down the order of greatness of the parameters, doing a scan for all the parameters in values of 0.1, 1, 10 and 100 to get their first approximation size of values, after that I focused the analysis on the orders of magnitude that gave the best results for each parameter.

Once I found the combination of parameters that give a reasonable behaviour for the first steps of the pathway I could move on to obtain the remaining parameters, so to complete the set required to model the pathway and have an output of results that are similar to the results obtained for the YMLO-4 cell cultures in the reference experiments.

After obtaining a set of parameters I can apply it to the system, where the Hill equation is applied to every reaction in the pathway. Even if the relation between the number of broken processes and the concentration of RankL was initially approximated as linear, analyzing the results from Simbiology I have found that using the Hill equation for this correlation gives more realistic results. One problem of using the Hill equation directly in the system is that it is a state equation, so to provide a viable response to the variation of inputs I had to apply integration on the release of RankL by broken processes, so that a repair of the crack does not affect retroactively itself. This integration causes a small increase in the growth of RankL, balancing some of the difference it has with the experimental data.

Noon - Lunch

1 p.m. - Training

5 p.m. - Dinner

6 p.m. - Drill Sergeant Time

8:30 p.m. - Personal Time

9:30 p.m. - Lights Out

(from the website www.baseops.net)

From this schedule I can model a stress layout for the whole day, making a distinction between 3 regimes: training, non-training and rest.

The training regime is when the soldier is engaged in training, as the name suggests. It is the more stress intensive regime and I have given to it a stress of 50 MPa. To set a value to the training stress I can compare it to running a long march with a full set of equipment on (a typical exercise of the army training regime); supposing that the average recruit weights 70 kg and wears an equipment load of around 35 kg, comparable to 50% of his weight and observing the variation of stress on lower limbs during a fast marching pace [Genk *et al*(26)] I can suppose that during the training period the stress on the bones is increased by a factor of 2.5, changing so a physiological stress of around 20 MPa into a stress of 50 MPa.

The non-training regime is the regime of near physiological stress that can be expected during the other activities of the day, like lunch or personal time. I have modelled 20 MPa of stress for this regime.

The rest regime is the state of almost complete inactivity that the soldiers have between the "lights out" command and the "wake up" time. I have modelled a stress of 10 MPa for this period, leaving a light stress to simulate small movements and the effect of gravity even during sleep.

The assumption on the amount of stress made in this paragraph probably overestimate the stress on military trainees, but as this simulation is mainly a failure study, I have decided to put the simulator in a "worst case" scenario. As the system is very sensitive to stress (see stability analysis), this will probably cause an increased number of crack failure in our simulation, as it is probable than a real life trainee will stop to catch breath, reducing locally the stress applied in an unpredictable way.

number of osteoclasts and osteoblasts can be used to provide the balance between bone removed and restored; balance that can be tweaked changing the multiplicative coefficients that give how much bone is removed by osteoclasts and added by osteoblasts. This balance of bone mass can be converted into a modifier on the bone strength that changes the characteristics of the simulated bone applying Equation 24.

$$\%Variation\ of\ strength = Q \sum B_p - B_r$$

Equation 24. Variation of Strength in the system to simulate the effects of Wolff's Law.

Where Bp is the quantity of bone placed by osteoblasts, Br the quantity of bone removed by osteoclasts and Q is a constant. The value of Q is related to the ratio between the number of cracks observed and the total number of cracks in the whole bone.

Simulation of the risk of fracture in lower limbs for military personnel

Bones are made to sustain everyday stress without breaking, unless there are pathologies involved that reduce its physical qualities to the point they aren't able anymore to sustain the stress. When stress grows Wolff's Law tells that the bone is able to adapt to the increased stress given time, but on the other hand, low everyday stress causes the bone to reduce its resilience to match the lower stress. When people enlist in the army, they subject themselves to an intensive training regime, which increases the stress on the bones, especially the lower limbs. This increased stress is the cause of one of the main forms of injury in the army, lower limb fractures that tend to occur in the first few weeks of training, when the bone is still reacting to the new stress levels (82). The incidence of fractures in this specific population is high enough to allow isolating the increased stress as its cause.

Stress: To simulate the microcrack behaviour for a new recruit of the army I have first modelled the increased load of stress an army recruit faces. In the army the schedules of training and rest are strictly enforced. This allows to reproduce the daily routine of a trainee and simulate the load on his bones. The normal day for a trainee is as follows:

5 a.m. - Wake up

5:30 a.m. - Physical Training

6:30 a.m. - Breakfast

8:30 a.m. - Training

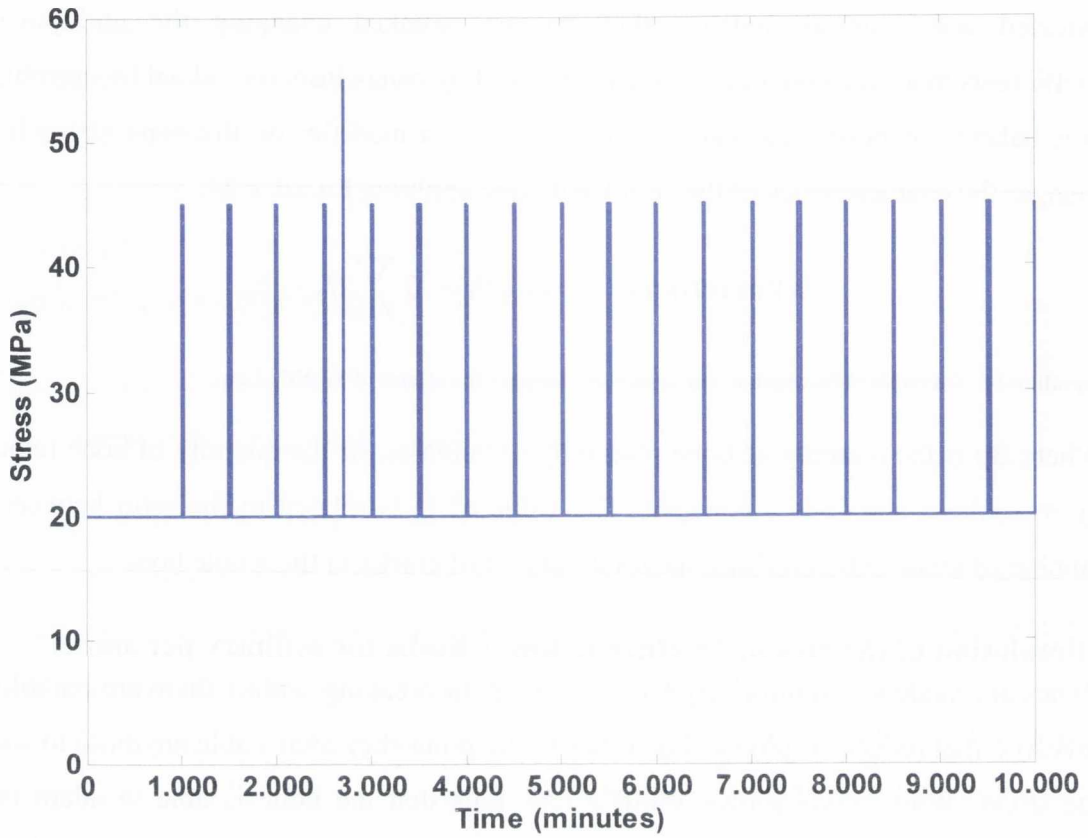

Figure 46. Stress layout with an "accident". The plot shows the alternating "low" and "high" stress periods and the peak caused by the "accident".

Effects of age, disease and drugs

The parameters of the simulation have been calculated for young, healthy persons. Modifying the parameters I can simulate various different effects, like age and disease.

To simulate age I have reduced the value of ΔKth as reported by Ager *et al* (27), while at the same time reducing the value of d, which is also noted to be reduced by age because of the increased presence of secondary osteons. I have reduced the mean value of ΔKth to 0.5 to simulate the osteons' reduced strength according to the reference that shows a reduction of 50% of both the crack propagation and initiation strength with age and the average value of the distance between osteons d of 25% according to Ager *et al* (27).

To simulate osteoporosis I have reduced the effectiveness of osteoblasts in the system by 90%. I have reduced the effectiveness of osteoblasts by this high ratio because I want the

The behaviour of stress with time in the simulator can be shown as in Figure 45.

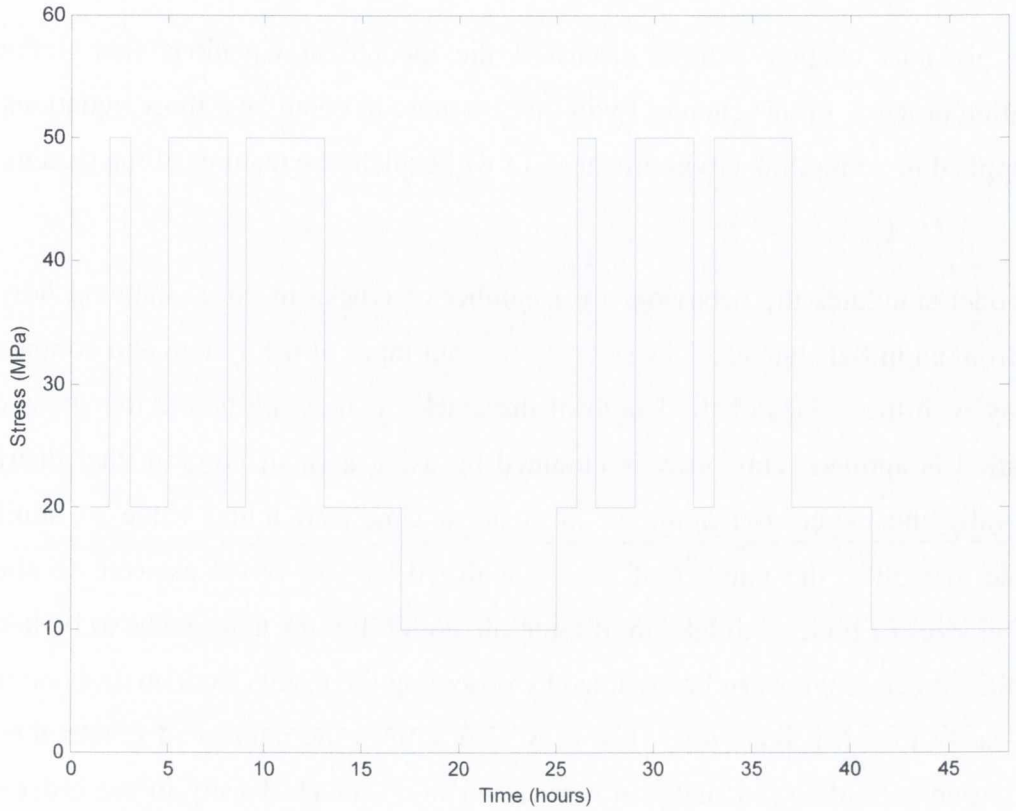

Figure 45. Stress Layout for the first 48 hours in the simulator. This pattern is repeated for all the simulation and replies the alternating training, non-training and rest periods.

Simulation of unexpected temporary overloads

To simulate the effect of traumatic events on bone I have created a stress layout in which the bone experiences a 2-phase cycle of activity during its everyday life. One longer period at 20MPa of stress (that I call here the low stress) and a 45 MPa shorter period (the high stress) that alternate themselves. One day, during the low stress period, the bone has an accident that brings for a short time the stress to 55MPa (see Figure 46).

Chapter 4: The simulator model

In the previous chapter I have discussed the theoretical equations that define the simulation process. In this chapter I will discuss more in detail how those equations have been applied in a Simulink environment and I will explain the features of the system.

Inputs

The model simulates the behaviour of a number of cracks in bone, showing how they grow from an initial state a0. This state is the main input of the system and composed of an array with the values of the length of the cracks as they are before the stress of the simulation is applied. This array is obtained by using a small program that distributes statistically the expected lengths so to create a simulated initial value as similar as possible to reality, the number of cracks analyzed can be varied as well, to simulate different sizes of bone or to take in account the possibility for new cracks to be initiated. The initial crack lengths can be obtained by observing the results from analysis on *in vivo* bone, easily found in literature. This array also defines the number of cracks that I am checking and simulating; usually in bone I can find a crack density in the order of 0.1 cracks per mm^2 (36), depending on the age of the bone, the species of the donor and the stresses applied to it before the analysis. If I approximate the crack density as a constant, then the number of elements in the array can be used as function of the size of the bone, instead of its crack density. To obtain the crack lengths of human bone *in vivo* I have used Figure 21 from a paper written by Martin(48), I have measured the values on the graph and I have extracted the Weibull distribution of the crack lengths. For the crack lengths in different animals I have used the results from other authors reported in Presbitero *et al* (39).

To measure the number of cracks to analyze I need to have two values: the volume of bone subjected to the maximum stress and the crack density for that volume. The volume of bone subjected to the maximum stress in a human femur can be found in Taylor and Kuiper (42). And crack density can be calculated by using Equation 6. Equation 6 applied to the stressed volume gives 250 cracks for 20MPa of stress and 1250 for 50 MPa of stress.

effects of osteoporosis, which usually take years to appear, to be evident in a shorter period of time.

To simulate the effects of anti-osteoporotic drugs (Bisphosphonates) I will modify the reaction coefficients that give birth to a BMU so that the effects of osteoclastic resorption are slowed. Bisphosphonates act both by preventing osteoclasts from initiating new BMUs and also by reducing the amount of bone removed (71), so I have simulated their effect by modifying the activation coefficient of the osteoclasts generation reaction increasing the value of K_2 by 5 times (so that the formation of the BMU is delayed) and by changing the effect of bone removed in the balance of bone mass so that the imbalance is reduced. This implies an increased risk of fracture, as the cracks will grow more, but will also delay and reduce the loss of strength of the bone. The resorption width of the BMU is reduced to around 90% of its control value in (71) so I have reduced the amount of crack length removed accordingly.

The simulation of crack length growth

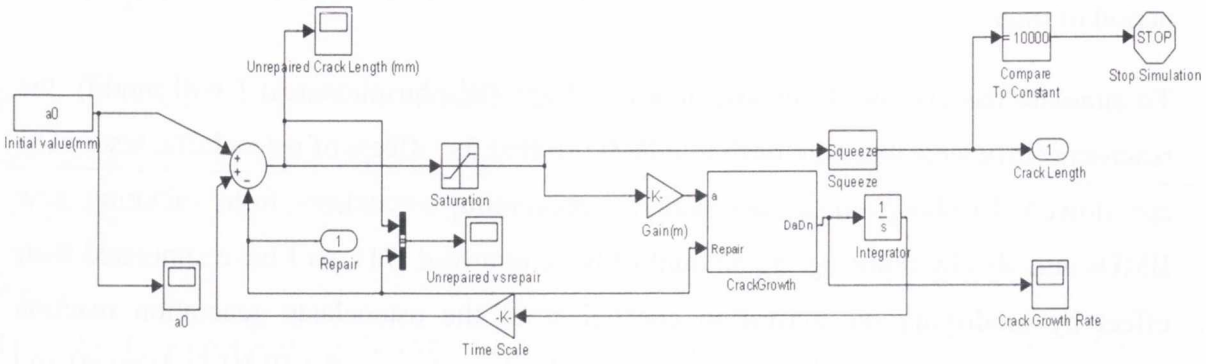

Figure 48. Subsystem: Bone Crack

The first part of the system is focused to simulate how damage accumulates with time. It is a closed loop subsystem where the value of crack length is used to calculate at every cycle of simulation how much the crack length is increased following Equation 1 in the subsystem *Crack Growth.* The subsystem (in Figure 49) is composed of 3 other subsystems that measure 3 different parts of the equation and a fourth one that calculates if the crack is stable.

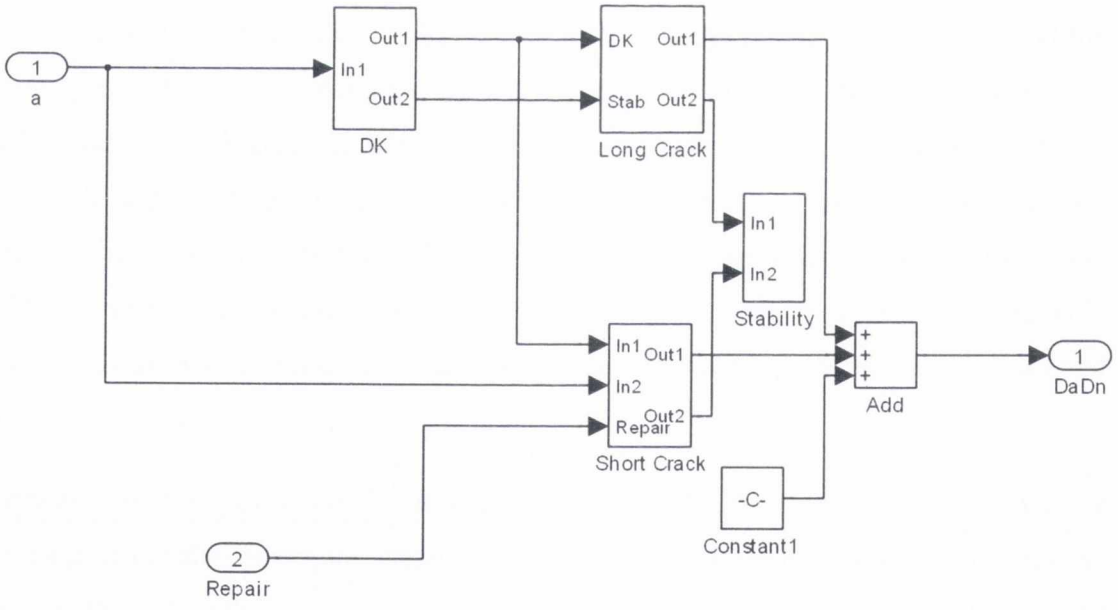

Figure 49. Subsystem: Crack Growth

The subsystems generate the value of ΔK, the long crack and the short crack behaviour and the *Add* block adds the last two together. The *Constant1* block adds a small growth independent of the crack length, to simulate any extra growth that cannot be predicted. The default value for this block is zero.

Layout of the simulator

The simulator's flow of information has been shown in Figure 36.

The value of crack length a is made by the contributions of the initial value a0, the repair and the growth by fatigue Δa. The value of broken processes (Bp) and the value of Δa are dependent on the value of a, closing the loop twice. In Simulink™ the system appears as in Figure 47

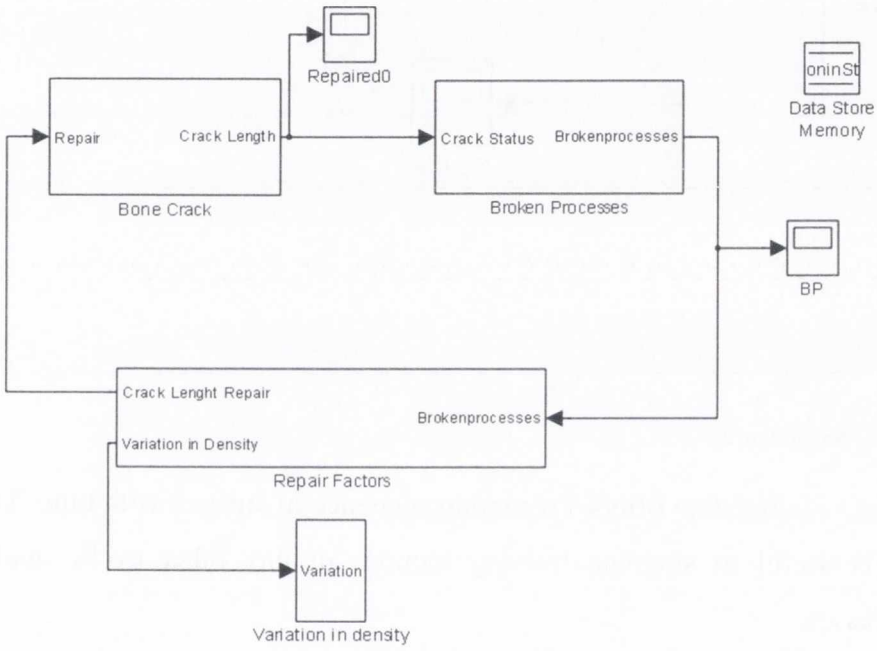

Figure 47. Main System

The system is a closed loop, the value of crack length calculated in the *Bone Crack* block is converted in a number of broken processes in the block of the same name; this number is changed into a repaired length of crack in the third block that reduces the value in the first block. The subsystem *Variation in density* analyzes the balance between bone removed and restored by the repair process and simulates the effects of this variation on the strength of the bone.

This subsystem creates a stress that has two alternating regimes, one with a low stress and another with a higher stress, and the presence of a single impulse of stress for a short time. Another possible stress subsystem is in Figure 52

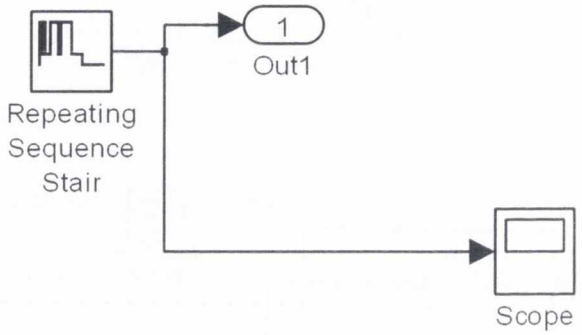

Figure 52. Stress Subsystem 2

This alternative subsystem offers a repeating sequence of stresses with time. This kind of subsystem is useful to simulate training regimes or any other cyclic application of different stresses.

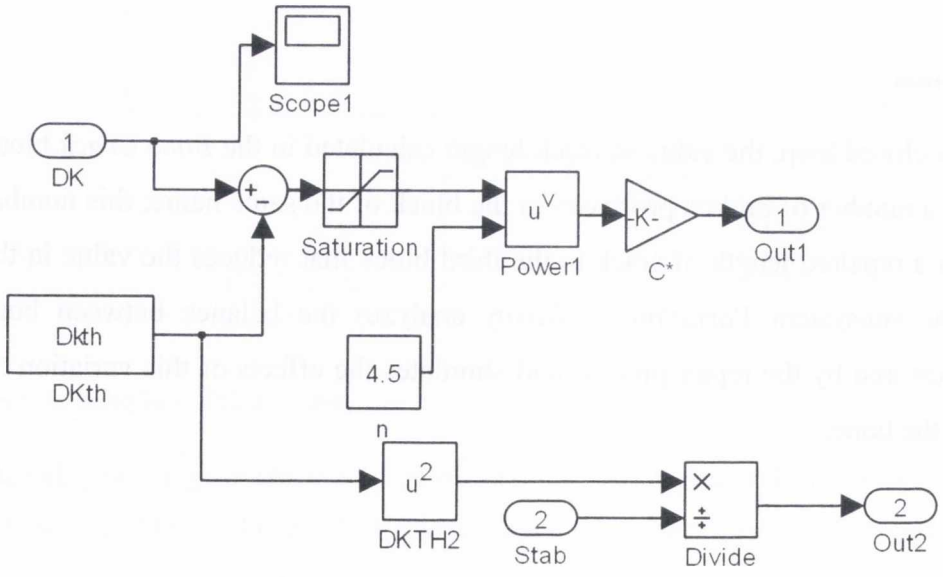

Figure 53. Subsystem Long Crack

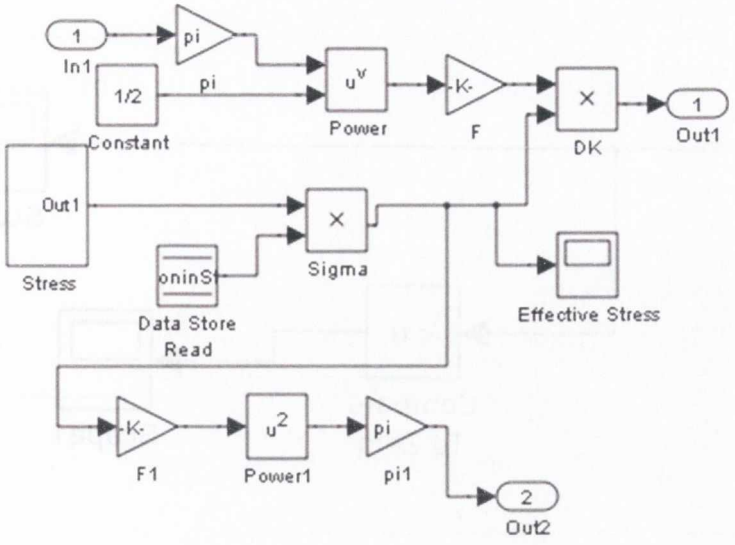

Figure 50. Subsystem: DK

The subsystem *DK* calculates the value of stress intensity range ΔK from the value of crack length and the stress. The blocks replicate the mathematical operations that compose the equation. The stress block can be either a simple constant or a subsystem in its own right. An example of stress subsystem is in Figure 51.

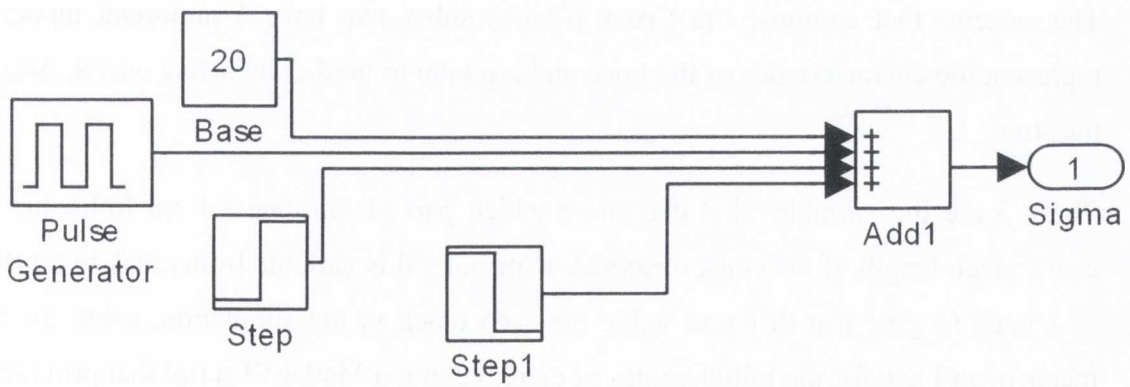

Figure 51. Stress Subsystem

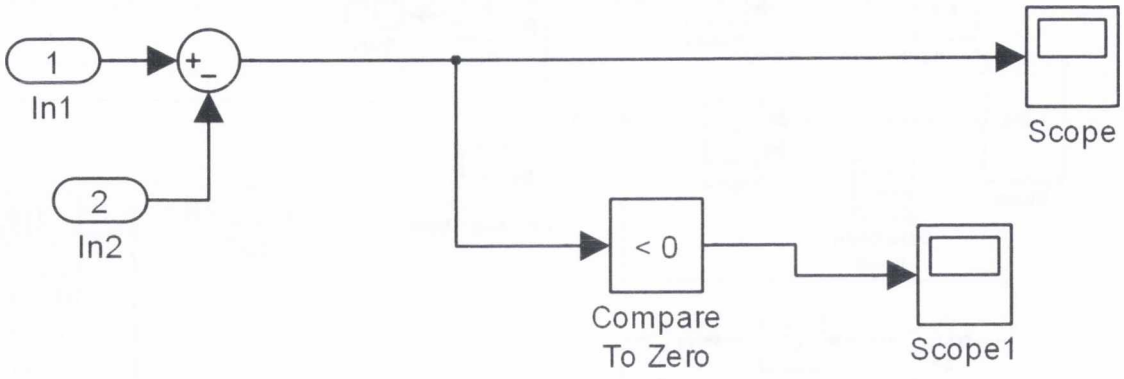

Figure 55. Subsystem Stability

The subsystem *Stability* is very simple as the two components of Equation 20 have been already calculated in the *Long Crack* and *Short Crack* subsystems. Here the two components are subtracted from each other and the relation between them is shown both numerically as the difference of the two values or as a logical TRUE/FALSE output after a comparison to zero.

The systems that compose the *Crack Growth* subsystem have 3 important inputs that represent the characteristics of the bone and are vital to predict its behaviour: d, ΔK_{th} and the stress $\Delta\sigma$.

These 3 are the variables that determine which part of Equation 1 I am following with every given length of the crack observed. Especially d is variable from crack to crack and so I need to give it a different value for each crack in the simulation, using the same mechanism I use for the initial values of crack length, a Matlab™ script that provides the values for all the different cracks using data obtained by experiments in the literature. Usually to obtain the distribution of d I have used the approaches shown Presbitero *et al* (39), either using data from fatigue tests or measuring directly the distance between osteonal barriers in images from microscopic analyses. ΔK_{th} on the other hand is a very delicate part of the equation; physically it represents the stress intensity needed for a crack to grow following the fracture mechanics equation, like a crack in a mostly

The subsystem *Long Crack* simulates the first part of Equation 1. The saturation block limits its outputs to positive values, giving an output of zero if the block input is negative, as required by the equation. The system calculates also one of the two components of the equation of stability.

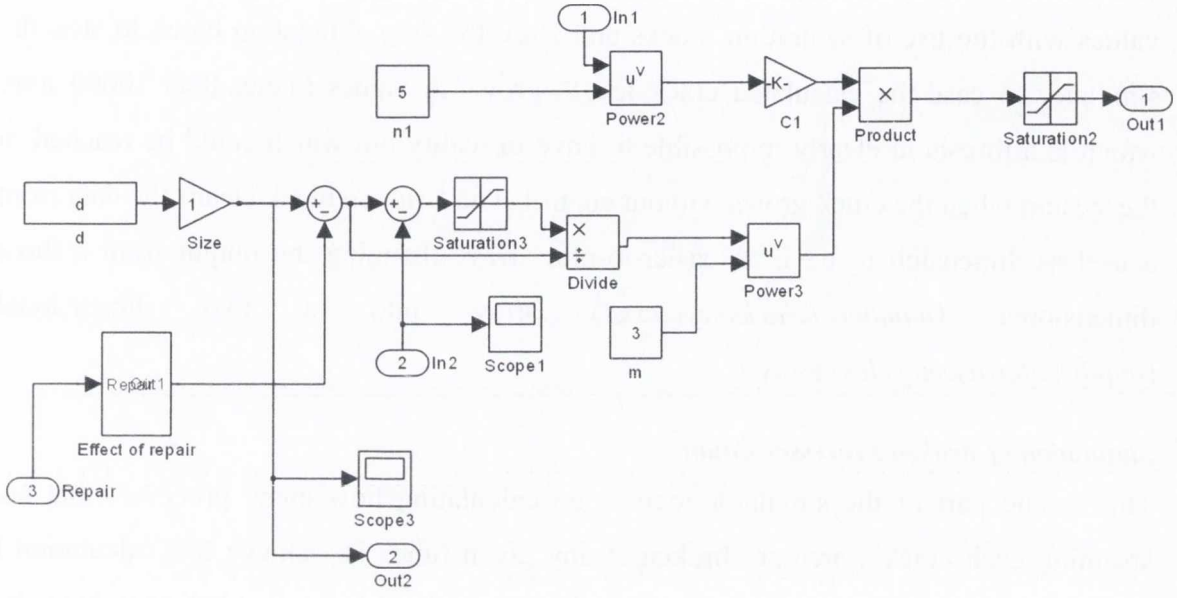

Figure 54. Subsystem Short Crack

This subsystem calculates the second part of Equation 1, which simulates the "short crack" behaviour of crack growth. The system has a saturation block to have only positive outputs and calculates also the remaining part of the stability equation. The output of the subsystem called *Effect of repair* is subtracted from the value of the input d to simulate the effect of bone remodelling in the case of incomplete crack repair (as will be explained more in detail in the paragraph on the effects of repair).

second, but it has the drawback of being a "hidden" property of the system, that cannot be immediately seen if you are not looking for it, so it is better to rely on this last method when starting a new simulation environment. Finally this part of the system has a couple of extra features done to avoid mathematical situations that represent physically impossible settings. I keep the values that are supposed positive from reaching negative values with the use of saturation blocks and I use the stop simulation block to stop the simulator in case the calculated crack length grows to values higher than 10000 mm, which is a threshold clearly impossible to have in reality but which could be reached in the system when the crack grows without control. The *Squeeze* block cleans the data from a useless dimension to have an easier-to-plot array, changing the output from a three dimensional (*numberofcracksxcyclesx1*) array into a two dimensional (*numberofcracksxcycles*) array.

Simulation of Broken Processes Count

The second part of the simulator focuses on calculating how many processes that are spanning each crack's area are broken at any given time. To achieve this calculation I convert in blocks the operations shown on the scripts that I have used before to have the same mechanics converted in a way that allows keeping the versatility of Simulink without any compromise on the quality of calculations.

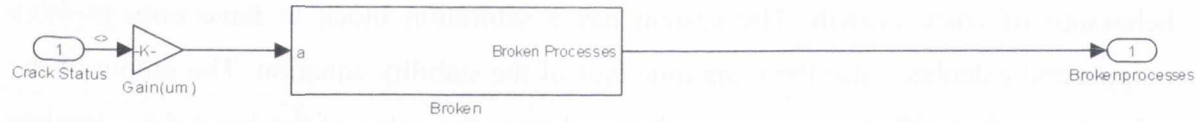

Figure 56. Subsystem BrokenProcesses. The only relevant block is the Gain(um) which converts crack length from millimetres to micrometres for unit coherence in the Broken subsystem

homogeneous material. In many studies I have found how the main factor of resilience of bone is given by the presence of osteons, so I can, with a good deal of approximation, interpret this value as a measure of the strength of the osteons to crack propagation. Shelton *et al*(37) reported a typical value for $\Delta K_{th} = 2$ for horses, this value has offered good results when applied in the simulation for bovine bone, suggesting than equine and bovine bone have similar behaviours. For human bones I have found the best adherence with experimental values with values around 1 (see results chapter), a value that is coherent with the values given for it in Taylor and Lee (32), where the authors gave ΔK_{th} a normal distribution of mean value 1 and variance 0.3.

$\Delta\sigma$ is the amplitude of the stress applied and the only parameter that affects the bone from the outside, as opposed to the other two that are intrinsic characteristics of the bone. This parameter can be applied as a non-constant value with time, as it is often applied in real life loading. As shown before, I can have a dedicated, albeit simple, subsystem to apply a load that can be as simple as a constant value or as complex as I want. Using a combination of step functions and pulse generator I can simulate an alternation of values able to reproduce the variation in stress that can be found in reality or to investigate the effect of rest.

Apart from the way of introducing these variables this section of the simulator has another important part, even if it is for addressing a weakness of the simulating program instead of a real biomechanical problem. After I calculate the increase Δa by integrating the output of the *Crack Growth* block, I have included a gain block called *Time Scale* that can multiply its results by a constant. In this way I can change the number of cycles of fatigue for every time unit of simulation (by default every time unit of simulation calculates a cycle of fatigue) and calculate in a single step the growth of several cycles of fatigue. This can be used to reduce the weight of computation when I need to simulate in the order of one million cycles or more by changing the number of effective calculations to a more manageable number. Opposing the benefits given by this technique, it also creates a linearity effect on the simulation, especially when the crack growth is in the "small crack" behaviour. This usually has the effect of increasing somehow the crack growth in this instance, increasing the crack size, while slightly downplaying the fast growth experienced in the second instance (long crack behaviour), but it is usually a negligible difference, provided that the factor used to increase it is not too high. An alternative method is changing the step size of the simulation, which is left to a cycle per

The subsystem replicates Equation 23 using the value of stress and crack length provided as input of the system and as result of the subsystem Crack Length.

Simulation of repair

The last part of the simulation applies the equations of system biology to predict the growth of a BMU able to restore the damage of the crack.

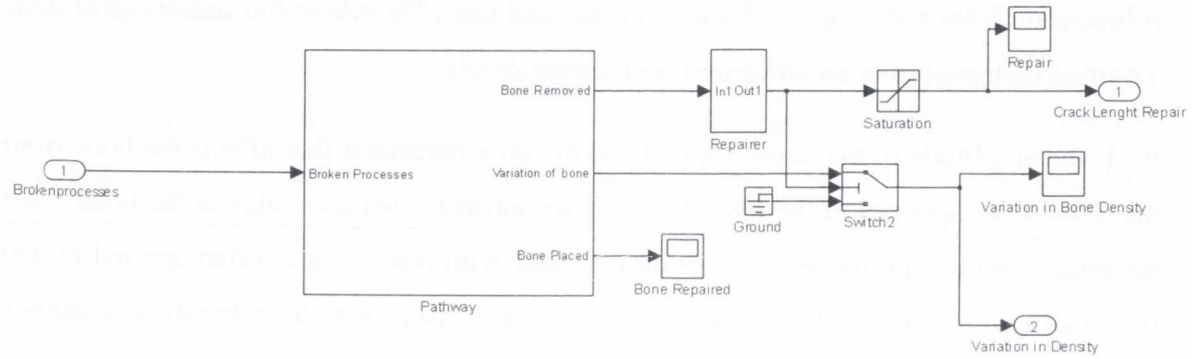

Figure 59. Subsystem Repair Factors

The subsystem is mainly composed of 2 systems: the Pathway that simulates the values of the actors in the BMU formation and the Repairer, which simulates the shape and movement of the BMU. The balance between bone placed and removed is the second output of the system, but it is sent to the appropriate system only when the BMU has reached its crack. To obtain the growth of osteoclasts and osteoblasts for every given crack I need to apply the pathway shown in Figure 44 using a subsystem representing the

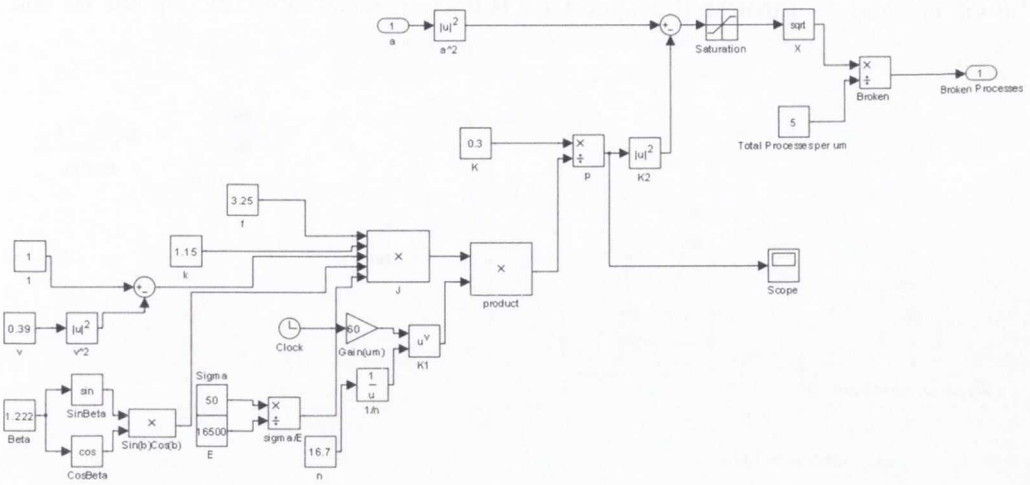

Figure 57. Subsystem Broken

An interesting extra feature of this part is the ability to calculate time using the clock utility of Simulink™ that allows for the simulation of fatigue effects on the processes without need for a new loop.

Simulation of mechanostat signal

Applying a different theory to our simulator is simple, for example to use the mechanostat model instead of the "scissors" model I only need to change the subsystem Broken with the subsystem Mechanostat shown in Figure 58

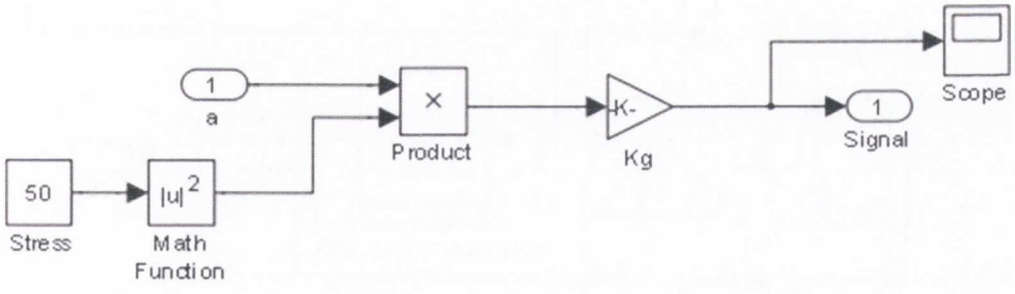

Figure 58. Subsystem Mechanostat

block is used to throttle the speed of RankL release with the speed of the simulator.

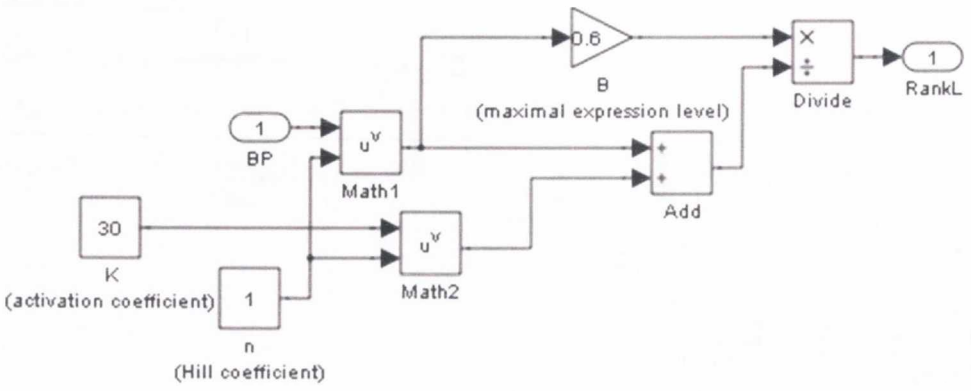

Figure 62. Subsystem RankL Generation. The shape of the subsystem is identical to the shape of all the subsystems in Reactions, as they all apply the same equation

The *RankL Generation* system is identical to the other systems that apply the equation of Hill, except for the coefficients, of course. The blocks are arranged to simulate the Hill equation.

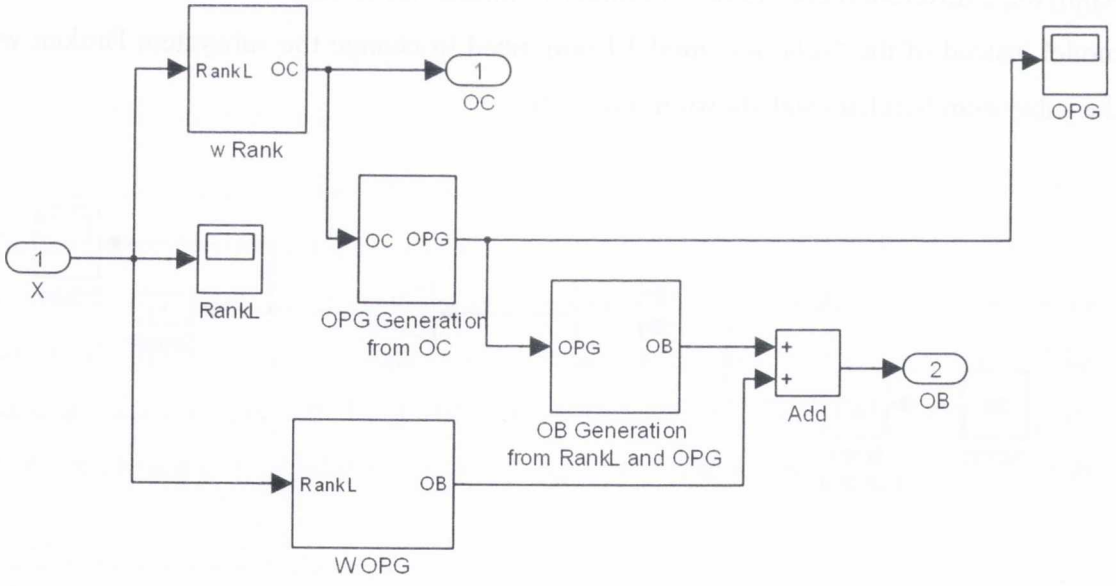

Figure 63. Subsystem Reactions

The *Reaction* subsystem is composed of 4 subsystems representing the other 4 Hill equations in the pathway. The shape of the model composed of these subsystems is that of a Feed Forward Loop (FFL), a network motif that is usually found both in engineering control theory applications and in system biology (70). An FFL is a motif where the first component of the pathway regulates both the end component and the intermediate

Hill equation for every reaction.

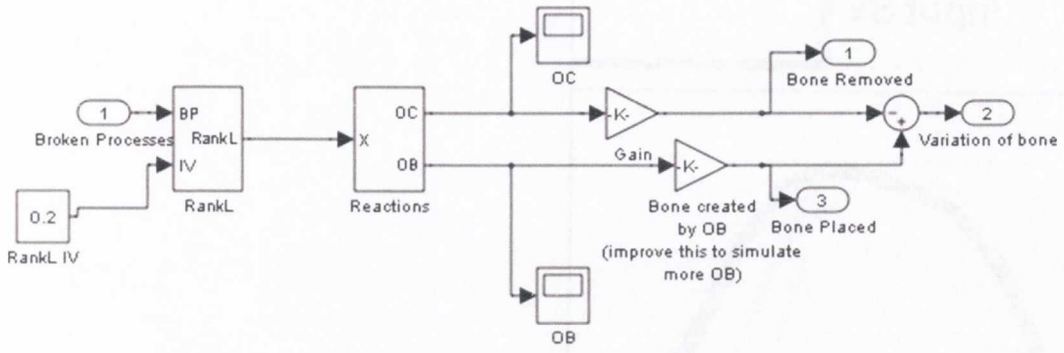

Figure 60. Subsystem Pathway

The subsystem Pathway is composed of a subsystem that replicates the formation of RankL because of damage (turning the Broken Processes input in a RankL output) and a subsystem that replicates the RANK-RANKL-OPG pathway, which turns the concentration of RankL in the values of osteoclasts and osteoblasts. The system then multiplies the values of osteoclasts and osteoblasts for the size of these cells, to have the amount of bone removed by osteoclasts and restored by osteoblasts. The difference between these two values is the variation of bone caused by the BMU.

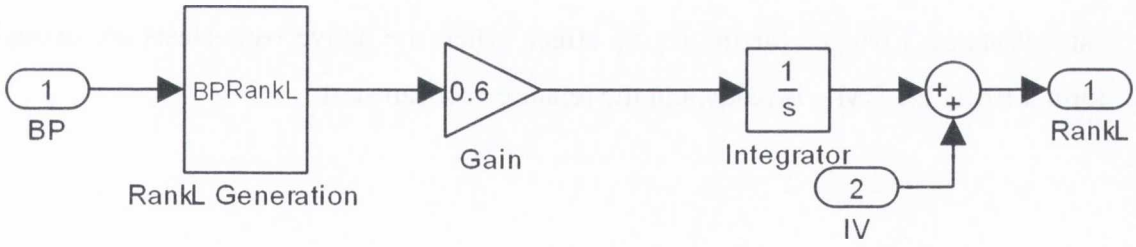

Figure 61. Subsystem RankL

The *RankL* subsystem applies the Hill equation to the number of broken processes that acts as an input (in the *RankL Generation* subsystem) and then integrates the result to have a value that varies with time (applying only the Hill equation would leave the RankL value to a level constant with the number of broken processes, contradicting the results in Mulcahy *et al* (54) that clearly show that RankL grows with constant damage). The gain

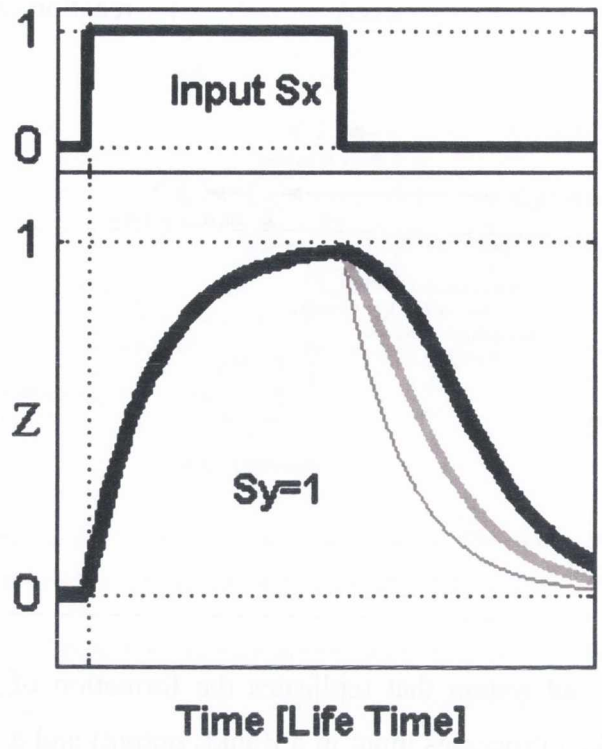

Figure 65. Graph of the reaction of a Feed Forward Loop to a step input. Notice how the negative step (or "brake") has a delayed reaction from Z. This is the reason the OR FFL is so common in repair processes. Adapted from Alon (70)

Applying the pathway allows the system to provide the number of active osteoclasts knowing time and the number of broken processes for every crack. As I know that the BMU is first formed and then moves to reach the crack I can use the number of osteoclasts as a trigger for the repair effect, when the active osteoclasts are enough to form a BMU the BMU is ready and the repair effect can start.

component that regulates the end component too. In this case the shape is a bit different than the standard FFL (see Figure 64) as the first component (RankL) does not directly regulate OPG (that regulates osteoblasts together with RankL) but regulates osteoclasts that regulate OPG.

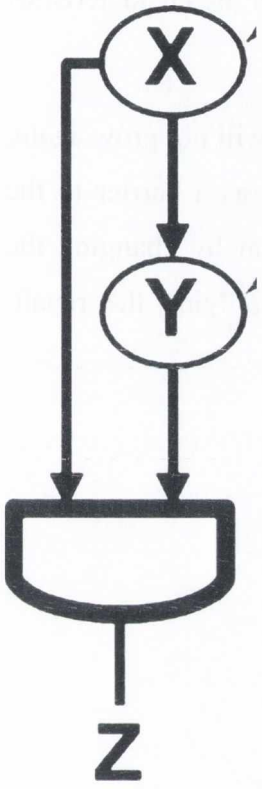

Figure 64. Feed Forward Loop. The FFL can be either of the OR type, when Z requires either X or Y to be active to be active, or of the AND type, when Z requires both X and Y to be active. When it is regulating a repair effect, the FFL is usually an OR type. Adapted from Alon (70)

The FFL makes the pathway signals act like there is a delay on the interruption of the reaction, making so that, even if the starting event (in this case, the RankL release) stops, the reaction will continue producing the last effect (the osteoblasts) until all the pathway components have been used, making the effect more "robust" against variations, exactly as it is needed for a repair process (see Figure 65).

Other effects of crack repair

Apart from the above mentioned effect of repairing the crack, the bone has extra effects from the repair process and the system has been able to replicate some of them. The effects are both local and global. Locally the repair has created a new section of bone that has a very low probability of further crack in the short period and globally the balance of bone mass removed by osteoclasts and replaced by osteoblasts affects the characteristics of the bone either improving or worsening them.

The local effect of repair makes so that if a crack has been repaired it will not grow again, even if the crack wasn't repaired completely, as the new bone acts as a barrier to the growth of the remaining crack. This has been applied to the system by changing the parameters for the area of bone represented in the array after applying the repair.

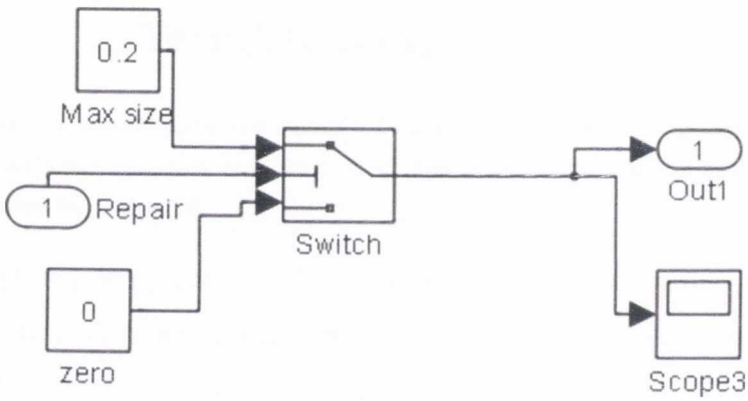

Figure 67. Subsystem Effect of Repair

By changing the value of d in the Equation 1 I can simulate the repaired bone's increased resilience without excluding the possibility of a crack growth with an eventual increase of stress. The subsystem *Effects of Repair* regulates this reduction of the factor d by applying it in the moment the osteoclasts have finished removing bone, simulating the variation in the histological structure in the area of the bone that is being remodelled.

To simulate the global effect I can use the data that I get by simulating the activation of the BMU to have the balance of bone removed by osteoclasts and applied by osteoblasts,

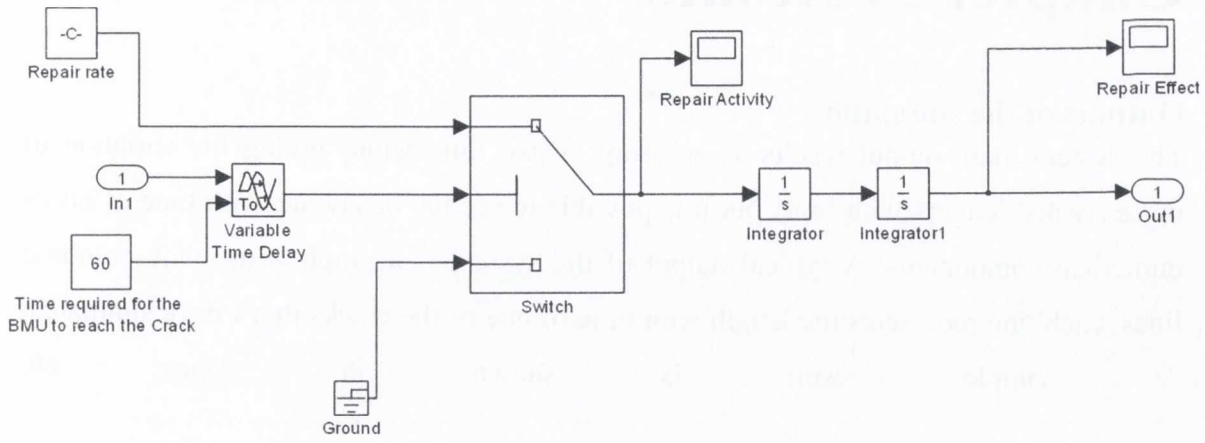

Figure 66. Subsystem Repairer

The repair effect can be simulated imagining the BMU as a round eraser deleting the old damaged bone and restoring it with new bone. This simplification is not too far from reality (BMU images have shown an overall round shape) and allows using a simple quadratic equation to simulate how crack length is reduced by repair. I have given to this round shape a cross section value of 200 μm at 100 μm of penetration in the crack. So applying the equation of a conical section to the values of r(t0)=0 and r(tf)=200 where t0=0 and tf is the time when the BMU has penetrated in the crack by 100 μm (100/40=> tf=2.5days) I have, among the other possible solutions, Equation 25:

$$r(t) = 32t^2$$

Equation 25. Crack erasing by BMU.

Equation 25 is easy to implement in the system as it can be obtained by integrating a constant value twice. In *Repairer* I have regulated the effect of the BMU by activating it via the switch only when the number of osteoclasts is enough to create a BMU (as the BMU is 200 μm large and osteoclasts are 40 μm in diameter, the number of OC necessary to create a BMU is easily calculated). The effect of the BMU on crack length is also delayed by the time required for it to reach the crack, which is 5 days (1). It should be noted how the crack continues growing even if it is been repaired. This can create some problem with the larger cracks as it will be shown in the following chapters,

Chapter 5: Results

Outputs of the simulator

The system main output results as an array in two dimensions giving the variation of these cracks' lengths with time, but it is possible to see the behaviour with time of all its numerical components. A typical output of the system is a graph with many coloured lines; each line represents the length with time of one of the cracks that I have simulated. A sample result is shown in Figure 69.

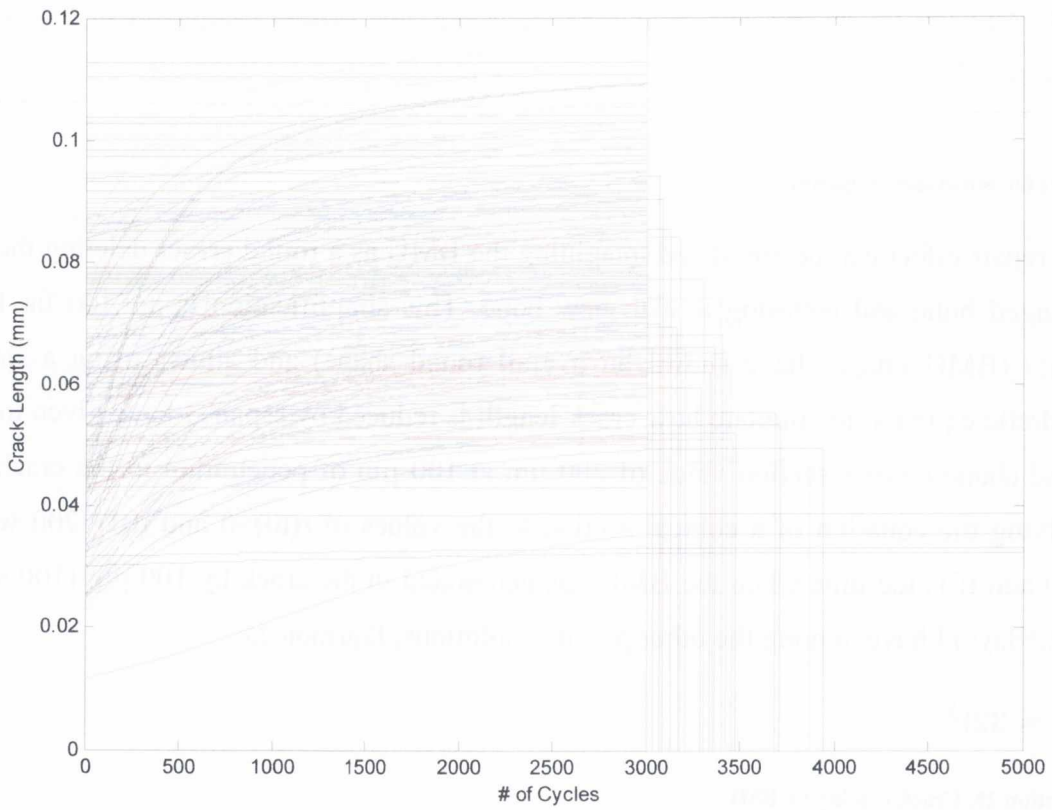

Figure 69. Results of simulation. Each line represents the value of crack length for a single crack during the simulated experiment's time. It can be noted how cracks are repaired in order of size and how the smaller cracks do not get repaired, as they do not show enough signal for the cells to activate a BMU. In the simulations done with the mechanostat signal theory all cracks get repaired, as the signal has no minimum damage thresholds, but the time required for a small crack to be repaired can exceed the simulation time.

The typical result shows how the cracks are repaired in order of size and how some of the cracks are not repaired at all because they are too small to be a danger. If one crack brings the bone to failure the plot becomes different, as the crack that grows without control is much bigger that the others, so the image shows only one crack because the others are too

this balance can be translated in a variation of strength of the bone.

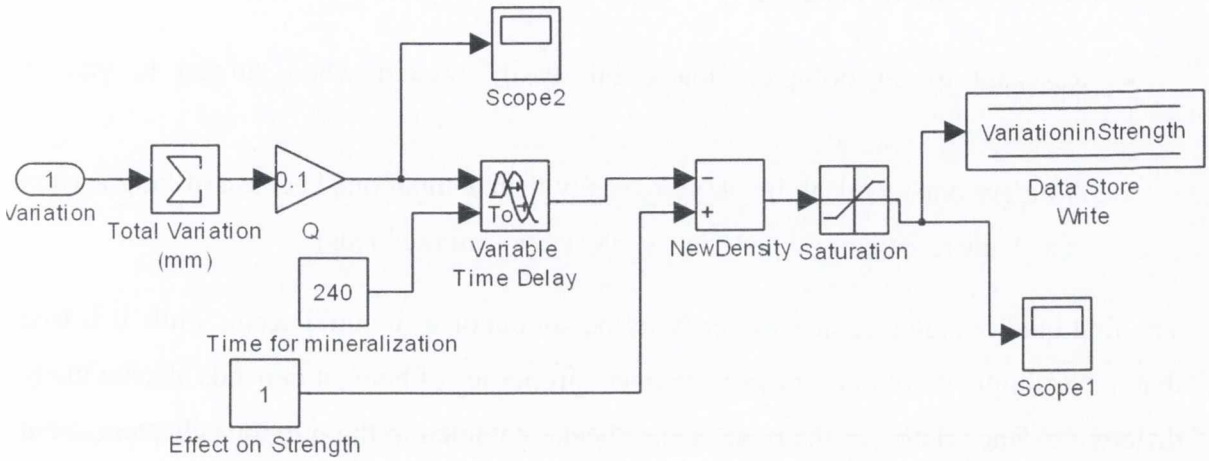

Figure 68. Subsystem Variation

In the subsystem *Variation* I apply the variation of bone strength by increasing the stress applied by a factor proportional to the amount of bone created or removed by the remodelling process after the time required for mineralization (10 days, according to (1)) has passed from the BMU action. The variation of stress is written in model-wide data storage, this way it can be applied in the *DK* subsystem in the other part of the system without even if they aren't directly connected to this block.

system that simulates the behaviour of bone without effects of repair. This is the part that can be more easily compared to literature, as analyses on dead bone are by far the most common and easiest to do.

Qualitative properties of bone are:

- Resistant to physiological loads, but easily broken when subject to greater stresses.
- A bigger bone tends to break more easily than a small one because of fatigue (this is a characteristic of all materials subjected to fatigue loads).

The first quality is not as easy to verify in the simulator as it could seem, while it is true that it is a simple definition of the mechanical properties of bone, it depends also on many different characteristics of the bone, as has been explained in the previous chapters about the stability of cracks. In that chapter it was shown how a risk factor for the crack can be predicted by observing the relationship between the constants that define Equation 1. Looking at Equation 20, I can see how it changes with stress at the power of 2. This means that as the stress grows and given a distribution of the values of ΔK_{th} and d, the probability that the relation is verified and so that a crack is unstable grows fast, as can be seen in Figure 71 and Figure 72, which show the distributions of the two parts of the relation graphically for 20 and 80 MPa. The area sustained between the two curves of stability limit distribution and d distribution shows the probability that one crack is inherently unstable, or the percentage of cracks that are unstable given the distribution of d and the stability limit at a given stress. By looking at the two images is clear how the differences between the two levels of stress are evident: in the simulation at 20 MPa the area sustained between the curves is almost invisible, while for 80 MPa the number of unstable cracks is a sizable percentage of the total. This difference shows how the system is highly sensitive to stress.

small to appear in scale. Equation 1 predicts a fast growth, so the simulated crack can grow to unrealistic values (in the order of meters) in a few cycles, even if the system is instructed to stop when crack length exceeds a security value. This can be solved by plotting the data on a logarithmic scale for the crack length. By changing the scale from linear to logarithmic and changing the y axis scale also the other cracks can become visible as shown in Figure 70.

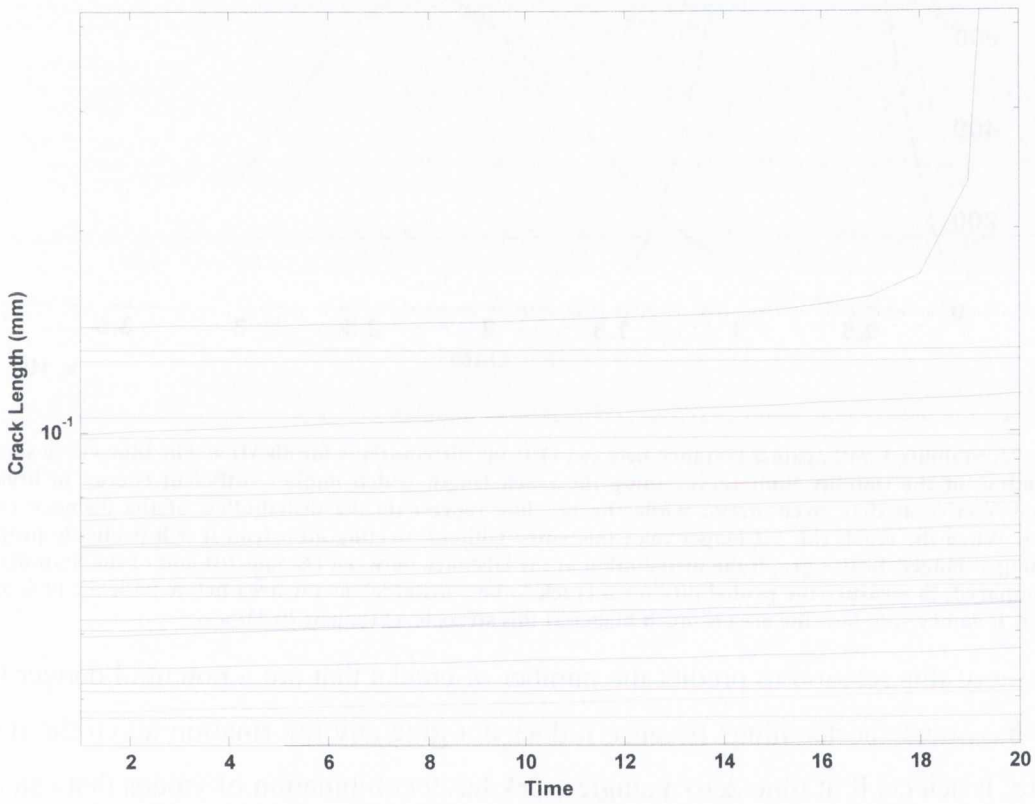

Figure 70. Crack Failure on a logarithmic scale. I have removed some of the cracks to increase visibility. It is easy to see how the crack growing to failure is only one, while the other cracks do not show a comparable growth.

Similar plots can be obtained for every variable in the system, like the number of broken processes or the levels of any actor in the repair process.

Simulation of crack growth in fatigue tests

To assess the capabilities of the simulator I need to see if its behaviour is consistent with the properties that are known of the target I am going to simulate. In this case the target is a given section of the bone so I need to confirm that the behaviour of the system is similar to that of a bone section. The first thing I can start to verify is the first main block of the

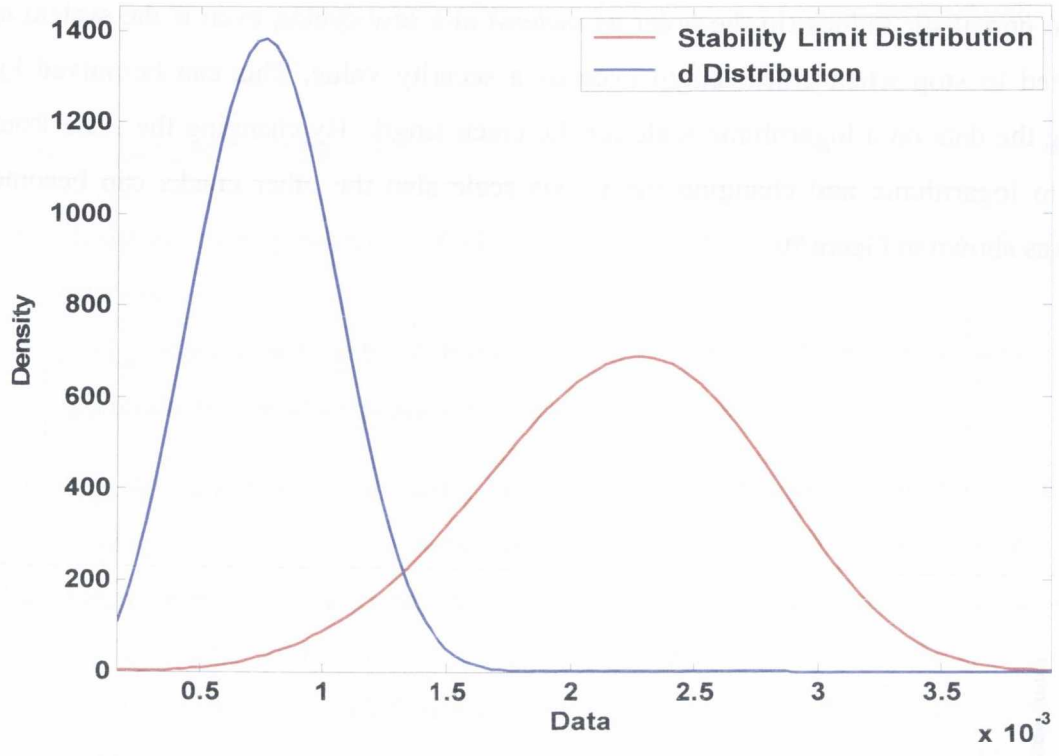

Figure 72. Stability Limit against Distance between Osteons distributions for 80 MPa. The blue curve shows the distribution of the stability limit representing the crack length which implies sufficient energy to breach an osteonal barrier at that given stress; while the red line represents the distribution of the distance between osteons. When the crack can get longer than this value without meeting an osteon it will probably propagate, becoming a danger. In this graph the distribution of the Distance between Osteons (d) and of the Stability Limit are compared, to measure the probability for a crack to be "unstable" as the area below both the blue and the red line. It can be seen how the area is much bigger at this stress level than at 20 MPa

The use of this relation to predict the number of cracks that are a potential danger to the bone has some shortcomings because it does not give any information about the time of failure: it detects if at time zero a single crack has a combination of values that can allow a fracture, but if during the time between the start of the simulation and the possible crack some of those values change because of other effects (for example an improvement of the bone strength) then the crack could not cause a failure. The opposite is also true, giving the possibility of a false negative. The simulation returns that the probability of unstable cracks for bovine bones at 80 MPa (shown in Figure 72) is equal to 0.1596, meaning that the stable cracks are 84%. This agrees very well with results by Taylor and Lee (32) where the number of "dormant" cracks found in the experimental data from O'Brien *et al* (34) on the same type of bone at 80MPa is 85%.

The second quality is justified by the nature of fatigue damage that accumulates itself in the material as a discrete number of microcracks; every crack has a probability to grow to failure, so it is a logical conclusion that bigger samples with the same crack density have

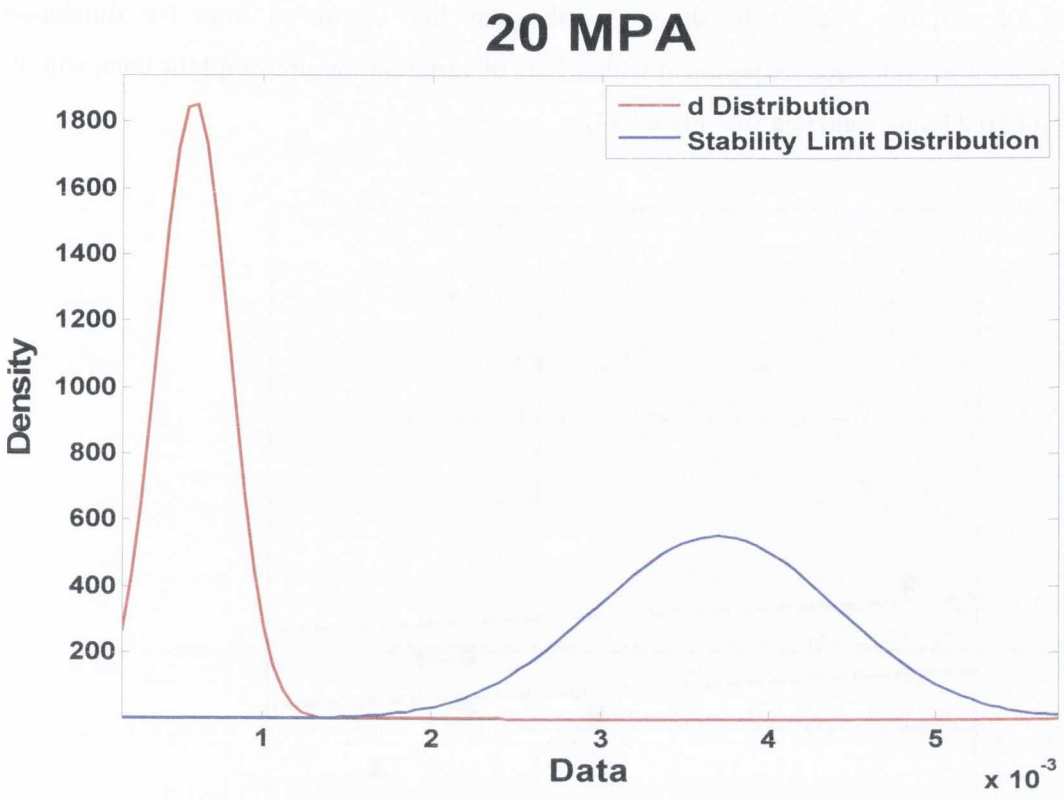

Figure 71. Stability Limit against Distance between Osteons distributions for 20 MPa. The blue curve shows the distribution of the stability limit representing the crack length which implies sufficient energy to breach an osteonal barrier at that given stress; while the red line represents the distribution of the distance between osteons. When the crack can get longer than this value without meeting an osteon it will probably propagate, becoming a danger. In this graph the distribution of the Distance between Osteons (d) and of the Stability Limit are compared, to measure the probability for a crack to be "unstable" as the area below both the blue and the red line, as can be seen at this stress level the area (and thus the probability of an unstable crack) is almost zero.

function of volume. The results show how the blue line calculated from the simulations approximates the results from experiment with a 20% of variation for almost all the data, with the exception of old human and dog (see Figure 74)

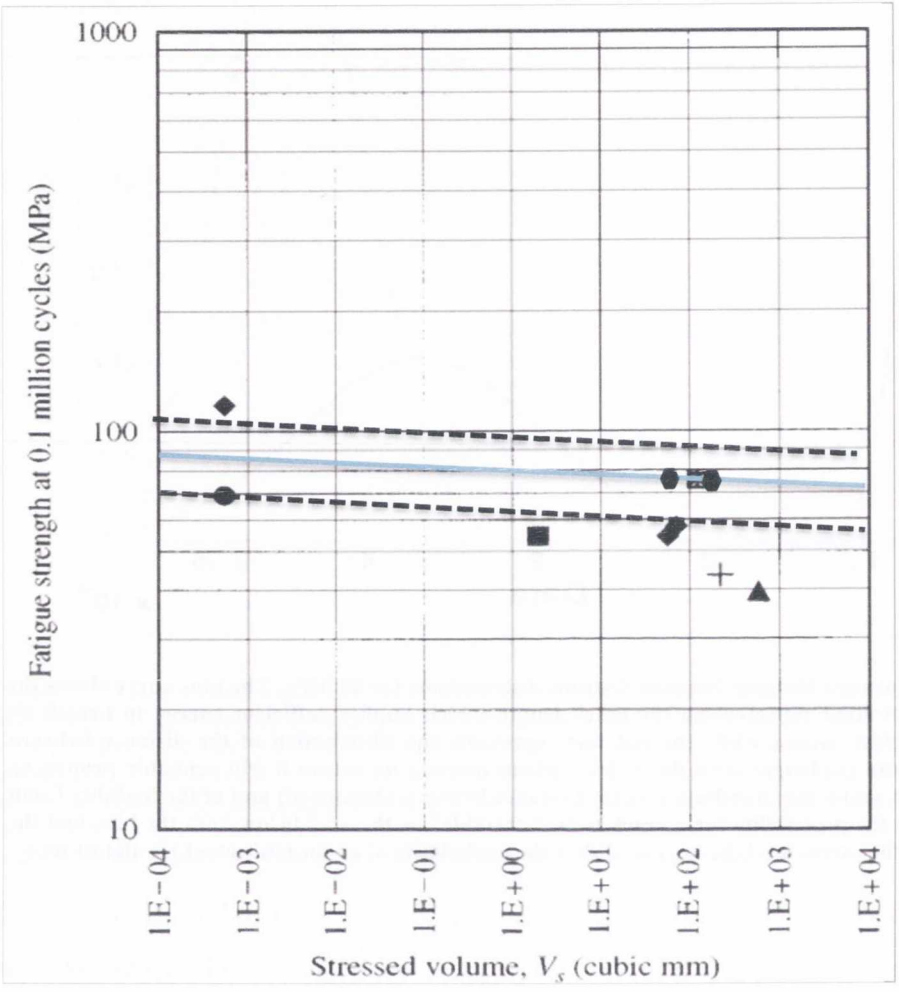

Figure 74. Experimental data on the fatigue strength of bone from different animals plotted as a function of the stressed volume of the bone or sample from Taylor 2000 (38), compared to the results of the simulation from figure 90. The blue line represents my prediction with the two dotted lines showing a ±20% variation from the prediction. The points represent the experimental data for mouse (●), rat (■), dog (▲), old human (♦) and cow (✱). The two hexagons are the points obtained by the simulation.

To verify the efficiency of the simulator in predicting crack growth by fatigue, I can use as reference the results of fatigue tests performed on bones. These results are readily available in the literature, where they have been obtained in controlled environments with simple distributions of stress applied to the bones and usually come with a study of the initial condition of the bones, which simplifies the research of the same parameters for the simulator. It is not possible to analyze the status of a bone before and after the fatigue test, as the cracks are situated inside the bone and they aren't visible unless it is cut,

a larger probability of failure simply because of a higher number of cracks. To simulate this effect in the system I have done a number of simulations keeping all other values as constant as I could but varying the number of cracks I are observing. I have counted the number of cycles to failure in all these cases and obtained a distribution of those both for the small bone (with the least number of cracks) and the big bone. The results are below and show how with a large bone the cycles to failure are less than those observed for a smaller bone.

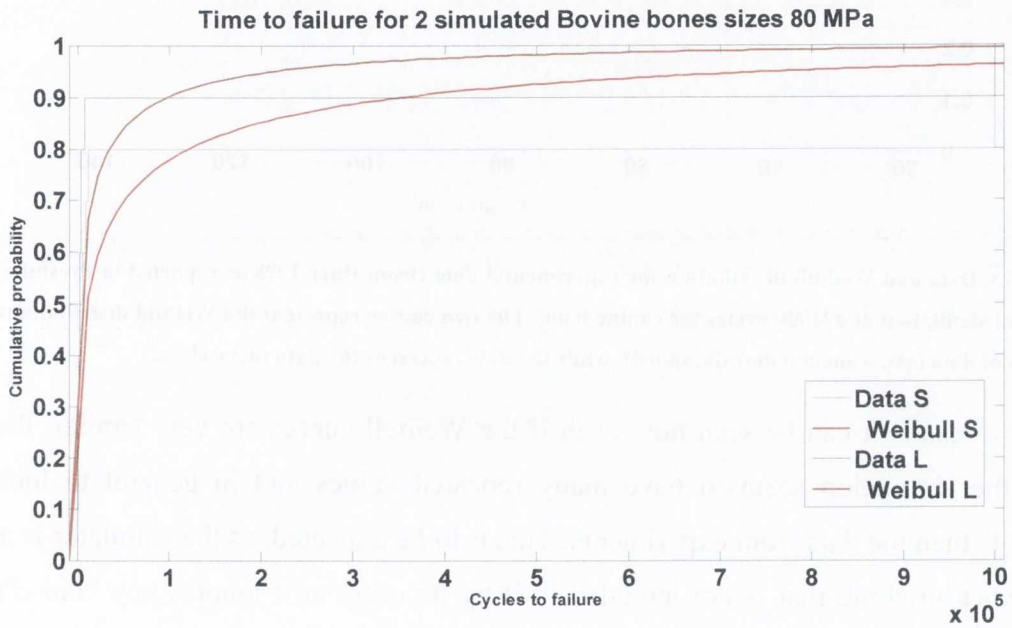

Figure 73. Distribution of failure times for large and small bovine bone. The small bone data show an increased probability of long life compared to the bigger bone.

These results can be verified by comparing them to those in a paper from David Taylor written in 2000 (38). In the paper the experiments proved that the probability of failure of a bone changes with its volume following Equation 4

From the simulation I have the cumulative probability of failure at 0.1 million cycles of 0.9 and 0.78 respectively for the large and small sample; the two values are in a ratio of 1.15 while the two volumes are in a ratio of 2. To compare the results with Equation 4 I applied the equation for the two volumes using the constants m, V_{so} and $\Delta\sigma_0^*$ as written in the Taylor 2000 (38) and in Taylor & Kuiper (42). I have found a ratio between the probabilities of 1.22, with an error from my part of 0.06, an acceptable degree of error. To compare this prediction to the experimental value from Taylor 2000 (38) I can use the results from the simulator to calculate the fatigue strength of the simulated bone as a

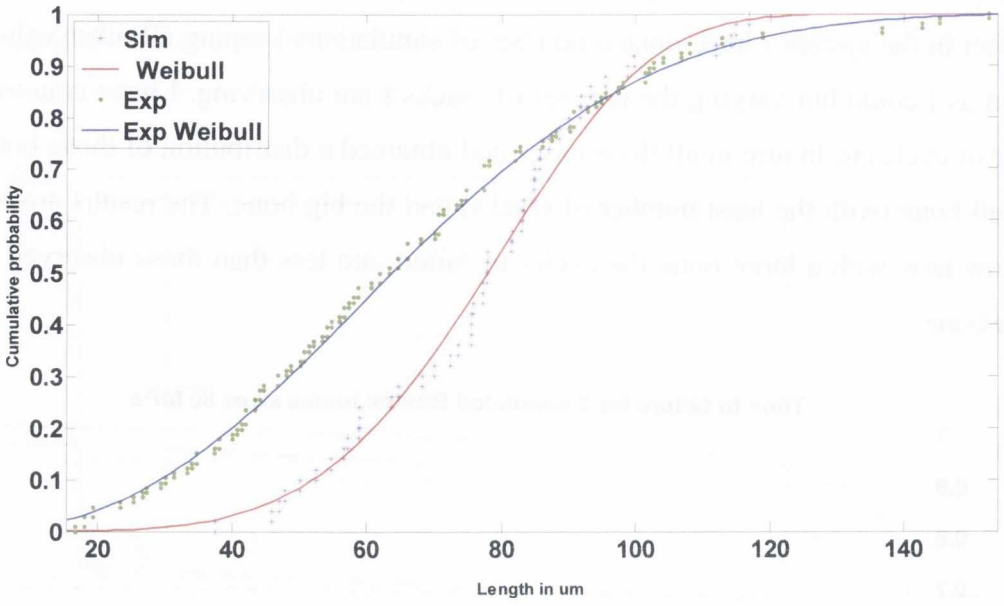

Figure 75. Data and Weibull distribution for experimental data (from Burr 1998 as reported in Presbitero, *et al* (39)) and simulation at 426000 cycles for canine bone. The two curves represent the Weibull distributions of the two sets of data (experimental and simulated), while the dots represent the data themselves.

In these results it can be seen how even if the Weibull curves are very similar, the data from the simulation seem to have many repeated values and in general to look less "varied" than the data from experiments. This is to be expected, as the simulator is unable to predict anything that is not included in it by its user, so it ignores any "noise"(as in unexpected input) in the real application. Anyway the similarities in the distribution prove that these differences are not statistically relevant.

The results of the simulation and their Weibull distributions have been compared to all the experimental data reported by Presbitero *et al* (39) and the collection of all these results has been written in Table 4. As said before, there is usually less variability in simulation that in real life and this, in this case, translates itself into a different value for the β parameter (the shape parameter). The use of a distribution of values for the d parameter of the simulation reduces greatly this difference. In the Table 4 I have also reported the value of a where the cumulative probability is 0.9: comparing this value gives a good measure of how much the simulation is approximating the distribution in experiments. The results show how the use of an average value of d in the simulation improves the accuracy, but also how in the 50000 cycles simulation, even with the distribution of d the results do not improve. This is probably caused by the linearization effect mentioned in the previous chapter, whose effect is clearly more evident when

which is an unrepeatable and destructive process. But I can take the data obtained from *in vivo* bones and obtain the statistical distribution of their values, to simulate the results that I can obtain with the system from an input that follows the same distribution. After obtaining a statistical distribution of the end values for loaded bone I can compare it to the values obtained by the experiments. The distribution that was shown to be the most suited to replicate the distribution of microcrack length in bone is the Weibull distribution (39)(38)(42). The Weibull distribution is very flexible and can have a large variety of shapes varying its coefficients. For this study I make use of the cumulative distribution of Weibull which is:

$$F(a) = 1 - \exp\left[-\left(\frac{a}{\vartheta}\right)^{\beta}\right]$$

Equation 26. Weibull equation,

By setting the system accordingly I can obtain the values of the crack lengths at the time when the physical experiments end by observing the output file at the specified time. I have used the data from experiments recorded in Presbitero *et al* (39) to obtain both the initial and final condition of those sets of data. These values can then be uploaded in Matlab™ to fit them into a distribution to compare to the distributions calculated on the experimental values. Using the distribution fit module of Matlab is possible to generate the curves representing the Weibull distributions which better approximates the experimental values and the results from our simulator, these two curved can then be plotted, offering a graphical comparison of the similarities between the results and the experiments. A few examples of these comparisons are shown in Figure 75.

Table 4: Results of the simulation compared to experiments. The simulations are characterized by a darker hue in the table.

Species	Bone type	β	θ(μm)	a (μm) (P=0.9)	Error	Stress	Number of cycles	References
Canine	Femur, radius	3.2	69.7	90.1	n/a	*In vivo*	*In vivo*	(Burr 1998; Gellasch 2002)
Bovine	Tibia	3.1	88.9	116.9	n/a	*In vivo*	*In vivo*	(O'Brien 2003; Presbitero *et al* 2012)
Canine	Femur	3.1	78.5	102.8	n/a	2600 με	426000	(Burr 1998)
Canine	Femur	4.6	84.4	101.1	0.01	2600 με	426000	Simulation with random values of d
Bovine	Tibia	2.7	101.6	137.9	n/a	70 MPa	50000	(Presbitero *et al* 2012)
Bovine	Tibia	7.6	108	125	0.1	70 MPa	50000	Simulation with average value of d
Bovine	Tibia	2.2	108.7	158.5	n/a	80 MPa	50000	(O'Brien 2003)
Bovine	Tibia	2.67	133.5	182.5	0.13	80 MPa	50000	Simulation with random values of d
Bovine	Tibia	2.3	126.0	180.0	n/a	70 MPa	Million cycles	(Presbitero *et al* 2012)
Bovine	Tibia	5.2	139	174	0.03	70 MPa	Million cycles	Simulation with average value of d
Bovine	Tibia	2.0	129.4	198.5	n/a	80 MPa	88000	(O'Brien 2003)
Bovine	Tibia	21.0	130.8	136	0.31	80 MPa	100000	Simulation with average value of d
Bovine	Tibia	2.63	137.2	188.9	0.05	80 MPa	100000	Simulation with random values of d

applied to a simulation with a smaller number of iterations as I have kept the time scale constant, which has caused the shorter simulations to be excessively fractioned.

As said in the previous chapter the system is composed of different subsystems that simulate different parts of the process of crack growth and repair. One advantage of this approach is the ability to isolate subsystem to observe the behaviour of different parts of the process that is used to simulate the crack behaviour. To prove this ability I have compared the behaviour of crack growth rate with stress intensity range shown by Kruzic *et al* (33) and the same behaviour reproduced by the appropriate part of the simulator. The results show how experimental data for long cracks are included in the range of results of the simulator for long cracks (Figure 77).

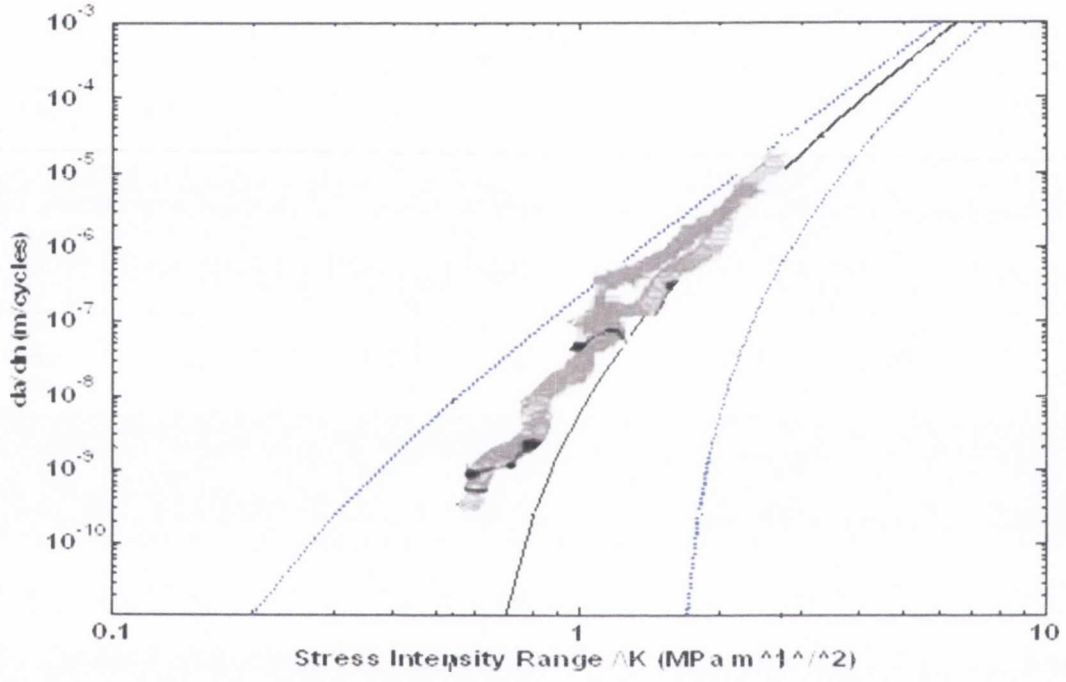

Figure 77. Simulation of crack growth rate with stress intensity range for long cracks. The two dotted lines represent the values of average $\Delta K_{th} \pm 1.5$ times the standard deviation and the gray area is composed from the reference points from Kruzic *et al* (33)

Because the short crack behaviour depends from three variables (ΔK, a, d), while the long crack behaviour depends only from two (ΔK and ΔKth), the results for short cracks need to be plotted in multiple images to be reproduced in two-dimensional images. Another problem for the simulation of short crack behaviour as function of ΔK is that ΔK varies with stress and with crack length (equation 32) and because of this I should know in advance the crack length of each point to calculate the stress applied. In Kruzic *et al* (33) the stress intensity range is calculated by measuring the surface stress the crack length, while the crack growth rate is given by the crack length divided by the number of cycles of fatigue the specimen has sustained before the crack was measured. As both the crack

An interesting application of the system shows how, because of the osteons acting as barriers stopping crack growth, the initial value of cracks is not as important to the end result as it could initially seem. To observe this effect I have created a simulation that shows the behaviour of a bone where all the cracks are initially of the same length (20 um) but the distances between the osteons for every crack are still randomized. The simulation shows how the cracks grow with different curves because of the different amounts of space available to them. The top crack shows an almost unrestrained growth, even remaining in the "short crack" behaviour, until it reaches almost 150 μm of size, where finally its growth starts slowing down. Observing the input of the system it can be seen that the top crack is regulated by a value of the parameter d=180 μm, which means that the crack has a relatively large length to reach before meeting an osteon, while all the other cracks have are smaller values for the same parameter that implies that they will meet an osteon relatively soon, explaining their slow growths (Figure 76).

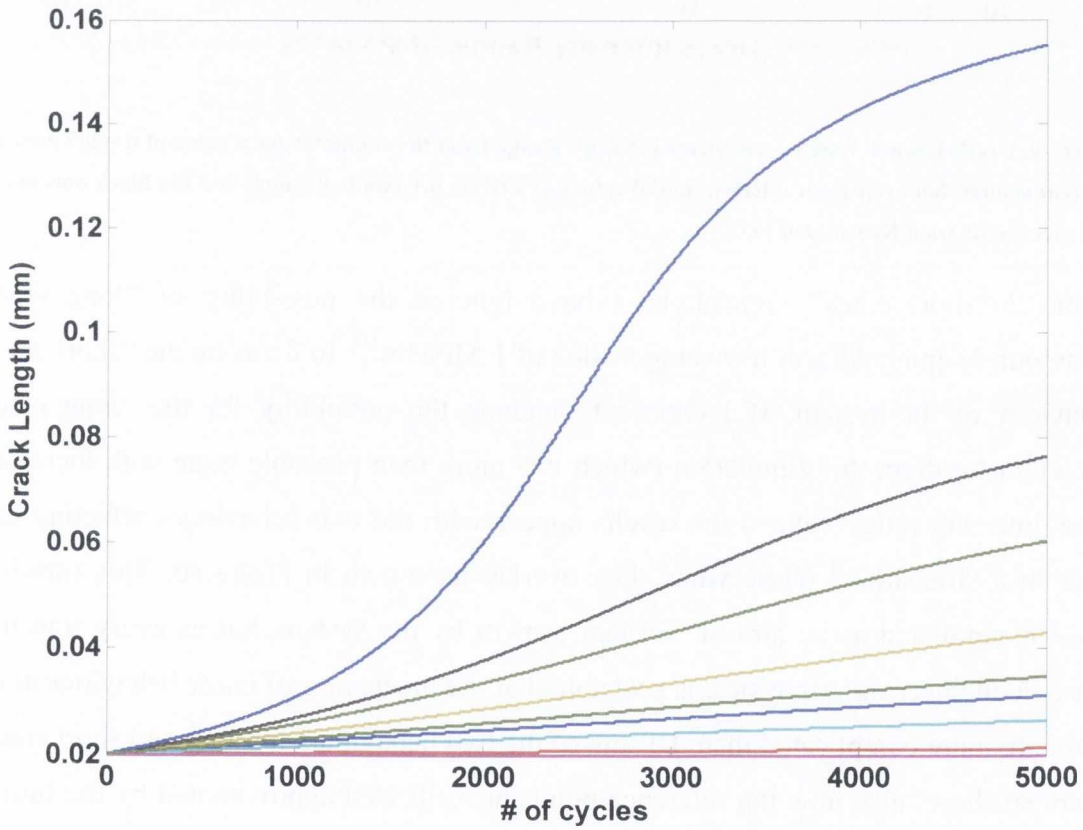

Figure 76. Different behaviours from the same initial size. The plot shows how even with the same initial value the cracks grow differently based on how much space they have to grow. It shows also how the crack growth tends to be small at first, then as the crack grows the growth rate increases until it slows when the crack tip is approaching an osteon, which usually blocks the crack growth.

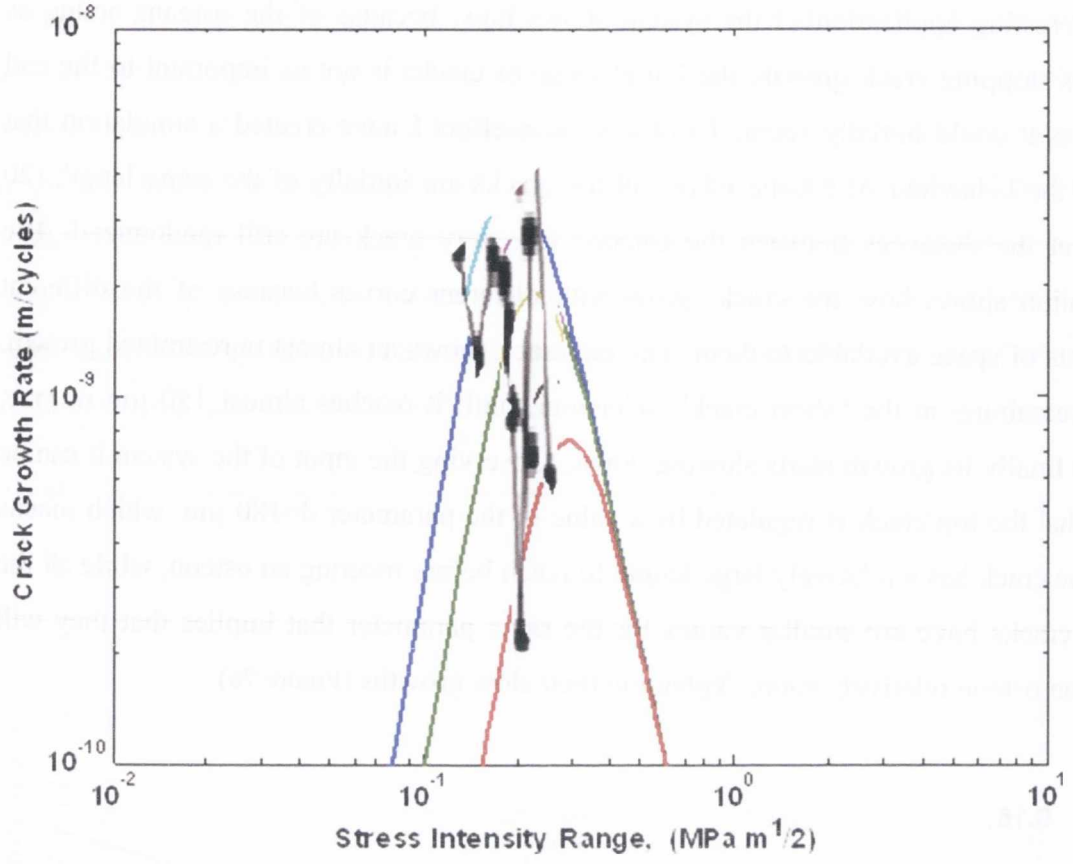

Figure 79. Crack Growth Rate versus Stress Intensity Range from the simulator for a value of d = 0.5 mm. The different colored lines represent different initial values of a (from 0.1 mm to 0.3 mm) and the black dots are the reference points from Kruzic *et al* (33)

In the 2 "short crack" simulations I have ignored the possibility of "long crack" behaviour, keeping ΔK_{th} at its average value of 1 MPa*$m^{1/2}$, to focus on the "short crack" behaviour of the system. If I choose to include the possibility for the "long crack" behaviour to affect this simulation (which is a more than probable issue with increasing stress intensity range values) the results appear with the two behaviours affecting each other in a "transition" phase when they overlap as shown in Figure 80. This transition phase is simulated as an almost constant growth by the system, but as every transition phase in engineering or physics, is probable that the mechanics of crack behaviour in this phase are more complicated than the sum of the two behaviours for long and short cracks. Figure 80 shows also how the reference points are still well approximated by the lines of

lengths and the cycles of fatigue between measuring in the paper are not directly stated in the paper, where both the values are reported as ranges, it is not possible to exactly recreate the condition of the experiments, but the simulation manages to replicate the behaviour of crack growth rate with stress intensity range observed in the experiments: small cracks grow at lower stress intensities than large cracks until they reach a size where the toughening effects slow their growth. The results show also how the reference points from Kruzic *et al* fall into the area of our simulation (Figure 78 and Figure 79)

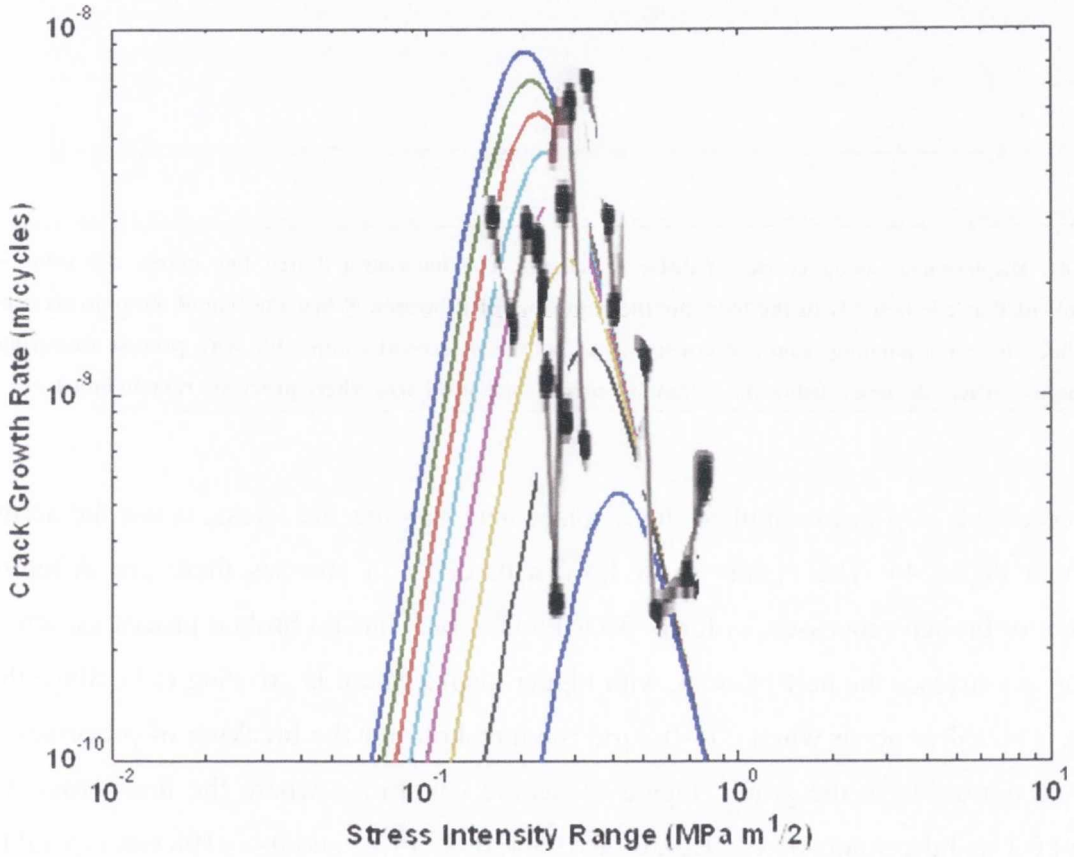

Figure 78. Crack Growth Rate versus Stress Intensity Range from the simulator for a value of d = 1 mm. The different colored lines represent different initial values of a (from 0.1 mm to 0.8 mm) and the black dots are the reference points from Kruzic *et al* (33)

all its length, while a 400 μm crack will have almost all of its length with broken processes.

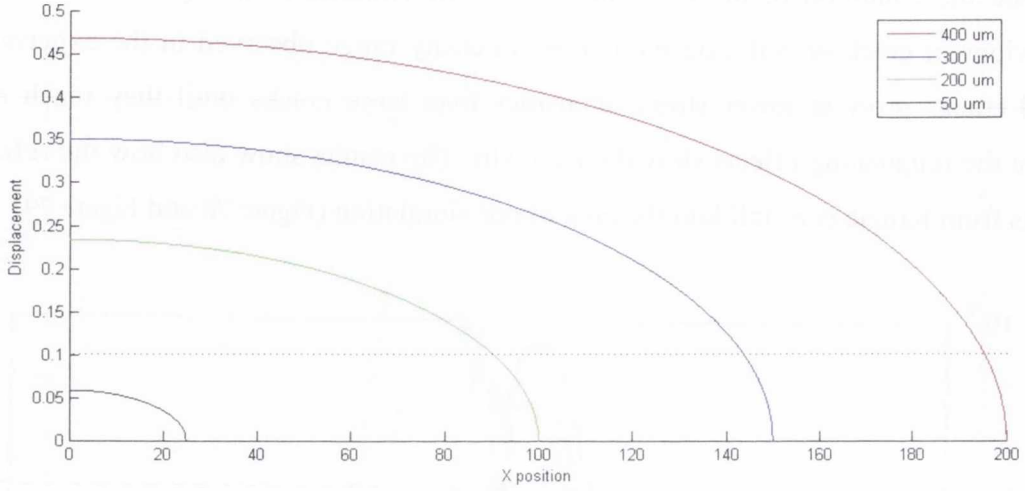

Figure 81. Displacement along cracks of different lengths. The horizontal dotted line marks the value of displacement that corresponds to the limit for the rupturing of processes. When the line of shear is over the dotted line, the corresponding length of crack has a shear displacement compatible with process rupturing; while the area where the line is below the dotted line corresponds to an area where processes remain intact.

The successive step is to simulate the displacement varying the stress, using the script shown in Figure 40. The results show how with different stresses there are different numbers of broken processes, as for σ=30 MPa the crack has no broken processes, while with bigger stresses the part of crack with bigger displacement is growing (51). Since the failure is stated to occur when $2\delta s>0.2$ μm the threshold for the breaking of processes is easily recognizable in the graph (Figure 82) as the value of x where the lines cross the limit of 0.1 and the points $0<x<191.9$, $0<x<195.4$, $0<x<197.2$ and $0<x<198$ correspond to the 95.95%, 97.7%, 98.6% and 99% of the complete length of the crack for the 4 stresses plotted

the simulator for the large part of the experiments copied.

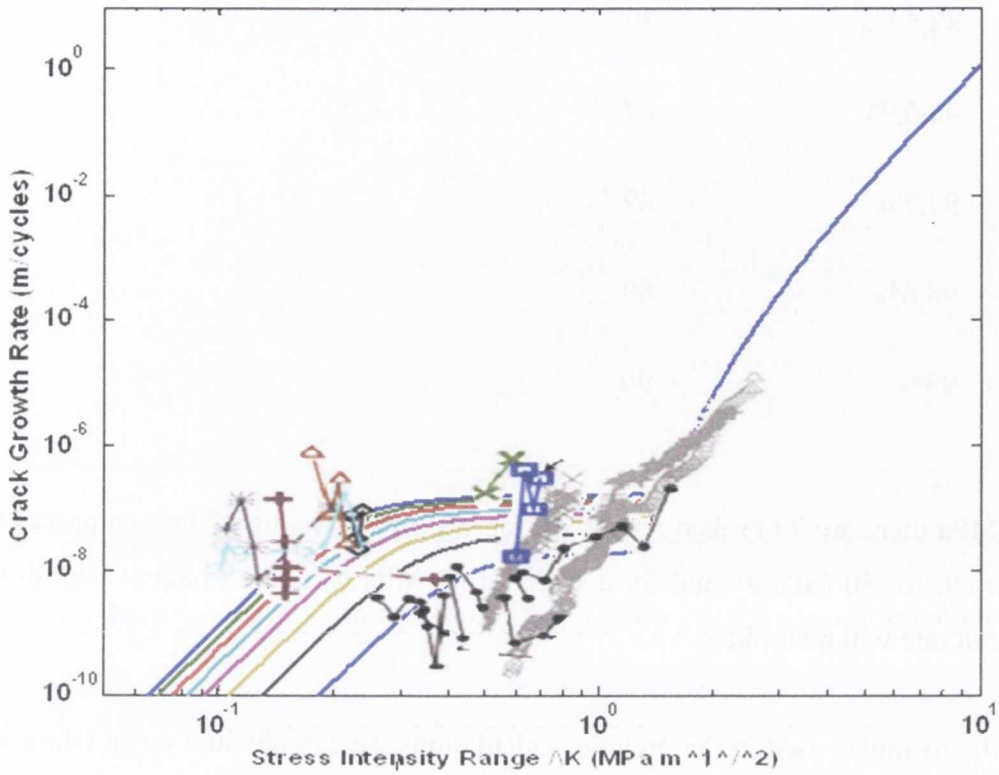

Figure 80. Crack Growth Rate versus Stress Intensity Range from the simulator with ΔK_{th} = 0.8. The different coloured lines represent the different values of a (from 0.1 mm to 0.8 mm) and the gray area and the differntly coloured points and markers are the reference points from Kruzic *et al* (33).

Simulation of broken processes

Shear Results

I have compiled a simulator for the number of broken processes by taking successive steps into simulating the shear and displacement layouts along the axis of a crack. The first step is to simulate the displacement with cracks of different lengths, using the model shown in Figure 39. That model generates a graphical output showing the displacement along the layout of 4 cracks of different sizes, as shown in Figure 81.The horizontal dotted line marks the value of δs=0.1 that corresponds to $2\delta s$=0.2: the limit for the rupturing of processes. When the line of shear is over the dotted line, the corresponding length of crack has a shear displacement compatible with process rupturing; while the area where the line is below the dotted line corresponds to an area where processes remain intact.

From the graph it can be seen how different sizes have different behaviour, for example the 50 μm crack has no broken processes, since the line remains under the threshold for

Table 5: Broken Processes along a crack. With increasing stress the ratio of processes that are broken by shear displacement on the total number of processes increases, for high stresses is safe to assume that almost all the processes that cross the crack are broken by the shearing of crack faces.

Stress	Broken processes %	Broken Processes #
17 MPa	83,50%	79
30 MPa	95,95%	87
40 MPa	97,7%	89
50 MPa	98,6%	89
60 MPa	99%	90

So for 17 MPa there are 79 broken processes, for 30 MPa there are 87 broken processes, for 40MPa 89, for 50 MPa 89 and for a stress of 60 MPa it is safe to admit that all the processes but one will be broken.

Inverting the formulas used in the previous calculations we can obtain a script (shown in Figure 41) which directly transforms the crack length in the number of broken processes at a given length.

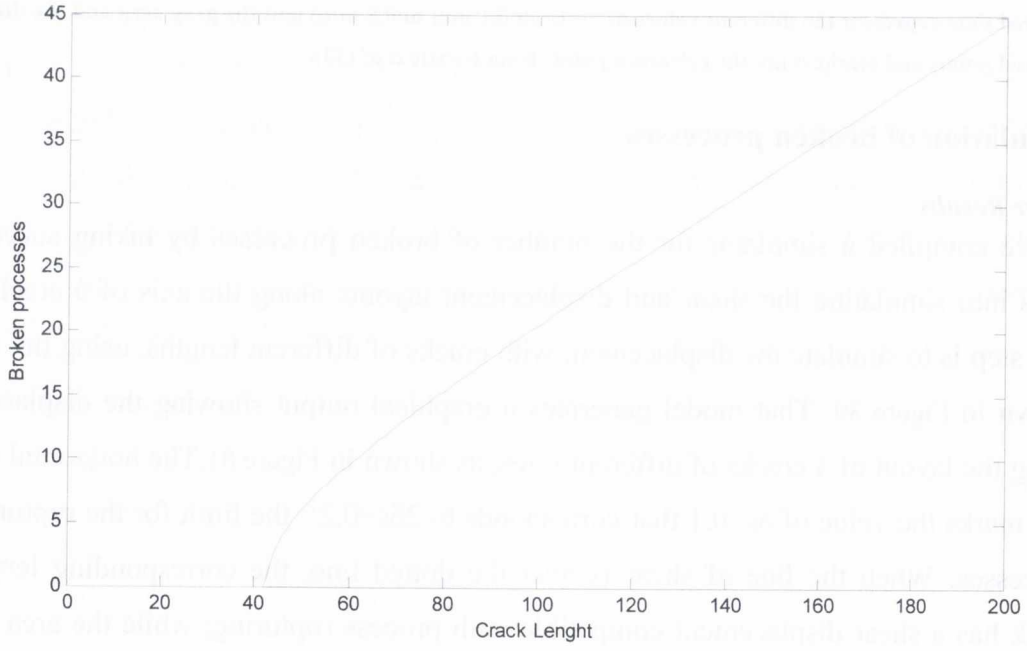

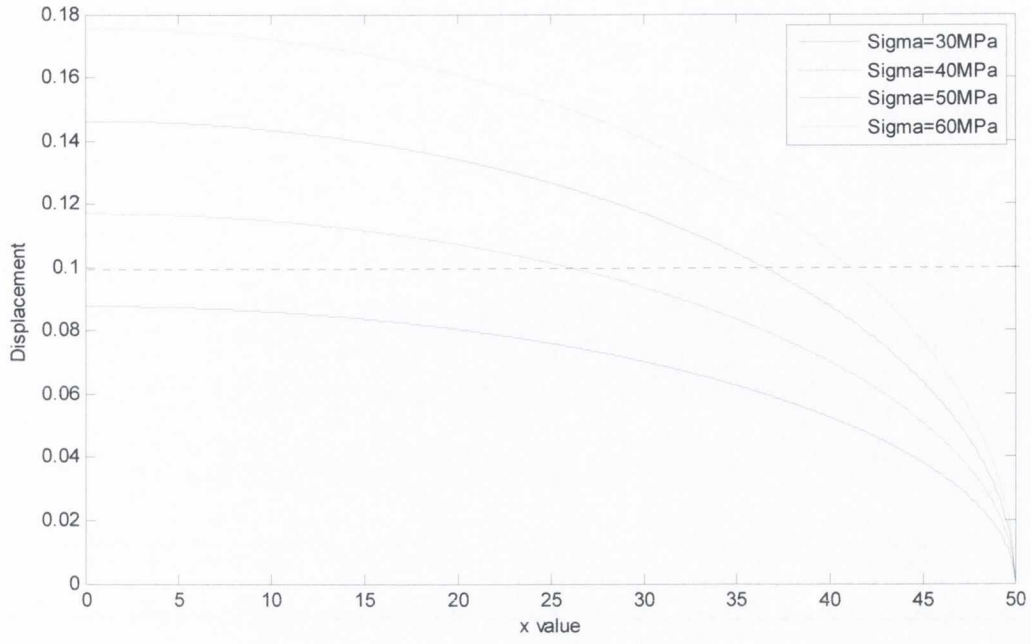

Figure 82. Displacement along a 100 μm crack with different stresses. The horizontal dotted line marks the value of displacement that corresponds to the limit for the rupturing of processes. When the line of shear is over the dotted line, the corresponding length of crack has a shear displacement compatible with process rupturing; while the area where the line is below the dotted line corresponds to an area where processes remain intact.

Number of broken processes

Applying the percentage from before to the number of total processes crossing a crack obtained combining the data from Mullender et al (62) and from Sugawara et al (63) we can calculate the number of broken processes that can be seen along the crack at different stresses as in Table 5

Figure 83. Broken Processes against crack length. It can be seen how when the crack is small there is no process that is broken, while at large crack sizes the number of broken processes is equal to the number of processes along the crack, resulting in a linear behaviour of the curve.

To confirm the efficiency of the simulation in predicting the number of processes broken by stress applied to the cracks I have compared its results to those of a series of SEM analysis done on bones subjected to fatigue tests (SEM data courtesy of Clodagh Dooley, TCD).

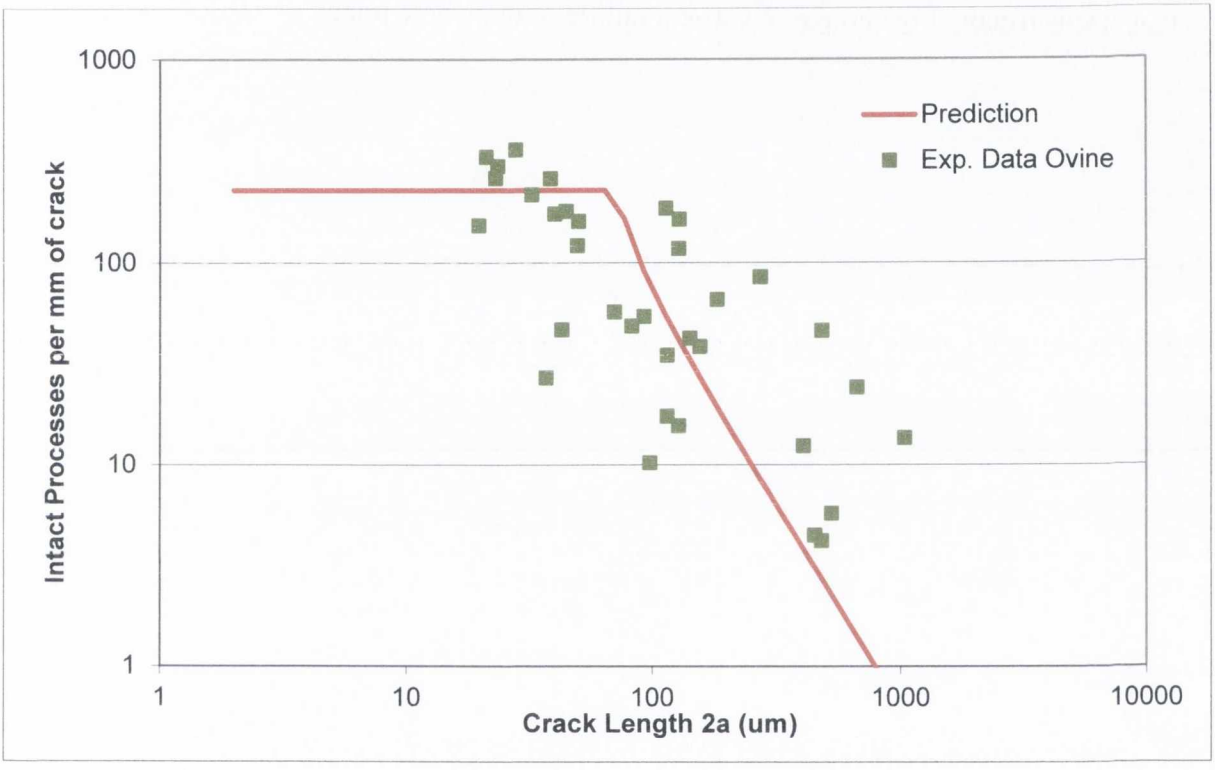

Figure 84. Intact Processes per mm, simulation against experiments at *in vivo* levels of stress. Experimental data courtesy of Clodagh Dooley, TCD. The first part of the line is horizontal, as for those crack sizes there is not enough displacement to broke any process, then the number of intact processes per mm decreases with size, as the length of low displacement along the axis of the crack falls. The graph has been published in Dooley, Tisbo *et al* (92).

The results of the comparison show how the curve from the simulator approximates the behaviour seen in the experiments, keeping in mind the presence of scatter in the experimental behaviour, as shown in Figure 84. The first part of the line is horizontal, because for small crack lengths, as has been showed before, the number of broken processes is zero and so the number of intact processes per mm is constant. Looking at the experimental data it can be seen how, for the same crack length, there can be different results. The reason for this scatter is probably the distribution of processes: the processes that I have modelled as evenly distributed along the cracks are not arranged in such order

in real bones and because of this the number of processes per mm is not constant even when the length of the crack is not enough to have broken processes. The greater difference between the simulator and the experimental data is at the highest values of crack length, where a difference of 1 order of magnitude between the prediction and the experiments can be found. Because I have very few reference points for that crack length I cannot be sure that the difference is because of scatter, but as the size of the crack is around 1 mm the problem of this difference is not relevant to the simulator as a crack of that size is usually big enough to cause a failure of the whole bone.

The final analysis performed on the number of broken processes along a crack is shown in Figure 42, where I have introduced the condition of fatigue disruption of processes calculated with the use of the script in Figure 42. The results from that script show how the process count grows smaller with time, in accordance with the experimental observations. They show also how, except for the smaller crack, the processes break very early in the analysis, meaning that approximating the breaking of the process to a simple shear displacement effect is an acceptable simplification in most cases (Figure 85).

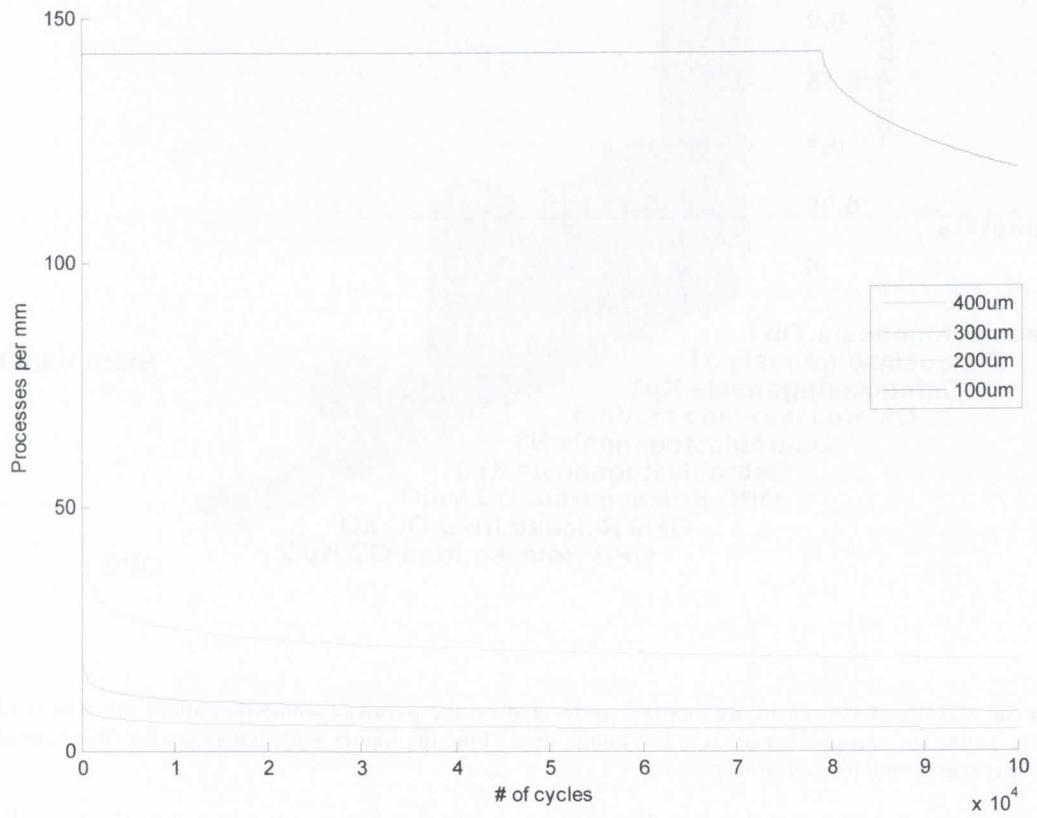

Figure 85. The number of intact processes per mm against number of fatigue cycles for cracks of four different lengths. The graph shows how with the longer lengths the number of broken processes reaches its maximum value in around 100 cycles, therefore the approximation of all the processes getting broken immediately is not excessive.

Biological reactions

The presence of broken processes ignites the reactions that activate the cells composing a BMU. In chapter 3 I have shown how the system reproduces the biological reaction pathway that activate a BMU and how I have obtained the parameters that define quantitatively the reactions comparing them to experimental data from Mulcahy *et al* (54). The values of the parameters required solving the pathway of osteoclasts and

osteoblasts activation has been obtained by performing a sensitivity analysis with Simbiology™ and then performing multiple parameters scan to individuate the set of parameters which better approximates the results from experiments.

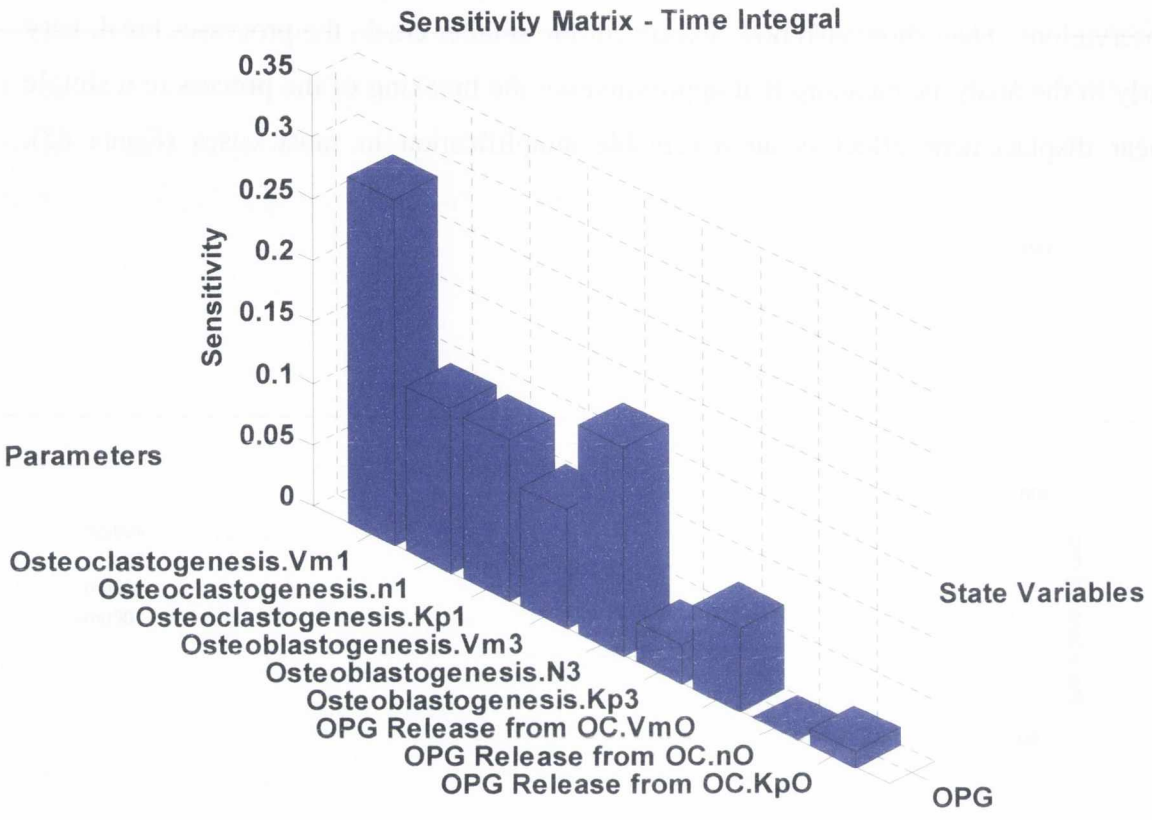

Figure 86: Results of the sensitivity analysis performed on the pathway simulation about the release of OPG after damaging the osteocyte processes. The image shows how the higher sensitivities are for the parameters of osteoclastogenesis and osteoblastogenesis.

The parameters chosen allow replicating the values of the experiments when applied to the system, allowing a fair deal of adherence to reality. Even if the value of the simulated output of RankL is lower than the experimental results, these results follow the behaviour shown by the experiment and this difference is subsided in the system by the absence of a mechanism for the reduction of RankL with time, which is otherwise present in SimBiology™.

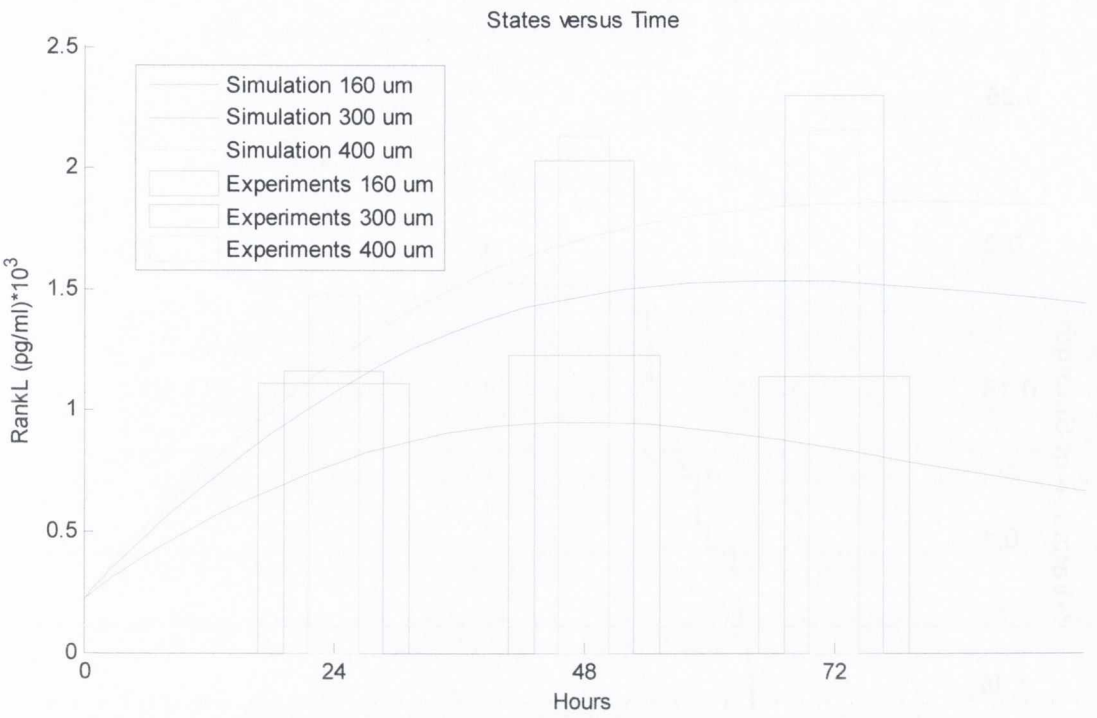

Figure 87. Values of RankL with time for different amounts of injury. It shows both the results from the Simbiology™ simulation (the lines) and the results from experiments from Mulcahy *et al* (54)(the histograms). It is shown how the behaviour has been reproduced nicely even if the value of the simulation is slightly lower than the experimental data.

Wolff's law simulation

The simulator is also able to model the effects of Wolff's law on the strength of bone by simulating the effects of the variation in bone mass because of the repair effect. The use of Equation 24 to simulate the variation in strength shows that the simulator calculates an increase of the strength of almost 25% during a simulation of 8 weeks of military training, as shown in Figure 88. This result is coherent with the results shown Notomi *et al* (80) where the training had resulted in a 33% increase of strength in rats after 4 weeks of training. Given the relative simplicity of the equation used in our model, this result show

good adherence to reality.

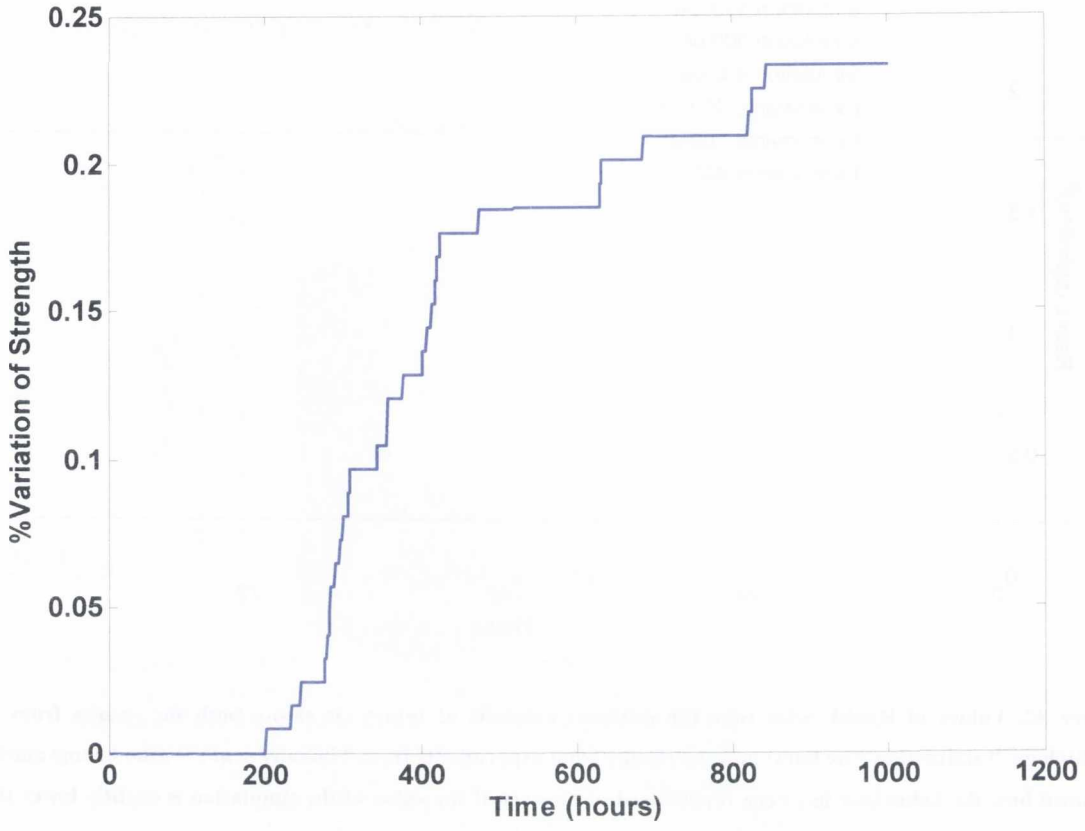

Figure 88. Variation of strength with training. The results show how the increasing need for repair caused by the increased load on the bone caused the bone mass to increase, therefore reducing the effect of stress on the trained bone.

Simulation of crack growth and repair

The most advanced property of the system is the ability to model the mechanics of bone repair and so to offer a way to predict the behaviour of living bone. Verifying the results of a simulation of this scope is not an easy task: microcracks that are part of a bone cannot be seen without cutting open the bone itself, which is not something that can be done on a living, healthy individual. Despite this obvious inconvenience there are studies that show the effects of repair on animals by euthanizing the animals after the stress loads to count the number of cracks and BMUs. The simulator offers a different kind of output, showing the behaviour of the cracks during the stress application and the timings of the BMUs in the repair effect, but thanks to its versatility, I can adapt it to output results that can be compared to those in literature, with a little extra calculation. In literature some authors have observed a linear relation between mean crack length and the number of resorption spaces left from BMUs (48) (27). The simulator is able to reproduce both the

number of BMUs and the crack lengths in every second of the simulation I am able to observe if the results respect this linearity. As the simulation is done on a number of cracks rather than a definite area, the variable on the x axis will be the number of resorption spaces. As Figure 89 shows, this linear relation is accurately predicted.

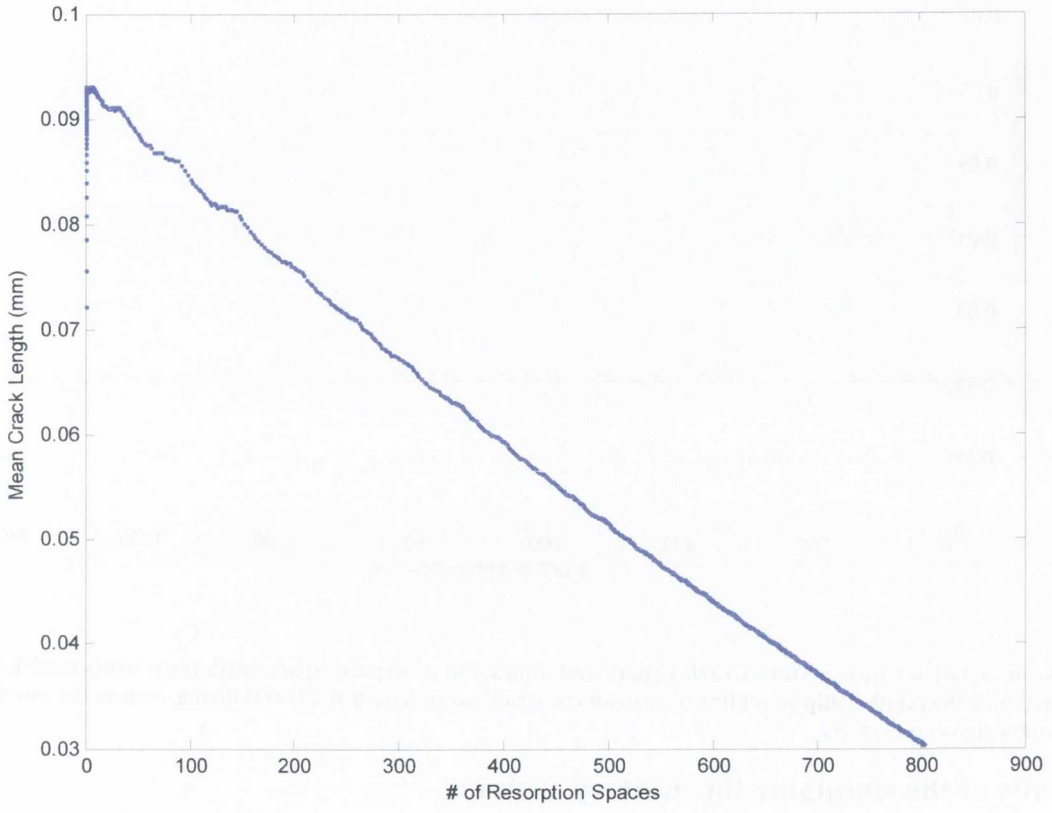

Figure 89. Relation between Mean Crack Length and number of resorption spaces with the scissors model. It can be noted how the relationship is linear.

Using the mechanostat signal model the behaviour of this curve changes into a less linear shape, shown in Figure 90. The reason for this difference is the fact that I have not inserted any threshold value for the signal (which is instead present in the scissors model), so the signal is always greater than zero, even if it is small with smaller cracks. Because of this the cracks get repaired even if they are very small, causing a variation in the ratio between the number of BMUs and the crack length which is effectively repaired by them. This reduced "ratio of effectiveness" of the BMUs causes this non linear behaviour when the number of BMU increases. In the scissors model the BMU ratio remains constant, as the repair is activated only for cracks above a certain length.

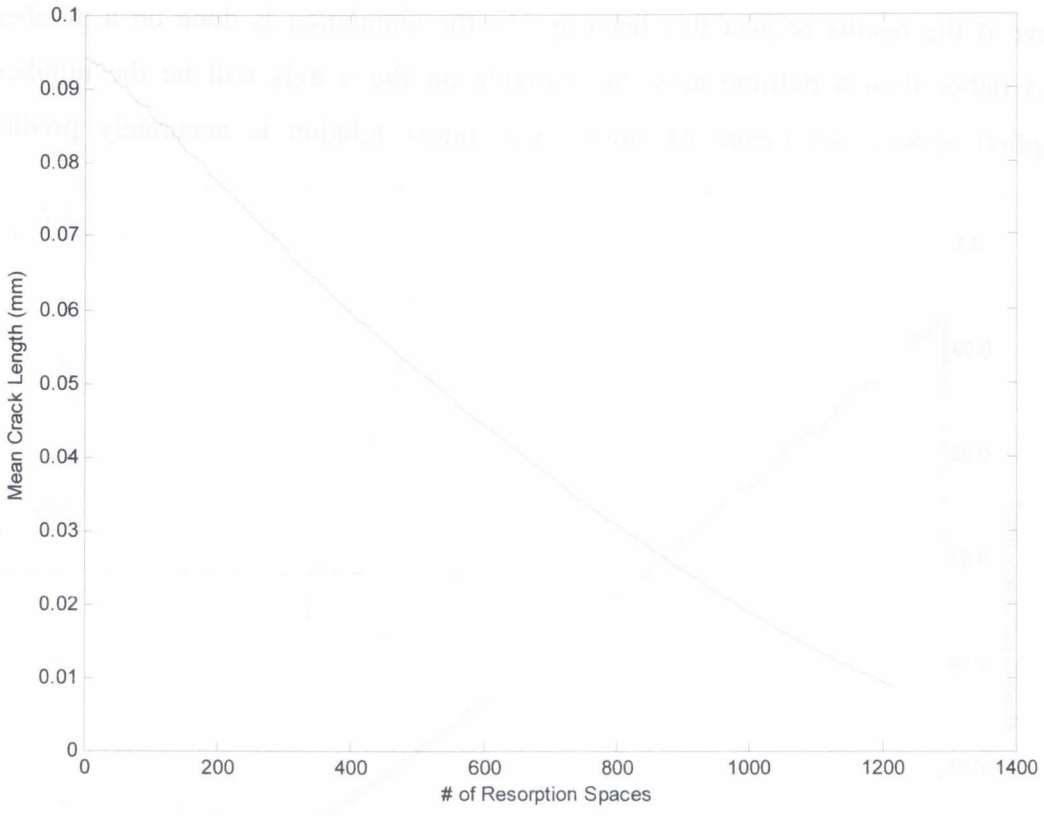

Figure 90. Relation between Mean Crack Length and number of resorption spaces with the scissors model. It can be noted how the relationship is not linear, instead the crack mean length starts stabilizing even as the number of resorption spaces increases.

Results of the simulator for military training

I have first activated the simulator to run a number of cycles that are coherent with at least a couple of weeks of training course. For this first analysis I have set the simulator so that every second of simulator time is equivalent to a minute of "real time". I will simulate a small number of cracks (25 cracks) to avoid memory errors and to have a better visibility. So to simulate two weeks I need to do a simulation for 20000 cycles (actually 20160).

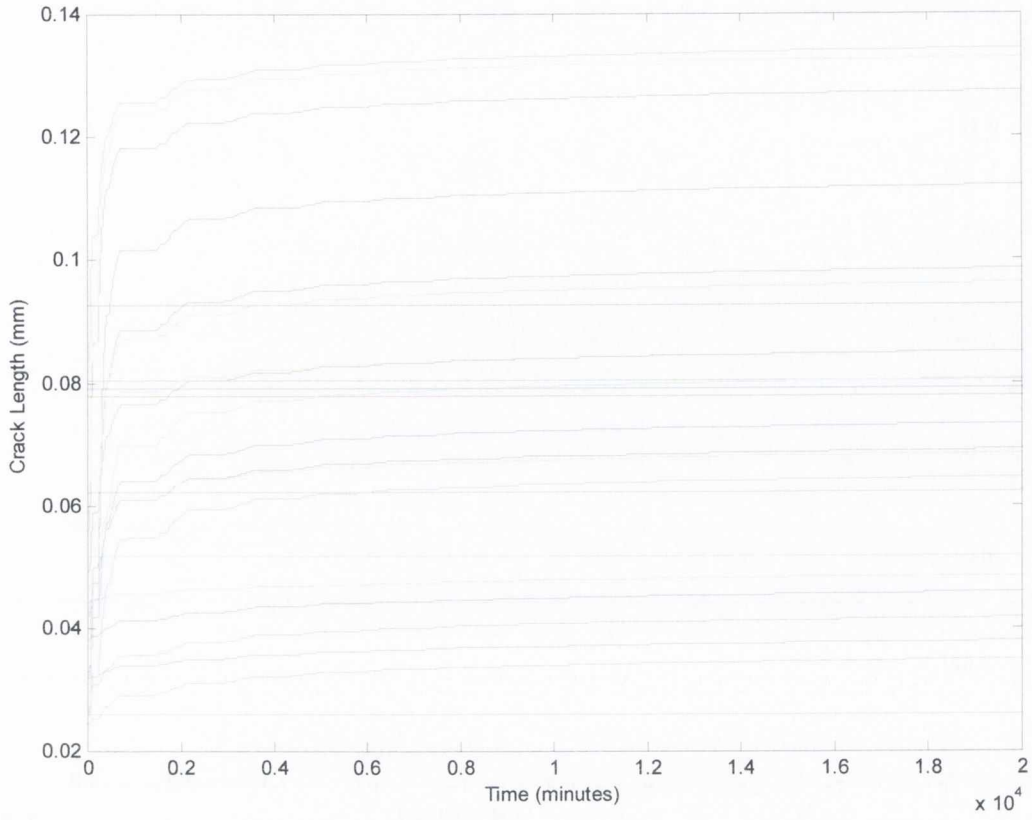

Figure 91. Simulation for two weeks (no repair). The simulation shows how the cracks grow faster during the training periods than in the rest periods. As in a week there are 10080 minutes in a week the value of 10^4 minutes can be exchanged for a week with a negligible error.

The first simulation does not include a failure, so it runs all 20160 cycles without stop. The end result shows a final mean value for crack length of 76 μm. Running another 10000 cycles increases the average crack length by 0.5 μm, not enough to bring any failure in the system.

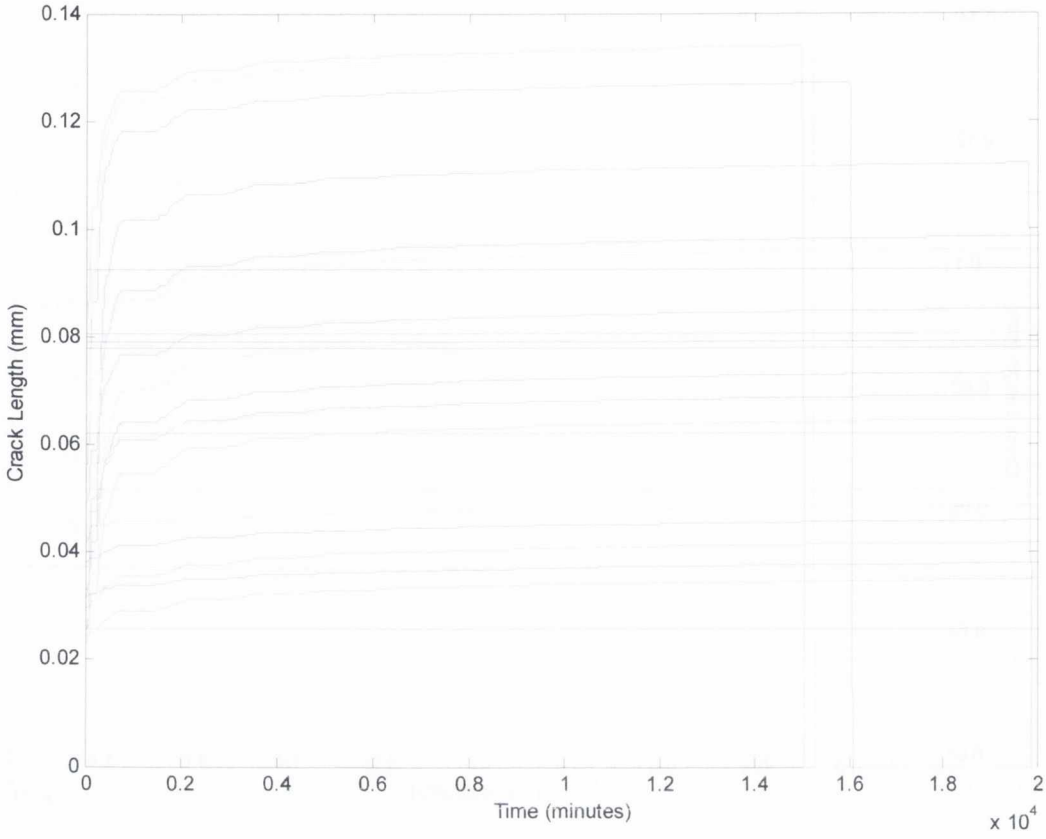

Figure 92. First two weeks of simulation with repair. The simulation shows how the cracks grow faster during the training periods than in the rest periods. As in a week there are 10080 minutes in a week the value of 10^4 minutes can be exchanged for a week with a negligible error. Only 3 cracks are repaired before the 2 weeks' time is expired.

Activating the repair it can be seen that only 3 cracks get repaired in the first 2 weeks' time. Running the simulator for 3 weeks it can be seen that the repair system has affected 3 more cracks. In the 4^{th} week the repair affects one more crack. In the 5^{th} week there is no crack repair. In the 6^{th} week two more cracks are repaired. In the 7^{th} and 8^{th} weeks there is no repair, the only cracks remaining are small enough to have very few broken processes. 3 of them (size 82, 80 and 79 μm) have less than 3 broken processes each, so there is a probability that they will be eventually repaired, as the broken processes will continue to slowly release RankL, and another crack (size 78 μm) is just starting to have broken processes. The other cracks are all below 75 μm, which is a value barely able to have 1 broken process even after all this time. The balance between the bone removed by osteoclasts and restored by osteoblasts is positive, so the bone has increased its mass reducing the effective stress on the bone in the training regime from 50 to 46.4 MPa, which is a more manageable stress for bone, even if it is more than double the

physiological stress, showing the possibilities of bone to adapt to stress changes with time. From the results it can be seen how the simulator reacts to damage by reducing first the bigger, more dangerous cracks because of their increased number of broken processes. The results shown in this paragraph replicate a case similar to those of the majority of subjects training in the Army, those who do not experience fatigue fractures.

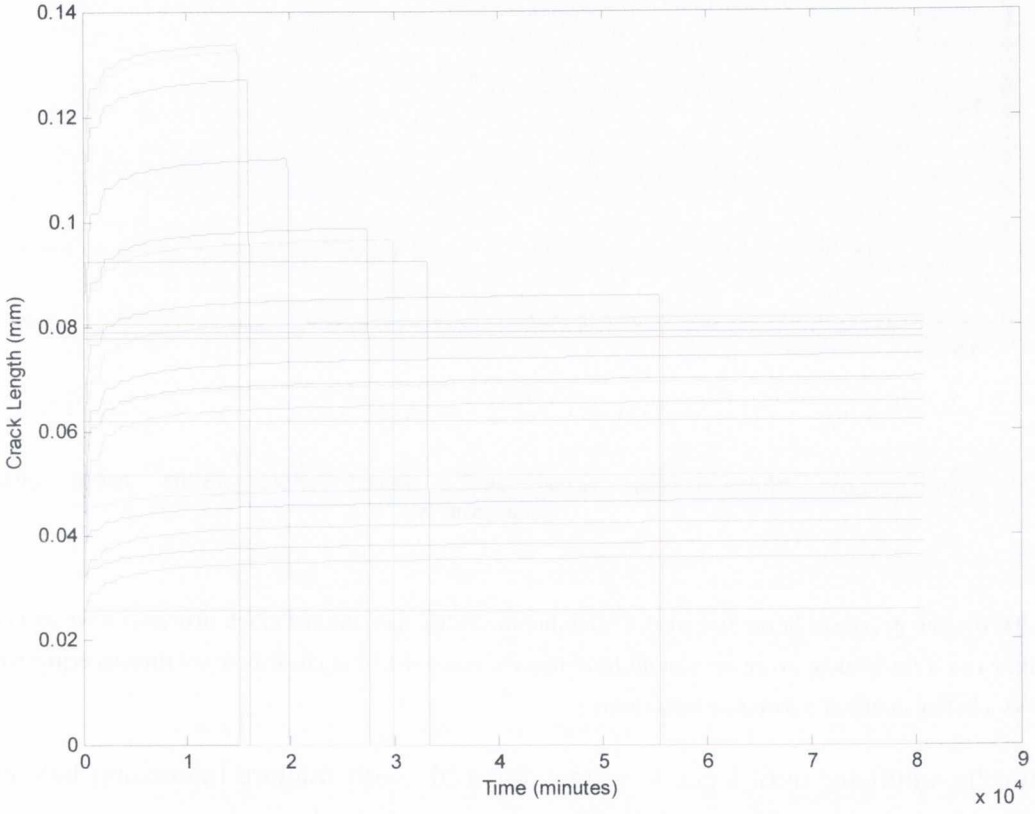

Figure 93. Simulation of 8 weeks. T As in a week there are 10080 minutes in a week the value of 10^4 minutes can be exchanged for a week with a negligible error.

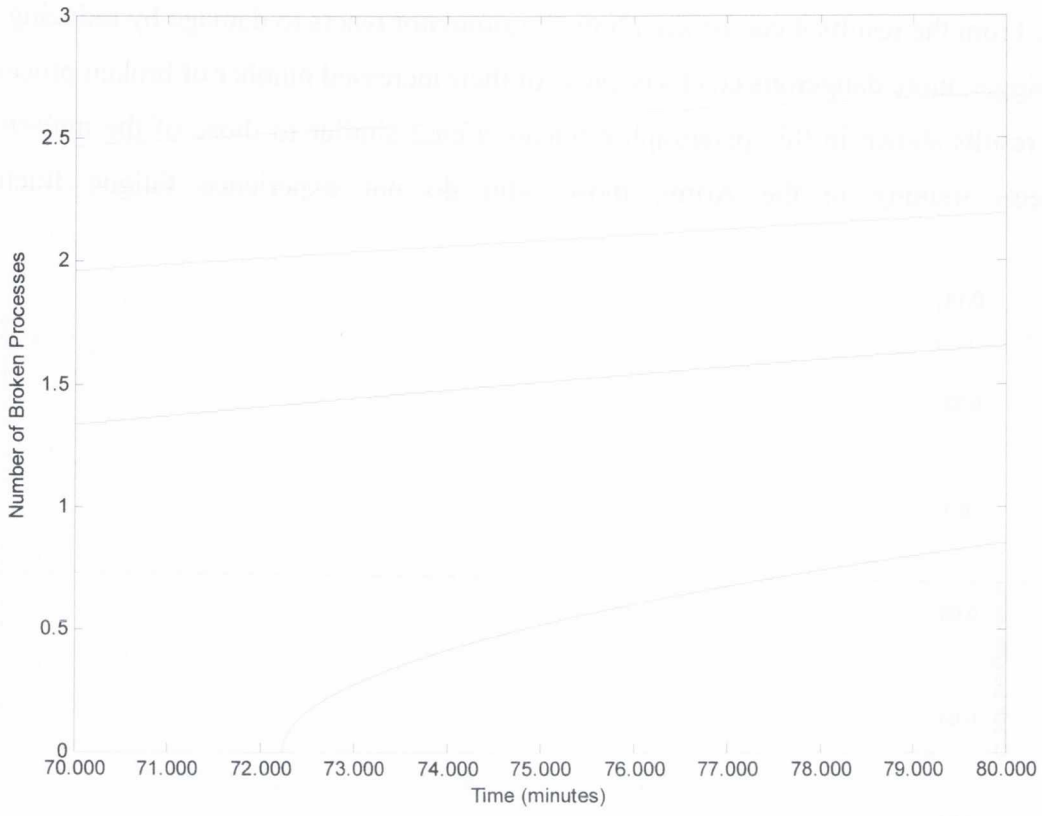

Figure 94. Broken processes in the last week of simulation. Notice how the red crack processes have just started to break. Even if the broken processes should be a discrete number I have chosen the continuous representation as it gives a better image of a dynamic behaviour,

If I run the simulator until I get a value compatible with fracture interesting behaviours appear. First of all it can be seen how the cracks grow until they meet osteons to stop their growth even at low stresses, but at higher stresses the process is much faster.

I have used the simulation with a time scale of minutes to show a general behaviour of cracks that are already in the bone when the stress begins. To simulate all the cracks that are formed because of the increased stress of training (50 MPa) I need to use a different time scale, because the number of cracks that are present in the higher stress volume according to Equation 6 is 1250, a number that must be multiplied for 80000 cycles, generating memory issues. So I use another scale to simulate this larger number of cracks, using the simulation with a cycle per hour. This simulation is less precise but can be used to simulate more cracks in less time. In Figure 95 there is the output of 1250 cracks for 8

weeks

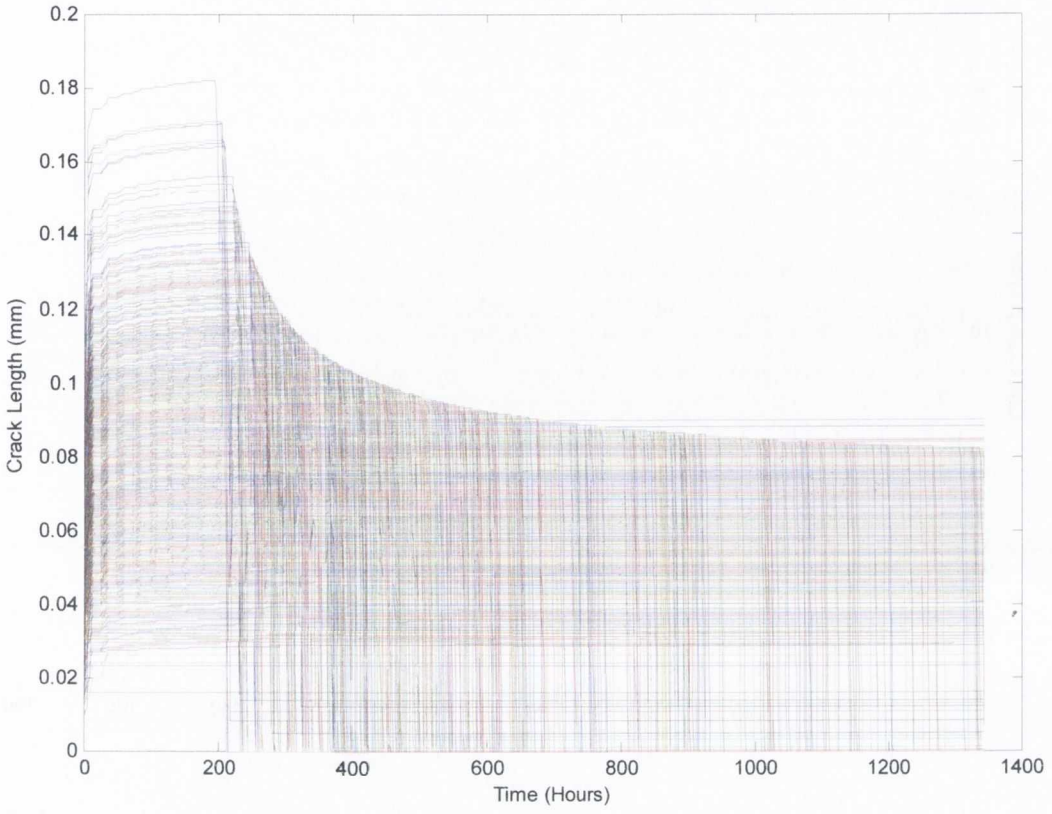

Figure 95. Simulation of 1250 cracks in 8 weeks. The image shows how the largest cracks are repaired first, while the smallest are never repaired.

Figure 95 shows how the greater number of cracks means that more cracks get repaired, but the pattern is the same than the previous simulation: the larger cracks get repaired first and then the repair affects the other cracks unless they are small enough to not be seen as a danger from the body.

There is a different pattern when we have a result which corresponds to a stress fracture. Observing the output of such a case it can be seen how one crack goes in the "Long Crack" behaviour because of the stress and starts diverging from the group and how the shape of the curve shows a flex, representing when the short crack behaviour was slowing to a stop, but the long crack behaviour took over to bring the crack to larger sizes and at a probable failure before the repair reduces the crack size to more manageable levels as shown in Figure 96.

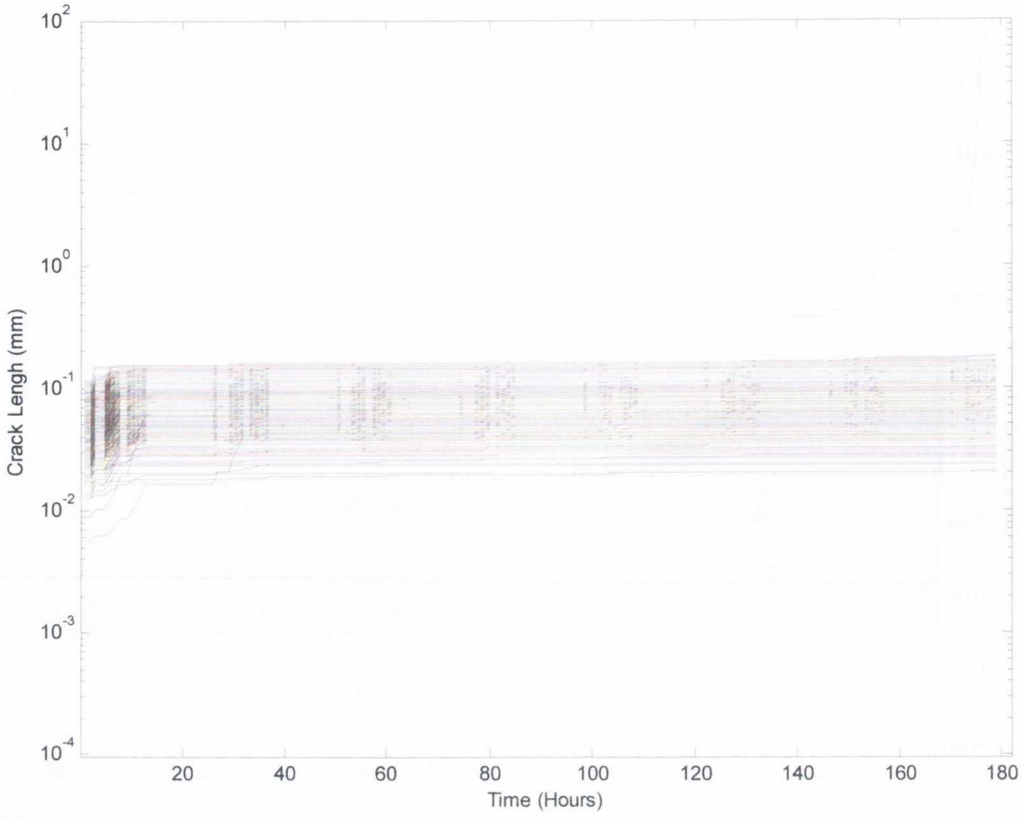

Figure 96. Simulation of stress failure in military training. The image shows how only a crack causes the failure, while the others remain stable.

If I isolate the growing crack to analyze it in detail I can observe how the crack had a slow growth at the beginning, but started growing faster and faster with every time period

of increased stress, as seen in Figure 97.

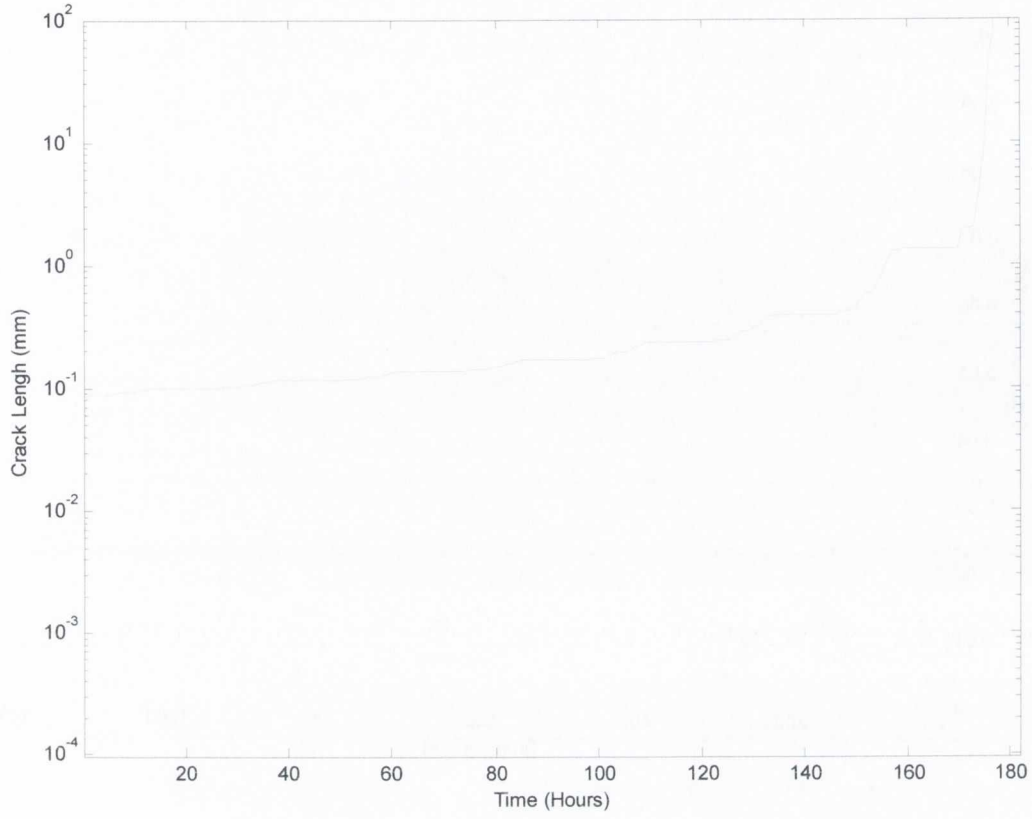

Figure 97. Simulation of stress failure in military training. The single crack which has generated the stress fracture has been isolated and shown in detail. The plot shows how the crack alternates between "rest" periods and "growth" periods according to the layout of stress, until it becomes big enough to grow during the low stress periods too.

If I simulate the same crack (with the same initial values) without the increase of stress caused by the training regime I can observe a different outcome of the simulation. Even if the crack continues to grow their growth is slower and it doesn't reach the "long crack" behaviour thanks to the reduced stress that reduces its stress intensity preventing it from growing beyond the osteons' barrier. Having the stress reduced by a factor of 2.5 increases the crack's "critical size" by a factor of 6.25 thus giving a huge difference in the danger of a single crack. The large crack gets also repaired without becoming a danger for the body, as shown in Figure 98.

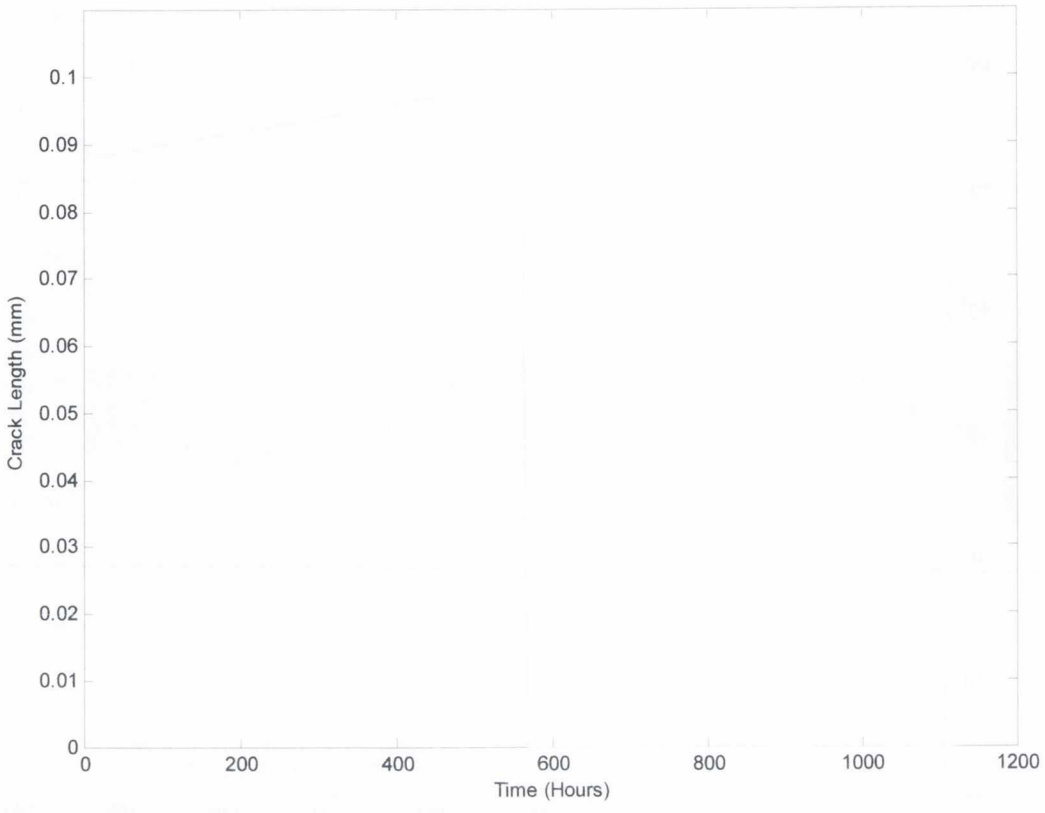

Figure 98. Simulation of a dangerous crack without training stress. The plot shows how the crack, even if relatively big, does not grow enough to be a danger before getting repaired.

It is shown that the lessened stress allows time for the repair of the longer cracks, which at bigger stresses would bring failure. This means that a crack of that size can be compatible with a regular lifestyle, but not with the extended loads experienced during an army training regime. The results obtained in this last simulation show how the danger of stress fracture can be avoided with sufficient rest and avoiding situations of excessive stress. This is one of the most powerful features of our simulator, as its modularity allows performing different analysis on the same set of initial data.

New cracks

The system is also able to simulate the behaviour of the new cracks that are born during the observation. Because of computational power limitations and for an easier application of the data, I have performed a second simulation showing only cracks that are born during the observation. Experimental data on dead bone (34) shows that cracks in bone tend to increase their number mainly in the first cycles of fatigue and when the bone is near failure, which is reasonable keeping in mind that cracks tend to appear where the

material has some invisible defects, but probably in living bone the behaviour is different, as data on humans show that it take years to observe significant variation in crack density (5). A probable behaviour is that cracks are born and repaired almost at the same rate, with a slightly positive trend. In the simulation of military training I am observing a situation which is a bit different from the normal stress layout for living bone, as I have a new stress regime that is applied to the trainees, stress regime that comports an increase in crack density following Equation 6. This new stress regime causes an increase in the number of cracks from 250 to 1250 and I can simulate these new cracks as immediate, following the theory of O'Brien *et al* (34). Because of the large number of cracks I have performed a simulation using a time scale of hours. The results of this simulation show how cracks grow from small values (I have given the initial value of the new cracks as 1 μm). The short crack growth rate is small at the beginning when the crack becomes a little bigger it grows faster until it reaches an osteonal barrier, when the crack growth slows and then (hopefully) stops. After this the behaviour of the crack is the same I have already shown in the previous simulations, as shown in Figure 99.

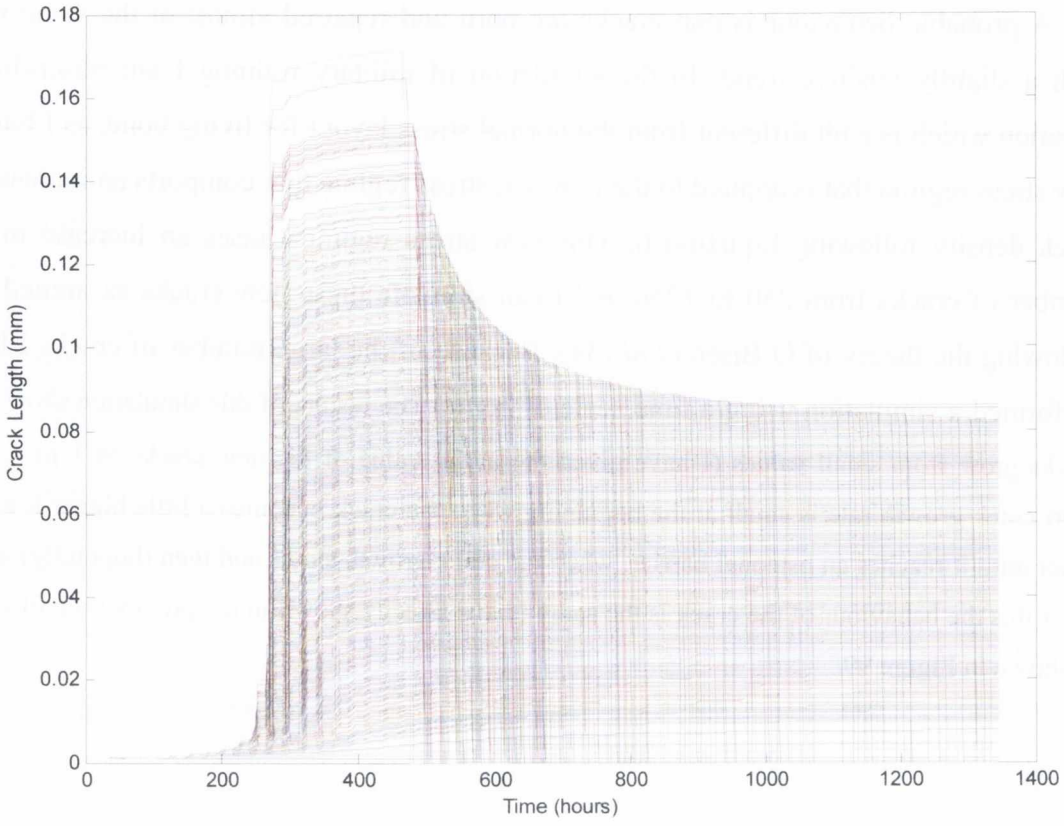

Figure 99. Simulation for new cracks appearing together at the same time. Each crack behaves differently because of the different boundary condition, but apart from that they tend to behave as in the other simulations.

To make the simulation of new cracks more useful I have done another simulation for a smaller number of new cracks whose birth is evenly distributed during the simulation time to have a better visibility. The results show how the repair prioritizes size over age for the cracks: as the "life" of the cracks is not constant, bigger cracks are repaired first. The cracks grow differently because of the different stress with time and of the distance between the osteons they are circled by. On a healthy individual it can be imagined that crack behaviour is exactly as shown in Figure 100: cracks appear, grow and get repaired continuously during the lifetime; bigger cracks are prioritized by the repair process, while smaller cracks are repaired slowly, if they are repaired at all.

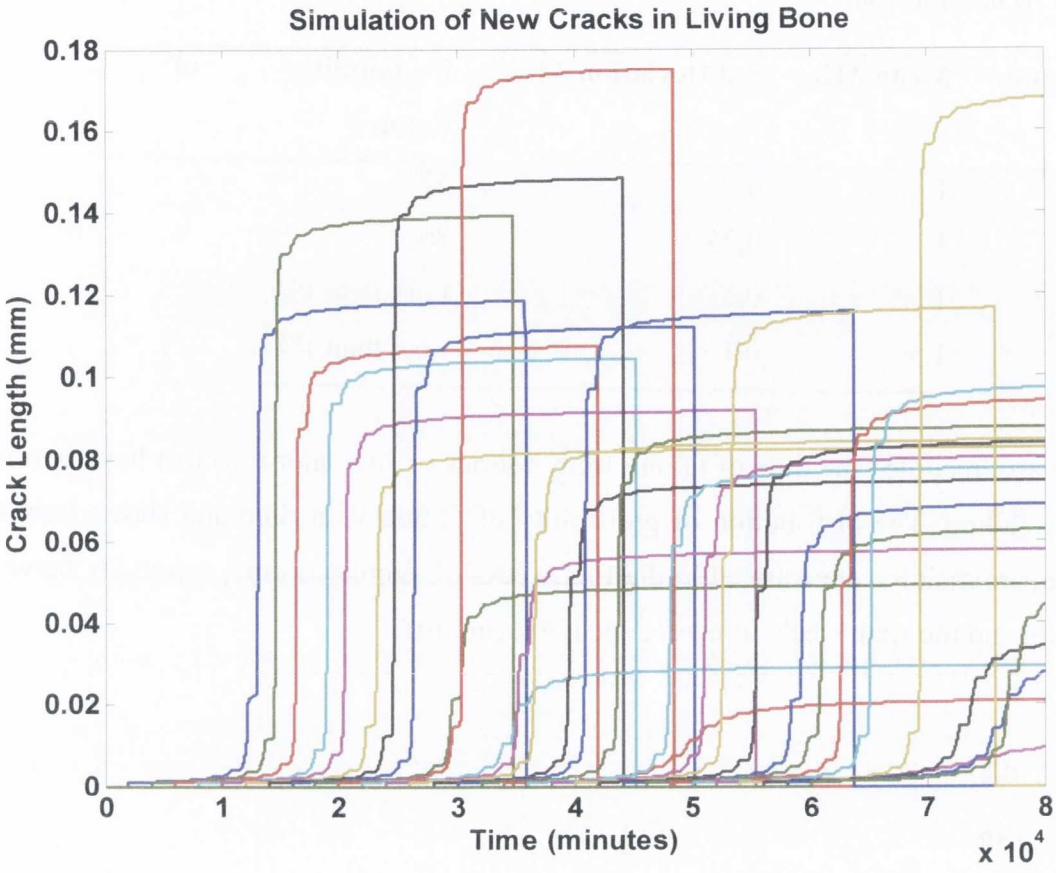

Figure 100. Simulation of new cracks. The graph shows the behaviour of newly formed cracks in humans following the loading regime used in the simulation for military training. It can be noted how cracks are repaired according to their size, not their age.

Probability of failure

A single simulation can offer results about a single simulated trainee in the amount of time that corresponds to the simulation period, but while interesting a single result cannot be used as a reference to prove the efficiency of the simulator. The simulation is based on 3 randomized variables that act as its inputs, allowing observation of the variability that can be expected from real life specimens. To confirm the accuracy of the system I need to compare its results to experimental data. To achieve a prediction of the probability of failure I need to run the simulator many times and register every failure. While the simulator is relatively fast (the simulation of 8 weeks takes less than 1 minute), the act of running it and retrieve the results performed for at least 100 times can take up to 2 hours. Because of this I have performed only 4 analyses for the probability of failure, each with a different distribution of ΔK_{th}, whose results are in Table 6.

Table 6: Prediction of failure

Simulation	Mean ΔK_{th}	Std Deviation ΔK_{th}	Probability of Failure
1	1	0.3	42%
2	1	0.25	8%
3	1	0.2	Less than 1%
4	1.5	0.1	Less than 1%

I have also recorded the time of failure from a series of simulator runs that have returned a bone failure. The distribution of probability of failure with time and shows how the failures are mainly concentrated in the first weeks of simulated time, especially between the third and the sixth week, as can be seen in Figure 101.

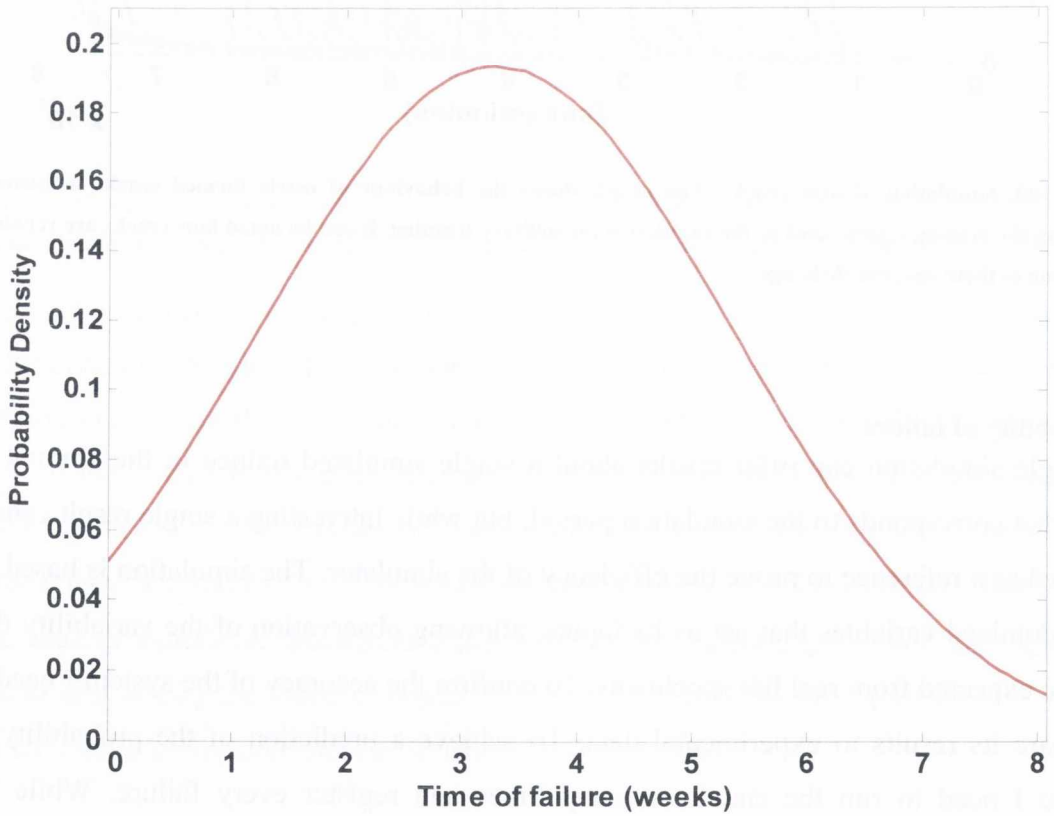

Figure 101. Distribution of time of failure for the simulator. The plot shows how the times of failure are concentrated in the first weeks of training, especially between the third and sixth week.

Simulation of special scenarios

It is interesting to see what happens when I change some of the parameters of the simulator. The results show an interesting shape, different from the behaviour observed in "younger" simulated bone. The shape of the curves of crack length with time is different from the shapes shown in other simulations. The reason for this shape is that the cracks in this simulation alternate between a prevalent long crack behaviour in the training period and a short crack behaviour in the rest and non training periods, as shown in Figure 102.

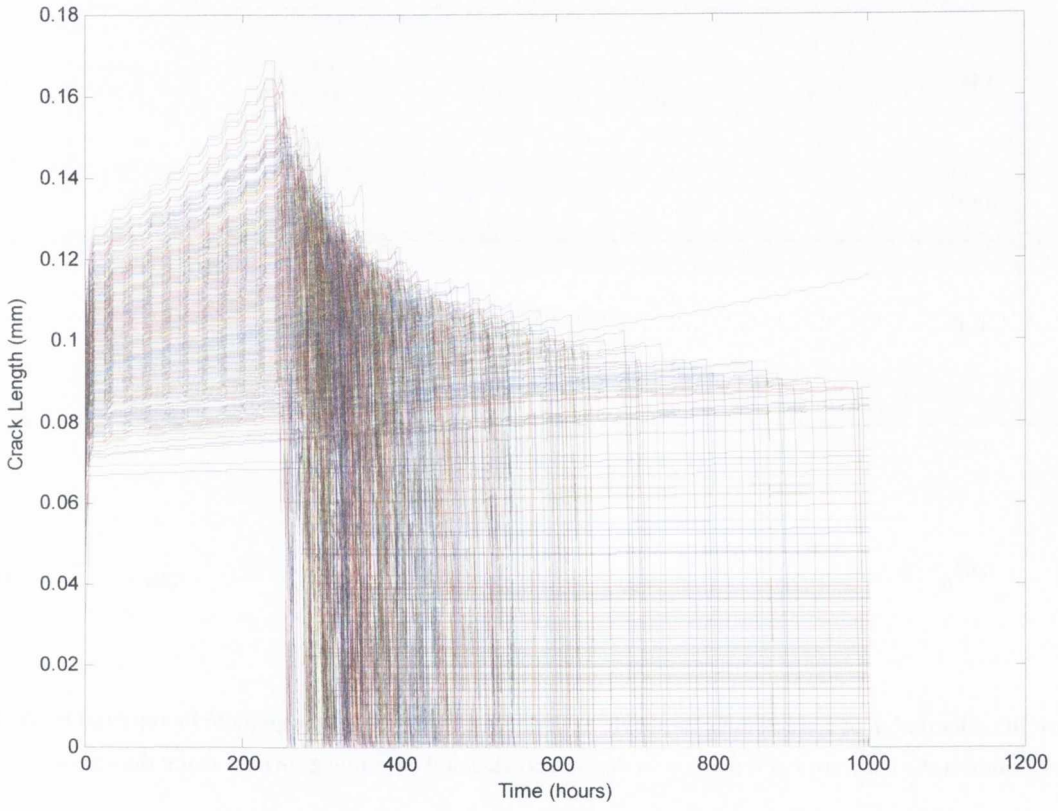

Figure 102. Simulation of military training with aged bone. The results show how the status of an aged bone affects the behaviour of cracks by reducing their resistance to high stresses. The cracks are usually smaller than for younger subjects when the stress is low, but they grow more easily when the stress is high.

An increased risk of fracture is present as it is possible that some cracks cannot be repaired completely because of their fast growth. In fact the simulation above will have a failure because of a crack that has not been repaired completely. The crack is repaired by the BMU, but because of its growth and in part because of the linearization effect that makes it harder for the system to follow the crack (the crack continues growing as it is larger than it actually is, as the crack growth rate is updated every hour) the BMU does not remove all the crack. The remaining crack is big enough to grow following the long crack behaviour

because the osteonal barrier is weakened by age and so it can grow until failure. This effect can be observed in detail in Figure 103.

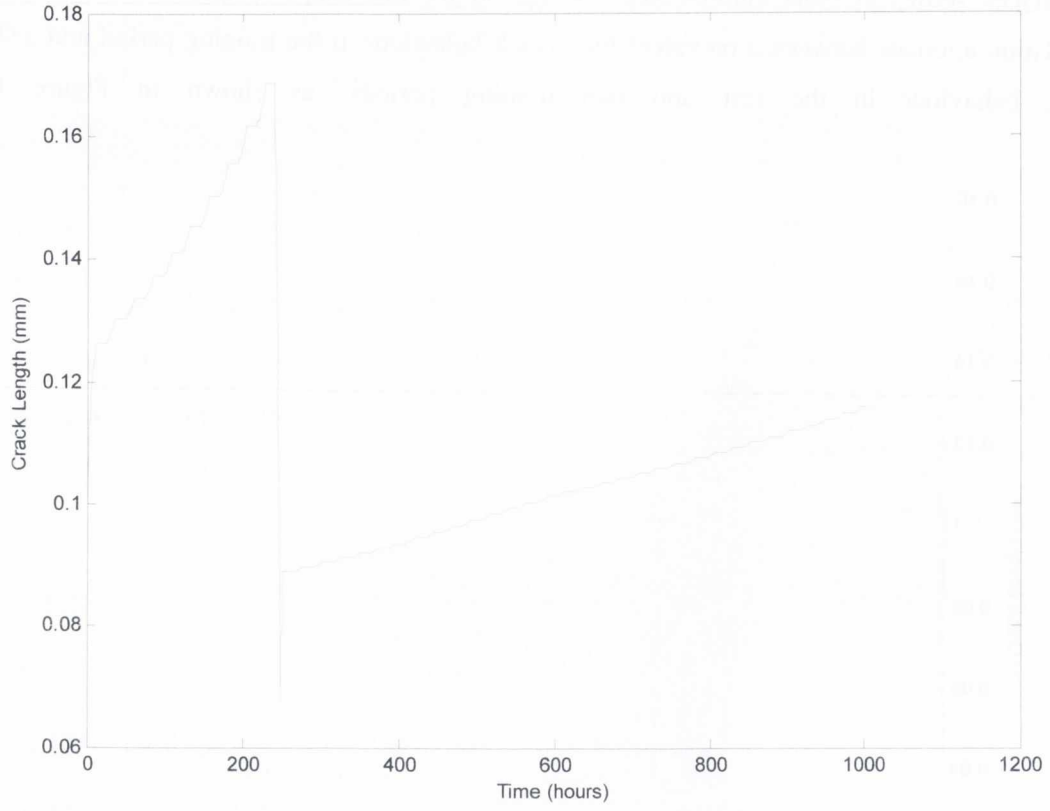

Figure 103. Simulation of a crack not completely healed. Even if the crack was going to be repaired by the BMU, the weakness of the bone around it made it so that the crack could continue growing during the repair.

Another possibility for the simulator is to replicate other conditions such as the presence of disease. Osteoporosis unbalances the remodelling process, causing a bone mass reduction that translates to an increase of the relative level of stress on the bone. This reduction increases at every repair until the bone is no longer able to sustain the stress, which causes a failure. In Figure 104 I have shown the results of a simulation under the same loading of military training, which results in failure. The results show also how more than one microcrack was growing toward dangerous values, as the reduced strength of bone made it more vulnerable to microcracks.

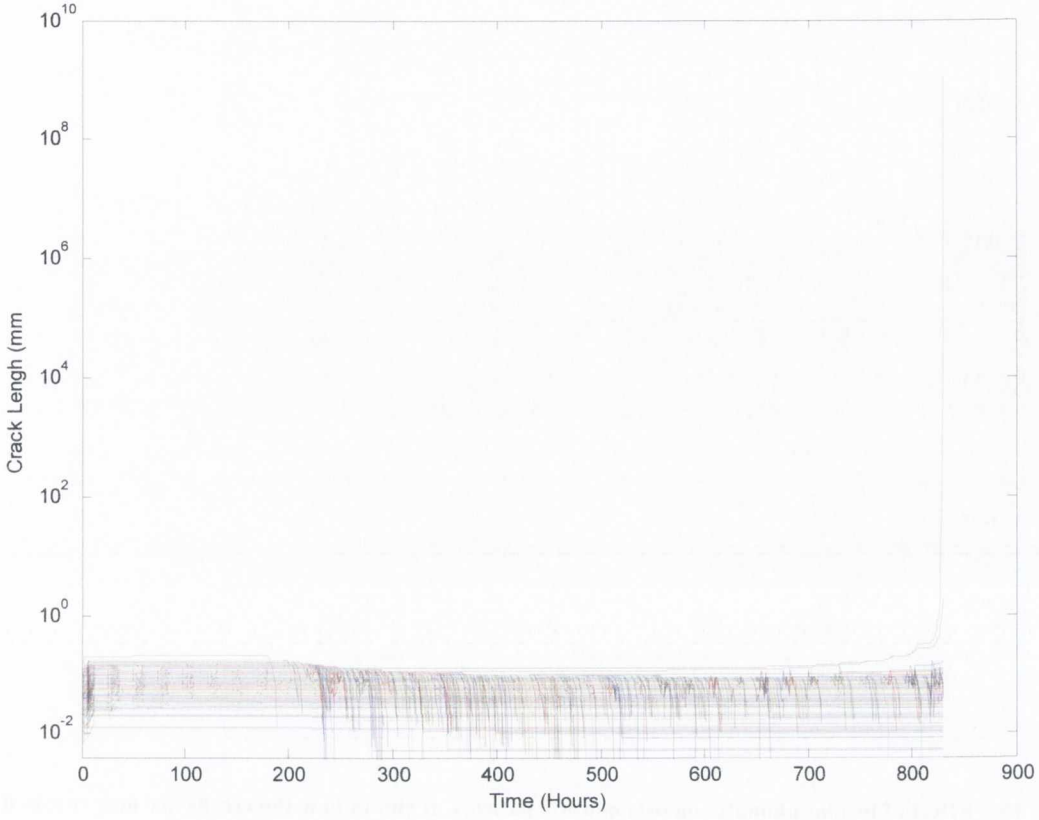

Figure 104. Simulation of osteoporosis, showing how with the loss of bone mass even cracks that were stable start becoming a danger. In the last few hours more than one crack are starting to diverge.

To counteract the effects of osteoporosis is become a clinical practice to use drugs like bisphosphonates. I have performed a simulation to replicate the effects of this kind of drugs on a subject affected by osteoporosis. The results show how the bisphosphonate extends the time needed for repair, allows the cracks to grow more and reduces the effectiveness of the BMU, which is not able to completely repair a 0.2 mm crack, but prevents the loss of bone mass and consequent reduction of bone strength that has brought failure to the previous simulation (Figure 105).

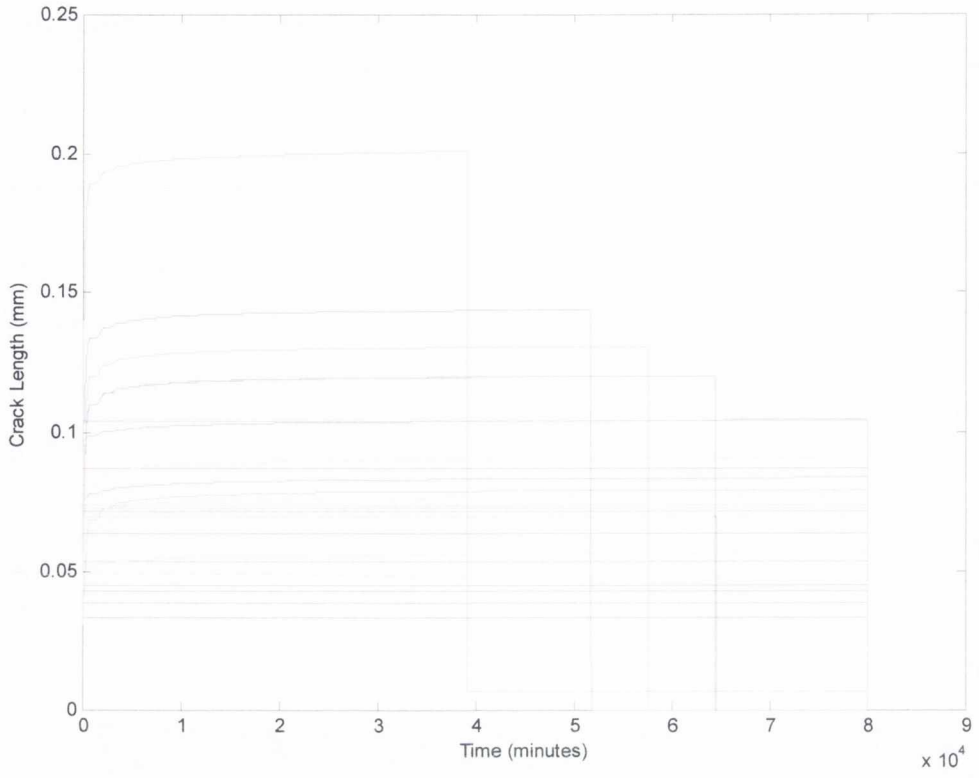

Figure 105. Effect of bisphosphonates on osteoporotic patients. It shows how the cracks are now repaired more slowly and the amount of crack removed is smaller than normal (usually a 0.2 mm crack should be completely repaired), but the strength of the bone is not affected by the repair as in Figure 104.

Another possible application of the simulator is to observe the effect of temporary overloads on the bone. A temporary overload is when a traumatic event, like a fall or a shock, causes the bone to experience a load that is lower than the stress required for the bone to break instantly, but high enough to be dangerous, if it were not temporary. One of the microcracks in the subject's bone grows during the accident. This crack reaches a size which is not dangerous during the "low stress" period, but that is enough to have it grow during the "high stress". As it can be seen from the simulation results below the crack size remains constant in the low stress period, then grows faster and faster every time it crosses the high stress period, until the failure. The repair effect heals the crack before it can reach dangerous levels; this is because the high stress periods are short in relation to the low stress periods, which allowed the crack the time to heal. So I have found again a clear motif of my simulation, which is how the presence of rest affects the health of the

bone, allowing the cells to repair cracks.

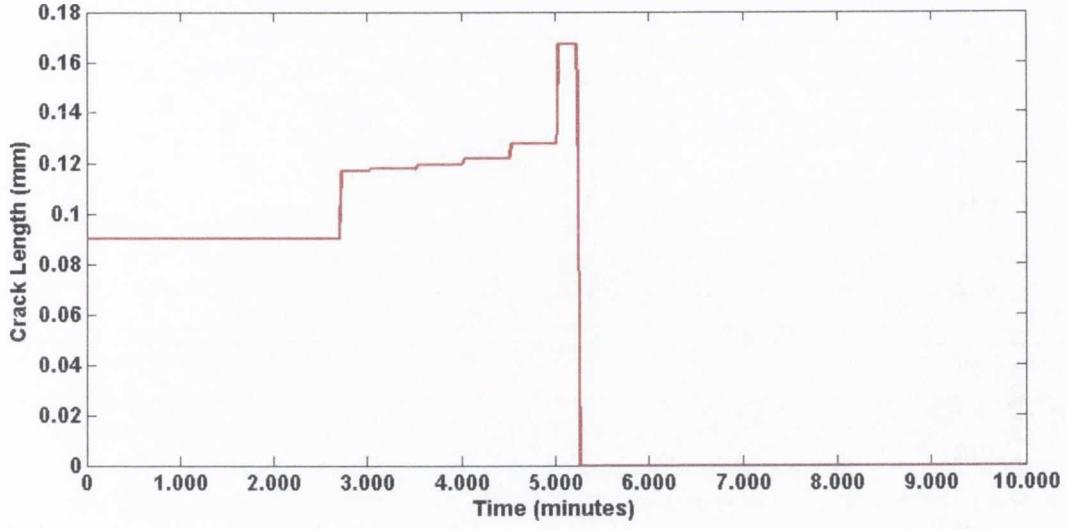

Figure 106. Behaviour of a microcrack in the "accident" simulation. It shows how the extra stress causes the crack to grow to a level where the "high stress" level is enough to cause crack growth, while the "low stress" does not cause growth. The crack gets repaired, but at every cycle of "high stress" the growth was greater than in the previous, a clear sign of danger.

Mechanostat signal model

Performing the simulation using the model for mechanostat signalling instead of the scissors model does not cause the results to differ much, except for the already mentioned difference in the "effectiveness" of the repair shown in Figure 90, caused by the generation of BMUs to repair very small cracks over long periods of time. The main difference between the two theories for the simulator is that Equation 23 provides a signal to insert in the model instead of the number of broken processes obtained by the "scissors" model, but the signal has a different behaviour with crack length when compared to the output of the "scissors" model with the same variable. The output of Equation 23 is linear with crack length, this means that all the cracks, even the smallest, will release signal when the crack length and the stress have a value. Also, while the number of processes along a crack is limited, the energy at its tip can be extremely high, thus the mechanostat signal can be hypothetically very high when the stress is big enough. Apart from that the simulator does not change its behaviour as long as the two models show coherent outputs. This confirms the initial hypothesis I have stated in the previous chapters about the interchangeability of the two theories for almost all the

applications of this simulator.

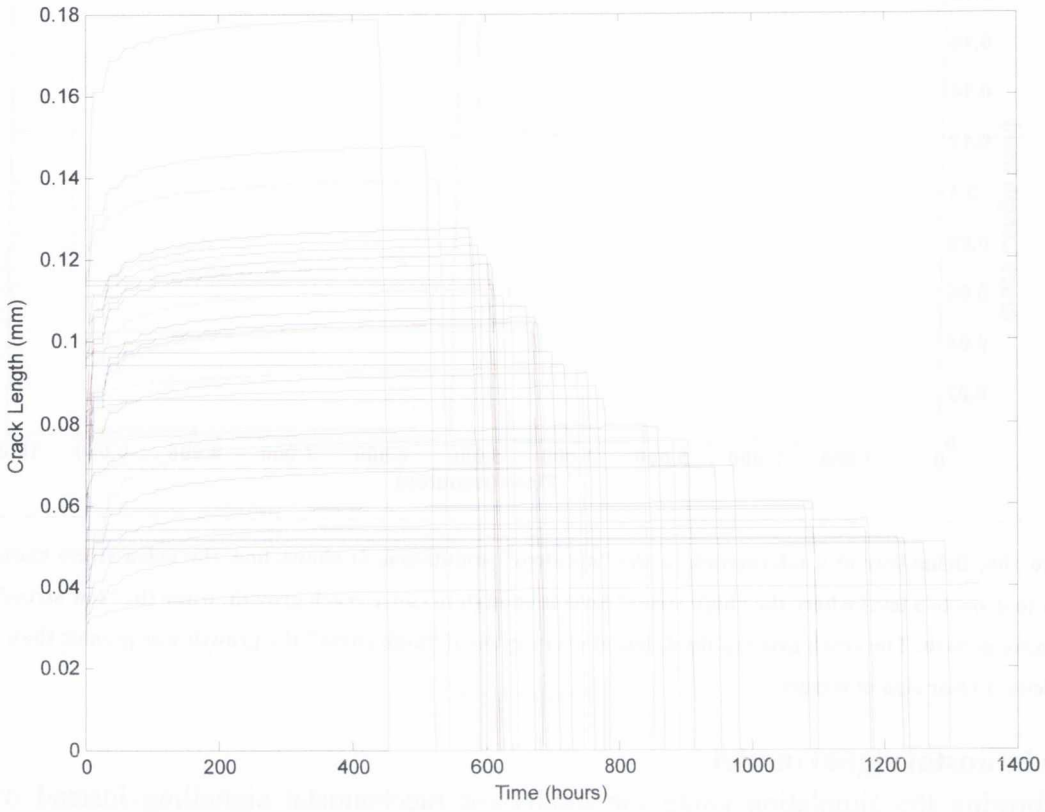

Figure 107. Simulation of military training performed with the mechanostat model. The behaviour is not drastically different from the simulation performed with the "scissor" model, but it can be noticed how the smaller cracks continue to be repaired even if they are not growing or potential risks.

Chapter 6: Discussion

This work describes how a simulation model to simulate the behaviour of microcracks in cortical bone has been developed by modelling independently the phases of crack growth, damage detection and crack repair. Predicting the behaviour of bone microdamage "*in vivo*" is a complex feat, requiring a multiscale approach to the problem. The application of control theory to this purpose has its advantages and disadvantages. First of all, this approach allows applying equations developed in different backgrounds and using them to observe all the variables that I included in the system. The system is open, every part of it can be observed singularly; in Simulink every subsystem is an equation, every block is either a variable or an operator. The degree of control granted by this approach has given the possibility to constantly improve the system and to reach a final degree of versatility so that one system can reproduce a large range of experiments with very small variations of its structure. The system is light and relatively fast, can simulate different patterns of stress and can be adapted to simulate the presence of diseases or the effects of age on the properties of bone. It can also show what happens when a single part of the crack growth and repair loop is not working properly, just by changing a few variables. On the other hand the system has been modelled by using data obtained from experiments and some of its equations are state equations, meaning that they simply tell the value of one variable when the other variables involved are at a given value. This means that the system can have difficulties simulating dynamic variations in some of its parameters that have been addressed by modifying a few relations, especially in the blocks simulating the interactions between crack growth and repair. Having differential equations for all the relations would provide for a smoother and more responsive system. Another problem of the simulator is the relative difficulty to obtain its parameters, as some of them are relatively uncommon and hard to find in literature. To simulate crack system requires knowledge of the microstructure at osteonal level of the bone (the value of the half-distance between osteons d), which is not widely shown in literature. A fundamental mechanics affecting the risk associated with the crack is linked to the stress intensity threshold ΔK_{th}; the value of this threshold affects at the same time both the size of the crack that can be dangerous at a given stress level and the speed of the crack growth when the crack reaches the "long" behaviour. The lower this value, the faster the crack will grow once it has breached an osteon. Finding a good value for this variable is very

important for the simulation. For large animals (equine and bovine) I have used the value in Shelton (37) and I have had satisfying results. For human bone I have used the value in Taylor *et al* (31), but since this value has been deduced in the paper instead of being obtained by experimental data, I have used other experimental results, mainly from Kruzic *et al* (33), to confirm this value. While the simulator is light for many of its applications its load increases when the number of cycles and the number of cracks increase, as the number of calculations required increase in a multiplicative way. A simulation for 20 cracks in 5000 cycles can take less than 3 seconds, while a 100 crack simulation for 80000 cycles takes more than a minute. The system is pretty fast and can be used easily for a large number of simulations, but it has difficulties when simulating large numbers of cracks, requiring a tuning of the time scale to avoid incurring memory errors.

As far as I know, this is the first time that Simulink™ has been used to simulate the mechanics of bone damage and repair. Simulations of bone under fatigue load are usually performed using Finite Element Analysis (FEA) (67) (85) (94). My approach has the advantage to allow complete freedom of choice of the equations I want to implement in the system, FEA programs have a usually more restricted choice of equations to use and are generally bound to the mathematical resolution of continuity equations. In other works, the repair mechanisms have been usually simulated by using differential equation systems (65) (22) (68) (95) and having them solved by the computer. This last approach is similar to mine, but in many occasions the system are based on empirical equations and finding. In this work I have tried as much as possible to use analytical equations which reproduce in detail the actual mechanics of bone crack growth and repair at the different scales. The equations used to model the system descript mechanical processes, structural effects and chemical reactions to reproduce the behaviour of microcracks in an accurate way and this is the first time that these different equations and models have been used together in the same simulation.

The use of analytical equations is at the same time the strongest and weakest point of the simulation. They allow the simulation to not have any "blind" spot where the empirical equations would not be able to predict the coincidence of different mechanics, but they require, as written before, the use of specific variables which sometimes are difficult to retrieve, thus affecting the precision of the model when they have to be extrapolated from different sources, some of which could not be perfectly fit to the simulation in case.

Luckily, the structure of the system gives it a good level of "robustness" as the errors tend to be confined to the section of the model where they generate, without affecting negatively the other sections because of the way the equations are arranged. For example a variation in the number of broken processes because of an erroneous calculation of the number of processes crossing a crack would not have a large effect on the time of creation of a BMU because the Hill equation acts as a dampener of the output (but would affect the amount of signal released and change the priority of repair) and an error in the choice of the parameters for the BMU formation would not have a large effect on crack length because the BMU size is given as constant (but it would change the timing of the BMU formation).

Simulation of crack growth in fatigue tests

The first set of results I have shown in this work is composed of simulations of crack behaviour in dead bone during fatigue tests (Table 4). These simulations have been performed without using the sections of the simulator that regulate damage detection and repair, so their results are depicting the behaviour of dead bone. Comparing the results of these simulations with those of similar experiments done in literature it can be observed how the simulator is able to replicate the effects of fatigue of crack length with a usually low degree of error (see Table 4), but the results also tell how the simulator's precision is linked to its different settings, a good lesson to learn how to better tune the simulator for more complex tasks. Using randomly distributed variables the results' accuracy improves and the accuracy is better when simulating a large number of cycles in relation to the time scale than when simulating a smaller number of cycles. The time scale is an artifice I have used to allow the simulator to replicate a large number of cycles without having outputs too big and without having memory issues, but its effects of linearization on the results need to be accounted for in the analysis of the results; low levels of linearization are observed when the value of time scale is in the order of the hundreds of cycles per second of simulation, but when the time scale is greater the reactivity of the system to changes is much slower.

Simulating the time to failure of a bone section requires the simulator to run to the failure of the bone multiple times, recording the times at every failure. The effect of linearization affects also the results of this kind of analysis, but only because the registered times need to be multiplied for the time scale to have the number of cycles. This simulation has been performed to observe how the system reacts to different sizes in two samples of the same

material under the same stress. The results from these simulations have been compared with the theoretical equations backed by experimental results found in Taylor 2000 (38) and have shown good adherence to their results, proving how the system is able to realistically reproduce the behaviour of a bone under fatigue load (Figure 74).

Simulation of repair

The most advanced feature of the simulator is the ability to predict the mechanics of repair in living bone. In the simulation the repair timings are coherent with the results in literature, but the use of the "scissors model" to define the time of activation of the BMU has another interesting feature: the BMU is activated by a combination of damage and stress. In other words, making the BMU react to broken osteocyte processes implies that the time of BMU activation is linked both to damage and stress, the same crack at lower levels of stress has less broken processes, so it would be repaired later. For a given level of stress it can be seen how cracks are repaired in order of size, more than in order of age, this mechanism could also explain why some cracks are never repaired (see Figure 100), while other cracks are repaired in a matter of days. This difference in the treatment of cracks cannot be observed in experiments, as observing a crack, let alone determining its "age", before it is repaired is impossible, so it is clearly a result with is only obtained by this simulation. I have also compared the effect of repair to the effect that appears in literature (48) where the correlation between average crack length and the number of resorption spaces left by BMUs is shown as linear. My simulation has shown a linear behaviour, coherently with the experimental data, where the slope/intercept ratio should represent the size of the BMUs (see Figure 89). My simulation differs from the experimental study because the simulation was done on a number of microcracks, while the study was done on a section of bone, so while the authors of the study had to use the density of resorption spaces, I had the simulator telling the exact number of BMUs that have repaired cracks. Another difference is that the graph in the study was used to demonstrate that the repair process in bone is not a casual mechanism, but a targeted action used by the bone to repair its microdamage; in the simulation I have used this approach from the beginning, as the repair in the simulation is not only a targeted process, but also an exclusive process, as every BMU repairs one and only one microcrack. Comparing the results of the simulation using the "scissors" model to those obtained using the mechanostat model has shown a difference between the two models which would have been otherwise difficult to notice. While the "scissors" model result prompts

a linear correlation between BMUs and average crack length the mechanostat model results in a nonlinear correlation, with the BMUs losing "effectiveness" when the average crack length is low, because of the fact that they continue to repair even small cracks (Figure 90). This difference between the two models has not been found before and is one of the findings that can be obtained with this simulator.

Military stress fracture simulation

I have used the simulator to predict the behaviour of microcracks in the lower limbs of army trainees during 8 weeks of training I have modelled the load caused by training by simulating a whole day in the life of a soldier and dividing it in periods to simulate the training, non-training activity and rest the soldiers perform during a typical day. The simulation has given the behaviour of the bone microcracks during the simulation period (Figure 93): the cracks grow in the phases of increased stress, while at the same time the body activates the repair system to reduce the more dangerous cracks' length before they grow enough to cause bone failure. The results show how this balance between crack growth and repair is usually such that the cracks are repaired before is too late, given enough rest. I have calculated the probability of stress fracture for different distributions of ΔK_{th} and the results have confirmed how important that variable is to quantify the risk of fracture; in three distributions with the same mean value but only slightly different standard deviations I have found dramatically different results. I have surely overestimated the stress in the training, as the simulation does not calculate the inevitable stops to catch breath that a soldier will take, simulating hours of uninterrupted training. When present, failure appears in the first weeks of training, as has been noted in the reference literature (83) (Figure 101). The results have also shown how the danger of a crack is directly related to the stress it is subject to. Even when the crack was large enough to be the cause of stress fracture in a training environment, the same crack in a normal stress layout would have not caused a stress fracture. Moreover, given enough time the crack would have been repaired and the bone would have been able to sustain the training stress afterwards, showing how rest can be an extremely good treatment for stress fractures, as it was also hypothesised by real life reports on army trainees (84).

Simulation of special scenarios

A goal for the system was to achieve a simulation able to replicate the effects of disease and of variable load conditions. The results have shown that the versatility of the system is one of its strong points, showing the possibility to reproduce special scenarios.

I have performed a simulation to model the effects of old age on the bone during the training regime, this simulation shows a different behaviour, as because of the reduced strength of the bone, the short and long crack behaviours overlap, causing a rising trend of crack length (Figure 102). Even repair is not sufficient to prevent failure, as the weakened osteons are unable to contain the cracks even at short lengths. The other concurrent effect of age, the increased number of secondary osteons, does not affect the crack lengths enough to prevent the crack from reaching dangerous size.

In another simulation I have tried to replicate the effects of osteoporosis in a patient (Figure 104). Clinical osteoporosis is characterized by a level of bone density that is below 2.5 standard deviations from the average value. The status of osteoporotic patient is easy to simulate with an enhanced level of stress, but I have used a different approach. Instead of simulating the osteoporosis as a static weakening of bone, I have tried to simulate the imbalance of bone damage and remodelling that causes the loss of density. To do so I have reduced the effectiveness of osteoblasts in the balance of bone density, to see how the disease turns an otherwise useful process as repair in a harmful process for the bone. The results show as expected how after the unbalanced remodelling takes place the imbalance causes even small cracks to become a danger for the body, because the reduction in bone density causes a reduction in the strength of the bone .

After simulating the effect of an osteoporotic condition I have simulated also the effects of a drug made to counter the disease (Figure 105). I have simulated the effect of bisphosphonates, a class of drugs that are currently in use for the treatment of osteoporosis. These drugs affect the activation of osteoclasts to delay the repair and to reduce the unbalance of bone removed and replaced caused by osteoporosis. I have simulated the first effect by increasing the activation coefficient for osteoclasts in the pathway simulation and reducing the coefficient of bone removed from the BMU simulation. In the simulation the effect of the drugs delays the activation of the BMUs and counter the effect of bone loss, but according to experimental data the BMUs, removing less bone, are also impaired in their crack repair effectiveness, reducing their efficiency in repairing damage.

These simulations are able to give us results and findings that would be impossible to obtain experimentally. The possibility to replicate the different conditions of health and age, together with the possibility to submit the bone to any sort of loads allows for

generating infinite different situations, even those that are impossible or too dangerous to be reproduced in real-life experiments, like having an elderly or osteoporotic person sustain a workload comparable to that of an army trainee.

Simulation of an accident

To prove the versatility of the system I have also applied the simulation to the task of predicting the effect of an unexpected overload in an otherwise manageable stress layout. I have showed only one crack to better focus on its behaviour. The crack growth because of the overload changes a manageable crack in a dangerous crack, which grows during every high stress period more than in the previous, rapidly reaching dangerous length. The presence of a low stress period allows the bone to repair the damage before failure, preventing an almost certain failure. This simulation replicates a known occurrence in the clinical casuistry: the stress fracture of a bone even 7 days after a traumatic event. This events cause a single crack to grow beyond an osteon, making it more susceptible to stress and causing a stress fracture if the patient does not recognize the danger and rests consequently (Figure 106). The use of the simulator has shown us how these "delayed" stress fractures could work, emphasizing again the usefulness of rest in the treatment of traumatic events, even when the residual damage could remain unseen because of a relative lack of symptoms.

Conclusions

The idea of approaching a simulation of microcracks in bone with the instruments of control theory is new and some of the instruments are not completely fit to this task, but the results obtained are encouraging. I have managed to create a system that is able to simulate the behaviour of cracks in bone during fatigue regimes and the process of repair caused by the damage represented by these cracks. The system is able to offer the values at every time of simulation of the crack growth, the amount of signal, the presence of RankL and other actors in the generation of a BMU, the number of BMU created since the start of the simulation and the number of osteoclasts and osteoblasts that are forming new BMUs, their balance and the amount of bone that will be removed and added by those BMUs for a number of different cracks. The simulator has been able to model the effects of diseases or drugs and the effects of old age on the mechanics of bone fatigue. I have shown the results of simulations of different load regimes, from the standard fixed load on the samples during fatigue tests to a complex time-dependant load simulating military training. The system allows monitoring of different parameters and shows adherence to the theory and experiments performed on this topic. As the variables are easily controllable the system is able to reproduce situations that are not easily controlled in experiments and the full control allows for reproducing situations which are too dangerous or painful to be seen in experiments, like an elderly person training for weeks like an army trainee. What makes this simulator different from every other is the fact that every equation, every step and every variable are visible in a graphical form and all the flux of information in the system is easily recognizable in the Simulink™ interface, allowing even inexperienced users to easily understand the relations among equations and modify the system when needed. This versatility makes for a system that is easily accessible for potential variations and improvements, allowing for example to change the pathway that generates the BMU with a different one to accommodate a different theory of damage detection or to calculate the effects of other actors in the formation of osteoclasts or osteoblasts. As the topic of bone damage accumulation and repair is still an evolving discussion in the scientific community and there is still room for new discoveries to confirm or dismiss the different theories that try to understand these mechanics, this model can become a useful tool to replicate the mechanics of bone damage and repair and to compare theories and experimental data. This system has

allowed to create an interface able to model the mechanics of bone microcrack in different situations, offering an insight on how the different mechanics obtained in different scales and different experiments are able to coexist and to interface with each other creating an harmonious system, which has been replicated in this model, but is a reproduction of how the different mechanics interact with each other in real life. This is the most revolutionary finding of this simulation, the ability to reproduce the links that connect different mechanics in real bone and to explain the way whose mechanics interact with each other into creating the cycle of bone damage accumulation and repair.

Possible improvements

The simulator can be improved in many ways, apart from the abovementioned problems with dynamic equations there is room for improving the response and reduce the approximations, by obtaining a better understanding of the reactions that bring the repair process to start I can modify the repair block to include in its variables other actors that have been suggested as involved in the BMU creation and in its cells' effectiveness. To insert the simulation of the pathway in the system I had to convert the pathway in a cascade of subsystems that replicates the reactions in the pathway. At the moment Simulink™ does not have a way to directly insert a Simbiology™ model in it, but as soon as this feature will be added I could also integrate more complex models with greater ease. The properties of bone are given as standard in the simulation, but calculating them from characteristics like mineralization and a study on bone "quality" could add an extra layer of depth to the simulation An improved management of the mechanics of bone strengthening with higher levels of stress and weakening with lower stresses would give an increased edge to the system, with more possibilities for long-term analysis. I have simulated the behaviour of bone in cases like osteoporotic diseases and the effects of drugs, but knowing the pharmacokinetics of those drugs could allow for a better simulation of their effects. The system can simulate many cracks at the same time but the statistical analysis of the probability of failure requires the system to be run at least 100 times and to register the failures in an external array, finding a way to make this process automatic would allow for a more practical approach. Simulink™ is also able to use more advanced functions, like real time replies and I/O interfaces. With more study and the adequate hardware, this system could be modified to simulate in real time the behaviour of a bone under a load detected by an external force feedback apparatus, to better simulate the effects of load on a real bone. Another possible future study would involve different

modes of application of strength, which are easy to model in the simulation but would require special arrangement to be shown in experiments. For example, would the bone be more at risk of failure after being under a fatigue load whose amplitude rises from a value A to a value A+B of would it be more dangerous a load whose amplitude goes from A+B to A? The system would be able to predict this, but without experiment there would be no way to say if the prediction is right. The application of control theory and system biology could also inspire new projects, as the creation of a simulator of a more complex biological process already mapped, for example a complex bacteria.

Appendix: List of Matlab™ scripts and functions

Script to measure displacement along a crack

```
E=9.6; %E22 Module of Young%;
f=3.25; %I work on shear
v=0.39; %Poisson Module
a=15; %width
b=4*a; % length
sigma=17; %average load
beta=70; %angle of effect
x=[1:0.1:15]; %position on the x axis
dss=(f*1.15*(sigma/E)*(1-v^2)*sqrt(a^2-x.^2)*(sin(b)*cos(b))); %displac.
plot (x,dss)
```

Program to observe the displacement on 4 cracks at the same time

```
%Orthotropic Elasticity%
E=17.4; %E11 Module of Young%;
f=3.25; %I work on shear
v=0.39; %Poisson Module
a1=200;
a2=150;
a3=100;
a4=25;
sigma=0.040; %average load equivalent to 40 Mpa
beta=1.222; %angle of effect 70°
x1=[0:0.1:200];
x2=[0:0.1:150];
x3=[0:0.1:100];
x4=[0:0.1:25];
ds401=(f*1.15*(sigma/E)*(1-v^2)*sqrt(a1^2-x1.^2)*(sin(beta)*cos(beta)));
ds402=(f*1.15*(sigma/E)*(1-v^2)*sqrt(a2^2-x2.^2)*(sin(beta)*cos(beta)));
ds403=(f*1.15*(sigma/E)*(1-v^2)*sqrt(a3^2-x3.^2)*(sin(beta)*cos(beta)));
ds404=(f*1.15*(sigma/E)*(1-v^2)*sqrt(a4^2-x4.^2)*(sin(beta)*cos(beta)));
hold off
hold on
plot (ds401, 'color', 'red')
plot (ds402, 'color','blue')
plot (ds403, 'color', 'green')
plot (ds404, 'color', 'black')
```

Program to observe the behaviour of the crack with different stresses

```
%Orthotropic Elasticity%
E=17.4; %E11 Module of Young%;
f=3.25; %I work on shear
v=0.39; %Poisson Module
a=50;
b=4*a;
sigma=[0.030; 0.040; 0.050; 0.060]; %average load equivalent to 30, 40, 50 and 60 Mpa
beta=1.222; %angle of effect 70°
x=[0:0.1:50];
dsv10=(f*1.15*(sigma/E)*(1-v^2)*sqrt(a^2-x.^2)*(sin(beta)*cos(beta)));
plot (x,dsv10)
```

Program to evaluate the number of broken processes by measuring displacement

```
%Orthotropic Elasticity%
E=17.4; %E11 Module of Young%;
f=3.25; %I work on shear
v=0.39; %Poisson Module
a= [0:200];
b=4*a;
sigma=0.040; %average load equivalent to 40 Mpa
beta=1.222; %angle of effect 70°
limit=0.1;
x=sqrt(a.^2-(limit/(f*1.15*(sigma/E)*(1-v^2)*(sin(beta)*cos(beta))))^2);
Percx= ((a-x)./a)*100;


broken=(x/4.4);


plot (a,broken)
```

Function to obtain the number of broken processes by shear displacement with crack length

```
function [ br ] = brokenprocesses( a)
%Brokenprocesses gives the number of broken processes in a crack of lenght
%a under the stress of 80 MPa and with an angle of 70°
E=17.4; %E11 Module of Young%;
f=3.25; %I work on shear
```

```
v=0.39; %Poisson Module
sigma=0.080; %average load equivalent to 80 Mpa
beta=1.222; %angle of effect 70°
limit=0.1;
x=sqrt(a.^2-(limit/(f*1.15*(sigma/E)*(1-v^2)*(sin(beta)*cos(beta))))^2);


if (a<=0);
   br = 0;
else
br=(x/4.4);
end


end
```

Program to simulate the number of broken processes with time following the fatigue theory

```
%Orthotropic Elasticity%
E=17.4; %E11 Module of Young%;
f=3.25; %I work on shear
v=0.39; %Poisson Module
d=4.4; %ovine bone distance between processes
a1=200;
a2=150;
a3=100;
a4=50;
n=16.7;
k=0.4;
sigma=0.080; %average load equivalent to 80 Mpa
beta=1.222; %angle of effect 70°
Nf=[1:100000];
J=(f*1.15*(sigma/E)*(1-v^2)*(sin(beta)*cos(beta)));
x1=sqrt((a1.^2)-(k./(J.*(Nf.^(1/n)))).^2);
x2=sqrt((a2.^2)-(k./(J.*(Nf.^(1/n)))).^2);
x3=sqrt((a3.^2)-(k./(J.*(Nf.^(1/n)))).^2);
x4=sqrt((a4.^2)-(k./(J.*(Nf.^(1/n)))).^2);
i1=a1-x1;
i2=a2-x2;
i3=a3-x3;
i4=a4-x4;
```

```
y1=i1/(d*a1);
y2=i2/(d*a2);
y3=i3/(d*a3);
y4=i4/(d*a4);
hold off
hold on
plot (Nf,y1, 'color', 'red')
plot (Nf,y2, 'color','blue')
plot (Nf,y3, 'color', 'green')
plot (Nf,y4, 'color', 'black')
```

Program to plot a 3-dimensional surf of intact processes per mm against time and crack length for bovine bone.

```
%Orthotropic Elasticity%
E=20; %E11 Module of Young%;
f=3.25; %I work on shear
v=0.39; %Poisson Module
d=7; %bovine bone distance between processes
a=[1:100:4000]; %Length of the crack
n=16.7; %Exponent in the Fatigue Equation
k=0.4; %constant of the Fatigue Equation
sigma=0.080; %average load equivalent to 80 Mpa
beta=1.222; %angle of effect 70°
Nf= [1:100:10000]; %time
x=zeros(40,100);
J=(f*1.15*(sigma/E)*(1-v^2)*(sin(beta)*cos(beta)));
for i=1:40
    x(i,:)=sqrt((a(i).^2)-(k./(J.*(Nf.^(1/n))).^2));  %Length  of  crack
affected by fatigue damage with time
end
uno=Nf'.^0;
ax=uno*a;
i=ax-x'; %Unaffected length of crack
i=real(i);
Pmm=(i./ax)*1000/d;
surf (Pmm) %surface with the intact processes per mm
```

Bibliography

1. **Martin, RB, Burr, DB and Sharkey, NA.** *Skeletal tissue mechanics.* New York, USA : Springer-Verlag, 1998.

2. *Bone Maintenance and Remodeling:A Control System Based on Fatigue Damage.* **Taylor, D.** 1997, Journal of Orthopaedic Research, pp. 601-606.

3. *Bone remodelling algorithms incorporating both strain and microdamage stimuli.* **McNamara, L. M. and Prendergast, P. J.** 2007, Journal of Biomechanics, pp. 1381-1391.

4. **Wolff, J.** *Das gesetz der transformation der knochen.* Berlin : Hirchwald, 1892 .

5. *Bone Microdamage and Skeletal Fragility in Osteoporotic and Stress Fractures.* **Burr, D. B., et al.** 1997, Journal of Bone Mineral Research, pp. 6-15.

6. **Gray, H.** *Anatomy of the human body.* Philadelphia, USA : Lee and Febiger, 1959.

7. **Gibson LJ, Ashby MF.** *Cellular solids—structure and properties.* Oxford : Pergamon Press, 1997.

8. **Netter, Frank H.** *Musculoskeletal system: anatomy, physiology, and metabolic disorders.* Summit, New Jersey : Ciba-Geigy Corporation, 1987.

9. *The role of osteocytes and bone microstructure in preventing osteoporotic fractures.* **Hazenberg, J. G., Taylor, D. and Lee, T. C.** 2007, Osteoporosis International, pp. 1-8.

10. *Effects of loading frequency on the functional adaptation of trabeculae predicted by bone remodeling simulation.* **Kameo, Yoshitaka, Adachi, Taij and Hojo, Masaki.** 2011, Journal of mechanical behavior of medical materials, pp. 900-908.

11. *Characterization of the Spatial Arrangement of Secondary Osteons in the Diaphysis of Equine and Canine Long Bones.* **SHAHAR, R., et al.** 2011, THE ANATOMICAL RECORD, pp. 1093-1102.

12. *Trabecular bone structure and strength - remodelling and repair.* **Mosekilde, L., Ebbesen, E.N. and Tornvig, L. and Thomsen, J.S.** 2000, Journal of Musculoskeletal Neuronal Interaction, pp. 25-30.

13. *The nature of fatigue damage in bone.* **Lee, T. C., O'Brien, F. J. and Taylor, D.** 2000, International Journal of Fatigue, pp. 847-853.

14. *The effect of bone microstructure on the initiation and growth of microcracks.* **O'Brien, F.J., Taylor, D. and Lee, T. C.** 2005, Journal of Orthopaedic Research, pp. 475-480.

15. *The real response of bone to exercise. .* **Boyde, A.** 2003, Journal of Anatomy, pp. 173-189.

16. *The cellular transducer in bone: What is it?* **Taylor, D. and Hazenberg, J. and Lee, T. C.** 2006, Technology and Health Care, pp. 367-377.

17. *Response of the osteocyte syncytium adjacent to and distant from linear microcracks during adaptation to cyclic fatigue loading.* **Colopy, S.A., et al.** 2004, Bone, pp. 881-891.

18. *Fracture and repair of bone: a multiscale problem.* **Taylor, D.** 2007, J Mater Sci, pp. 8911-8918.

19. *Bone Remodeling in response to in vivo fatigue microdamage.* **Burr, D.B., et al.** 1985, Journal of Biomechanics, pp. 189-200.

20. *Model structure and control of bone remodeling: A theoretical study.* **Pivonka, P., et al.** 2008, Bone, pp. 249-263.

21. *Targeted and nontargeted remodeling.* **Burr, D. B.** 2002, Bone, pp. 2-4.

22. *THE CELLULAR DYNAMICS OF BONE REMODELING: A MATHEMATICAL MODEL.* **RYSER, M. D., KOMAROVA, S. V. and NIGAM, N.** 2010, Journal of Applied Mathematics, pp. 1899-1921.

23. *Osteoprotegerin ligand is a cytokine that regulates osteoclast differentiation and activation.* **Lacey DL, Timms E, Tan HL, Kelley MJ, Dunstan CR, Burgess T, Elliott R, Colombero A, Elliott G, Scully S, Hsu H, Sullivan J, Hawkins N, Davy E, Capparelli C, Eli A, Qian YX, Kaufman S, Sarosi I, Shalhoub V, Senaldi G, Guo J, Delaney J, Boyle WJ.** 1998, Cell, pp. 165-176.

24. *RANK, RANKL and osteoprotegerin in bone biology and disease.* **Wright, H. L., et al.** 2009, Current Reviews in Musculoskeletal Medicine, pp. 56-64.

25. *Confounders in the Association between Exercise and Femur Bone in Postmenopausal Women.* **BECK, T. J., et al.** 2010, MEDICINE & SCIENCE IN SPORTS & EXERCISE, pp. 80-89.

26. *Enhanced daily load stimulus to bone in spacefl ight and on Earth.* **GENC, K.O., HUMPHREYS, B.T. and CAVANAGH, P.R.** 2009, Aviat Space Environ Med, pp. 919-926.

27. *Fracture, aging, and disease in bone.* **Ager III, J.W., Balooch, G. and Ritchie, R.O.** 2006, Journal of Material Research, pp. 1878-1892.

28. *Damage accumulation in compact bone: a fracture mechanics approach to estimate damage andrepair rates.* **Taylor, D. and Prendergast, P.J.** 1995, Advances in Bioengineering, pp. 337-338.

29. *Microcrack growth parameters for compact bone deduced from stiffness variations.* **Taylor, D.** 1998, Journal of Biomechanics, pp. 587-592.

30. *Mechanical and morphological effects of strain rate on fatigue of compact bone.* **Shaffler, M B, Radin, E L and Burr, D B.** 1989, Bone , pp. 207-214.

31. *Modelling of fatigue crack growth at the microstructural level.* **Taylor, D.** 2002, Computational Material Science, pp. 228-236.

32. *A crack growth model for the simulation of fatigue in bone.* **Taylor, D. and Lee, T.C.** 2003, International Journal of Fatigue, pp. 387-395.

33. *Propagation of surface fatigue cracks in human cortical bone.* **Kruzic, J.J., et al.** 2006, Journal of Biomechanics, pp. 968-972.

34. *Microcrack accumulation at different intervals during fatigue testing of compact bone.* **O'Brien, F. J., Taylor, D. and Lee, T. C.** 2003, Journal of Biomechanics, pp. 973-980.

35. *Bone as a composite material: The role of osteons as barriers to crack growth in compact bone.* **O'Brien, F. J., Taylor, D. and Lee, T. C.** 2007, International Journal of Fatigue, pp. 1051-1056.

36. *The behaviour of microcracks in compact bone.* **O'brien, F.J., et al.** 2005, European Journal of Morphology, pp. 71-79.

37. *Transverse fatigue crack propagation behaviour in equine cortical bone.* **SHELTON, D. R., et al.** s.l. : JOURNAL OF MATERIALS SCIENCE, 2003, JOURNAL OF MATERIALS SCIENCE, pp. 3501-3508.

38. *Scaling Effects in the Fatigue Strength of Bones from Different Animals.* **Taylor, D.** 2000, Journal of Theoretical Biology, pp. 299-306.

39. *Distribution of microcrack lengths in bone in vivo and in vitro.* **Presbitero, G., et al.** 2012, Journal of Theoretical Biology, pp. 164-171.

40. *Microstructural mechanical study of a transverse osteon under compressive loading: The role of fiber reinforcement and explanation of some geometrical and mechanical microscopic properties.* **DeMicheli, P.O. and Witzel, U.** 2011, Journal of Biomechanics, pp. 1588-1592.

41. *Osteonal structure in the equine third metacarpus.* **Martin, R.B., et al.** 1996, Journal of Biomechanics, pp. 165-171.

42. *The prediction of stress fractures using a 'stressed volume' concept.* **Taylor, D. and Kuiper, J.** 2001, Journal of Orthopaedic Research, pp. 916-926.

43. *The importance of mechanical loading in bone biology and medicine.* **Martin, R.B.** 2007, Journal of Musculoskeletetal Neuronal Interactions, pp. 48-53.

44. *Computational modeling of bone density profiles in response to gait: a subject-specific approach.* **Pang, H., et al.** 2011, Biomechanics and Modeling in Mechanobiology, pp. 379-390.

45. *Strength of human compact bone under repetitive loading.* **Evans FG, Lebow M.** 1957, Journal of Applied Physiology, pp. 127-130.

46. *MICROMECHANICS THEORY OF FATIGUE CRACK INITIATION AND PROPAGATION.* **GHONEM, H. and PROVAN, J. W.** 1980, Engineering Fracture Mechanics, pp. 963-977.

47. *Micro- and nano-structural analyses of damage in bone.* **Sahar, N. D., Hong, Sun-Ig and Kohn, D.H.** 2005, Micron, pp. 617-629.

48. *Targeted bone remodeling involves BMU steering as well as activation.* **Martin, R. B.** 2007, Bone, pp. 1574-1580.

49. *Measuring the shape and size of microcracks in bone.* **Taylor, D. and Lee, T. C.** 1998, Journal of Biomechanics, pp. 1177-1180.

50. *Microdamage: A cell transducing mechanism based on ruptured osteocyte processes.* **Hazenberg, J. G., et al.** 2006, Journal of Biomechanics, pp. 2096-2103.

51. *The cellular transducer in damage-stimulated bone remodelling: a theoretical investigation using fracture mechanics.* **Taylor, D., Hazenberg, J.G. and Lee, T.C.** 2003, Journal of Theoretical Biology, pp. 65-75.

52. *Fracture Mechanics.* **Ewalds, H.L., Wanhill, R.J.H.,.** s.l. : Edward Arnold, 1997.

53. *Mechanical loading: biphasic osteocyte survival and targeting of osteoclasts for bone destruction in rat cortical bone.* **Noble, BS, et al.** 2003, American Journal of Physiology - Cell Physiology, pp. C934-C943.

54. *RANKL and OPG activity is regulated by injury size in networks of osteocyte-like cells.* **Mulcahy, L. E., et al.** 2011, Bone, pp. 182-188.

55. *Sensitivity of osteocytes to biomechanical stress in vitro.* **Klein-Nulend, J.** 1995, FASEB Journal, pp. 441-445.

56. *Mechanotransduction in bone—role of the lacunocanalicular network.* **BURGER, E. H. AND KLEIN-NULEND,J.** 1999, FASEB Journal, pp. S101-S112.

57. *Mechanobiology of bone tissue.* **Klein-Nulend, J., Bacabac, R.G. and Mullender, M.G.** 2005, Pathologie Biologie, pp. 576-580.

58. *Osteocyte morphology in fibula and calvaria — Is there a role for mechanosensing?* **Vatsa, A., et al.** 2008, Bone, pp. 452-458.

59. *What is the importance of multiphysical phenomena in bone remodelling signals expression? A multiscale perspective.* **Lemaire, T., et al.** 2011, Journal of the Mechanical Behaviour of Biomedical Materials, pp. 909-920.

60. *Activation of bone remodeling after fatigue: Differential response to linear microcracks and diffuse damage.* **Herman, B.C., et al.** 2010, Bone, pp. 766-772.

61. *Activation of resorption in fatigue-loaded bone involves both apoptosis and active pro-osteoclastogenic signaling by distinct osteocyte populations.* **Kennedy, O. D., et al.** 2012, Bone, pp. 1115-1122.

62. *Osteocyte density and histomorphometric parameters in cancellous bone of the proximal femur in five mammalian species.* **Mullender, M.G., et al.** 1996, Journal of Orthopaedic Research, pp. 972-979.

63. *Three-dimensional reconstruction of chick calvarial osteocytes and their cell processes using confocal microscopy.* **Sugawara, Y., et al.** 2005, Bone, pp. 877-883.

64. *A computational model for cell differentiation.* **Ardelean, I., et al.** 2004, BioSystems, pp. 169-176.

65. *Mathematical model predicts a critical role for osteoclast autocrine regulation in the control of bone remodeling.* **Komarova, S. V., et al.** 2003, Bone, pp. 206-215.

66. *Smaller, weaker, and less stiff bones evolve from changes in substistence strategy.* **Nowlan, N. C., Jepsen, K. J. and Morgan, E. F.** 2011, Osteoporosis international, pp. 1967-1980.

67. *Simulations of trabecular remodeling and fatigue: Is remodeling helpful or harmful?* **van Oers, R.F.M., et al.** 2011, Bone, pp. 1210-1215.

68. *Mathematical Model for Repair of Fatigue Damage and Stress Fracture in Osteonal Bone.* **Martin, B.** 1995, Journal of Orthopaedic Research, pp. 309-316.

69. *Spatio-temporal structure of cell distribution in cortical Bone Multicellular Units: A mathematical model.* **Buenzli, P.R., Pivonka, P. and Smith, D.W.** 2011, Bone, pp. 918-926.

70. **Alon, Uri.** *An Introduction to Systems Biology: Design Principles of Biological Circuits.* s.l. : Chapman & Hall/CRC, 2006.

71. *Morphological Assessment of Basic Multicellular Unit Resorption Parameters in Dogs Shows Additional Mechanisms of Bisphosphonate Effects on Bone.* **Allen, M. R., et al.** 2010, Calcified Tissue International, pp. 67-71.

72. *A Crack in the System.* **Ouslander, Joseph G.** 2010, Journal of the American Geriatric Society, pp. 1593-1594.

73. *Cost-effectiveness of a multifaceted intervention to improve quality of osteoporosis care after wrist fracture.* **Majumdar, S. R., et al.** 2011, Osteoporosis International, pp. 1799-1808.

74. *Perspective: Genetic and hormonal roles in bone disorders: Insights of an updated bone physiology.* **Frost, H.M.** 2003, Journal of Musculoskeletal and Neuronal Interactions, pp. 118-135.

75. *Small-Animal PET/CT Assessment of Bone Microdamage in Ovariectomized Rats.* **Zhan-Chun Li, Sheng-Dan Jiang, Jun Yan, Lei-Sheng Jiang, and Li-Yang Dai.** 2011, THE JOURNAL OF NUCLEAR MEDICINE, pp. 769-775.

76. *Effects of Estrogen Deficiency and Bisphosphonate Therapy on Osteocyte Viability and Microdamage Accumulation in an Ovine Model of Osteoporosis.* **Brennan, O., et al.** 2011, JOURNAL OF ORTHOPAEDIC RESEARCH, pp. 419-424.

77. *Relative importance of body composition, osteoporosis-related behaviors, and parental income on bone speed of sound in adolescent females.* **Holmes, B. L., et al.** 2010, Osteoporos International, pp. 1953-1957.

78. *Modeled microgravity and hindlimb unloading sensitize osteoclast precursors to RANKL-mediated osteoclastogenesis.* **Saxena, R., et al.** 2010, Journal of Bone Mineral Metabolism, pp. 111-122.

79. *Evidence for an additional effect of whole-body vibration above resistive exercise alone in preventing bone loss during prolonged bed rest.* **Belavý, D. L., et al.** 2011, Osteoporos International, pp. 1581-1591.

80. *A comparison of resistance and aerobic training for mass, strength and turnover of bone in growing rats.* **Notomi, K., et al.** 2000, European Journal of Applied Phisiology, pp. 469-474.

81. **AA., VV.** Physical Fitness and Physical Training for Military Performance. [book auth.] J. A. and Patton, J. F. III Vogel. *Rehabilitation of the Injured Combatant Vol 2.* Washington : Office of The Surgeon General, Department of the Army, United States of America, 1999.

82. *Stress fracture injury in young military men and women.* **Armstrong, D. W. III, Rue, J. H. and Wilckens, J. H. and Frassica,F.J.** 2004, Bone, pp. 806-816.

83. *STRESS FRACTURES IN MILITARY RECRUITS: A PROSPECTIVE STUDY SHOWING AN UNUSUALLY HIGH INCIDENCE.* **MILGROM, C., et al.** 1985, THE JOURNAL OF BONE AND JOINT SURGERY, pp. 732-735.

84. *How stress fracture incidence was lowered in the Israeli army: a 25-yr struggle.* **Finestone A, Milgrom C.** 2008, Medicine and Science in Sports and Exercise, pp. 623-629.

85. *The finite cell method for bone simulations: verification and validation.* **Ruess, M., et al.** 2011, Biomechanics and Modeling in Mechanobiology, pp. 425-437.

86. *Multiscale prediction of crack density and crack length accumulation in trabecular bone based on neural networks and finite element simulation.* **Hambli, R.** 2011, INTERNATIONAL JOURNAL FOR NUMERICAL METHODS IN BIOMEDICAL ENGINEERING, pp. 461-475.

87. *Anisotropic gradient elasticity for modelling bone tissue.* **Gitman, I.M.** 2011, Computational Materials Science, pp. 136-138.

88. *The use of the flexible multibody approach for lower body skeletal loading analysis.* **Krodowski, A., et al.** 2011. Symposium on Human Body Dynamics. pp. 93-100.

89. *Multibody biomechanical models of the upper limb.* **Ambrósio, J., et al.** 2011. Symposium on Human Body Dynamics. pp. 4-17.

90. *Development of a Full Body CAD Dataset for Computational Modeling: A Multi-modality Approach.* **GAYZIK, F. S., et al.** 2011, Annals of Biomedical Engineering, pp. 2568-2583.

91. *Microdamage and mechanical behaviour predicting failure and remodeling in compact bone.* **Taylor, D. and Lee, T. C.** 2003, Journal of Anatomy, pp. 203-211.

92. *Rupture of osteocyte processes across microcracks: the effect of crack length and stress.* **Dooley, Clodagh, et al.** 2012, Biomechanics and Modeling in Mechanobiology, pp. 759–766.

93. *Living with cracks: Damage and repair in human bone.* **TAYLOR, D., HAZENBERG, J. G. and LEE, T. C.** 2007, Nature materials, pp. 263-268.

94. *Bone morphology allows estimation of loading history in a murine model of bone adaptation.* **Christen, P., et al.** 2011, Biomechanics and Modeling in Mechanobiology, pp. 483-492.

95. *A mechano-regulation model for tissue differentiation during fracture healing: analysis of gap size and loading.* **Lacroix, D. and Prendergast, P.J.** 2002, Journal of Biomechanics, pp. 1163-1171.

96. *Examination of compact bone microdamage using back-scattered electron microscopy.* **Schaffler, M.B., et al.** 1994, Bone, pp. 483-488.

97. *Fatigue failure and skeletal evolution.* **Martin, R. B.** 2007, International Journal of Fatigue, pp. 1019-1023.

98. *Loss of Osteocyte Integrity in Association with Microdamage and Bone Remodeling After Fatigue In Vivo.* **Verborgt, O. and Gibson, G. J. and Schaffler, M. B.** 2000, Journal of Bone Mineral Research, pp. 60-67.

99. *On the effect of X-ray irradiation on the deformation and fracture behaviour of human cortical bone.* **Barth, H. D., et al.** 2010, Bone, pp. 1475-1485.

100. *Predicting stress fractures using a probabilistic model of damage, repair and adaptation.* **Taylor, D., Casolari, E. and Bignardi, C.** 2004, Journal of Orthopaedic Research, pp. 487-494.

101. *Presence of microscopic cracks in vivo in bone.* **Frost, H. M.** 1960, Henry Ford Hospital Medical Bulletin.

102. *Stress intensity variations in bone microcracks during the repair process.* **Taylor, D. and Tilmans, A.** 2004, Journal of Theoretical Biology, pp. 169-177.